12-1993

Dynamic Response of a Compressor Research Facility

Janet W. Grondin

AFIT/GAE/ENY/93D-16

DYNAMIC RESPONSE OF A COMPRESSOR RESEARCH FACILITY

THESIS

Janet W. Grondin, Captain, USAF

AFIT/GAE/ENY/93D-16

AFIT/GAE/ENY/93D-16

DYNAMIC RESPONSE
OF A
COMPRESSOR RESEARCH FACILITY

THESIS

Presented to the Faculty of the Graduate School of Engineering
of the Air Force Institute of Technology
Air University
In Partial Fulfillment of the
Requirements for the Degree of
Master of Science in Aeronautical Engineering

Janet W. Grondin
Captain, USAF

December 1993

Preface

The purpose of this thesis effort was to find the resonant frequencies of the Compressor Research Facility located at Wright-Patterson AFB, Ohio. The general approach to the study was to treat the facility as a fluid transmission line and solve for the transfer function of the facility. The solution is analogous to electrical theory where the gain and phase shift of an alternating input signal is determined at the output end of the line.

I had the good fortune to be advised by Dr. Milton Franke, who has established an outstanding reputation for his work in fluid transmission lines, as well as in other areas of mechanical and aeronautical engineering. Dr. Franke's guidance through the project was the primary reason this thesis effort was successful.

This project involved both theoretical and experimental efforts and the latter could not have been accomplished without the help of Andy Pitts of the AFIT Aeronautical Engineering Laboratories. Andy's help with setting up the transducers, plumbing, data acquisition system, and pneumatic valve was essential to the success of the experiment. Also, Mr. Jan LeValley and Mr. David Driscoll at the AFIT model shop constructed the CRF model with superb accuracy, resulting in excellent experimental data.

The support from Dr. Douglas Rabe, of the Compressor Research Facility, was greatly appreciated. Although often busy with the daily operation of the CRF, Doug always took the time to answer any questions I had concerning the facility.

Also greatly appreciated is the support and team-oriented efforts of Capt Brian Hull. Though busy with his own thesis, Brian worked with me to connect his control system design to my theoretical output. His faith in my work was crucial to my self-esteem as well as to the usefulness of the results in this thesis.

I would like to thank Maj Tom Buter and Capt John Doty, readers of this thesis, for their support of the project and helpful suggestions along the way. Their effort to understand the problem, theory, and conclusions was tremendously valuable to me, especially in learning how to present the information to other engineers.

Finally, it is hard to put into words how grateful I am to my loving and supportive husband. My husband, Pat, has had his own master's program to finish while I was finishing mine. Through all of the ups and downs, Pat has been by my side, encouraging me and showing his support, even during times when his own work was very demanding of his time and energy. Pat, I love you and can't wait to spend more time with you after graduation.

Janet W. Grondin

Table of Contents

List of Figures

List of Tables

Notation

A	area, ft^2
a	speed of sound in air, ft/s
c_p	specific heat at constant pressure, Btu/lbm-°F
CRF	Compressor Research Facility
D	diameter, ft
f	frequency, Hz or friction factor, nondimensional
J_0	Bessel function of the first kind, zero order
J_1	Bessel function of the first kind, first order
j	$(-1)^{½}$
K_L	loss coefficient, nondimensional
k	thermal conductivity of air, Btu/(h-ft-°F)
L	inertance, $lbf-s/ft^4$ or line length, ft
l	line length, ft
M	Mach number, nondimensional
$\dot{m}$	mass flow, slug/s
N_p	Prandtl number, dimensionless
P	pressure, lbf/ft^2
Q	volume flow, ft^3/s
R	resistance, $lbf-s/ft^5$ or radius, ft
R_{air}	universal gas constant for air, ft-lbf/slug-°R
R_c	compressor radius, ft
Re_D	Reynolds number based on diameter, nondimensional
r	radial distance, ft
T	temperature, °R

t	time, s
u	axial velocity, ft/s
V	velocity, ft/s
x	axial distance, ft
Y	admittance, $ft^4/lbf \cdot s$
Z	impedance, $lbf \cdot s/ft^5$
Z_{ca}	characteristic adiabatic impedance, $lbf \cdot s/ft^5$
Z_L	load impedance, $lbf \cdot s/ft^5$
β	porosity, nondimensional
Γ	propagation operator, 1/ft
γ	ratio of specific heats, nondimensional
ν	kinematic viscosity, ft^2/s
ρ	density, $slug/ft^3$
θ	phase angle, degrees
ω	frequency, rad/s
ω_v	characteristic frequency, Hz

Subscripts

c	characteristic
i	line input
l	line end
res, b	resonant frequency for a blocked line, Hz
res, o	resonant frequency for an open line, Hz
T	throughflow

Abstract

The response of the Wright Laboratory Compressor Research Facility to a small amplitude, acoustic, sinusoidal disturbance was investigated. The fluid transmission line equations for laminar, one-dimensional flow in a circular duct were solved and verified through a laboratory experiment using a scale model of the facility. The resonant frequencies of the facility were determined for a variety of flow conditions. Techniques for analytically modeling end impedance and flow straightening elements were also studied. The fundamental frequency of the facility was determined to be between 5.5 and 6.5 Hz depending on the flow conditions and geometry configurations specified.

DYNAMIC RESPONSE

OF

A COMPRESSOR RESEARCH FACILITY

I. Introduction

1.1 Background

The study of the dynamic response of the Air Force Wright Laboratory Compressor Research Facility (CRF) was proposed for the purpose of determining the resonant frequencies of the facility. Currently, a new inlet valve control system design is under development in a parallel effort (Hull:1993). This control system design requires accurate resonant frequency input in order to perform properly. This study determines the resonant frequencies through a modeling of the CRF as a fluid transmission line.

Fluid transmission lines have been studied in depth for over 40 years. In the early years, these studies were conducted to yield baseline equations and data for design of fluidic components to be used as amplifiers, diodes, switches, and other circuit elements. The early studies resulted in a sound knowledge base of fluid transmission line theory (Iberall:1950; Nichols:1962; Brown:1962; Kirshner and Katz:1975). In addition, efforts to gather baseline data resulted in theory verification for many types of fluid transmission lines (Krishnayer and Lechner:1967; Bergh and

Tijdeman:1965; Franke:1969, 1979, 1972). The theory and some experimental data from the early work apply to the solution of the CRF dynamic response.

1.1.1 Fluid Transmission Lines. The theory centers on the idea that, for a small amplitude input signal, fluid transmission lines are fundamentally similar to electrical transmission lines. To begin with, the fluid line is comprised of the same passive elements in an electrical line; namely, resistance, conductance, inductance, and capacitance. Viscous dissipation causes losses in the fluid line in the same manner as resistance and conductance cause losses in potential in an electrical line. Compressed fluid stores energy in the same manner as a capacitor in an electrical line. Boundary layer interactions cause a phase shift in the signal in the same manner as an inductor in an electrical line. Further, the pressure difference between the exit and inlet of a fluid line is analogous to voltage while the volumetric flow is considered the fluid equivalent of current. A circuit made up of passive elements has resonant frequencies and at these frequencies the output can be much larger than the input, resulting in a large gain. Given a sinusoidal input signal, the gain and phase shift of the signal at the output of the circuit can be calculated if the resistance, conductance, capacitance, and inductance are known. For a

simple electrical circuit design in which the passive elements are specified, finding the resonant frequencies, the associated gain, and corresponding phase shift is quite tractable. For transmission lines; however, considerable effort is required as values for resistance, conductance, inductance, and capacitance must be theoretically determined. Fortunately, these parameters can be found for the fluid line by solving equations developed by Iberall (1950:85-108) and Nichols (1962:5-14).

In this study, Nichols' work is used to determine the transmission line characteristics of the CRF. In particular, the study focuses on finding the resonant frequencies of the facility.

1.1.2 The Compressor Research Facility. The CRF is a unique facility used to test experimental jet engine compressors. Flow is introduced through five large butterfly valves at the inlet, drawn through several flow conditioning elements, and exhausted through the test article (compressor). The flow conditions are varied according to a test plan developed for each compressor that typically calls for several runs at different flow conditions. Often, specified flow conditions are met by setting a desired static pressure at the face of the compressor; thereby simulating a predetermined altitude for testing.

Operators of the CRF primarily control the pressure at the compressor inlet through the manipulation of the five butterfly valves. However, when the speed of the test article is changed, the static pressure at the compressor face also changes. Due to this effect, it is not a simple process to evaluate and test a compressor at different speeds and constant pressure. Presently, a feedback control system is being designed to read the static pressure change caused by a change in the compressor speed and accordingly adjust one or more of the five inlet valves to hold a constant pressure at the inlet of the test article.

However, when the control system adjusts the valves, the steady inlet flow will be disturbed. As a result, unsteady pressure waves, at a frequency corresponding the valve movement rate, will be produced and transmitted down the facility. These waves, should they be generated at one of the resonant frequencies of the facility, could become quite large and ultimately destroy the test article.

The control system, then, must be designed to avoid operation at the fundamental frequencies. The purpose of this study is to provide that frequency information to the controls designer so the control system can be developed with confidence that the resonant frequencies will be avoided.

1.2 Objectives

The primary objective of this study is to determine the resonant frequencies of the CRF. The frequencies are determined from the fluid transmission line theory presented by Nichols (1962). The Nichols equations are modified to account for the specific geometry of the facility and then solved for various mass flows and compressor radii. The solution process involves meeting the following specific objectives:

1. Write and verify a computer program that determines the frequency response of the CRF;
2. Design and test a scale model of the CRF and verify the analytical results;
3. Determine the correct analytical model of the screens and honeycomb elements in the CRF; and
4. Obtain the transient response of the laboratory model.

1.3 Thesis Outline

The entire discussion is comprised of eight chapters. First, the governing equations for fluid transmission lines are detailed in Chapter II. The physical systems are outlined in Chapter III, including the various configurations of the CRF and the laboratory model. The experimental apparatus and data acquisition equipment are described in Chapter IV.

Chapter V outlines the computer program written to solve for the frequency response of the CRF and laboratory model. The results of the program, as applied to the CRF are discussed and presented in Chapter VI. The experimental results from the scale model are presented in Chapter VII.

Conclusions on these results are discussed in Chapter VIII along with recommendations for future studies of this type. Finally, the results of several intermediate studies are presented in Appendices.

II. Theory

2.1 Introduction

In this chapter, the basics of pipe resonance are covered, followed by the circuit theory for fluid transmission lines, and a summary of the governing equations. The transmission line equations for a constant diameter circular line with a small, acoustic input signal are presented and modifications to include velocity effects discussed. The chapter is concluded with equations for more complex geometries, including cascaded and branched lines.

2.2 Basic Pipe Resonance Equations

The fluid transmission line theory is really an extension of the basic equations for a resonating pipe, such as an organ pipe. For a pipe of length, l, and air with speed of sound, a, the resonant frequencies are given by (Haliday and Resnick, 1981:326):

$$f_{reas,b} = \frac{na}{4l} \qquad (2\text{-}1)$$
$$n = 1, 3, 5, \ldots$$

for a blocked pipe. For an open pipe, the resonant frequencies are:

$$f_{res,o} = \frac{na}{2l} \qquad (2\text{-}2)$$

$$n = 1, 2, 3, \ldots$$

From Equations (2-1) and (2-2), the following observations are made. First, the resonant frequencies are inversely proportional to the length of the pipe. As such, long pipes will have lower resonant frequencies than short pipes. Second, for two pipes of the same length, one open and one blocked, the blocked pipe resonant frequencies will be one half of the open pipe resonant frequencies. Therefore, for the same length, the open pipe will have higher resonant frequencies than the closed pipe. Third, depending on the frequency range, length of pipe, and speed of sound, the blocked pipe can have more resonant frequencies in the range than the open pipe. The latter notion is more fully developed in Chapter III.

2.3 Circuit Theory for Fluid Transmission Lines

The circuit representation for a typical fluid transmission line with passive elements and a small, acoustic input signal is illustrated in Figure 2.1. P_i is the input pressure signal and Q is the flow rate. At some point along the line, the pressure signal is detected as P_1 and its value depends on the load impedance Z_L, as well as on the line impedance, Z, and admittance, Y.

For any given circular fluid line, knowledge of Z, Y, and Z_L allows solution of the system gain, P_l/P_i, and phase shift, θ, at any frequency. The result fully defines the dynamic response of the transmission line for a small sinusoidal input signal.

2.4 Governing Equations

Analytical methods for determining Z, Y, and P_l/P_i for the fluid transmission line have been developed from the Navier-Stokes equations (Nichols, 1962:5-14). The solution of the Navier-Stokes equations is reduced in complexity according to the following simplifying assumptions:

1. one-dimensional plane wave;
2. axial symmetry;
3. ideal gas;
4. small acoustic signals;
5. laminar flow;

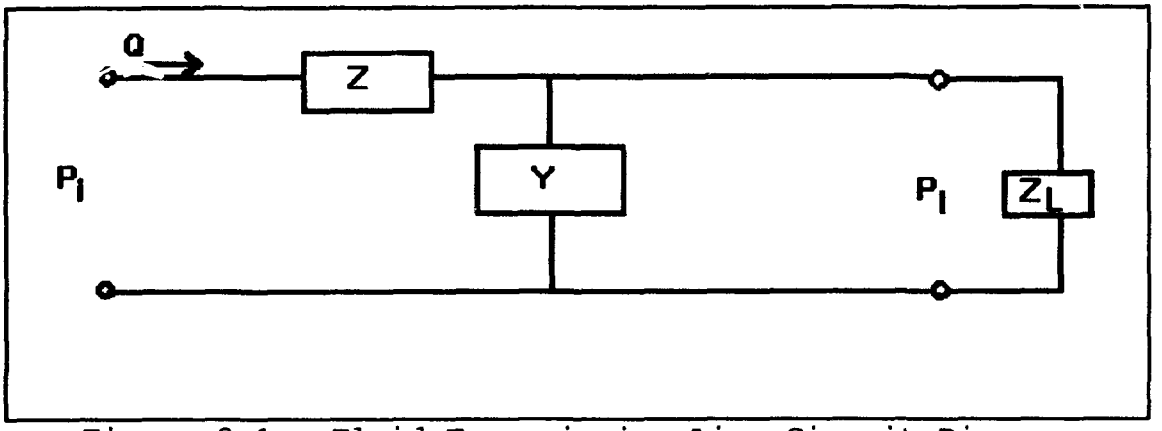

Figure 2.1. Fluid Transmission Line Circuit Diagram

6. first order approximations;

7. negligible axial velocity and temperature gradients;

8. uniform pressure at each cross section; and

9. no throughflow.

The simplified momentum, energy, and continuity equations are (Kirshner and Katz, 1975:76):

$$\frac{\partial u}{\partial t} = -\frac{1}{\rho}\frac{\partial P}{\partial x} + \nu\left[\frac{1}{r}\frac{\partial}{\partial r}\left(r\frac{\partial u}{\partial r}\right)\right] \qquad (momentum) \quad (2\text{-}3)$$

$$\rho c_p \frac{\partial T}{\partial t} = \frac{\partial P}{\partial t} + k\left[\frac{1}{r}\frac{\partial}{\partial r}\left(r\frac{\partial T}{\partial r}\right)\right] \qquad (energy) \quad (2\text{-}4)$$

$$\frac{\partial \rho}{\partial t} + \rho\frac{\partial u}{\partial x} = 0 \qquad (continuity) \quad (2\text{-}5)$$

Nichols (1962:9) has shown these equations reduce to the wave equation if, at the inlet (x = 0), the alternating pressure and alternating flow rate are specified:

$$\frac{\partial^2 P}{\partial x^2} = ZYP \quad . \qquad (2\text{-}6)$$

In the wave equation, the impedance, Z, and the admittance, Y, are given by

$$Z = j\frac{\omega\rho}{A}\left\{1 - \frac{2J_1\left[j^{3/2}(8\omega/\omega_v)^{1/2}\right]}{j^{3/2}(8\omega/\omega_v)^{1/2}J_0\left[j^{3/2}(8\omega/\omega_v)^{1/2}\right]}\right\}^{-1} \qquad (2\text{-}7)$$

$$Y = j\frac{A}{\rho a^2}\omega\left\{1 + \frac{2(\gamma - 1)J_1\left[j^{3/2}(8N_p\omega/\omega_v)^{1/2}\right]}{j^{3/2}(8N_p\omega/\omega_v)^{1/2}\,J_0\left[j^{3/2}(8N_p\omega/\omega_v)^{1/2}\right]}\right\} . \qquad (2\text{-}8)$$

Where the characteristic frequency for a circular line is given by:

$$\omega_v = \frac{8\pi\nu}{A} . \qquad (2\text{-}9)$$

The three parameters that completely characterize the transmission line are the end impedance, Z_L, the characteristic impedance, Z_c, and the propagation operator, Γ. The end impedance is comprised of a resistance and inertance and is discussed in detail in the next section. Z_c and Γ are dependent on Z and Y as

$$Z_c = (Z/Y)^{1/2} \qquad (2\text{-}10)$$

$$\Gamma = (ZY)^{1/2} . \qquad (2\text{-}11)$$

Finally, Kirshner & Katz (1975:68) give the gain of the line as:

$$\frac{P_l}{P_i} = \frac{(Z_L/Z_c)}{\sinh(\Gamma l) + (Z_L/Z_c)\cosh(\Gamma l)} \qquad (2\text{-}12)$$

and the phase angle as:

$$\theta = \arctan\left[\frac{Im(P_1/P_i)}{Re(P_1/P_i)}\right] . \qquad (2\text{-}13)$$

Given the flow conditions and geometry of the fluid line, the only remaining variable to be specified is the end impedance, Z_L.

2.4.1 End Impedance. The end impedance is comprised of a resistance, R, and an inertance, L:

$$Z_L = R + j\omega L \quad . \qquad (2\text{-}14)$$

In the case of a blocked line, Z_L is infinitely large. On the other hand, for an open line, Z_L is zero. For an orifice-terminated line, Z_L may be represented as (Kirshner and Katz, 1975:16):

$$Z_L = R = K_L \frac{\dot{m}}{A^2} \qquad (2\text{-}15)$$

where A is the area of the smallest cross section and K_L is the loss coefficient of the orifice.

According to Kirshner & Katz (1975:56), inertance is unimportant unless the orifice length is short in comparison to the wavelength of the input signal. When required, the inertance of a line is expressed as:

$$L = \frac{\rho l}{A} \qquad (2\text{-}16)$$

where l and A are the length and area of the orifice, respectively.

For a single, constant diameter line with no throughflow, the above equations satisfactorily describe the dynamic response of a system. However, the end impedance for an orifice-terminated line is strongly dependent on mass flow rate. As such, it is natural to extend the expressions for the propagation operator and characteristic impedance to include the effects of throughflow as well.

2.4.2 Throughflow Effects. If throughflow is present, an adjustment can be made to the characteristic impedance and the propagation operator. Katz, Housner, and Eisenberg (1974:278-281) derived approximations to Γ and Z_c that incorporate velocity effects.

With these approximations, the propagation operator is adjusted for throughflow as follows:

$$\Gamma_T = \frac{\Gamma (1 + m^2)^{1/2}}{1 - M^2} \qquad (2\text{-}17)$$

where

$$m = \frac{M}{2}\left[\frac{Z_{ca}}{Z_c} - \frac{Z_c}{Z_{ca}}\right]$$

$$Z_{ca} = \left(\frac{\rho \gamma P}{A^2}\right)^{1/4}$$

The gain is then calculated as:

$$\frac{P_l}{P_i} = \frac{e^{bl}(1 + m^2)^{1/2}}{(1 + m^2)^{1/2}\cosh(\Gamma_T l) + [(Z_c/Z_L) - m]\sinh(\Gamma_T l)} \qquad (2\text{-}18)$$

with

$$b = \frac{M\Gamma g}{2(1 - M^2)}$$

$$g = \frac{Z_{ca}}{Z_c} + \frac{Z_c}{Z_{ca}} \quad .$$

The characteristic impedance then becomes:

$$Z_{cT} = Z_c[(1 + m^2)^{1/2} - m] \quad . \qquad (2\text{-}19)$$

2.4.3 Cascaded Lines. The theory for a single, constant diameter line is easily extended to a system of cascaded lines with different diameters. In a system of cascaded lines, the overall gain is found by multiplying the gains of the individual lines. Further, a new variable is introduced, Z_i, as the input impedance of a line. In general, Z_i is equal to the end impedance of the upstream line and is computed through (Kirshner and Katz, 1975:67):

$$Z_i = Z_c\left[\frac{Z_L\cosh(\Gamma l) + Z_c\sinh(\Gamma l)}{Z_L\sinh(\Gamma l) + Z_c\cosh(\Gamma l)}\right] \quad . \qquad (2\text{-}20)$$

Often, cascaded line behavior is significantly different from the behavior of a single diameter line of the same length. Depending on the length of the lines in the cascade, waves reflecting at the boundaries can change the resonant frequencies from those of a constant diameter line. Thus, the overall transfer function can change when the cascade is introduced.

2.4.4 Branched lines. A branched line allows for a second flow path and can also significantly alter the transfer function of a system. Figure 2.2 shows a branched line system.

Figure 2.2 shows that the branched line model assumes that the pressure, P, at the junction is the same for each line. As such, the load impedance for the input line (1) is a combination of the end impedances for lines 2 and 3. Thus, Z_{L1} is now given by (Kirshner and Katz, 1975:98):

$$Z_{L1} = \frac{Z_{i2}\, Z_{i3}}{Z_{i2} + Z_{i3}} \quad . \tag{2-21}$$

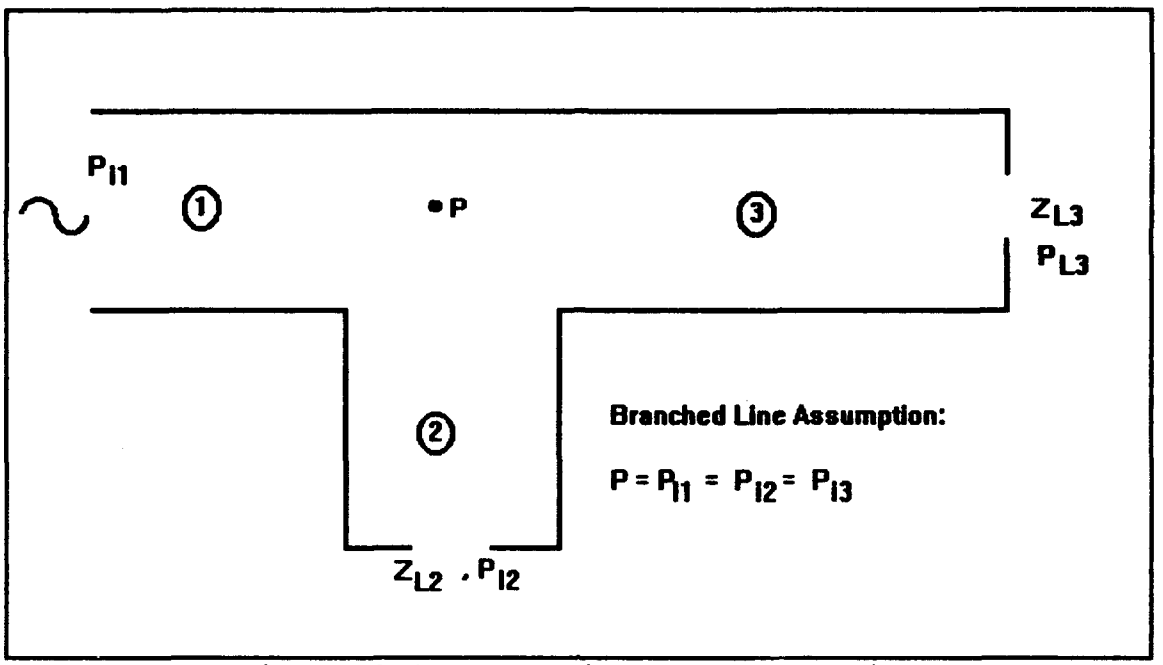

Figure 2.2. A Typical Branched Line

III. The Compressor Research Facility and Model

3.1 Introduction

In this chapter, the geometry of the CRF and the scaled laboratory model are detailed. During the discussion, correlations between the equations presented in Chapter II and the specific geometry of the facility are made.

3.2 The Compressor Research Facility

As illustrated in Figure 3.1, the CRF is 69.8 ft long and includes a 20 ft diameter inlet section (section 1), a 10 ft diameter flow conditioning section (section 2), and a 3.3 ft diameter section (section 3) at the inlet of the test article. Additionally, a 2.5 ft diameter pipe is connected to the inlet section and exhausted outside the main flow. Mass flow rates through the facility generally range from 20 lbm/s up to 250 lbm/s.

3.2.1 Section Lengths. The lengths of sections 1 and 3 (L1 and L3) can vary to accommodate different compressors. Changes in L1 are offset by an equal change in L3 such that the overall facility length of 69.8 ft remains unchanged. The maximum and minimum lengths of both sections are noted in Figure 3.1 and the three length configurations defined for this study are listed in Table 3.1.

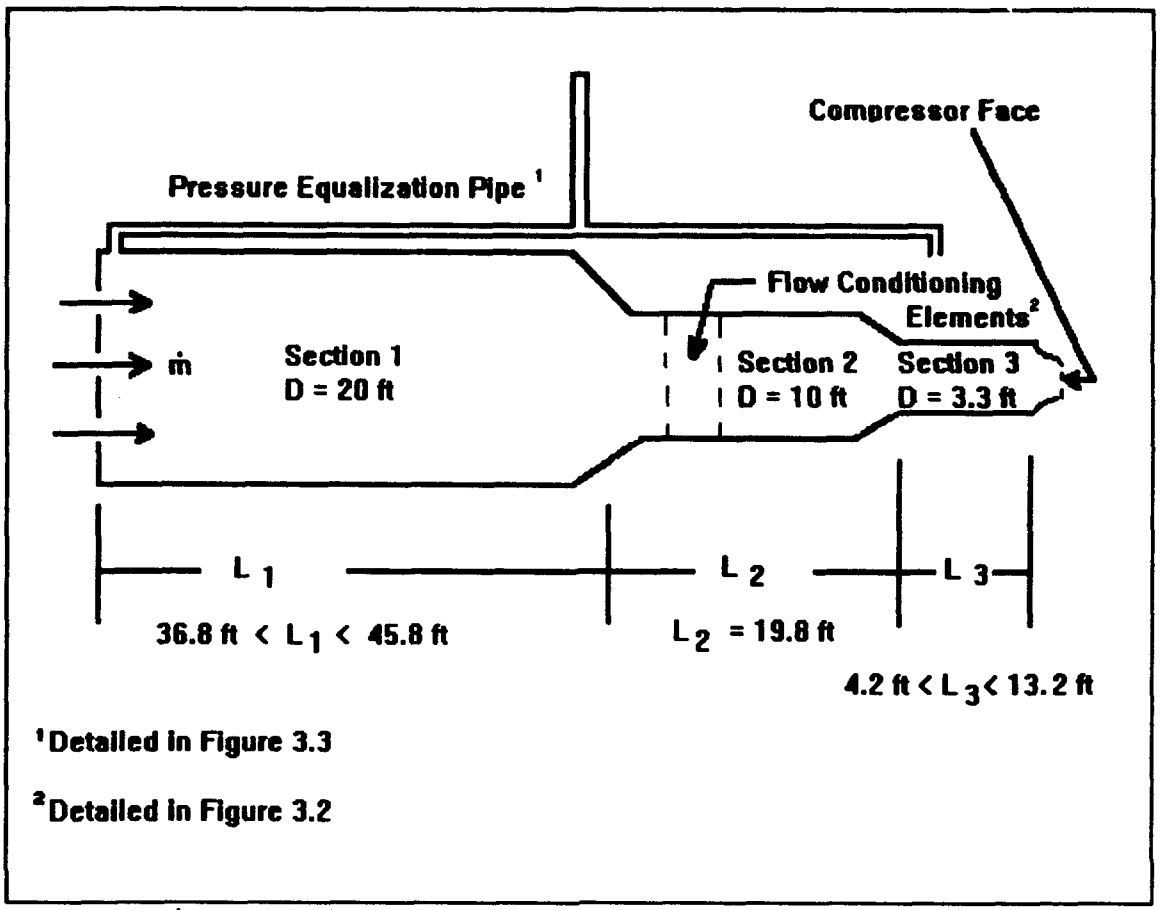

Figure 3.1. The Compressor Research Facility

Table 3.1. Length Configuration Definitions

Configuration	L1 (ft)	L2 (ft)	L3 (ft)
Basic	36.8	19.8	13.2
Intermediate	41.3	19.8	8.7
Extended	45.8	19.8	4.2

In Table 3.1, the basic length configuration is defined such that L1 is minimized and L3 is maximized. The extended length configuration is defined for L3 maximized and L1 minimized. The intermediate length configuration is defined for both L1 and L3 between their maximum and minimum lengths. For all configurations, the sum of L1, L2, and L3 is 69.8 ft.

3.2.2 Flow conditioning elements. Section 2 contains two sets of grids, screens, and honeycomb, called flow conditioning elements, that remove axial and radial turbulence in the throughflow. These elements improve the quality of the throughflow at the compressor face but also add impedance to the system. Figure 3.2 shows a breakdown of the flow conditioning elements and their locations. The upstream end, denoted as line A-A in Figure 3.2, is 39.4 ft from the inlet of the CRF (for the basic length configuration).

The impedance presented by the screens, honeycomb, and grid elements is modeled analytically as area reductions at the locations where they are mounted. These areas are determined by the porosity of the individual elements. For example, the equivalent open area of the 18-mesh screen is calculated as (Rae and Pope, 1984:76):

$$\beta_{18} = \frac{open\ area}{total\ area} = (1 - wd^2) \qquad (3\text{-}1)$$

where, for the 18-mesh screen:

$$w = 18\ wires/inch$$

$$d = 0.017\ inch\ (dia) \quad .$$

To find the diameter representing the equivalent open area:

$$\beta_{18} = 0.482 = \frac{\pi D^2}{\pi (10\ ft)^2}$$

$$D = 6.94\ ft$$

In the analytical model, the 18-mesh screen is represented by a line of diameter 6.94 ft and length 0.017 in.

The radius changes between the individual sections and the flow straightening elements requires that the facility be

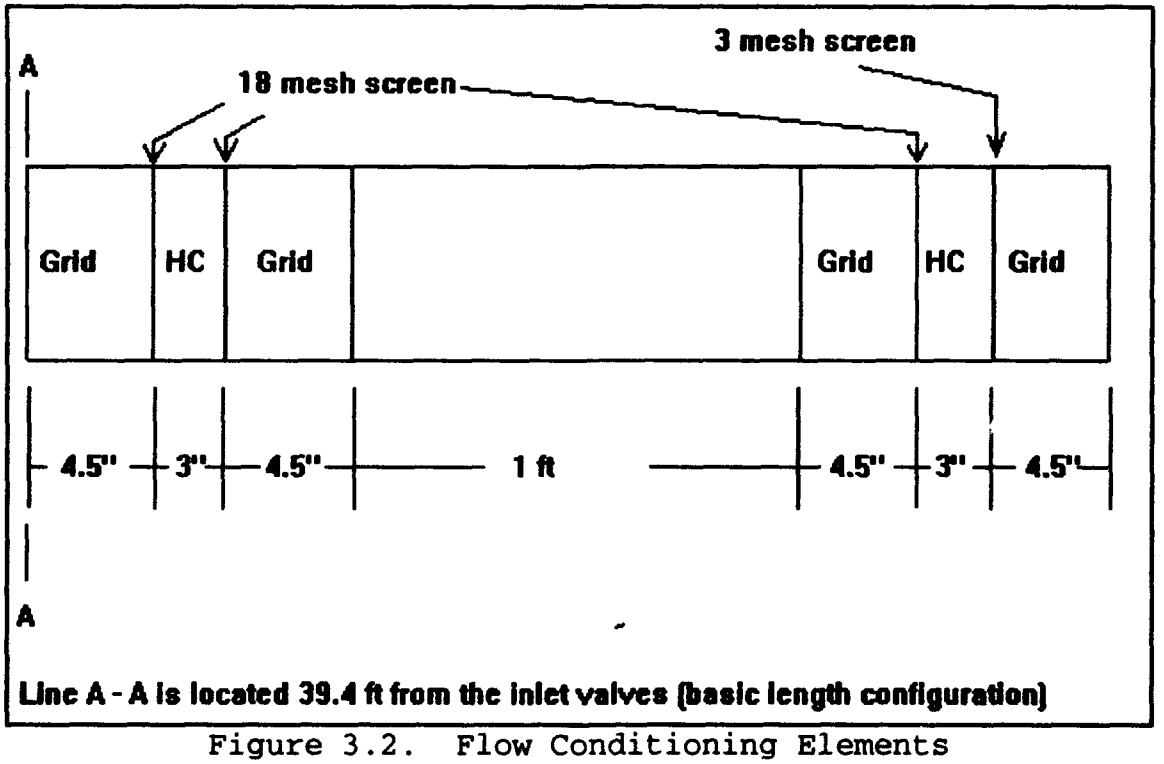

Figure 3.2. Flow Conditioning Elements

treated as a system of cascaded lines in the fluid transmission line equations. Thus, the gain for each line is calculated and multiplied by the gains of the other lines to find the overall gain for the facility.

3.2.3 Pressure Equalization Pipe. The pressure equalization pipe is detailed in Figure 3.3. The function of the pipe is to provide inlet flow to a large cavity surrounding the outside structure of sections 2 and 3 of the facility. Because the cavity surrounds the outside of sections 2 and 3, it is not in the main flow of the CRF. The

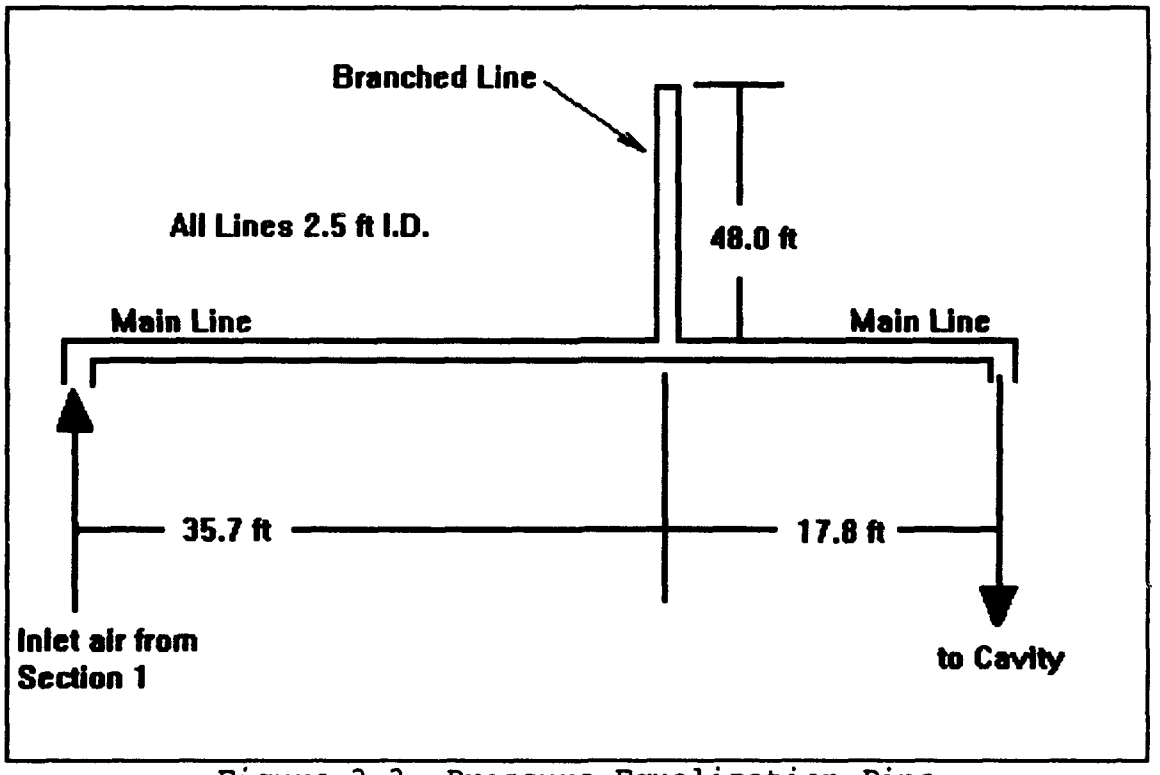

Figure 3.3. Pressure Equalization Pipe

pipe ensures the cavity is at the same pressure level as section 1.

For the purposes of this study, the pressure equalization pipe is simply a branched line that draws flow from the 20 ft diameter section and exhausts it outside the main flow. From Figure 3.3, it is clear that the branched line is composed of two lines. The 2.5 ft diameter main line is comprised of the 35.7 ft and 17.8 ft lines. The main line exhausts to the cavity and in the analytical model is considered a branched line (branching from section 1). The end of the main line is treated as fully open.

The 48.0 ft line, also of 2.5 ft diameter, branches from the main line to a valve. In the analytical model, the 48.0 ft line is considered a branched line (branching from the main line) and the end is treated as fully blocked.

3.2.4 Inlet Valves. The five inlet butterfly valves are arranged in a circular pattern about the centerline of the facility. The two largest valves have the same diameter, 36 in, while the other three valves have 24 in, 20 in, and 14 in diameters. These five valves, when moved while the facility is operating, produce the unsteady disturbances that are the input signals for the transmission line equations.

For the analytical model, the valves are not considered individually. Instead, it is assumed that a single sinusoidal

disturbance emanates from the point where the valves are located in the line (inlet, x = 0). This approximation was made in order to simplify the analysis; because, modeling the individual valves would be an effort in itself.

The transmission line equations depend not only on the inlet conditions but also on the end conditions. Here, too, the geometry is approximated to simplify the analysis.

3.2.5 Exit Geometry. The CRF exhausts the main flow through the compressor into a long, taurus-shaped pipe and eventually returns the flow to atmospheric conditions. For the purposes of this study; however, the compressor, taurus-shaped pipe, and eventual return of the flow to atmospheric conditions are all ignored. The validity of this assumption is discussed in Chapters VI, VII, and VIII.

Including the compressor in the analysis requires detailed knowledge of the energy added to the throughflow by each test article. Since each test article behaves differently, it would be a significant task to find a model that covers all of the potential compressors to be used in the facility. Because of this, the compressor and all downstream elements are ignored.

The analytical model instead assumes the flow in section 3 smoothly necks down to the compressor. The end of the transmission line is considered to be at the compressor face

and the compressor face is assumed to be at the end of section 3, 69.8 ft from the inlet valves. Modeling the system exit in this manner means that in the equation for end impedance (2-15), the loss coefficient, K_L, has a constant value of 0.05 (Kirshner and Katz, 1975:18). While far from exact, this model does serve the purpose at hand, which is to find the fundamental frequencies.

3.3 Theoretical Limitations on the CRF

This section details the theoretical limitations on the frequency range. Some of the discussion from Chapter II that was postponed is picked up again and resolved.

The one-dimensional, plane wave assumption places limits on the frequencies for which the Nichols theory is valid. F.T. Brown (1962:548) reports that for a valid solution:

$$f \ll \frac{2a}{D} \quad . \tag{3-2}$$

Thus, the limiting frequency depends on the largest diameter line in the system. For a = 1130 ft/s and D = 20 ft:

$$f \ll \frac{1130\ ft/s}{10\ ft} = 113\ Hz \quad . \tag{3-3}$$

The frequency response solution is limited to 112 Hz because of this restriction.

Now that a valid frequency range has been established, recall the postponed discussion in Section 2.1 on the number

of resonant peaks for simple constant diameter closed and open pipes in a given frequency range. The statement was made that under certain length and frequency conditions, the blocked pipe can have more resonant frequencies than the open pipe. At this time, the length of the CRF has been presented as 68.9 ft, the valid frequency range as 112 Hz, and the speed of sound can be assigned the standard sea level value of 1130.5 ft/s. Using the basic pipe resonance equations (2-1 and 2-2), the number of peaks for simple blocked and open lines of length 69.8 ft can be determined.

For the open line, the highest resonant frequency below 112 Hz occurs for n = 13 at 105.3 Hz. This means an open line of length 69.8 ft will have 13 resonant frequencies in the valid frequency range. On the other hand, for the blocked line of length 69.8 ft, the highest resonant frequency below 112 Hz occurs when n = 27 at a frequency of 109.3 Hz. This means that the blocked pipe of the specified length will have 14 resonant frequencies (recall only odd n are present for the blocked pipe) in the valid frequency range.

This is not a rigid analysis of the system but rather an attempt to gather additional background information to help with the analysis of the results of the study.

3.4 The Experimental Model

The model is constructed to incorporate as many of the transmission line characteristics of the CRF (full-scale facility) as possible. The length changes of L1 and L3 are incorporated in the model, along with the pressure equalization pipe, the inlet valves, and the flow conditioning elements. The end of the model is terminated with a short line and exhausted to the atmosphere. The schematic is equivalent to Figure 3.1, with the exception of the radii and end condition.

The model is constructed from high density polyethylene plastic tubing. This is a rigid material that allows the input signal to traverse the line without being absorbed by the structure.

3.4.1 Model Length and Radii. Table 3.2 illustrates the model dimensions in comparison to the full-scale facility. As shown in the table, the model length is equal to the length of the full-scale CRF. Each section is maintained on a 1:1 ratio with its counterpart in the CRF. The model was constructed to allow changing L1 and L3 from the basic to the intermediate and extended length configurations, although only the basic length configuration was tested. In order for the model to fit in the provided lab space, the tubing was coiled and contained in a 44 in square box.

Unlike the length, the radii are scaled significantly. Sections 1 and 2 and the pressure equalization pipe are scaled 1:120; whereas section 3 and the terminating line are scaled 1:106. The different scales are a result of standard sizes for commercially available tubing.

3.4.2 Flow Conditioning Elements for the Model. The model is constructed such that one of three flow conditioning sections can be used in section 2. Two of the sections are used to determine if the analytical model for the flow conditioning elements is valid while the third is used to verify the response of the full-scale CRF analyses. The three sections are illustrated in Figure 3.4.

The purpose of the washer configuration (top, Figure 3.4) is to physically model the analytical representation of

Table 3.2. CRF and Model Dimensions (Basic Length)

Dimension	Model	CRF
L1 (Basic)	36.8 ft	36.8 ft
L2	19.8 ft	19.8 ft
L3 (Basic)	13.2 ft	13.2 ft
R1	1.0 in	10.0 ft
R2	0.5 in	5.0 ft
R3	0.1875 in	1.65 ft

the flow conditioning elements that is used in the analysis. Since the analysis represents only area reductions at the locations of these elements, each element in the analysis can be physically described as a washer. Thus, the first of the three flow conditioning sections was constructed by installing washers, of inner radii equivalent to the area reductions calculated, in the locations where screens would normally be placed. The grid and honeycomb have very large porosity, therefore large equivalent radii, and were not modeled in this flow conditioning section.

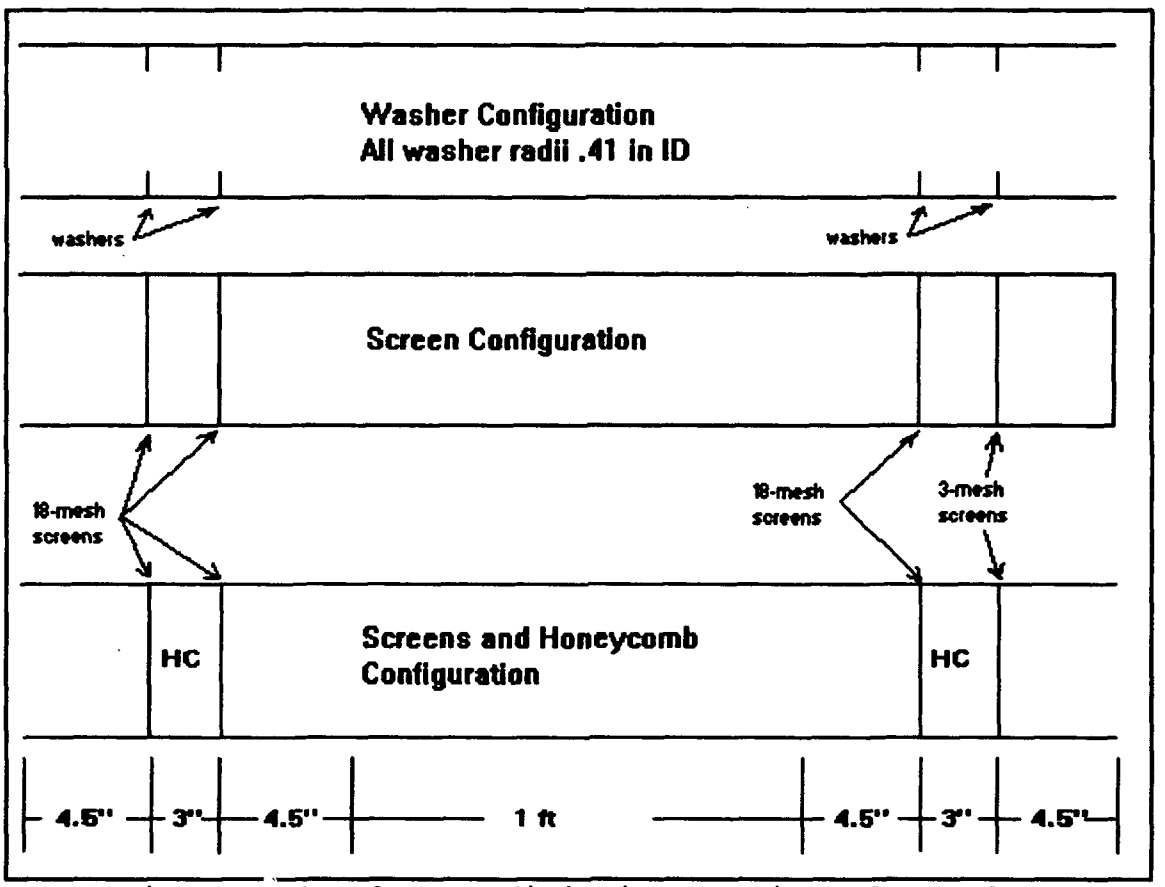

Figure 3.4. Flow Conditioning Sections for Model

The second flow conditioning section constructed (middle, Figure 3.4) is closely related to the first in that only the screens are modeled. Here, the washers are not present; instead, screens identical to the screens in the CRF are installed in the locations where the washers are installed for the first flow conditioning section model. Data taken with this section can be compared to data with the washer section to determine if the area reduction technique properly models the screens.

The third flow conditioning section (bottom, Figure 3.4) contains both screens and honeycomb in the locations where they are installed in the full-scale CRF. This model represents the most realistic configuration of the CRF and is used primarily to verify the analytical results for the response of the full-scale facility.

3.4.3 Pressure Equalization Pipe. The pressure equalization pipe is included in the model by branching a 0.25 in diameter line off of the inlet of section 1. Note that the diameter is scaled 1:120 from the full-scale value of 2.5 ft. The length, as with the other sections of the model, is not scaled.

The inlet to the pressure equalization pipe is located 0.33 in downstream of the inlet of the model and is detachable so the effect of its presence on the model response can be

assessed. Except the difference in radii, the analytical representation for the model pressure equalization pipe is identical to the analytical representation of the full-scale pressure equalization pipe.

3.4.4 Model Inlet and Exit. The inlet of the model is designed to represent the five butterfly valves. There are five input ports for accepting either the sinusoidal signal or throughfl w. The different valve sizes of the CRF inlet are not represented. Instead, the inner diameter of all ports is 0.25 in. The ports are installed in a 2 in diameter pipe with the relative spacing about the centerline equivalent to the relative spacing of the valves in the CRF inlet.

The physical exit of the model is slightly different from the analytical representation of the full-scale CRF exit. Where the CRF exit is analytically modeled as a smooth contraction to the compressor face, the laboratory model is physically terminated with a sharp contraction to the end radius. Flow through the model is exhausted to the atmosphere through the exit line; whereas, the analytical representation of the full-scale CRF exit does not assume the flow returns to atmospheric conditions.

The 1.0 in long end termination of the model is very short in length when compared to the rest of the model and is referred to as an orifice-terminated line. This type of

termination requires a different calculation for the loss coefficient than is required for the full-scale analysis. Whereas for the full-scale analysis, K_L was 0.05 for all end radius conditions, the model K_L depends highly on the radius of the termination since the flow returns to atmospheric conditions at the exit. For the model, then, the following equation, given by Kirshner and Katz (1975:15-31), applies for the loss coefficient in Equation (2-15):

$$K_L = 1.5 - \frac{R_c}{R3} + \left(\frac{R_c}{R3}\right)^4 + \frac{f}{24\ R3} \quad . \tag{3-4}$$

In Equation (3-4), f is the Darcy friction factor defined for laminar pipe flow as (Gerhart and Gross, 1985:422):

$$f_{laminar} = \frac{64}{Re_D} \tag{3-5}$$

and for turbulent pipe flow as:

$$f_{turbulent} = \frac{0.316}{(Re_D)^{.25}} \quad . \tag{3-6}$$

However, only the real part of end impedance is modeled using Equation (2-15). Recall from Chapter II that inductance, Equation (2-16), should be included when the line length is short. For the model, the terminating line is short, but finite, and the inductance is included as the imaginary part in the end impedance.

Several end radii are studied with the model. Under the open condition, the end radius is equal to R3 (0.1875 in).

For the blocked condition, the end radius is zero. All other end terminations are between the blocked and open conditions. These other radii are ¼R3 (0.04689 in), ½R3 (0.09375 in) and ¾R3 (0.141 in).

IV. Experimental Apparatus and Procedure

4.1 Introduction

This chapter is divided into two main parts. First, the experimental apparatus and procedure are described for the frequency response tests. Second, the transient response test set-up and procedure are discussed. Details on equipment specifications, such as manufacturer, model, and serial numbers, are available in Appendix C.

4.2 Frequency Response Set-Up and Procedures.

The end goal of the frequency response tests is to determine the gain and phase shift of an input signal at various locations along the line. Figure 4.1 is an overall schematic of the experimental apparatus used to accomplish these goals.

Figure 4.1 shows that pressurized air (house air) is fed to a pneumatic signal generator that produces a sinusoidal pressure wave. The sinusoidal wave is fed through one of the five input ports at the model inlet and allowed to traverse the length of the model. At four locations along the model length, the input signal is sensed by dynamic pressure transducers (PS, PR2, PR3, and PR4). The signals from these transducers are amplified and fed to a digital data acquisition system. The acquisition system is connected to

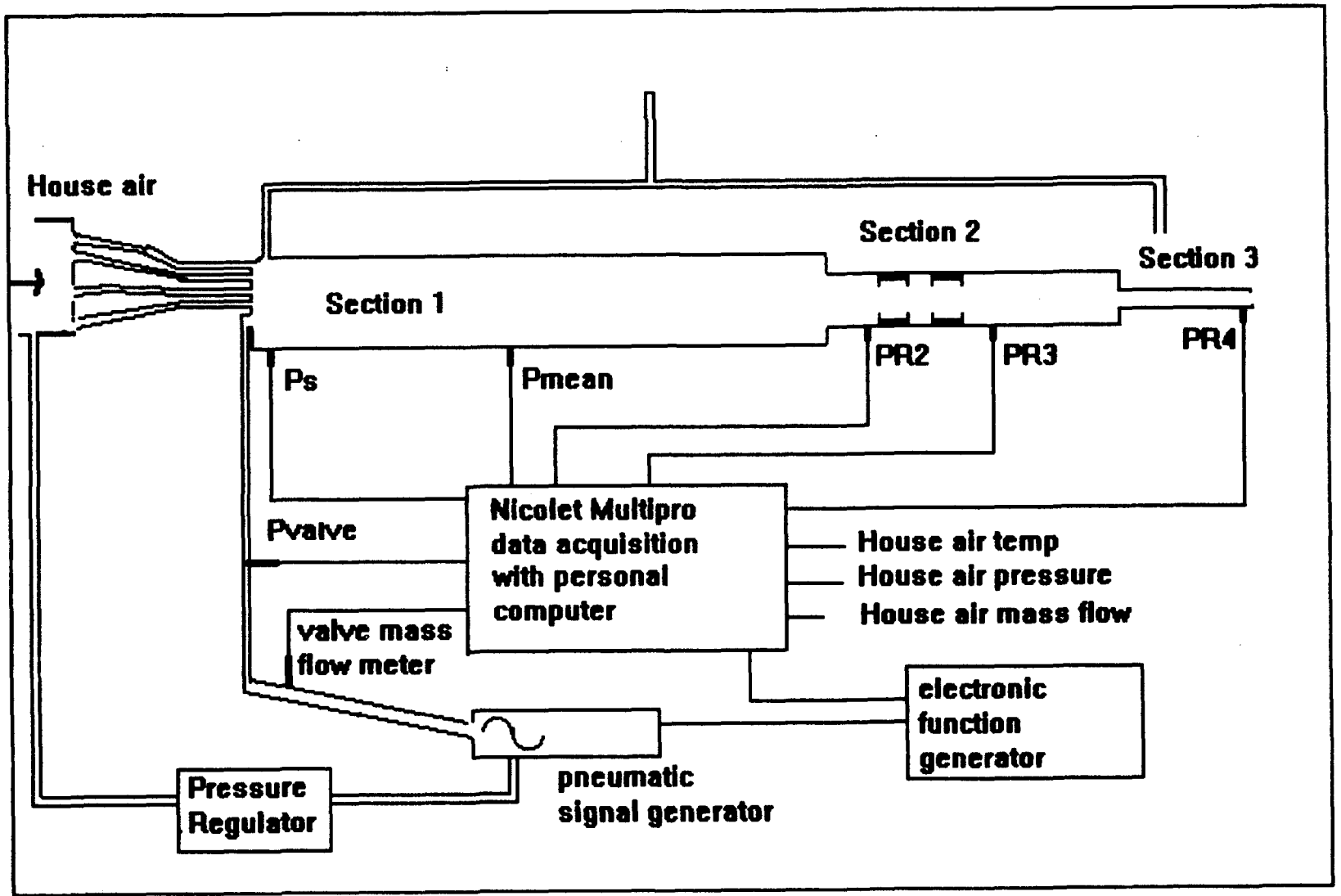

Figure 4.1. Experimental Apparatus

a personal computer that displays the signals and allows manipulation of the digital data. The manipulated data give amplitude and phase shift information for the pressure data collected at each transducer location along the line. The data are recorded and the gain and phase shift, relative to the inlet transducer, are computed.

Two types of experiments were conducted to determine the frequency response of the model. The first type is termed "no throughflow", indicating that the mass flow in the model is provided entirely by the pneumatic signal generator. In the no throughflow experiments, the signal was supplied to one inlet port and the rest of the ports were blocked. These experiments were conducted to gather baseline data so the effect of throughflow, end impedance, and the flow conditioning elements could be determined.

The second type of experiment is termed "with throughflow" and indicates that mass flow was provided by both the pneumatic signal generator and steady state throughflow. For the experiments with throughflow, all the input ports accepted flow; one accepted the pneumatic signal and the other four accept throughflow from the house air supply. These experiments were conducted to find the frequency response of the model under conditions similar to the flow conditions in the CRF.

4.2.1 House Air, Mass Flow, and Pressure Regulation. The house air is maintained at 100 psig by a large compressor. This is the air supplied to both the pneumatic signal generator and the model inlet.

The steady throughflow and alternating flow from the pneumatic signal generator parallel each other prior to entering the inlet of the model. As such, the pneumatic signal generator has its own mass flow meter and pressure regulating valve. The throughflow has a separate mass flow detector and pressure regulating valve (not shown in Figure 4.1).

The mass flow meter for the pneumatic signal generator flow is an electronic device that uses temperature measurements to calculate the flow rate with a high degree of accuracy. The mass flow for throughflow is determined from transducer readings on either side of an orifice plate using the following equation (Gerhart and Gross, 1985:486):

$$Q = C_D A_o \left(\frac{\Delta P}{\rho}\right) \qquad (4\text{-}1)$$

where C_D is the discharge coefficient for the orifice and ΔP is the pressure drop across the orifice plate.

Two regulating valves, one upstream of the pneumatic signal generator and another for throughflow control, are used to control the input pressure levels to well below 100 psig. The valve typically produces a small signal, on the order of

5 X 10^{-3} psig (peak-to-peak) in section 1. For experiments with throughflow, the alternating signal from the pneumatic signal generator is introduced along with throughflow. The amplitude of the alternating pressure signal remains on the order of 5 X 10^{-3} psig (peak-to-peak) but the steady pressure is increased from 0.0 psig (no throughflow) to around 5 psig in section 1.

4.2.2 Pneumatic Signal Generator. The pneumatic signal generator uses high voltage applied to a piezoelectric disk to produce a waveform. The waveform shape and frequency are determined by input from an electronic function generator. The pneumatic signal generator is capable of producing sinusoidal, triangular, and square waves at frequencies as high as 1000 Hz. For this study, only sinusoidal input signals below 113 Hz were produced.

These waveforms are fairly noisy below about 80 Hz. Above 80 Hz, the valve produces much cleaner signals. Figures 4.2a and 4.2b illustrate the waveform from the valve at 6.3 Hz and 93 Hz.

The input waveform is important because this is the signal that traverses the model and is to be sensed by the pressure transducers. If the signal has poor characteristics to begin with, it is probable that the same signal will be difficult to detect at the end of the model.

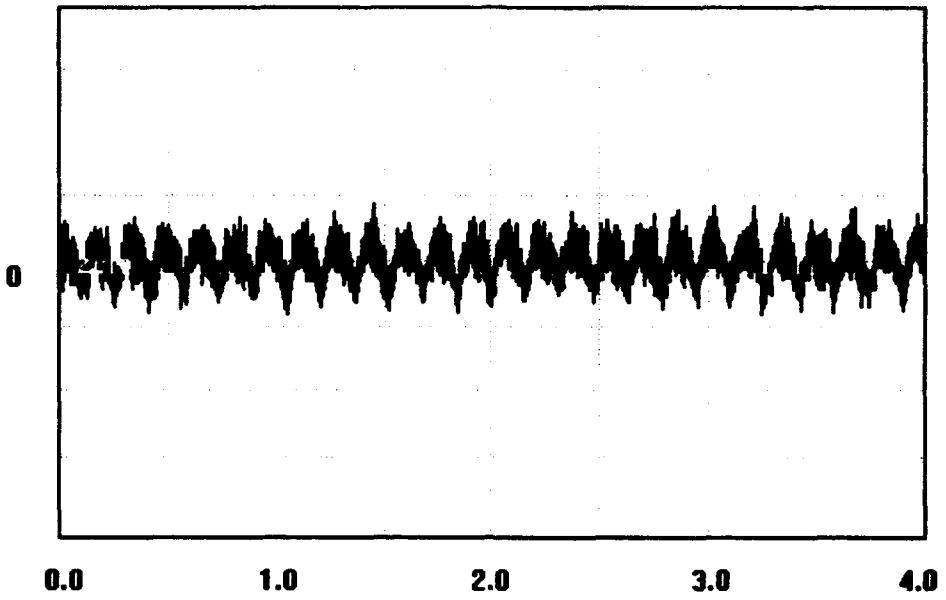

Figure 4.2a. Valve Waveform at 6.3 Hz

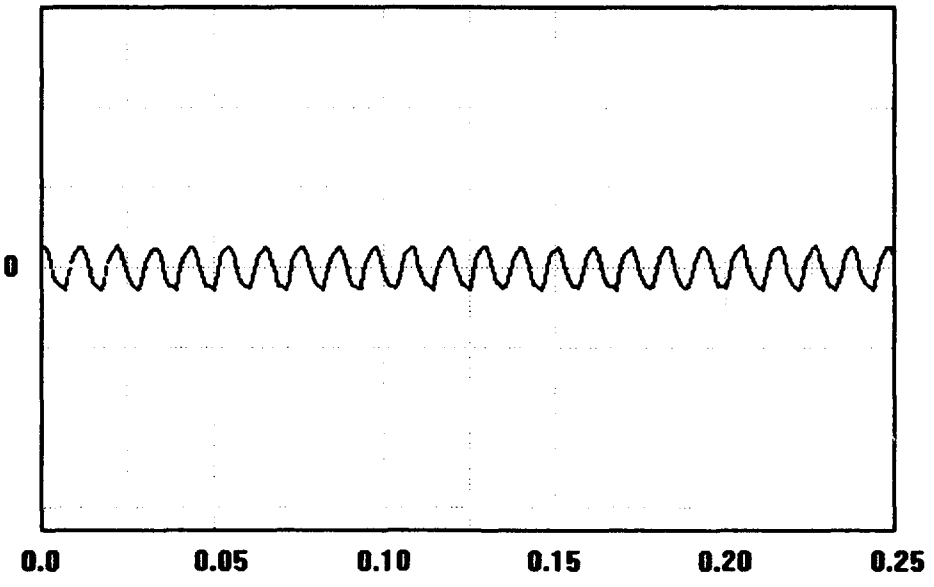

Figure 4.2b. Valve Waveform at 93 Hz

4.2.3 Transducers. Five transducers are located along the length of the model. Figure 4.3 is a schematic of the locations of the five transducers.

All of the transducers in the model are capable of sensing dynamic signals. Each has a differential pressure port that can be attached to a steady state pressure port in the line and remove the mean pressure signal. PS, PR2, PR3, and PR4 are the main sensors, set up with differential pressure to sense the unsteady flow only. The mean pressure transducer is not used as a dynamic sensor. Instead, for this transducer, the differential pressure port is open to atmosphere and the mean gage pressure in section 1 is sensed. The mean gage pressures in sections 2 and 3 are calculated based on the section 1 mean gage pressure and friction losses through the model.

The resonant frequency of the dynamic transducers used is 85 KHz (before installation), well above the highest pressure input frequency of 112 Hz. These transducers have a 5 psig range and output voltages, after amplification, between 0 and 6 volts.

The transducers are extremely accurate and are able to detect very low amplitude signals. After amplification, most signals detected during model testing were in the millivolt and microvolt range. These voltages correspond to pressure

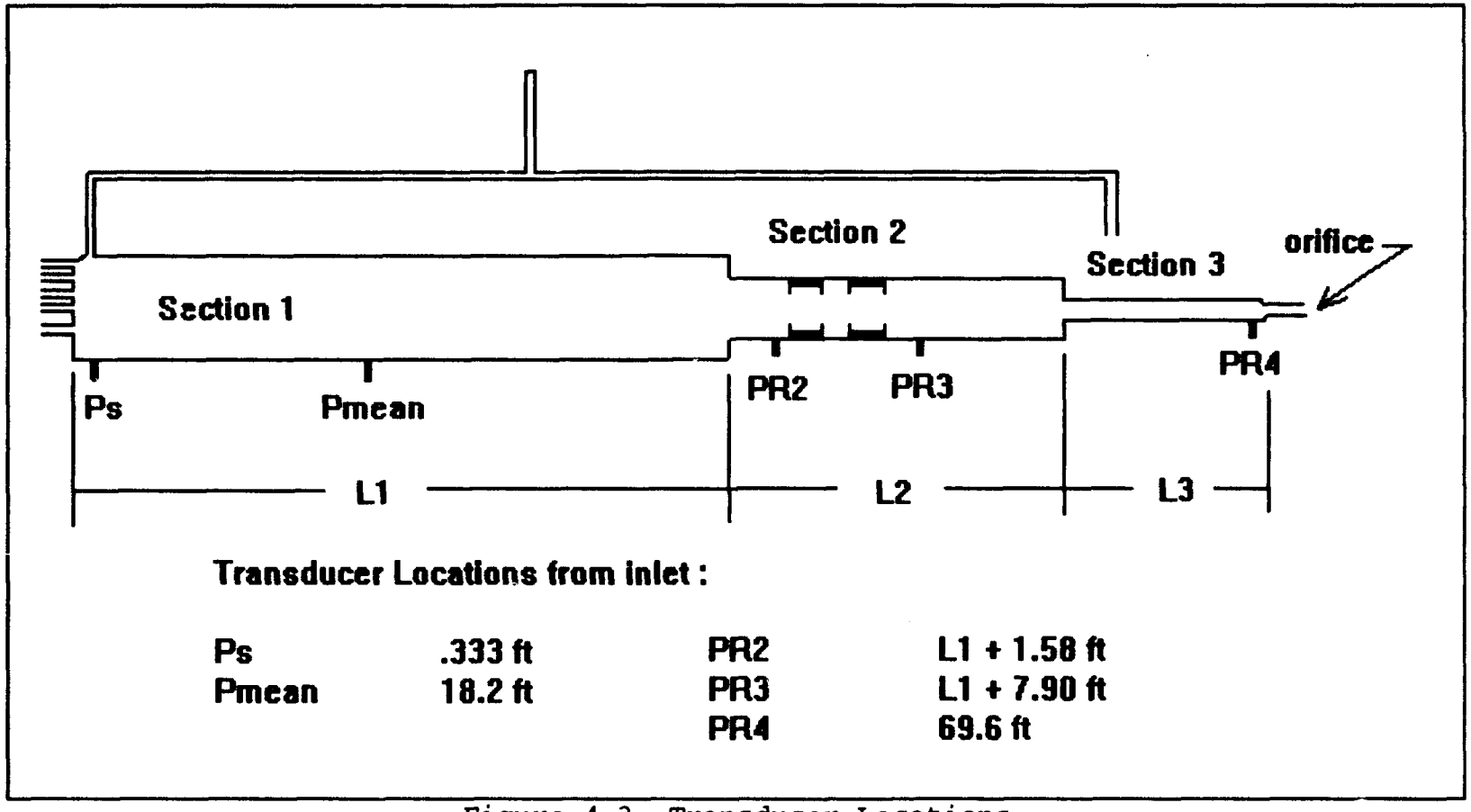

Figure 4.3. Transducer Locations

amplitudes between 0.02 psig for millivolt signals and 5 X 10^{-5} psig for microvolt signals.

Figures 4.4a and 4.4b illustrate the shape of the pressure signals at the transducer locations PS, PR2, PR3, and PR4 for the 6.3 Hz and 93 Hz input signals, respectively. The figures show that the input signals of Figures 4.2a and 4.2b are transmitted down the model and detected by all of the transducers. In Figure 4.4a, for the 6.3 Hz signal, the signal amplitude and shape are not as clearly defined as in Figure 4.4b. This is a result of the input signal at 6.3 Hz (Figure 4.2a) containing more noise than at the higher frequency of 93 Hz (Figure 4.2b).

4.2.4 Data Acquisition System. The system used for data acquisition is a 16 channel unit with 12-bit resolution. Each channel is referred to the same internal clock and therefore, all channels acquire data simultaneously. The data acquisition system includes a personal computer with software that allows manipulation of the dynamic signals.

Pressure levels and phase shift are easily determined using the spectral analysis software program (Nicolet, 1991:19-11,19-12) provided by the data acquisition system manufacturer. This program converts time domain data to the frequency domain.

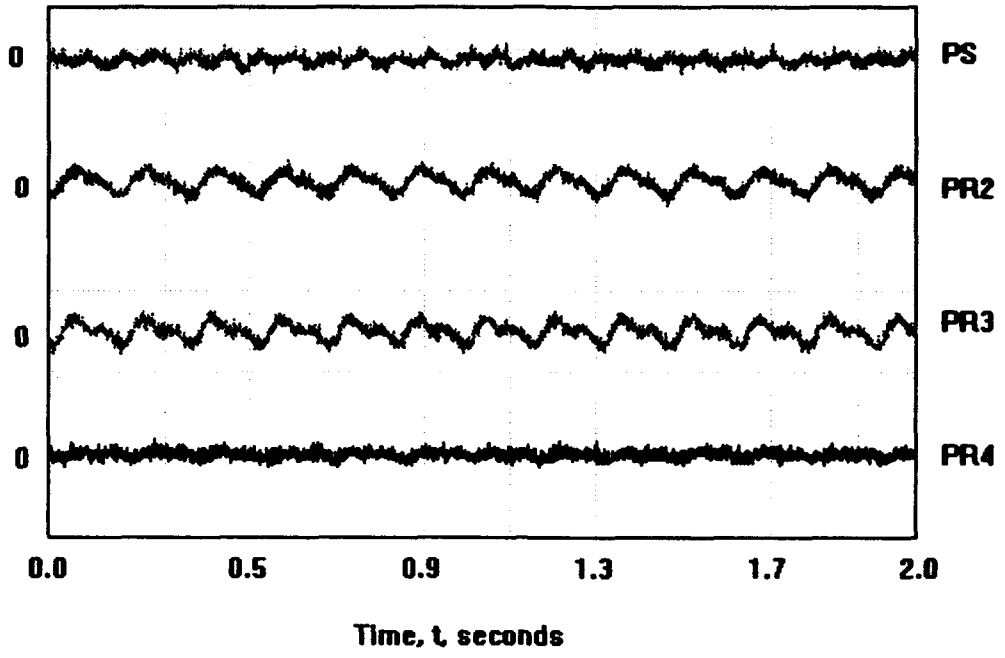

Figure 4.4a. Transducer Signals at 6.3 Hz

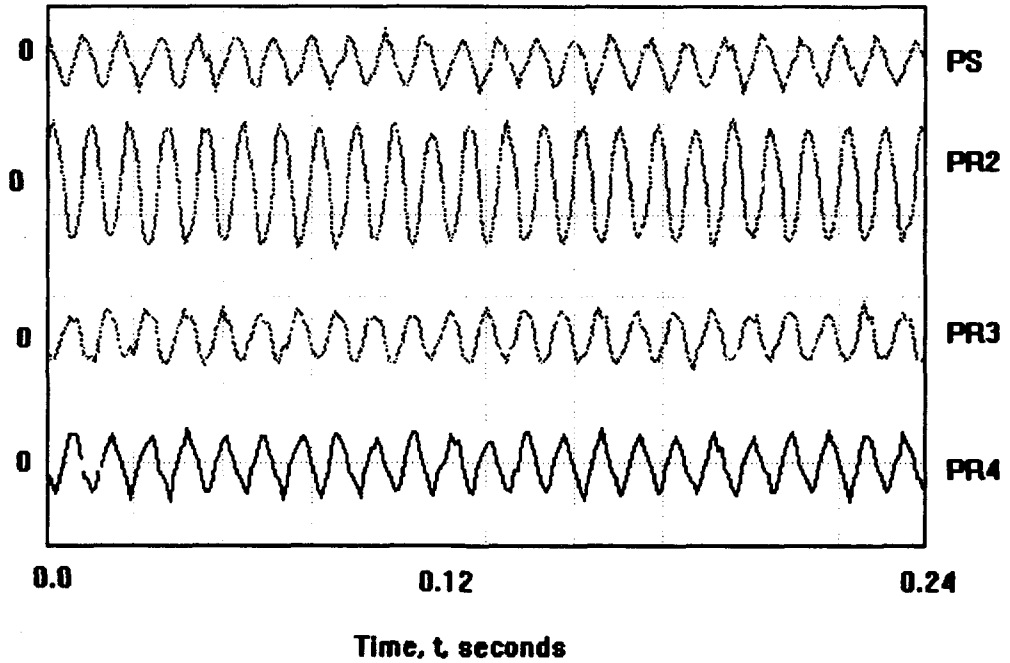

Figure 4.4b. Transducer Signals at 93 Hz

Figures 4.5a and 4.5b illustrate the amplitude of the 6.3 Hz and 93 Hz signals presented in Figure 4.4 after spectral analysis has been performed. Due to the input signal having more noise in the low frequency case (Figure 4.5a), the amplitude of the frequency domain "spike" is lower for the 6.3 Hz signal.

For the frequency response experiments, the sampling frequency was kept constant at 1 KHz, well above the 214 Hz aliasing frequency. Each sampling required approximately 3 seconds to gather 4000 points per channel. Primarily, these values were determined by trial and error, chosen because the data acquisition time was minimized without losing clarity of the signal.

4.2.5 Frequency Data Acquisition Procedure. Prior to running the first test of the day, the equipment was turned on and allowed to warm up for one hour. After warm-up, the individual test procedure began with recording the ambient conditions, configuring the data acquisition system, and setting up the model geometry.

Testing began by applying pressure to the pneumatic signal generator, applying steady inlet flow for test conditions requiring throughflow, setting a frequency on the electronic function generator, and allowing the system to

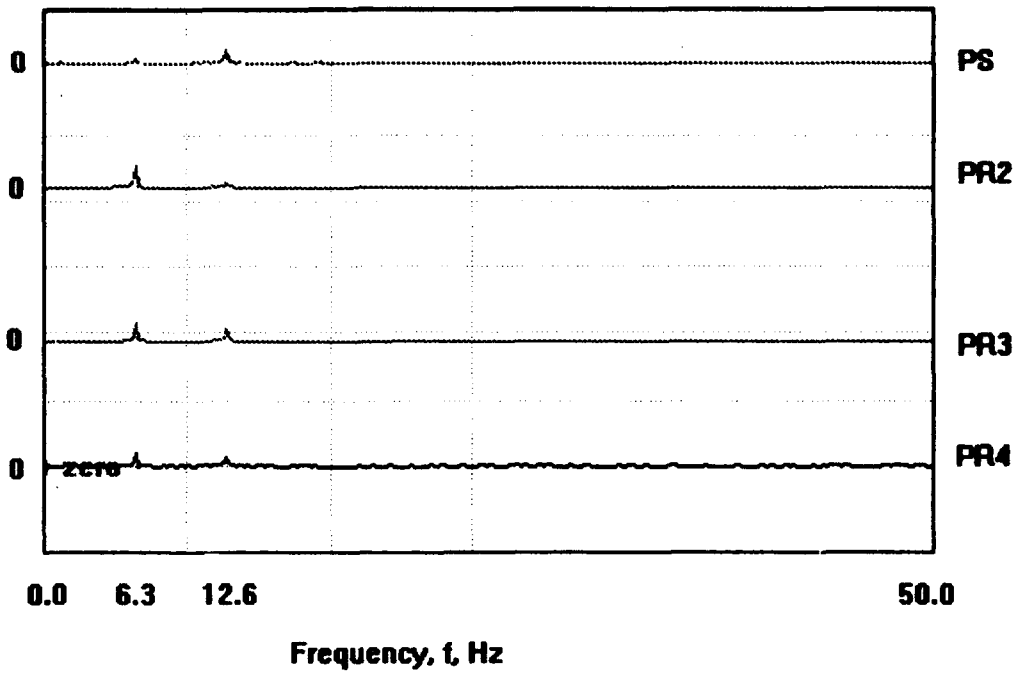

Figure 4.5a. 6.3 Hz Transducer Signals After Spectral Analysis

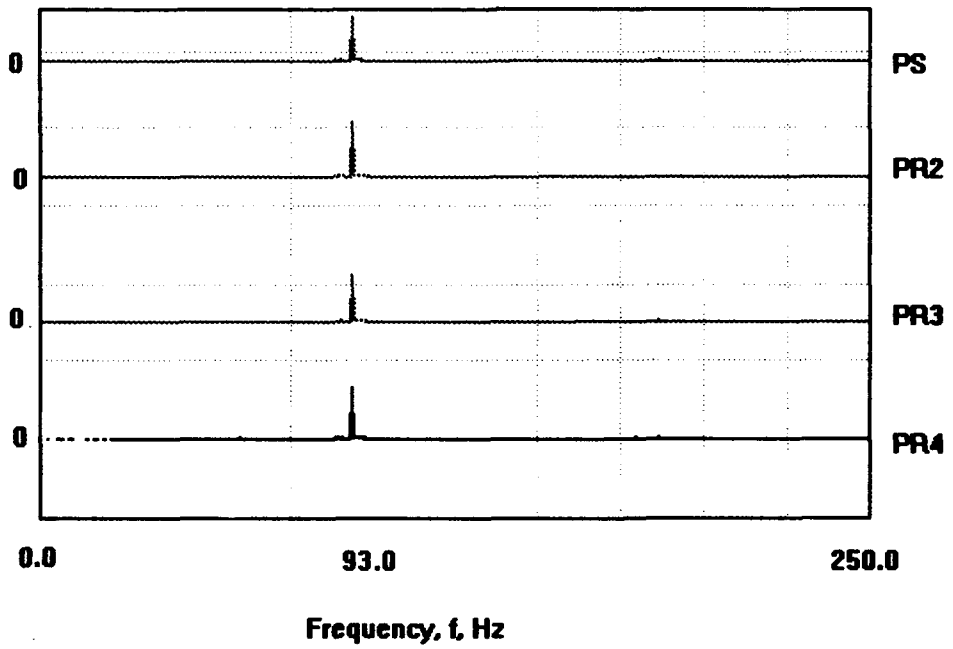

Figure 4.5b. 93 Hz Transducer Signals After Spectral Analysis

settle for a few seconds. When the system settled, the data acquisition system was commanded to take readings.

Once the data was acquired, mass flows and mean pressures were recorded. The dynamic signals for PS, PR2, PR3, and PR4 were transformed to the frequency domain using the spectral analysis program and the amplitude and phase shift of each transducer signal was recorded. A different frequency was set on the electronic function generator, the system allowed to settle, and the process repeated by commanding the acquisition system to acquire data.

4.3 Transient Experimental Set-Up and Procedures.

The transient tests were performed using a solenoid valve in place of the pneumatic signal generator. The procedures were the same as with the frequency experiments with the exception of the actual data acquisition.

In the transient tests with positive step inputs, the system was maintained at atmospheric pressure until the valve was opened. The acquisition system was triggered just prior to opening the valve.

Once the valve opened, the acquisition system acquired data for approximately 15 seconds. After the data acquisition was complete, the valve was closed. For these tests the sampling frequency was 4.35 KHz with 65,000 data points acquired per channel.

For negative step experiments, the solenoid valve was opened and the model allowed approximately one minute to reach steady state pressure. Just prior to closing the valve, the data acquisition system was triggered. The valve was closed and data acquired for 15 seconds at 4.35 KHz.

V. Computer Program

5.1 Introduction

The program calculates gain and phase at discrete frequencies by stepping through the valid frequency range in large increments. After the entire range is swept, the resonant frequencies are determined. The program then restarts the sweep, iterating around these frequencies in small increments.

5.2 Inputs and Output

The program accepts several inputs and produces multiple output variables. The inputs include geometry variables, ambient conditions, and mass flow rate.

The output is contained in several arrays. Each array contains either the gain or phase shift at a specified location in the line for the discrete frequencies in which the equations are solved.

Ambient conditions are used, along with mass flow rate and geometry, to solve for velocities and pressure drops in the line. The velocities in each section are calculated through:

$$V = \frac{\dot{m}}{\rho A} \qquad (5\text{-}1)$$

and the static pressure through Bernoulli's equation for incompressible flow:

$$P_s = P_{tot} - \frac{\rho V^2}{2} - \Delta P \quad . \qquad (5\text{-}2)$$

In Equation (5-2), ΔP is (Gerhart and Gross, 1985:415):

$$\Delta P = \frac{\rho V^2}{2}\left(f \frac{L}{D}\right) \qquad (5\text{-}3)$$

for a smooth-walled pipe of diameter,D, and length, L, where f is defined in Equation (3-5) for laminar flow and Equation (3-6) for turbulent flow. Through the flow conditioning elements, ΔP is calculated using equations developed by Luchuck and Prickett (1984:10,20):

$$\Delta P = \frac{\rho V^2}{2}(2.541 - 2.837\beta) \qquad (5\text{-}4)$$

where, for a screen and honeycomb set, β is the product of the porosities of the individual elements. For the CRF flow conditioning elements, $\beta = 0.06$.

The speed of sound is calculated as:

$$a = [\gamma R_{air} T]^{1/2} \qquad (5\text{-}5)$$

and the Mach number follows as:

$$M = \frac{V}{a} \quad . \qquad (5\text{-}6)$$

The Mach number is used in the equations for characteristic impedance (2-17), propagation operator (2-18), and line gain (2-19).

5.3 Program Limitations

The program is restricted both by theory and by the programming language. The range of frequencies calculated is limited to below 113 Hz, due to the restrictions on theory presented in Equation (3-2).

For small arguments, the programming language, MATLAB™, will compute the Bessel functions in the equations for impedance (2-7) and admittance (2-8). These intrinsic functions work well for the solution of the scaled laboratory model; however, due to the round-off errors associated with the CRF dimensions, these functions do not yield an answer for the full-scale solution. When full-scale dimensions are entered, the program uses an algebraic approximation devised by F.T. Brown (Kirshner and Katz, 1975:83) to solve for Z and Y. Although the intrinsic functions are used when possible, the approximation is generally twice as fast and nearly as accurate as the intrinsic functions.

5.4 Program Verification

A wealth of data already exist on fluid transmission lines as a result of previous work. These data are well established and were used to verify the program. Table 5.1 lists the conditions of verification and sources used to validate the output from this computer program. All of the configurations were tested using both the intrinsic Bessel functions and Brown's approximation. Although the data is not presented here, the results of Runs 1.1 through 1.6 in Table 5.1 showed that this computer program yields the same solution as presented in the sources, regardless of the calculation method used for the Bessel functions.

Additional program verification was accomplished using the laboratory model of the CRF. In Chapter VII, the results from the model tests are reviewed in light of the analytical results obtained for the full-scale CRF. First, the full-scale results obtained from several runs of the computer program are presented in the next chapter.

Table 5.1. Verification Matrix for Computer Program

Computer Run Number	Configuration Tested	Compared against published data
1.1	Attenuation	Karam and Franke, 1967:375
1.2	Volume Terminated	Franke et al., 1969:413
1.3	Cascaded	Franke, Karam, and Lymburner, 1970:9
1.4	Branched	Franke, Malanowski, and Martin, 1972:18
1.5	Orifice-terminated	Franke, Karam, and Lymburner, 1970:12
1.6	Mean flow	Franke, Karam, and Lymburner, 1970:12

VI. Full Scale CRF Results

6.1 Introduction

In this chapter, the results from several computer runs are presented for the full-scale facility. Several flow and geometry configurations are investigated and the relative importance of each are discussed.

All of the results presented in this chapter are for the full-scale facility with the flow straighteners and pressure equalization pipe. The lengths of sections 1 and 3 are varied, as are the mass flow rates and compressor radius.

6.2 Tabulated Results

Tables 6.1, 6.2, and 6.3 give the results of 63 computer runs for varied configurations of the facility. Each table represents specific length geometry. The basic length configuration is represented in Table 6.1, the intermediate length configuration in Table 6.2, and the extended length configuration in Table 6.3. For all runs, the ambient pressure is 14.3 psig and the ambient temperature is 72 °F, resulting in the same speed of sound for all cases.

In the tables, the end impedance is calculated through Equation (2-15) except for the no throughflow runs (8.18 - 8.21, 9.18 - 9.21, and 10.18 - 10.21). In the no throughflow runs, the end termination is artificially assigned a unit

Table 6.1. CRF Basic Length Results**

Run	Compressor (Exit) Radius*	Mass Flow Rate lbm/s	Fundamental frequency Hz	Fundamental Peak Amplitude dB	End Impedance $lbf \cdot s/ft^5$
8.1	0	0	6.5	70.9	∞
8.2	¼R3	20	6.8	24.4	0.0869
8.3	¼R3	100	6.6	31.5	0.4374
8.4	¼R3	180	6.5	36.2	0.7874
8.5	¼R3	250	6.5	39.2	1.0936
8.6	½R3	20	6.9	22.3	0.0055
8.7	½R3	100	6.9	23.7	0.0273
8.8	½R3	180	6.9	24.0	0.0492
8.9	½R3	250	6.9	24.3	0.0683
8.10	¾R3	20	6.9	18.2	0.0011
8.11	¾R3	100	6.9	22.6	0.0054
8.12	¾R3	180	6.9	23.6	0.0097
8.13	¾R3	250	6.9	24.3	0.0135
8.14	R3	20	6.9	12.1	3.4×10^{-4}
8.15	R3	100	6.9	20.0	0.0017
8.16	R3	180	6.9	22.0	0.0031
8.17	R3	250	6.9	23.3	0.0043
8.18	¼R3	0	6.7	62.0	$0.0012 + 0.1870j$
8.19	½R3	0	6.8	55.3	$0.0002 + 0.0466j$
8.20	¾R3	0	6.9	49.5	$4.6 \times 10^{-5} + 0.021j$
8.21	R3	0	6.9	44.7	$2.1 \times 10^{-5} + 0.013j$

**L1 = 36.8 ft, L2 = 19.8 ft, L3 = 13.2 ft
*R3 = 1.65 ft

Table 6.2. CRF Intermediate Length Results**

Run	Compressor (Exit) Radius*	Mass Flow Rate lbm/s	Fundamental frequency Hz	Fundamental Peak Amplitude dB	End Impedance $lbf \cdot s/ft^5$
9.1	0	0	6.0	68.8	∞
9.2	¼R3	20	6.3	22.5	0.0869
9.3	¼R3	100	6.0	32.3	0.4374
9.4	¼R3	180	6.0	37.4	0.7874
9.5	¼R3	250	6.0	40.5	1.0936
9.6	½R3	20	6.4	20.1	0.0055
9.7	½R3	100	6.4	20.9	0.0273
9.8	½R3	180	6.4	21.4	0.0492
9.9	½R3	250	6.3	21.9	0.0683
9.10	¾R3	20	6.4	17.4	0.0011
9.11	¾R3	100	6.4	20.3	0.0054
9.12	¾R3	180	6.4	20.9	0.0097
9.13	¾R3	250	6.4	21.2	0.0135
9.14	R3	20	6.4	12.7	3.4×10^{-4}
9.15	R3	100	6.4	18.7	0.0017
9.16	R3	180	6.4	20.1	0.0031
9.17	R3	250	6.4	21.2	0.0043
9.18	¼R3	0	6.2	61.9	$0.0012 + 0.1870j$
9.19	½R3	0	6.3	56.1	$0.0002 + 0.0466j$
9.20	¾R3	0	6 4	50.6	$4.6 \times 10^{-5} + 0.021j$
9.21	R3	0	6.4	46.3	$2.1 \times 10^{-5} + 0.013j$

**L1 = 41.3 ft, L2 = 19.8 ft, L3 = 8.7 ft
*R3 = 1.65 ft

Table 6.3. CRF Extended Length Results**

Run	Compressor (Exit) Radius*	Mass Flow Rate lbm/s	Fundamental frequency Hz	Fundamental Peak Amplitude dB	End Impedance $lbf \cdot s/ft^5$
10.1	0	0	5.5	69.2	∞
10.2	¼R3	20	5.6	21.9	0.0869
10.3	¼R3	100	5.5	34.7	0.4374
10.4	¼R3	180	5.6	32.4	0.7874
10.5	¼R3	250	5.5	43.3	1.0936
10.6	½R3	20	6.1	16.1	0.0055
10.7	½R3	100	6.0	17.2	0.0273
10.8	½R3	180	5.9	18.0	0.0492
10.9	½R3	250	5.7	20.4	0.0683
10.10	¾R3	20	6.1	15.1	0.0011
10.11	¾R3	100	6.1	16.1	0.0054
10.12	¾R3	180	6.1	16.4	0.0097
10.13	¾R3	250	6.1	16.5	0.0135
10.14	R3	20	6.1	12.7	3.4×10^{-4}
10.15	R3	100	6.1	15.5	0.0017
10.16	R3	180	6.1	16.2	0.0031
10.17	R3	250	6.1	16.6	0.0043
10.18	¼R3	0	5.7	61.6	$0.0012 + .1870j$
10.19	½R3	0	5.9	57.4	$0.0002 + .0466j$
10.20	¾R3	0	6.0	52.8	$4.6 \times 10^{-5} + 0.021j$
10.21	R3	0	6.1	49.0	$2.1 \times 10^{-5} + 0.013j$

*R3 = 1.65 ft
** L1 = 45.8 ft, L2 = 19.8 ft, L3 = 4.2 ft

length of 1.0 ft and the end impedance is calculated as the input impedance of the 1.0 ft line using Equation (2-20). These runs required this end impedance calculation because the zero mass flow rate condition forces $Z_L = 0$ in Equation (2-15), causing the solution to be undefined when Equation (2-15) is used.

6.2.1 Fundamental Frequency. The most notable difference between the three tables is the different fundamental frequencies for each length configuration. Specifically, note that the frequency varies from a low of 5.5 Hz (run 10.1, Table 6.3) to a high of 6.9 Hz (run 8.6 - 8.17, 8.20, 8.21, Table 6.1) depending on the length configuration and the end impedance.

6.2.2 Length Configuration Dependence. For all mass flow and end impedance conditions, the extended configuration yields the lowest fundamental frequencies. For the blocked cases (runs 8.1, 9.1, and 10.1), the frequency drops by 0.5 Hz from the basic to the intermediate configuration and by another 0.5 Hz from the intermediate to the extended configuration. The lowest drop in fundamental frequency is noted at the more open conditions where the compressor radius is equal to or larger than ½R3. Under these conditions, the frequency drops 0.5 Hz from the basic to intermediate length

configuration and 0.3 Hz from the intermediate to extended configuration.

In all cases, the fundamental frequency is lowest when L1 is maximized at 45.8 ft. As a check on these results, consider the basic pipe resonance equations [(2-1) and (2-2)]. Recall that for the simple lines represented in Equations (2-1) and (2-2), longer lines have lower fundamental frequencies, provided the speed of sound is constant. This is in accordance to what is found by comparing data in the tables. Although the overall length is constant at 69.8 ft, L1 drives the frequency low when it is maximized, similar to the basic pipe where the long pipe drives the fundamental frequency low.

The reason for this dependence on L1 and L3 is that the input signal partially reflects off of the junction between sections 1 and 2, where an impedance mismatch occurs. The impedance mismatch, caused by the different diameters of sections 1 and 2, is located a different distance from the inlet for the three cases. Signals have farther to travel in the intermediate and extended configurations before partial reflection, resulting in lower fundamental frequencies.

6.2.3 End Impedance Dependence. In general, higher end impedance (a small compressor and/or a high flow rate) results in lower fundamental frequencies. This is expected from the basic pipe resonance equations [(2-1) and (2-2)], where the

blocked (infinitely large end impedance) fundamental frequency is one half of the open (zero end impedance) fundamental frequency.

From Tables 6.1, 6.2, and 6.3, it is clear that the end impedance is higher for small compressors and high mass flow rates, as would be expected from Equation (2-15). In fact, for the ¼R3 cases (Runs 8.2-8.5, 9.2-9.5, 10.2-10.5), the combination of a small compressor and high flow rates causes the fundamental frequency to approach that of the blocked line (Runs 8.1, 9.1, and 10.1). The result of the high end impedance is the fundamental frequency is low, close to the frequencies found for the blocked line cases.

Comparing the unblocked, no throughflow cases (8.18 - 8.21, 9.18 - 9.21, 10.18 - 10.21) with the blocked line response (8.1, 9.1, 10.1), it is evident that increasing the end radius from zero changes the fundamental frequency. This is due to the fact that for the blocked line the portion of the input signal that propagates to the end is reflected entirely. For partially or fully open ends; however, only a portion of the signal is reflected at the exit. Part of the signal propagates through the opening and exits the line. This effectively changes the transmission line characteristics and the result, for the no throughflow conditions, is a change in fundamental frequency from the blocked line case.

With throughflow in the line, wave propagation is again affected, now due to the interaction of the throughflow velocities with the propagating signal. These interactions cause changes in the characteristics of the line without throughflow (Katz, Housner, and Eisenberg: 1972, 272), resulting in different resonant frequencies for the cases with throughflow. Runs with throughflow (8.2 - 8.17, 9.2 - 9.17, 10.2 - 10.17) can be compared to runs without throughflow (8.18 - 8.21, 9.18 - 9.21, 10.18 - 10.21) to illustrate this effect. For the higher mass flow rate runs where $\dot{m} \geq 180$ lbm/s, the throughflow velocity in section 3 can be significant compared to the speed of sound. At high flow rates, velocities at the compressor face can be as high as 500 ft/s ($M \approx 0.5$). These high velocities affect the propagation of the acoustic signal by altering the velocity of the wave. Waves propagating in the direction of throughflow travel at the speed of sound plus throughflow velocity; whereas, waves propagating against the throughflow direction have a velocity of the speed of sound minus the throughflow velocity. Because of the different velocities, the interaction between the waves propagating in the two directions is different than when no throughflow conditions exist.

6.2.4 Fundamental Peaks. The amplitude of the fundamental peaks is highest for high end impedance because

most of the waves are reflected at the end and not allowed to propagate out of the line. For example, note that for all of the blocked conditions (Runs 8.1, 9.1, and 10.1) the fundamental peak is quite large, around 70 dB. These high peaks are a result of the large radius and blocked end. Additional details on peak levels are available in Appendix B.

For the fully open cases with no mass flow (8.21, 9.21, and 10.21), the fundamental peak drops to just above half the decibel level of the blocked cases. The primary reason for this drop in amplitude is that the open condition provides very low impedance. Much of the signal is propagated out of the line, leaving little to be reflected.

In cases with throughflow, the amplitudes of the fundamental peaks are reduced not just below the blocked condition, but also below the open condition (Runs 8.14 - 8.17, 9.14 - 9.17, and 10.14 - 10.17). The peaks are highest for high mass flows and small compressor radii. This indicates that throughflow velocities, when added to the speed of the propagating waves, aids the signals in propagating out of the system; thereby reducing the gains.

6.3 Graphical Results

Six figures are presented and analyzed in this section for the valid frequency range. The solution for the entire

frequency spectrum is presented for the blocked line response of the basic, intermediate, and extended length configurations. Further, three plots, with the compressor radius fixed at ½R3, are presented for a single mass flow rate and varied length configurations.

The graphs present the overall gain and the phase shift of the signal at the end of the CRF as a function of frequency. The phase shift was forced to limits of ± 180° by using an intrinsic function in MATLAB™.

6.3.1 Blocked Line Results. Figures 6.1 through 6.3 illustrate the blocked line response for the basic, intermediate, and extended length configurations, respectively. These curves represent hypothetical situations because, with a compressor installed and under testing, the facility is definitely open to some degree. Although they represent a hypothetical situation, these conditions are a worst case scenario since the fundamental frequencies are the lowest of any case studied (Tables 6.1 through 6.3) and they have the highest fundamental peak amplitudes. Both low fundamental frequencies and high fundamental peak amplitudes present problems for the control system design (Hull:1993).

The peaks represent the gain of the CRF at the resonant frequencies. The lowest frequency peak is the fundamental and the rest are harmonics. There are 14 peaks present in all

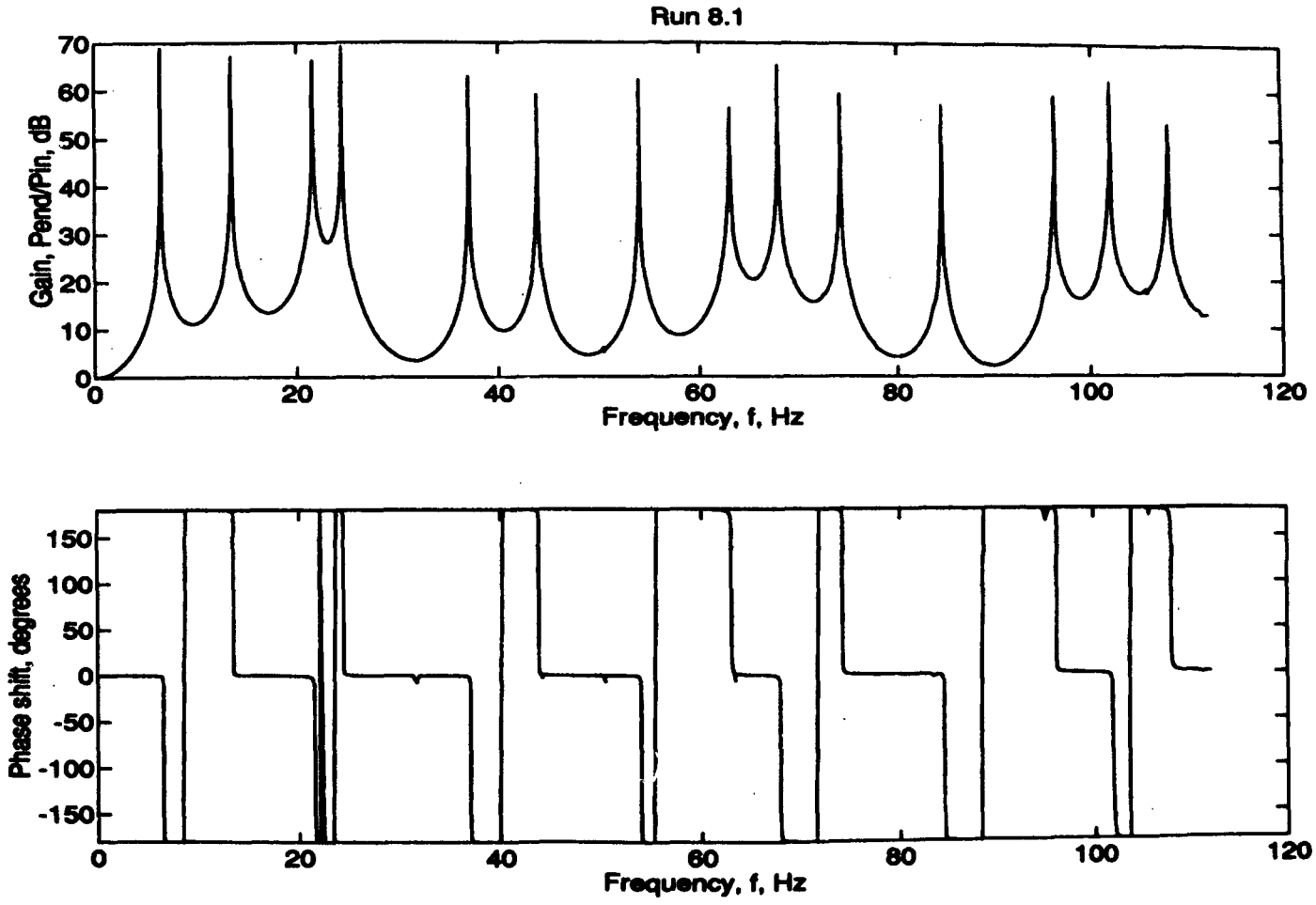

Figure 6.1. CRF Blocked Line Frequency Response (Basic Length). Conditions: R_c = 0.0 ft, $\dot{m}$ = 0 lbm/s. Fundamental Peak: 6.5 Hz at 70 dB.

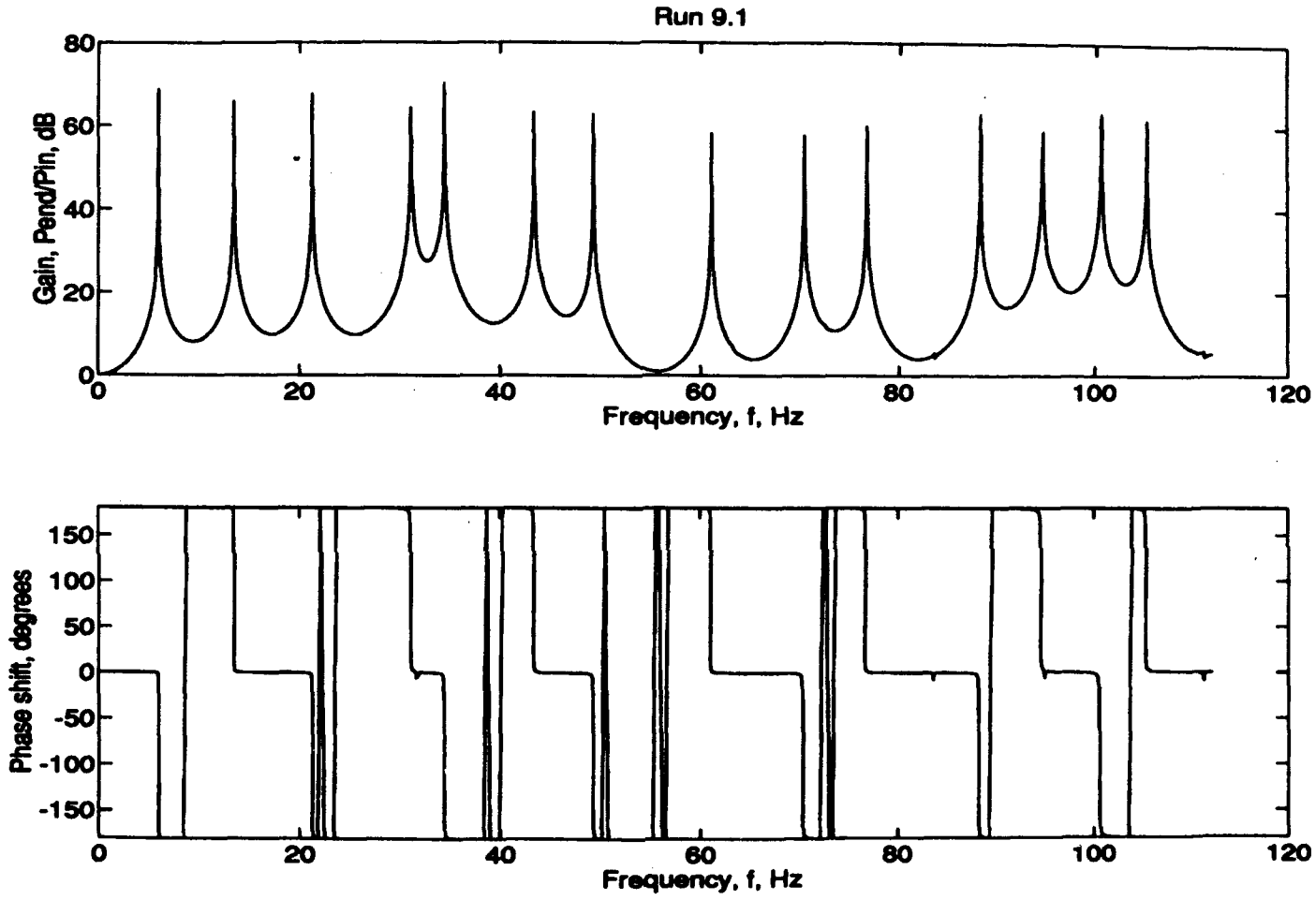

Figure 6.2. CRF Blocked Line Frequency Response (Intermediate Length). Conditions: R_c = 0.0 ft, $\dot{m}$ = 0 lbm/s. Fundamental Peak: 6.0 Hz at 68.8 dB.

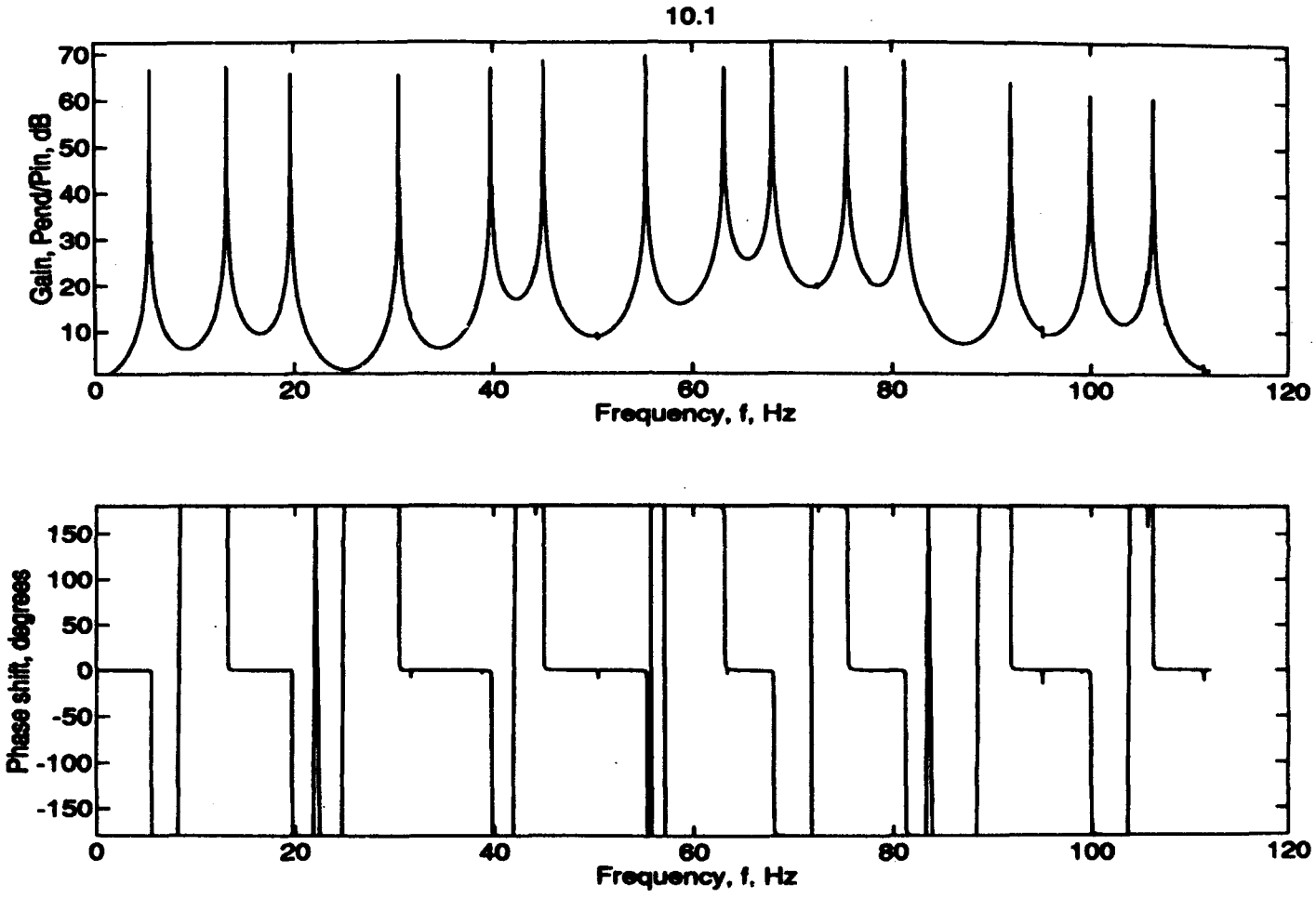

Figure 6.3. CRF Blocked Line Frequency Response (Extended Length). Conditions: R_c = 0.0 ft, $\dot{m}$ = 0 lbm/s. Fundamental Peak: 5.5 Hz at 69.2 dB.

plots, indicating the blocked behavior expected (Chapter III) from the basic pipe resonance equations(2-1).

Note that the higher frequency peaks are in the same decibel range as the fundamental. All of the peaks are high and very sharp. In contrast, off-peak gains are low and more rounded. The corresponding phase plots show the phase angle crossing zero at the peak frequencies with a nearly infinite slope, further illustrating the sharpness of the peaks. The off-peak phase angles are a maximum at ±180 degrees as is expected for low gains.

Note also the curves are generally the same shape for all three length configurations. However, note how drastically different the resonant frequencies are for the different length configurations above 20 Hz. Above 20 Hz, the resonant peaks clearly occur at different frequencies for the three length configurations, indicating the entire frequency spectrum is affected by L1 and L3.

6.3.2 Results for a Fixed Radius Compressor. The remaining three figures show the response for an exit radius 0.825 ft (½R3) and a mass flow rate of 180 lbm/s. Figures 6.4, 6.5, and 6.6 show the response for the basic, intermediate, and extended length configurations, respectively. The curves for a compressor radius of ½R3 and

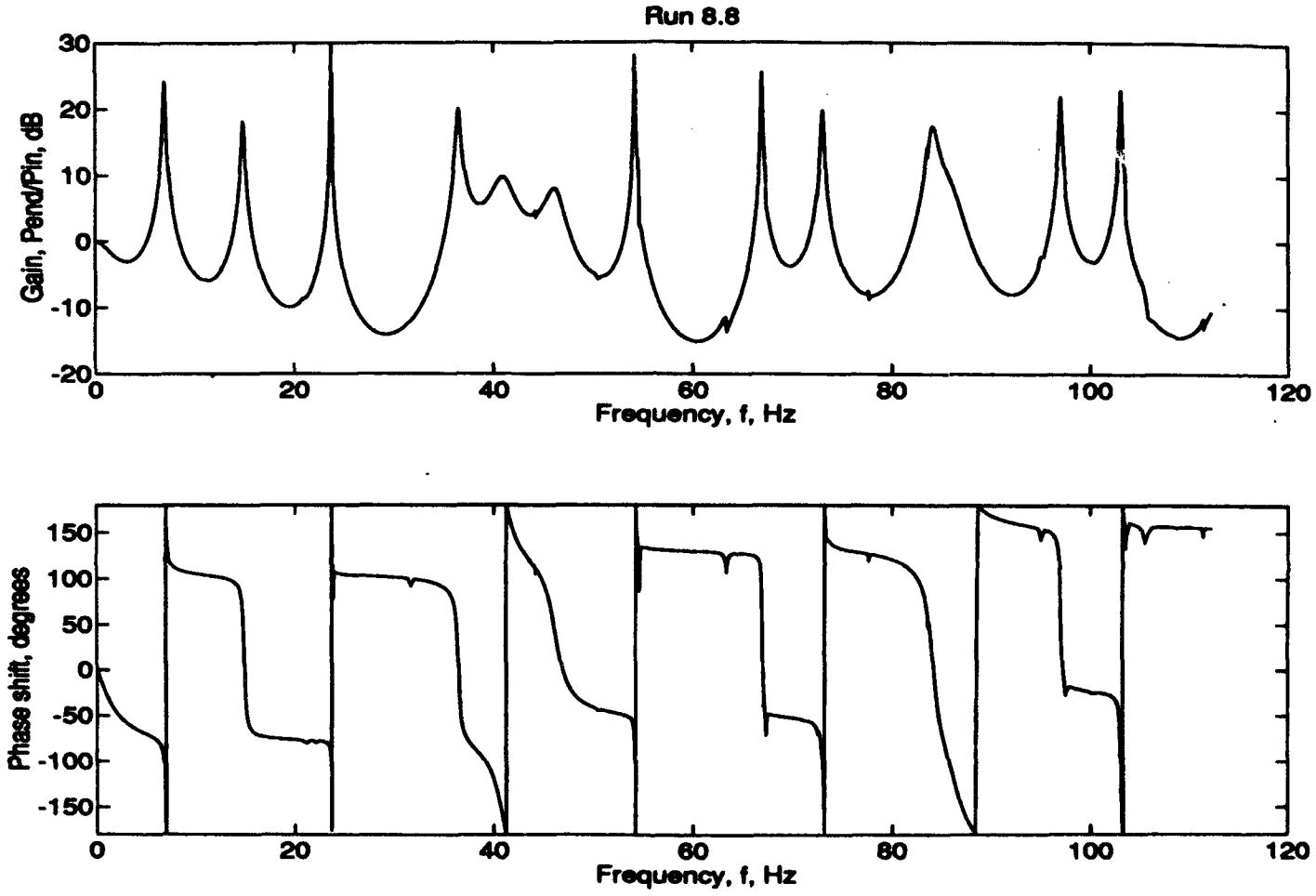

Figure 6.4. CRF Frequency Response for ½R3 End Radius (Basic Length). Conditions: R_c = 0.825 ft (½R3), $\dot{m}$ = 180 lbm/s. Fundamental Peak: 6.9 Hz at 24.0 dB.

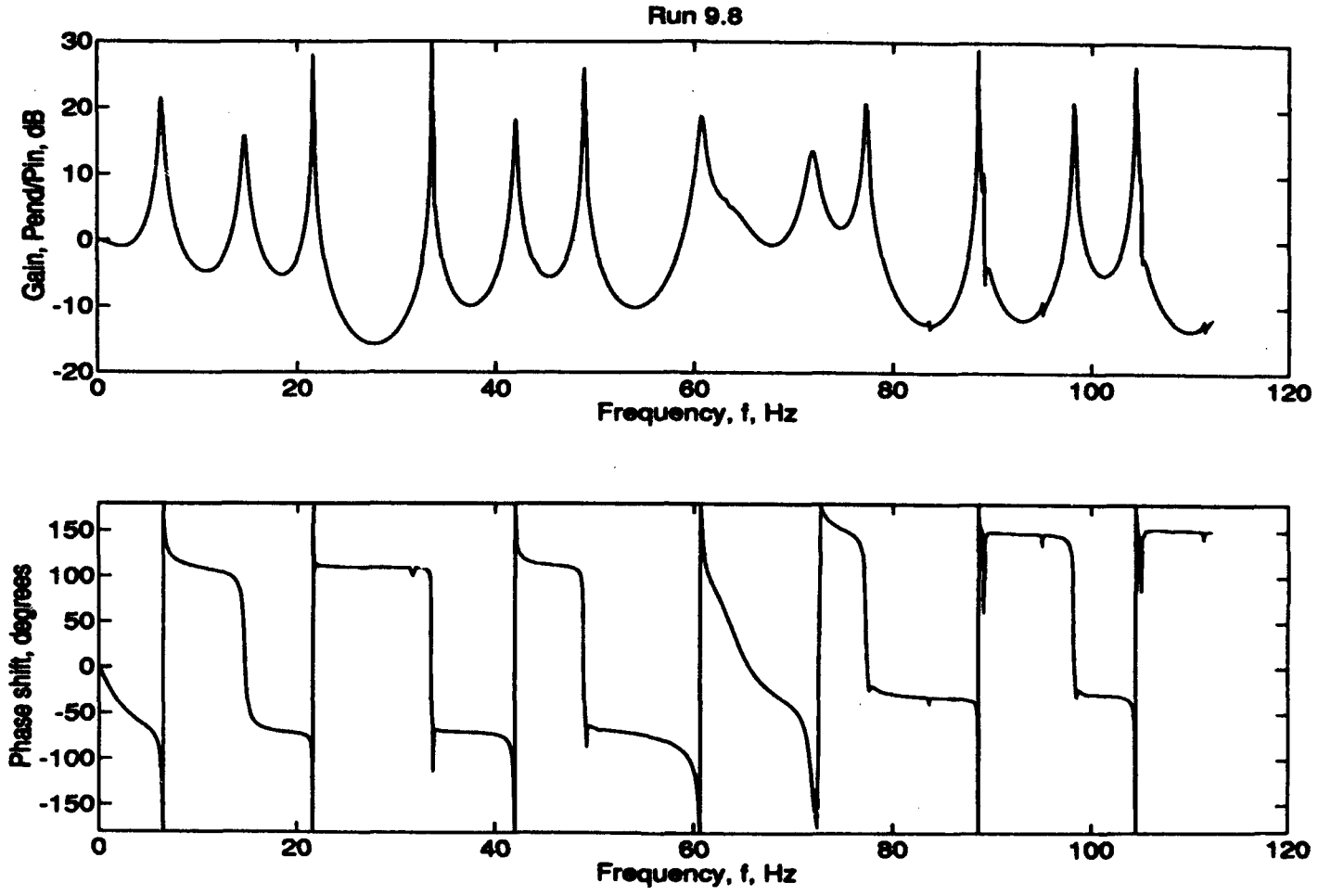

Figure 6.5. CRF Frequency Response for ½R3 End Radius (Intermediate Length). Conditions: R_c = 0.825 ft, $\dot{m}$ = 180 lbm/s. Fundamental Peak: 6.4 Hz at 21.4 dB.

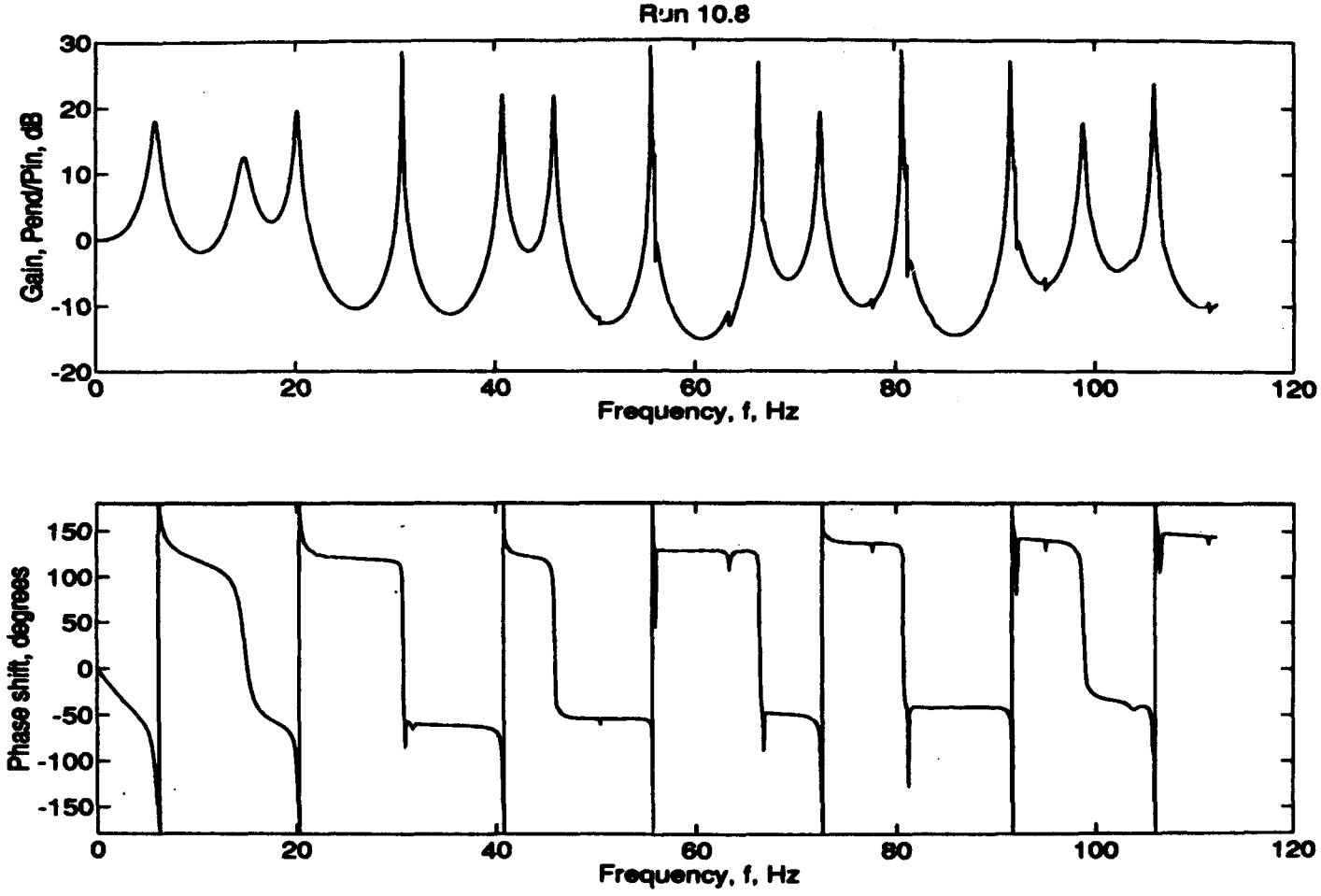

Figure 6.6. CRF Frequency Response for ½R3 End Radius (Extended Length). Conditions: R_c = 0.825 ft, $\dot{m}$ = 180 lbm/s. Fundamental Peak: 5.9 Hz at 18.0 dB.

mass flow rates of 20 lbm/s, 100 lbm/s, and 250 lbm/s are located in Appendix A, Figures A.1 - A.9.

Comparing Figures 6.4, 6.5, and 6.6, it is clear that the resonant frequencies are dependent on the length configuration. This is the same result as with the blocked line plots in Figures 6.1 - 6.3. For all cases in Figures 6.4 - 6.6, the number of peaks in the spectrum is lower than for the blocked case, varying only slightly between 12 and 13. The lower number of peaks is expected since the line is no longer blocked (Chapter III discussion).

All figures exhibit the same peak levels, relative to the fundamental, as in the blocked cases. The gains are lower than for the blocked cases, but rise with increasing mass flow conditions (Appendix A). The lower gains are again a result of the wave propagating out of the system through the open end. This also results in smoother phase transitions through zero and increased spacing between the peaks, as compared to the blocked line curves.

6.4 Summary

In summary, the data presented yields a fundamental frequency for the CRF between 5.5 Hz and 6.9 Hz, depending on the length configuration and end impedance conditions. The gains for the CRF range from 70 dB, for the blocked cases, down to 13 dB for the open end conditions with mass flow. The

frequency trends and number of peaks in the spectrum checks with the trends expected from the basic pipe resonance equations at varied length and end impedance conditions.

However, the gains cannot be checked against any basic equations since none exist. It turns out that when the gains are used to determine the damping characteristics of the CRF, the amplitudes indicate a very lightly damped system (Hull:1993). This presents a problem for the control system designer. Further discussion on this problem is postponed until after the experimental results are presented.

VII. Experimental Results

7.1 Introduction

In this chapter, the results of several experiments with the CRF model are presented and discussed. The first discussion centers on gain and phase shift results from data taken at discrete frequencies for no throughflow conditions. These results are compared with analytical solutions for the model at the flow and geometry conditions of the individual experiments. The second section discusses results for experiments with throughflow. In the last section, transient response test results for the model are presented and analyzed. All results presented are for the basic length configuration.

7.2 No Throughflow Model Response

Several data sets without throughflow were taken using the pneumatic signal generator as a sinusoidal pressure input. Only a sampling of the results is presented here; additional plots are located in Appendix A.

The condition of no throughflow simply means that the mass flow in the model is provided only from the sinusoidal input. As such, mean mass flow rates for these experiments are extremely low, on the order of 2×10^{-6} slug/s. This, in turn, yields velocities on the order of 1×10^{-4} ft/s in section 3 of the model. Arguably, these conditions are not

representative of the realistic flow in the CRF where the mass flow rate and velocities are much higher. However, these results provide insight into the accuracy of the analysis of the full-scale facility and are presented for that purpose.

Two groups of experiments are discussed in the following sections. The first group is comprised of four runs for the model configured with screens and honeycomb in the flow conditioning section. The end radius, R_c, varies with each run. These results are compared with full-scale analyses for the same flow, length, and end conditions.

The second group of experiments is nearly identical to the first, except for the flow conditioning elements in the model. The second set of data are taken with the washers installed in section 2 instead of the screens and honeycomb. These results are compared to the model results in the first group to determine the effects of modeling the flow conditioning elements as area reductions.

7.2.1 Screens and Honeycomb: Blocked Line Response. The blocked line response for the basic length model with screens and honeycomb in the flow conditioning section is presented in Figures 7.1a through 7.1c[1]. Data points are represented by

[1]Figure numbers appended with "a" show results for the end transducer (PR4) as compared to the inlet transducer (PS). Figures appended with "b" and "c" show results for the transducers near flow conditioning elements (PR3 and PR2, respectively). Transducer locations are defined in Figure 4.3.

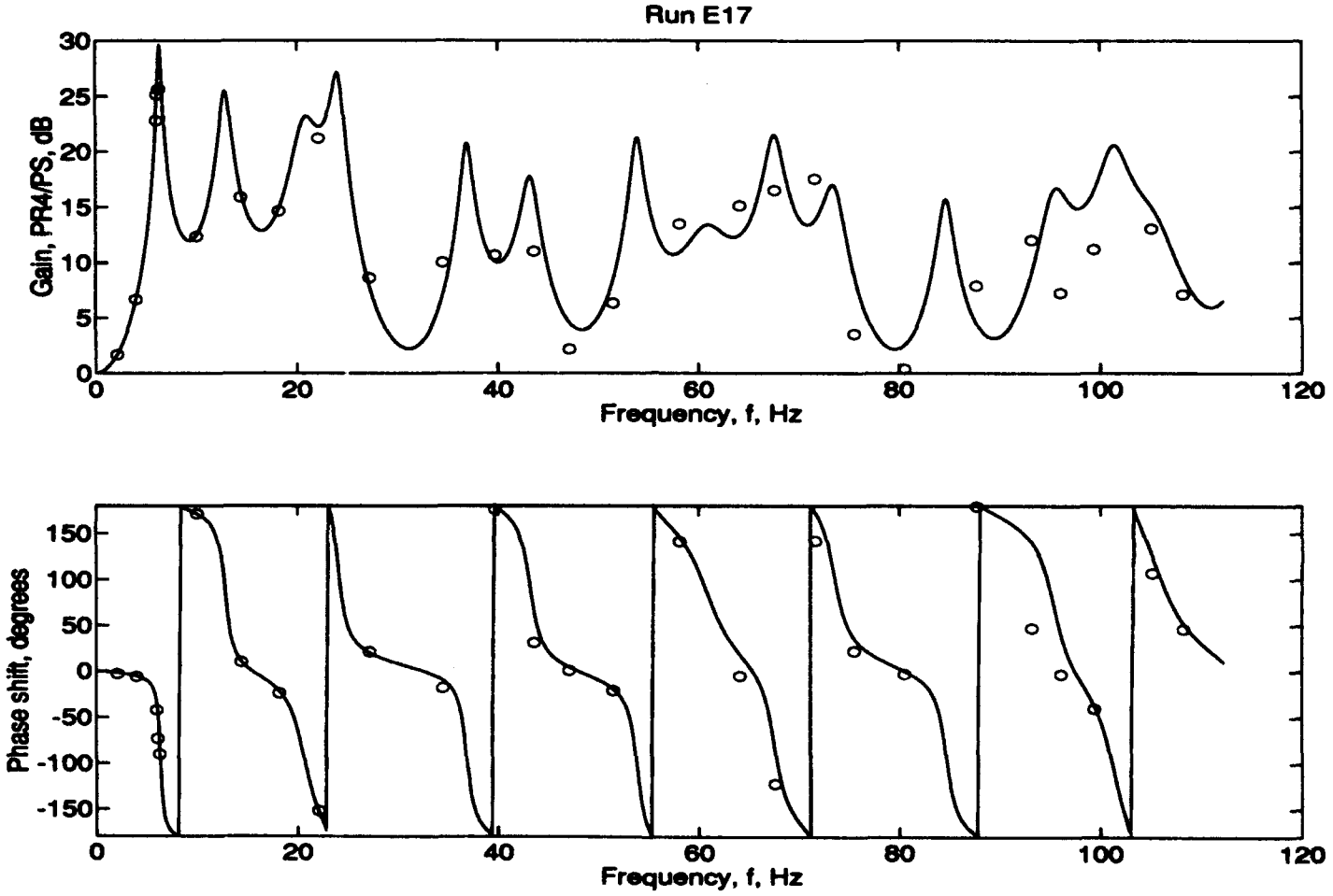

Figure 7.1a. Model Blocked Line Frequency Response (PR4). Conditions: R_c = 0 ft, $\dot{m}$ = 0 slug/s, basic length, screens and honeycomb. Fundamental peak: 6.3 Hz.

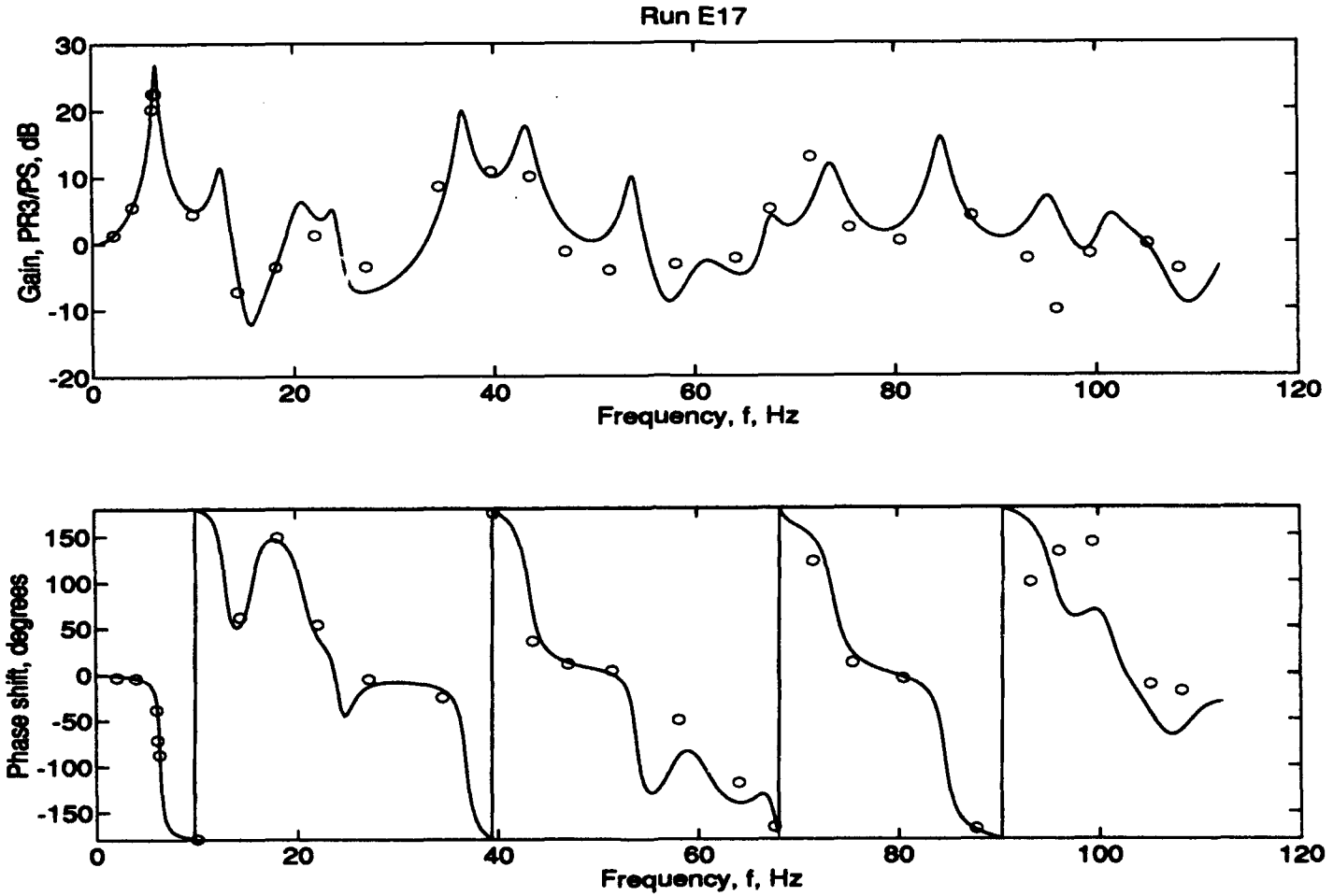

Figure 7.1b. Model Blocked Line Frequency Response (PR3). Conditions: R_c = 0 ft, $\dot{m}$ = 0 slug/s, basic length, screens and honeycomb. Fundamental peak: 6.3 Hz.

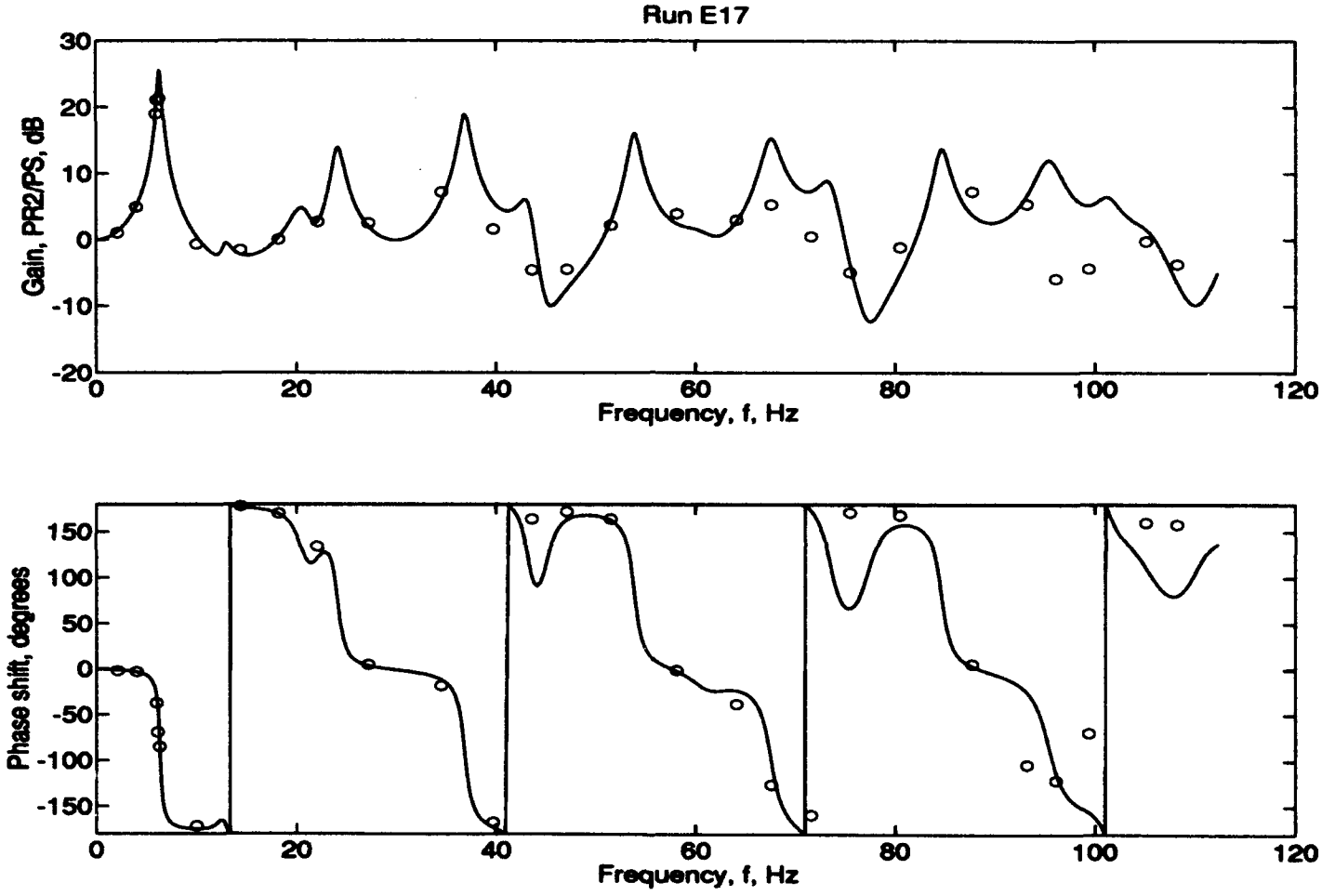

Figure 7.1c. Model Blocked Line Frequency Response (PR2). Conditions: R_c = 0 ft, $\dot{m}$ = 0 slug/s, basic length, screens and honeycomb. Fundamental peak: 6.3 Hz.

circles and the analytical solution for the model is represented by the solid line. The full-scale results for the same flow conditions are illustrated in Figures 7.2a through 7.2c. There is no full-scale experimental data; therefore, only the analytical curves are presented in full-scale plots.

The fundamental frequency for the model is 6.3 Hz; whereas, for the full-scale solution, the fundamental frequency occurs at 6.5 Hz. The fundamental frequencies of the model and CRF are nearly the same, as would be expected from the radius scale study performed (Appendix B).

Reviewing the gains in Figures 7.1a - 7.1c, note that most of the data fall on the analytical curves quite well at frequencies below 50 Hz. Above 50 Hz, the data fall in the vicinity of the curves until around 90 Hz where the data and analyses diverge. The corresponding phase plots show the same behavior although, in general, the phase data follow the analyses more closely than the gain data, especially at higher frequencies. The high frequency discrepancy between theory and experiment is common throughout all of the plots. Although the cause of the discrepancy is unknown, it is most likely due to losses in the model that are not accounted for in the analysis, such as the curvature of the coiled tubing.

The gains vary significantly for the different transducer locations. While PR4 (Figure 7.1a) decibel levels are all greater than zero, both PR3 (Figure 7.1b) and PR2 (Figure

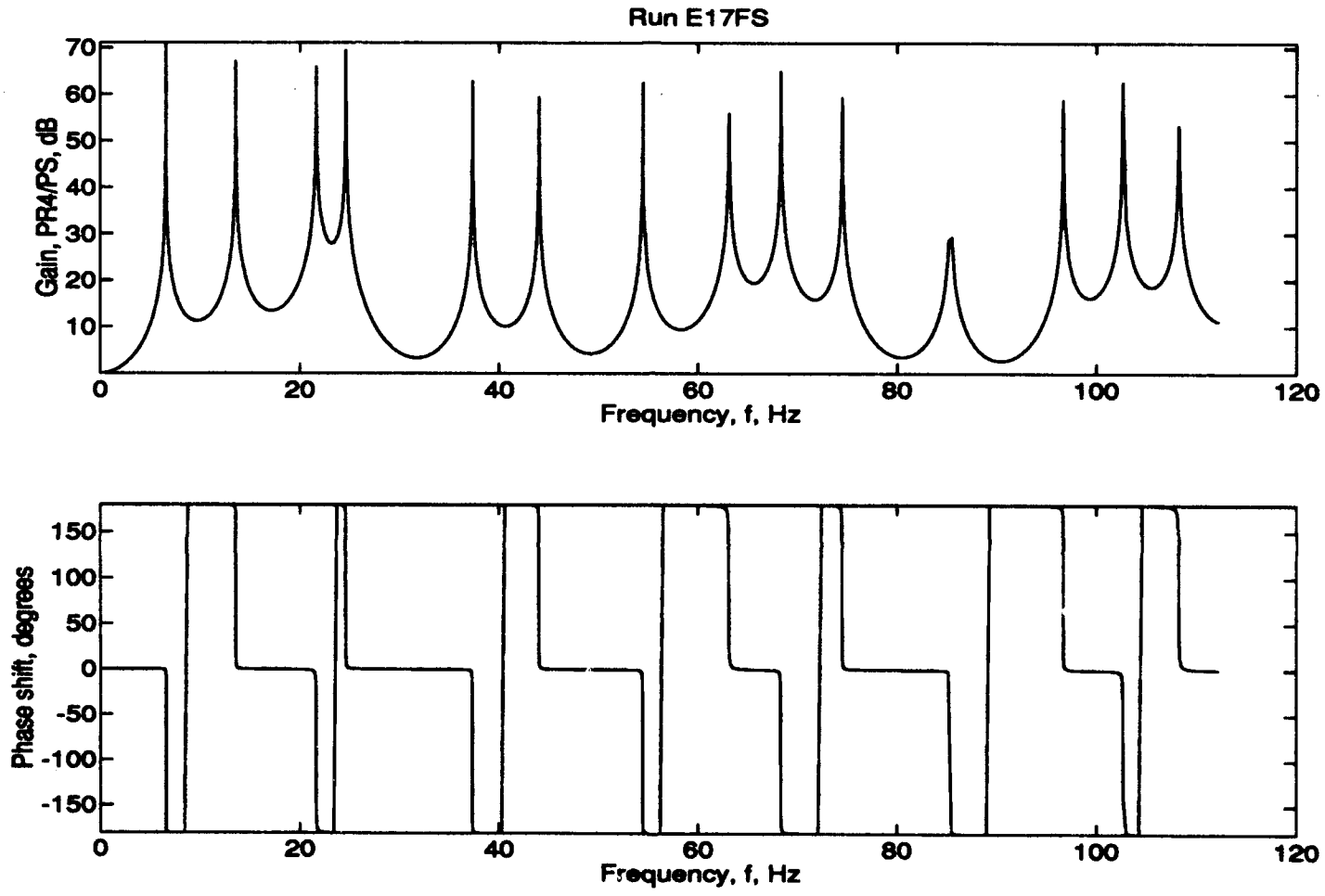

Figure 7.2a. CRF Blocked Line Frequency Response (PR4). Conditions: R_c = 0 ft, $\dot{m}$ = 0 slug/s, basic length. Fundamental peak: 6.5 Hz.

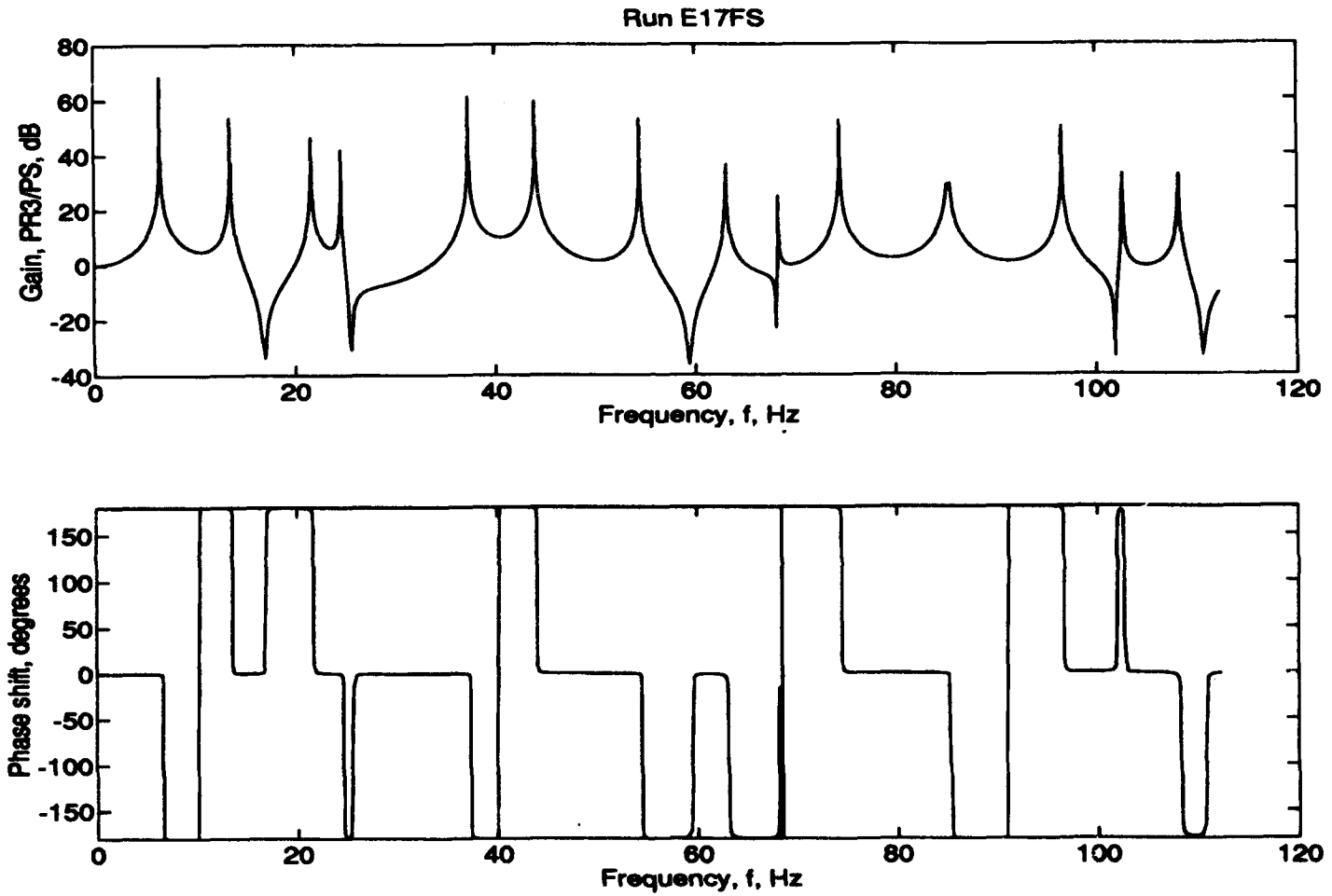

Figure 7.2b. CRF Blocked Line Frequency Response (PR3). Conditions: R_c = 0 ft, $\dot{m}$ = 0 slug/s, basic length. Fundamental peak: 6.5 Hz.

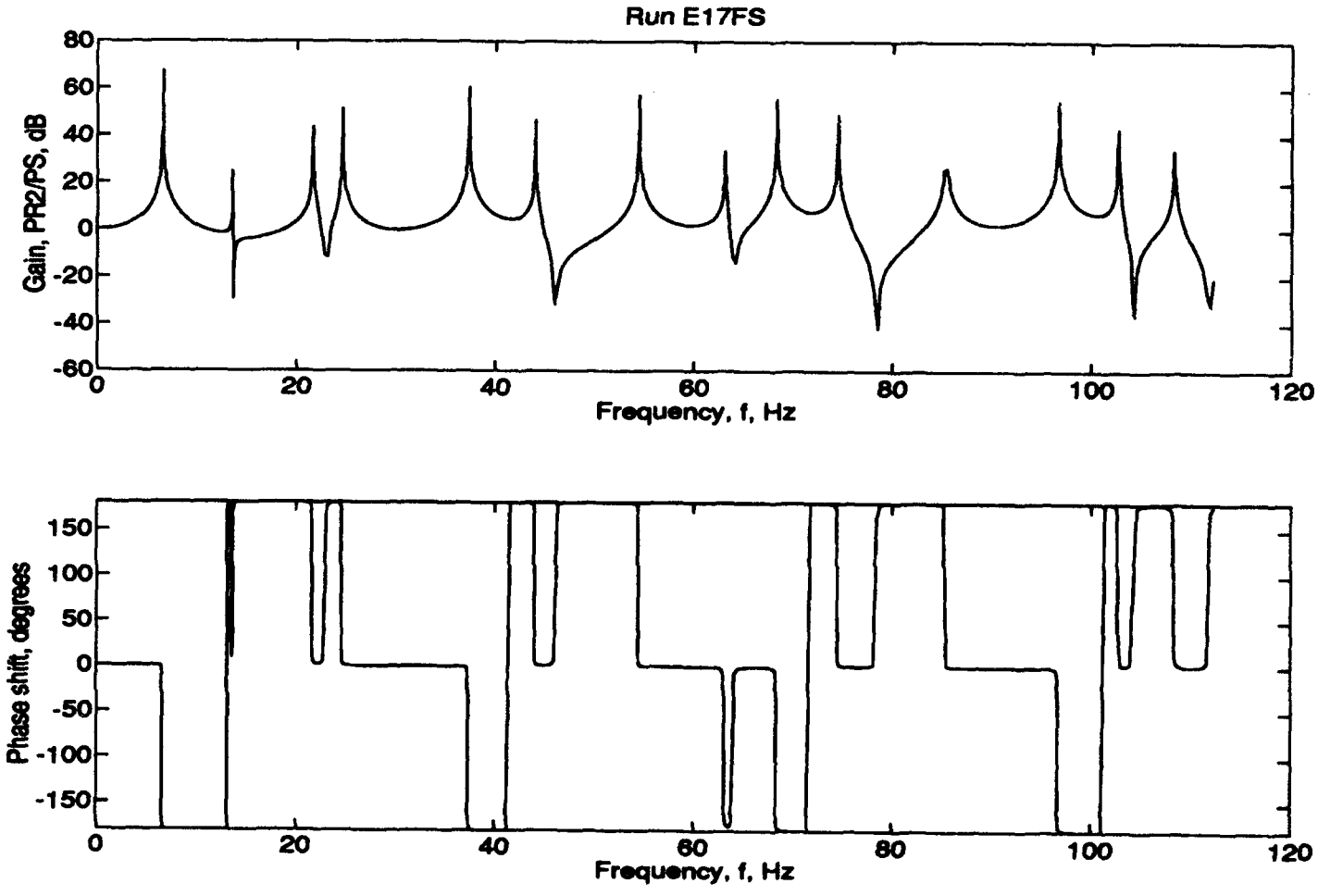

Figure 7.2c. CRF Blocked Line Frequency Response (PR2). Conditions: R_c = 0 ft, $\dot{m}$ = 0 slug/s, basic length. Fundamental peak: 6.5 Hz.

7.1c) gains fall below 0 dB at some frequencies. This is simply an indication that gains are a function of location in the line. The basic behavior of the line is not dependent on location since the peaks and valleys occur at the same frequencies for all three locations.

Finally, comparing Figures 7.1a - 7.1c with 7.2a - 7.2c, it is obvious that the gain decibel levels are significantly higher for the full-scale analysis than for the model analysis and data. This is a result of radius scaling. Additional details on radius scaling from a 20 ft diameter line to a 2 in diameter line and the associated peak decibel levels are located in Appendix B.

Four important characteristics of the model are found from the blocked line analysis, where infinite exit impedance exists. First, the data and theory are in good agreement for this configuration below 90 Hz. Second, the amplitude of the resonant peaks are dependent on location in the line. Third, the model peaks are significantly lower than the full-scale peaks for the same flow and geometry configurations. Fourth, both the theoretical and experimental results place the fundamental frequency for the model at 6.3 Hz. This is very close to the full-scale fundamental frequency of 6.5 Hz, illustrating that the experiment verifies the full-scale, blocked line frequency results.

7.2.2 Screens and Honeycomb: R_o = ¼R3. Figures 7.3a through 7.3c are presented in this section for the basic length configuration with screens and honeycomb as flow conditioning elements and the end radius fixed at ¼R3. The mass flow is again due only to the sinusoidal input from the pneumatic signal generator and for these figures, is computed to be 2.2×10^{-6} slug/s.

In Figures 7.3a through 7.3c, again note the data points fall closely to the analytical curves. However, in this case, the agreement is not as good as in the blocked case. This is a result of the end impedance equation used for the analysis. For blocked lines, the end impedance is infinite and no approximation of its value is necessary. However, for an orifice-terminated line, the end impedance is not well understood and approximations for the value must be made [Equation (3-4)]. The end impedance equation used (2-15) for the model analyses was determined by trial and error. Other representations in the analysis were tried but were much less successful. One representation tried was to use the Equation (4-1) for the pressure drop across and orifice plate. This representation was used by Ross (1983:20) with successful results. A second representation tried was to treat the orifice as a short, open line.

Computing the frequency response using Equation (2-15); however, produced the best match between analytical and

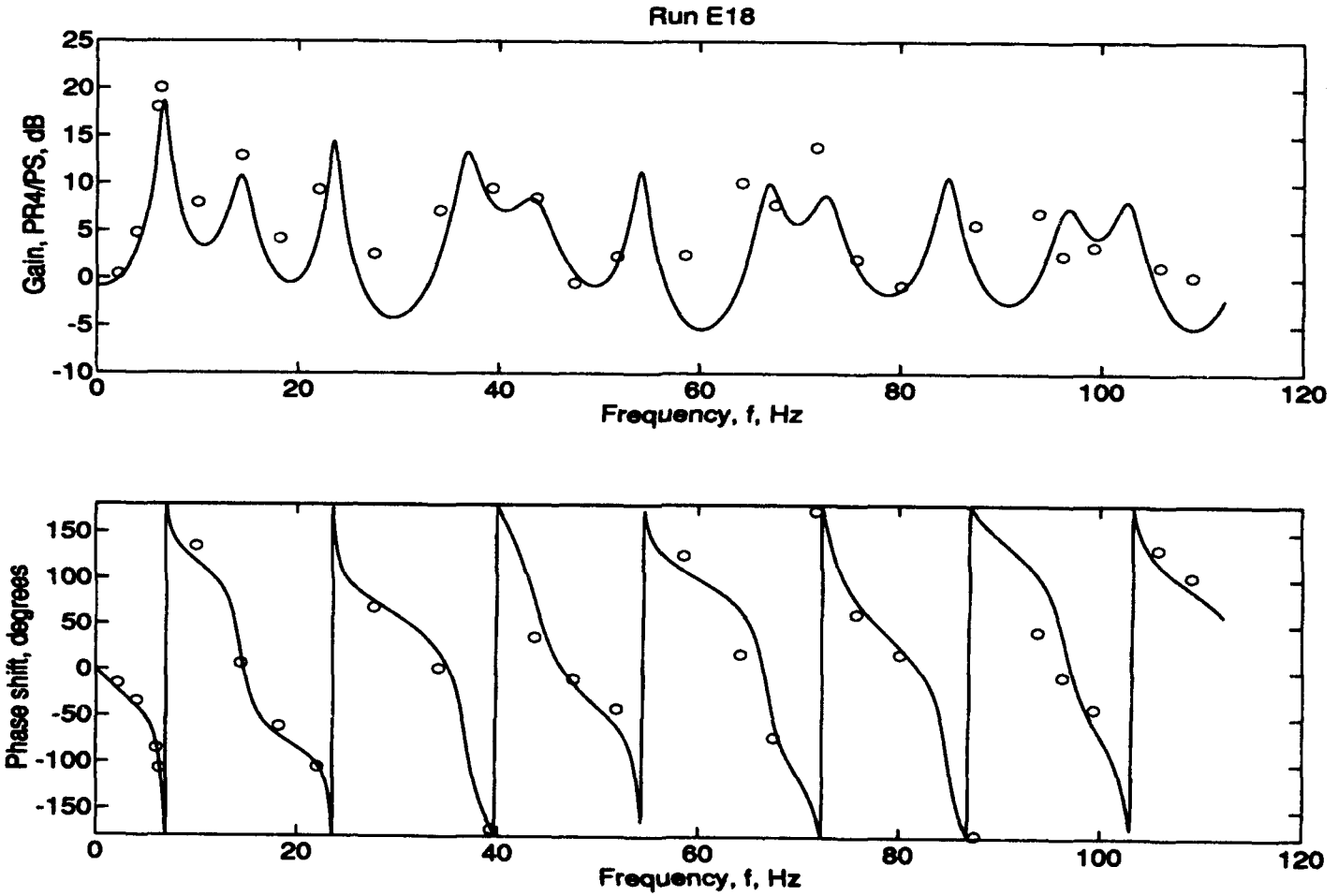

Figure 7.3a. Model No Throughflow Frequency Response (PR4) for R_c = ½R3. Conditions: R_c = 3/64 in, $\dot{m}$ = 2.2 X 10^{-6} slug/s, basic length, screens and honeycomb.

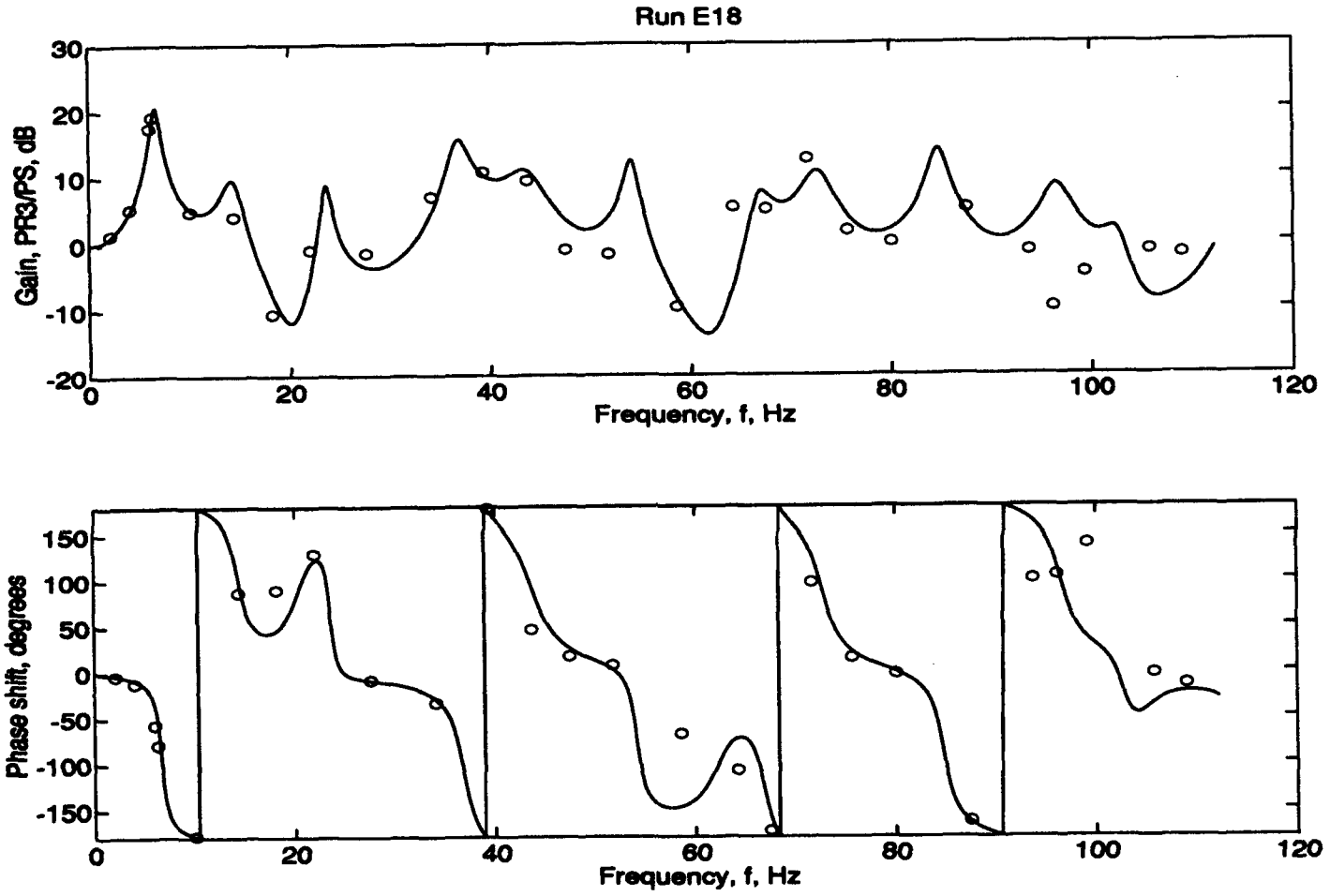

Figure 7.3b. Model No Throughflow Frequency Response (PR3) for R_c = ¼R3. Conditions: R_c = 3/64 in, $\dot{m}$ = 2.2 X 10^{-6} slug/s, basic length, screens and honeycomb.

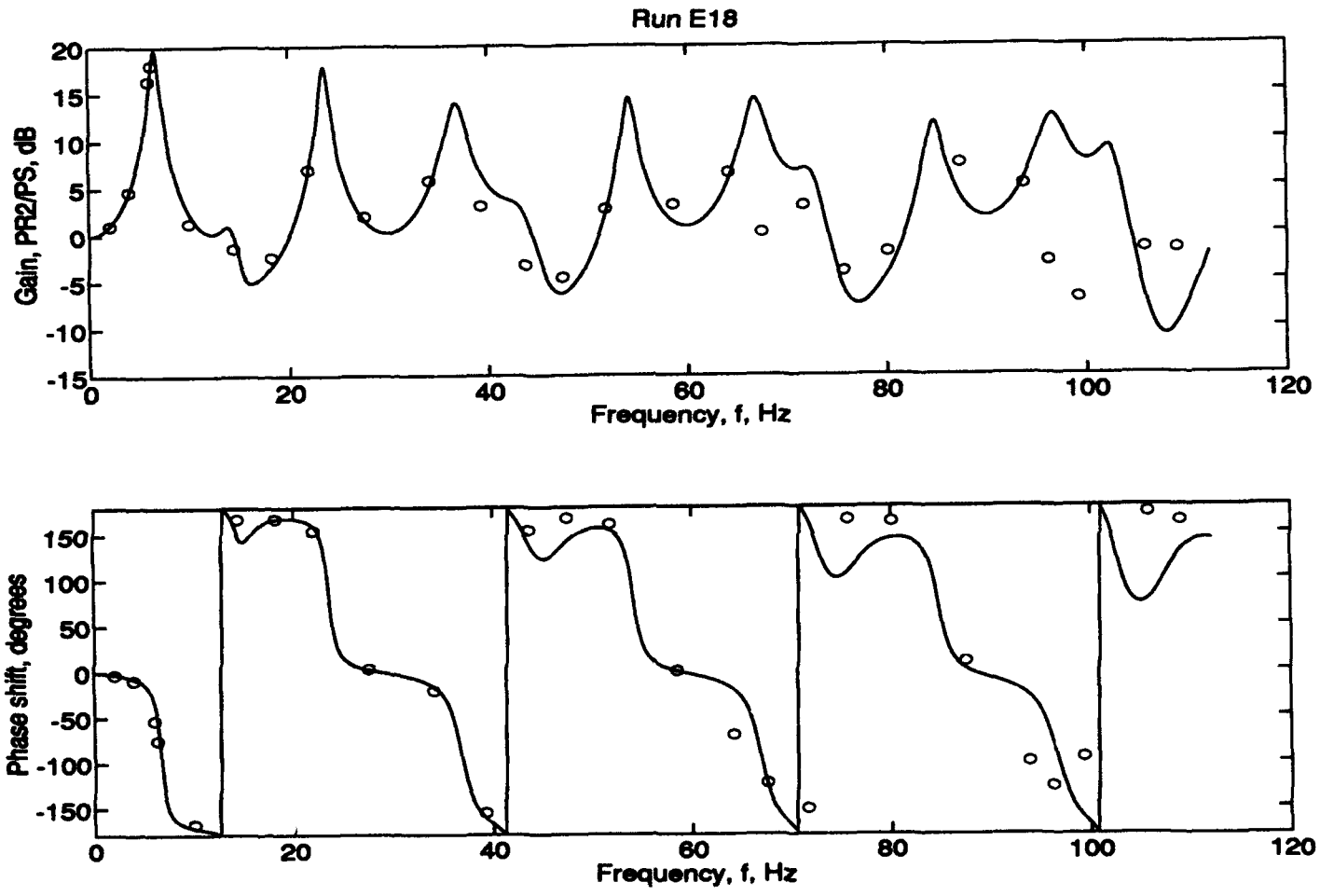

Figure 7.3c. Model No Throughflow Frequency Response (PR2) for R_c = ¼R3. Conditions: R_c = 3/64 in, $\dot{m}$ = 2.2 X 10^{-6} slug/s, basic length, screens and honeycomb.

theoretical results. The use of different end impedance equations, in general, vertically shifted the theoretical curve and slightly changed its shape. It is possible to devise a better analytical representation of the end impedance by further trial and error.

Comparing again the blocked and ¼R3 cases, note that the peak gains are reduced as the end condition changes from blocked to partially open. Particularly, the fundamental peak for PR4/PS (Figure 7.3a) drops to 20 dB from the blocked line level of 30 dB (Figure 7.1a). From the analysis in Chapter VI, this is an expected response when the end radius is increased. The peaks for the full-scale CRF also drop in magnitude with the increased end radius. These curves are in Appendix A (Figures A.10 - A.12). From Figures A.10 - A.12 and 7.3a - 7.3c, note the fundamental frequency for the full-scale CRF is 6.9 Hz; whereas, for the model, the fundamental frequency is 6.6 Hz. Again, the frequency data for the full-scale facility is verified through experimental results.

At this point, some attention should be given to the low frequency ($f << 1$ Hz) response of the CRF and model. Unlike the blocked case, Figure 7.3 (and A.10 as well) indicates that the gains are not zero when the frequency is zero. This is simply a consequence of the scale of the plots. Studies were conducted to determine if the analysis does go to zero at low frequency. It was found that in all cases considered, the

gains drop very rapidly, on the order of 10 dB/.001 Hz, for frequencies much less than 1.

As with the full-scale results in Chapter VI, these results show that the peaks reduce with increasing end radius. The data show good agreement with theory although the agreement is not as good as with the blocked line case.

7.2.3 Screens and Honeycomb: R_e = 1/2R3. Figures 7.4a through 7.4c illustrate the model response under the following conditions. The model is configured for basic length, screens and honeycomb for the flow conditioning elements, and an end radius of ½R3. The mass flow is due only to the sinusoidal input signal and is computed as 2.3 X 10^{-6} slug/s. The corresponding full-scale CRF plots are located in Appendix A in Figures A.13 through A.15.

Figures 7.4a shows the gain data again falling relatively close to the curves below 30 Hz, although when compared with the same curve for the blocked and ¼R3 cases, the data and analyses do not agree as closely. Again, this is a direct result of the end impedance equation used for the model and indicates the end impedance equation (2-15) is less accurate for the more open lines.

By increasing the radius to ½R3 from ¼R3 in the analytical solution for the model, the fundamental peak drops from near 20 dB (Figure 7.3a) to just above 0 dB (Figure

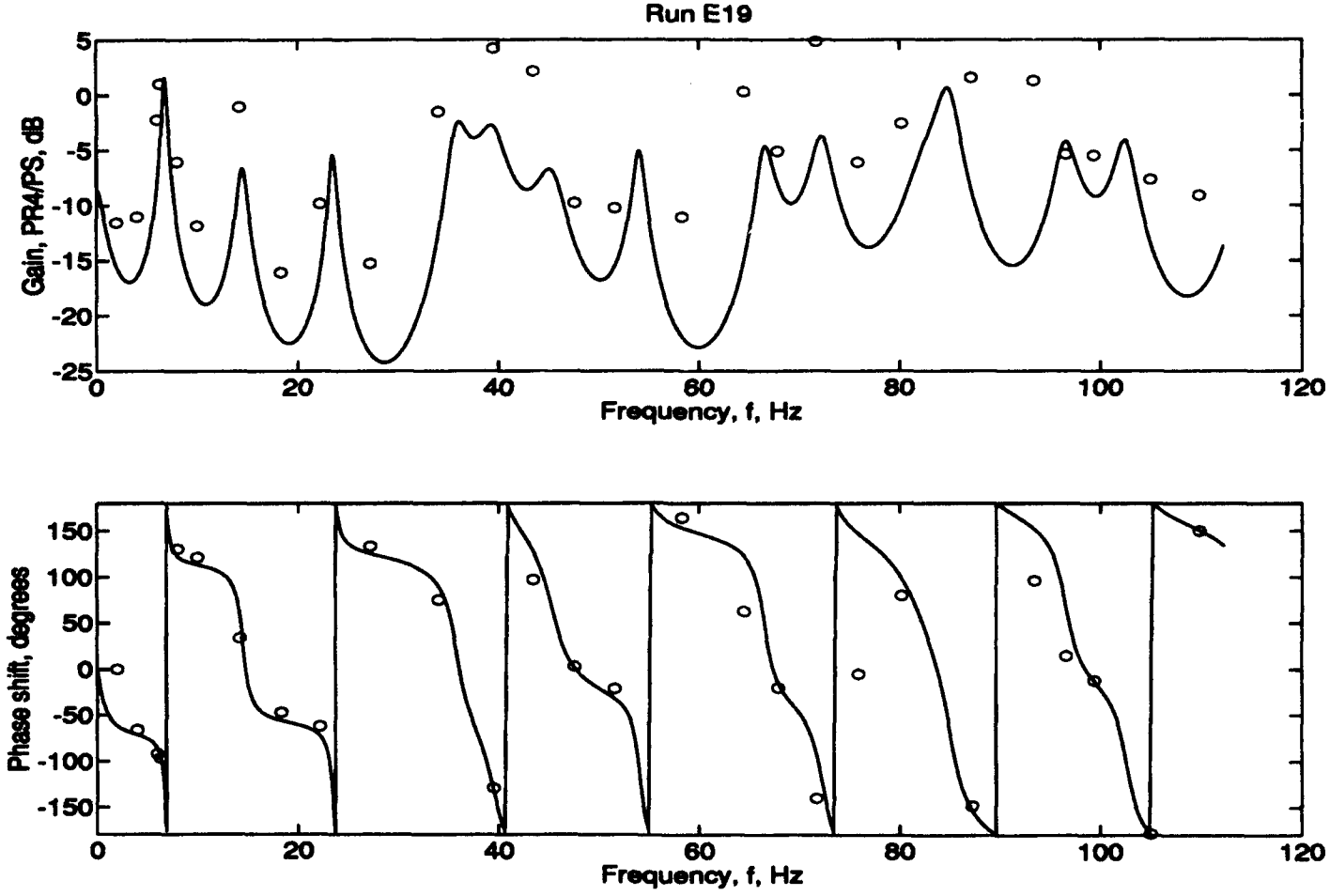

Figure 7.4a. Model No Throughflow Frequency Response (PR4) for R_c = ½R3. Conditions: R_c = 3/32 in, $\dot{m}$ = 2.3 X 10^{-6} slug/s, basic length, screens and honeycomb.

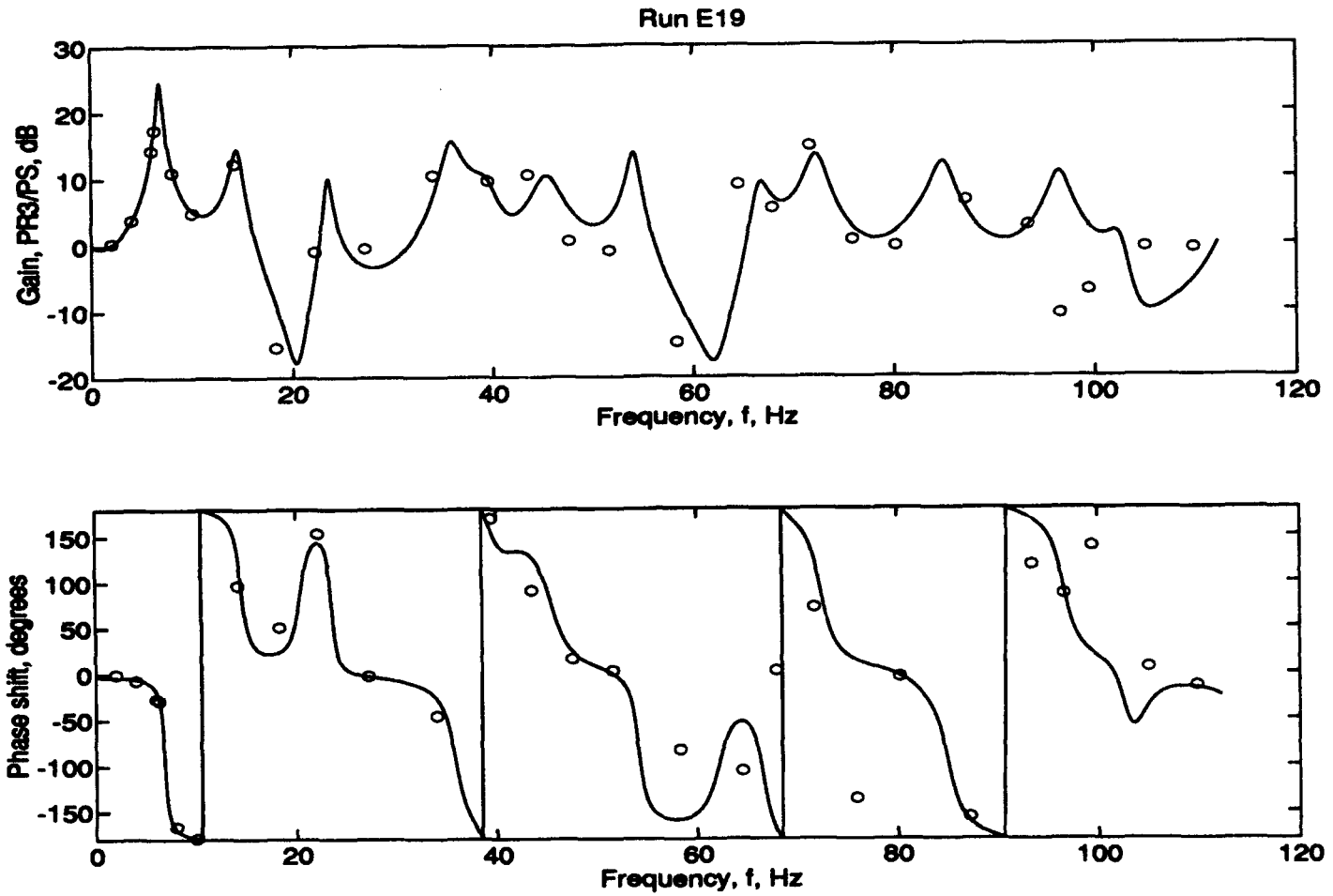

Figure 7.4b. Model No Throughflow Frequency Response (PR3) for R_c = ½R3. Conditions: R_c = 3/32 in, $\dot{m}$ = 2.3 X 10^{-6} slug/s, basic length, screens and honeycomb.

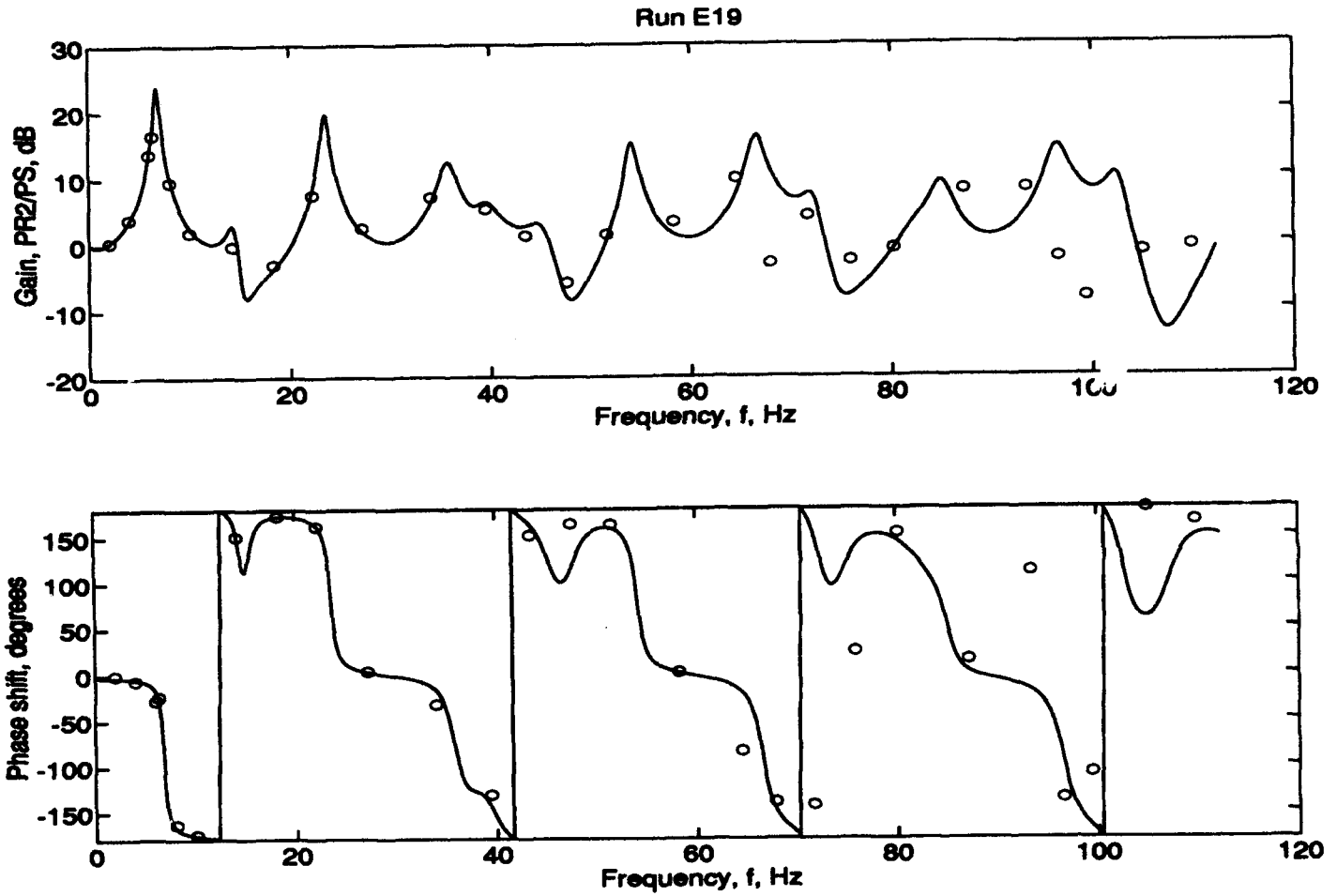

Figure 7.4c. Model No Throughflow Frequency Response (PR2) for R_c = ½R3. Conditions: R_c = 3/32 in, $\dot{m}$ = 2.3 X 10^{-6} slug/s, basic length, screens and honeycomb.

7.4a). The other transducer locations, however, are not affected as greatly by increasing the end radius. For PR3/PS, the fundamental peak increases 5 dB from the ¼R3 case (Figure 7.3b) to the ½R3 case (Figure 7.4b) and the fundamental peak for PR2/PS rises 5 dB from the ¼R3 case (Figure 7.3c) to the ½R3 case (Figure 7.4c). Primarily, these results show that the end impedance dependence of the line is a function of location. In particular, the end impedance strongly affects the end transducer but does not have a big effect on the upstream transducers. This is primarily due to the fact that the end impedance for the upstream transducers is more strongly dependent on the impedance mismatch at the junction of sections 2 and 3 of the model than on the orifice radius. This impedance at the junction of sections 2 and 3 is high due to the small radius of section 3 as compared to the radius of section 2. In effect, the end impedance for sections 1 and 2 is nearly that of a blocked line. Thus, changing the end radius has a minimal effect on the signal at the upstream transducer locations.

7.2.4 Screens and Honeycomb: Open Line Response. Figures 7.5a through 7.5c illustrate the fully open behavior of the model. The full-scale plots are located in Appendix A as Figures A.16 through A.18. This set of results is for the

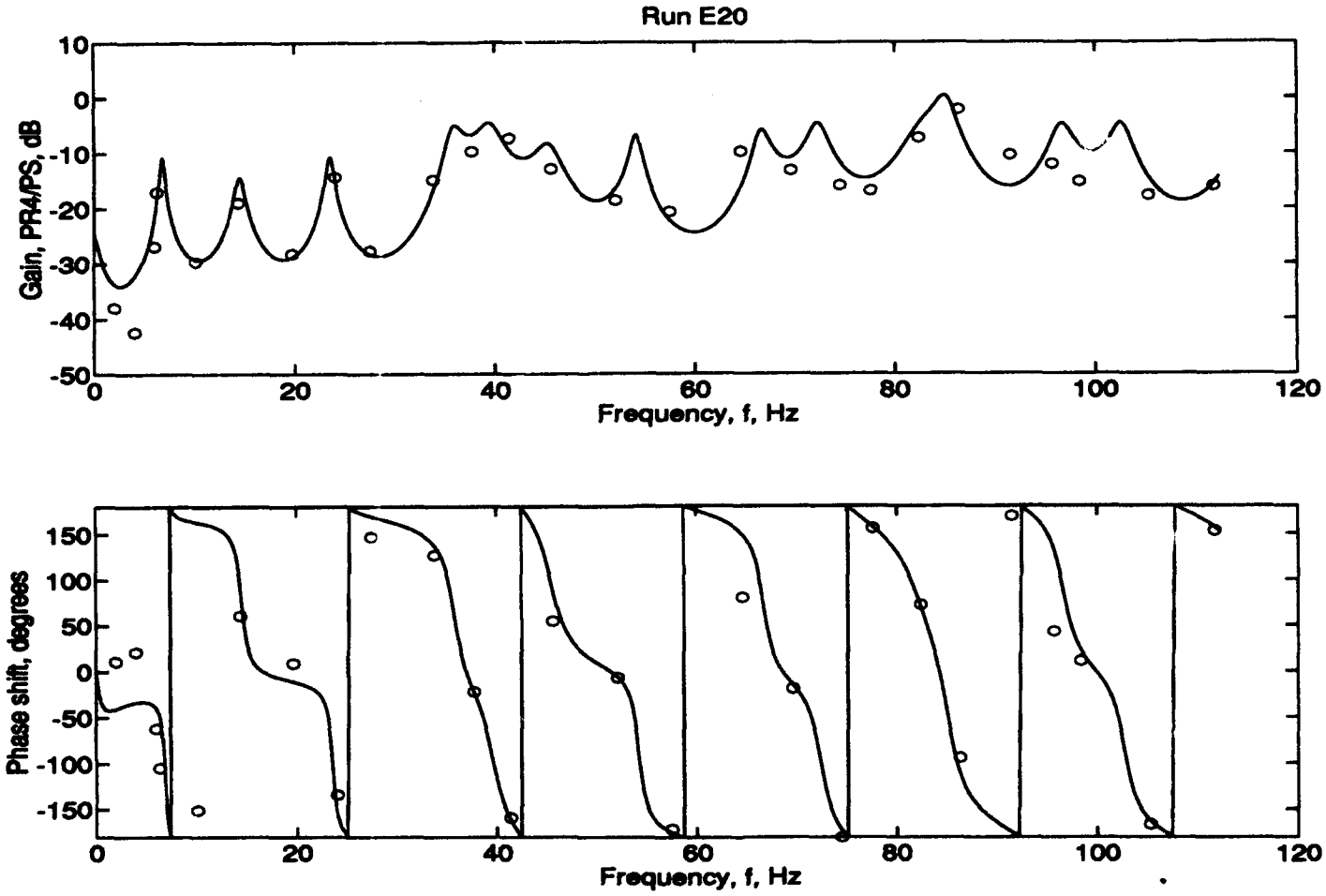

Figure 7.5a. Model No Throughflow Frequency Response (PR4) for R_c = R3. Conditions: R_c = 3/16 in, $\dot{m}$ = 2.1 X 10^{-6} slug/s, basic length, screens and honeycomb.

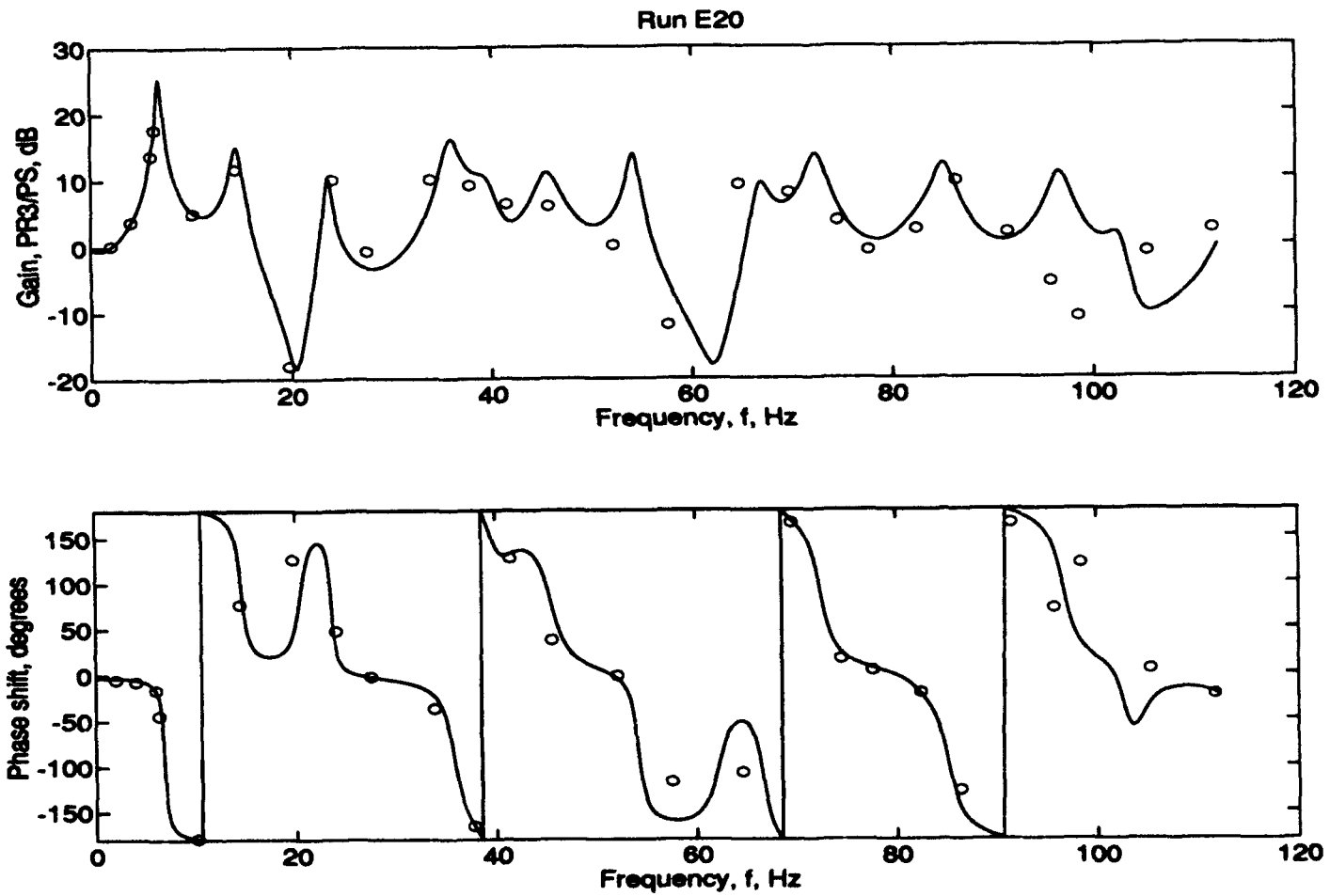

Figure 7.5b. Model No Throughflow Frequency Response (PR3) for R_c = R3. Conditions: R_c = 3/16 in, $\dot{m}$ = 2.1 X 10^{-6} slug/s, basic length, screens and honeycomb.

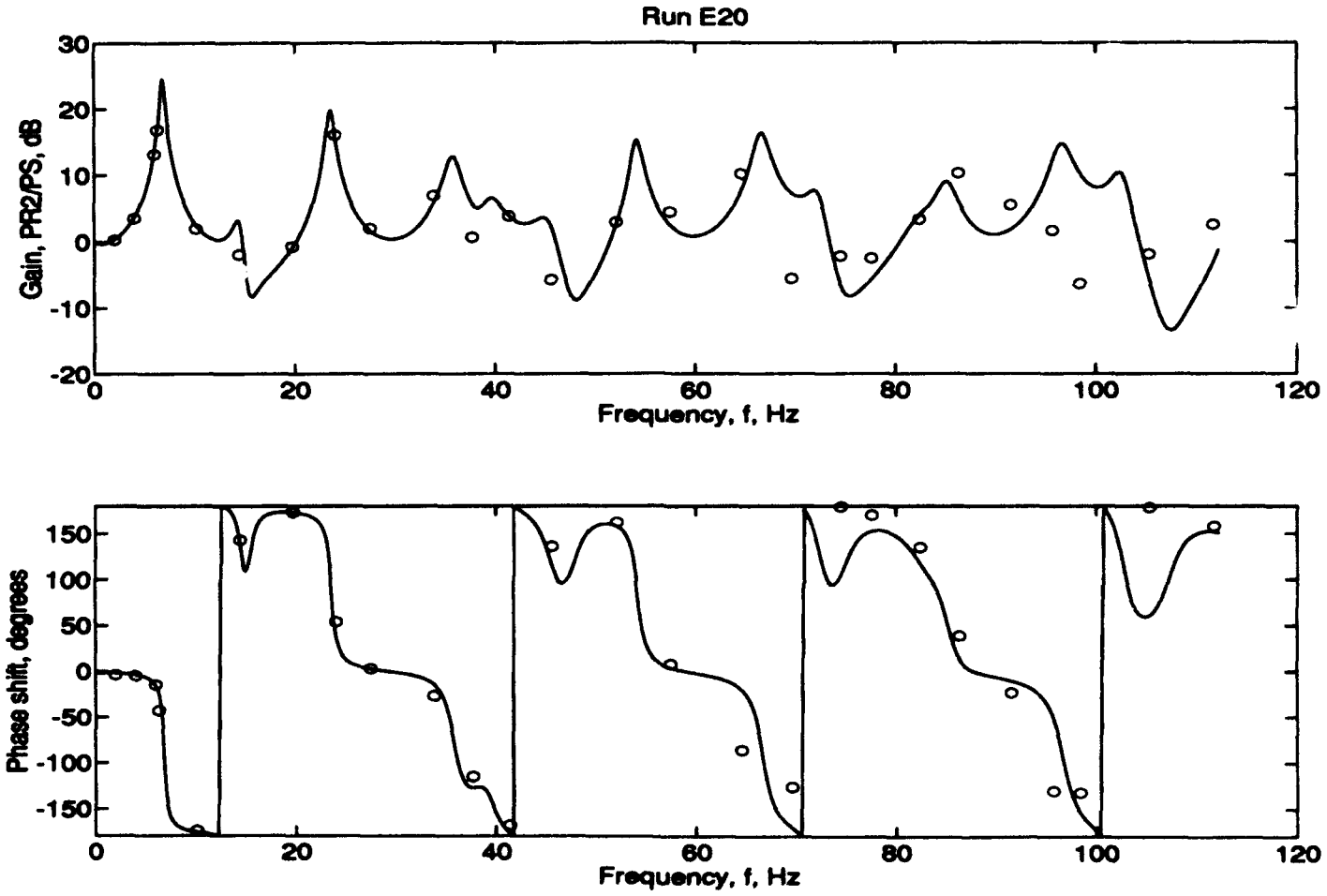

Figure 7.5c. Model No Throughflow Frequency Response (PR2) for R_c = R3. Conditions: R_c = 3/16 in, $\dot{m}$ = 2.1 X 10^{-6} slug/s, basic length, screens and honeycomb.

same configuration as the last three sets of results, except the end radius is now fully open and equal to R3.

Note first that increasing the end radius to R3 causes the data points to fall closer to the curve than in the two orifice-terminated cases. In fact, the data fall on the curve about as well as for the blocked case. This is due to the fact that the open line end impedance is zero; thus, no approximations are required.

Comparing Figures 7.5a and 7.4a, the fundamental peak drops 10 dB from the ½R3 case to the fully open case. However, the gains for PR3 (Figure 7.4b and 7.5b) and PR2 (Figures 7.4c and 7.5c) change very little, indicating these two locations are relatively unaffected by radius increases beyond ½R3.

The full-scale results are similar to the model results for PR2 and PR3 in that they change very little when the radius is increased from ½R3 to R3. Also, for the full-scale analysis, PR4/PS changes very little as well. This appears to contradict the results of Chapter VI where it was noted several times that the gain of the line overall facility is highly dependent on the end radius. The reasons for this seeming discrepancy are explained in the next section.

7.2.5 End Conditions, Transducer Locations, and Gain.

First, it is noted that PR4/PS is not the gain of the whole

system (PEND/PIN). PR4 is not located exactly at the exit and PS is not precisely located at the inlet. It turns out that, for the full-scale facility, these locations are very important to the gains when the end radius is greater than zero.

Second, the mass flows in the model are so low that the resistance at the exit is nearly zero for all cases terminated with an orifice. Recall that the end impedance equation (2-15) is directly proportional to mass flow and inversely proportional to area. For the full-scale analysis, the mass flow is very low and the area is very large. Under these conditions, PR4/PS is far enough upstream of the exit to be unaffected by the radius change at the exit and therefore the response, under all of the orifice-terminated conditions, is similar to the open line response.

In contrast, PEND/PIN is significantly affected by the radius changes as this location is right at the exit. Figures A.19 through A.21 show the full-scale CRF PEND/PIN response for the ¼R3, ½R3 and fully open cases presented in this chapter. The end impedances are extremely low for these cases (3×10^{-7} lbf-s/ft^5 for the ¼R3 case, 2×10^{-8} lbf-s/ft^5 for the ½R3 case, and 1×10^{-9} lbf-s/ft^5 for the R3 case).

This information is important and will be further discussed in section 7.5.1. For now; however, the discussion

will return to the lab model. In the next section, the second group of no throughflow results are presented.

7.3 Model Response with Washers. Three sets of figures, each representing a different end radius, are presented in this section for the basic length configuration with washers installed for the flow conditioning elements. Again, throughflow is provided only by the input signal. For all three figure sets, the mass flow is 2.3 X 10^{-6} slug/s.

The purpose of this analysis is to determine if the area reduction technique, used in the analysis to model the impedance of the flow conditioning elements, correctly predicts the gains and phase shift at the three transducer locations in the laboratory model.

Figure 7.6 shows the model response at the end transducer (PR4) for washers installed in section 2 with the end radius open to ¼R3. This plot can be compared with the identical screen and honeycomb results in Figure 7.3a. The data for the screens and honeycomb configuration fall closer to the analytical curve for PR4/PS than the data for the washer configuration at the same location. The other two transducer locations show the same good agreement with theory for both the washers and the screens and honeycomb (Appendix A, Figures A.22 through A.23).

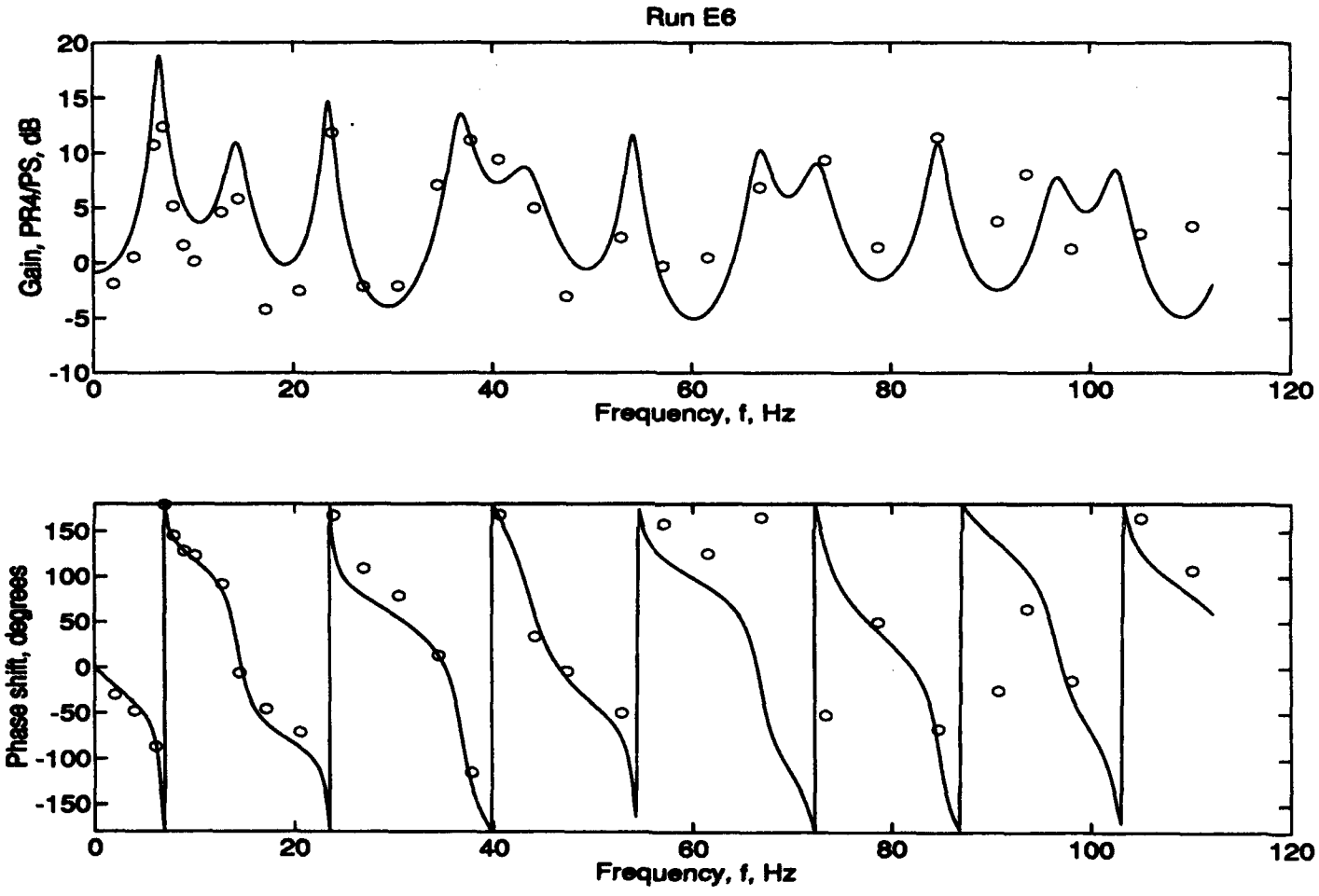

Figure 7.6. Model Frequency Response (PR4) with Washers for R_c = ½R3. Conditions: R_c = 3/64 in, $\dot{m}$ = 2.3 X 10^{-6} slug/s, basic length, washers.

Figure 7.7 shows the model response for washers in section 2 and the end radius open to ½R3. This plot is compared to the identical screens and honeycomb results in Figure 7.4a. For this configuration, the washer results show better agreement with theory for PR4/PS than the screens and honeycomb results. Near the flow conditioners (PR3 and PR2) both configurations again show excellent agreement with theory (Figures A.24 and A.25).

Finally, Figure 7.8 illustrates the model response for PR4 with washers in section 2 and the end radius fully open to R3. These plots compare with Figure 7.5a. In this case, neither configuration shows better agreement with theory than the other for any of the three transducer locations. PR2/PS and PR3/PS plots are in Appendix A, Figures A.26 and A.27.

The data appear to be independent of the flow conditioning elements as no one configuration is better matched to theory than another. The reason the flow conditioning elements do not affect the solution is because the impedance presented by these elements is small in comparison to the area changes that occur between sections of the facility. Under no throughflow conditions, since the area reductions are small, the flow straightening elements are virtually nonexistent and do not affect the analytical model. Unfortunately, this conclusion sheds no light on whether or not the area reductions are correct models for the flow

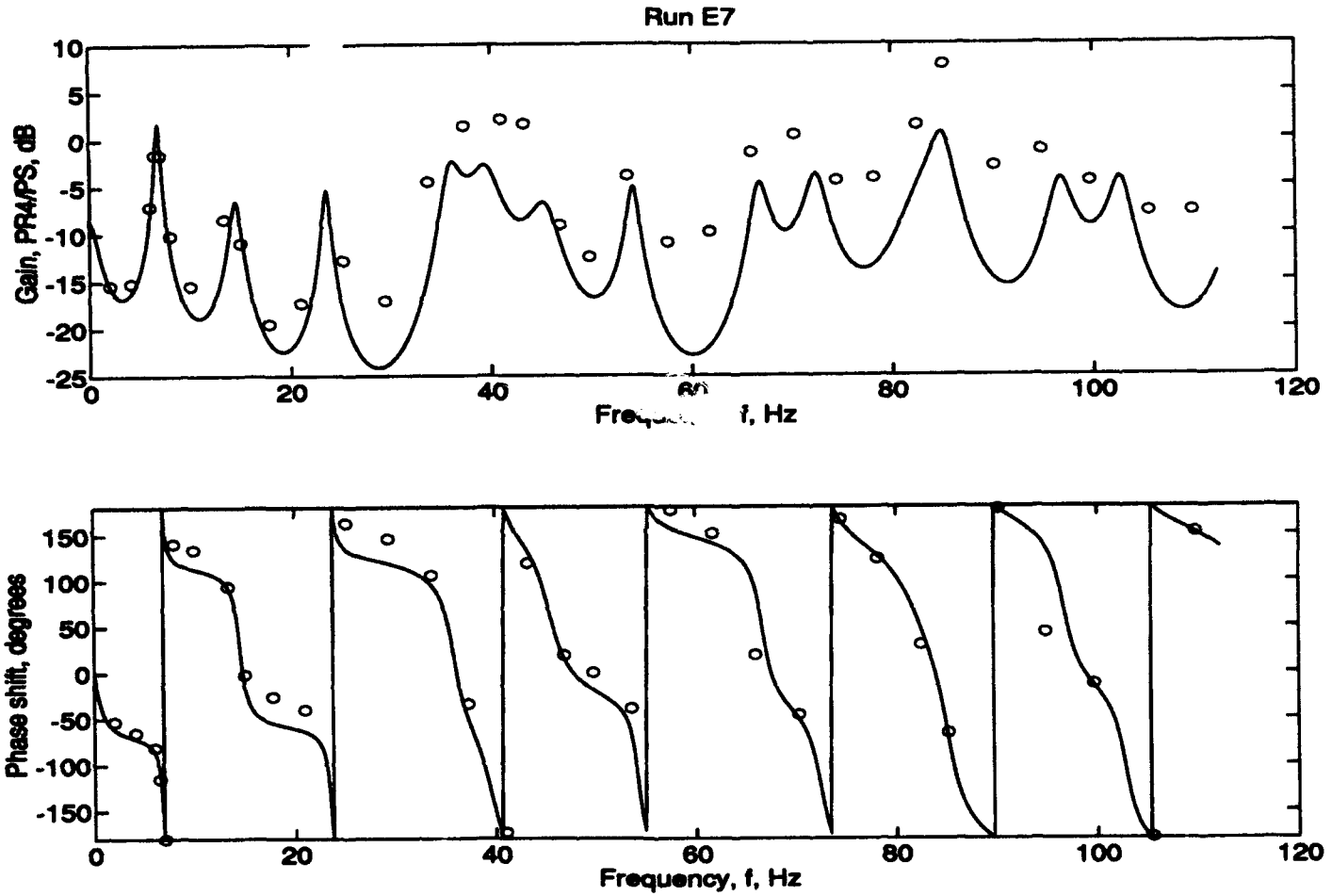

Figure 7.7. Model Frequency Response (PR4) with Washers for R_c = ½R3. Conditions: R_c = 3/32 in, $\dot{m}$ = 2.3 X 10^{-6} slug/s, basic length, washers.

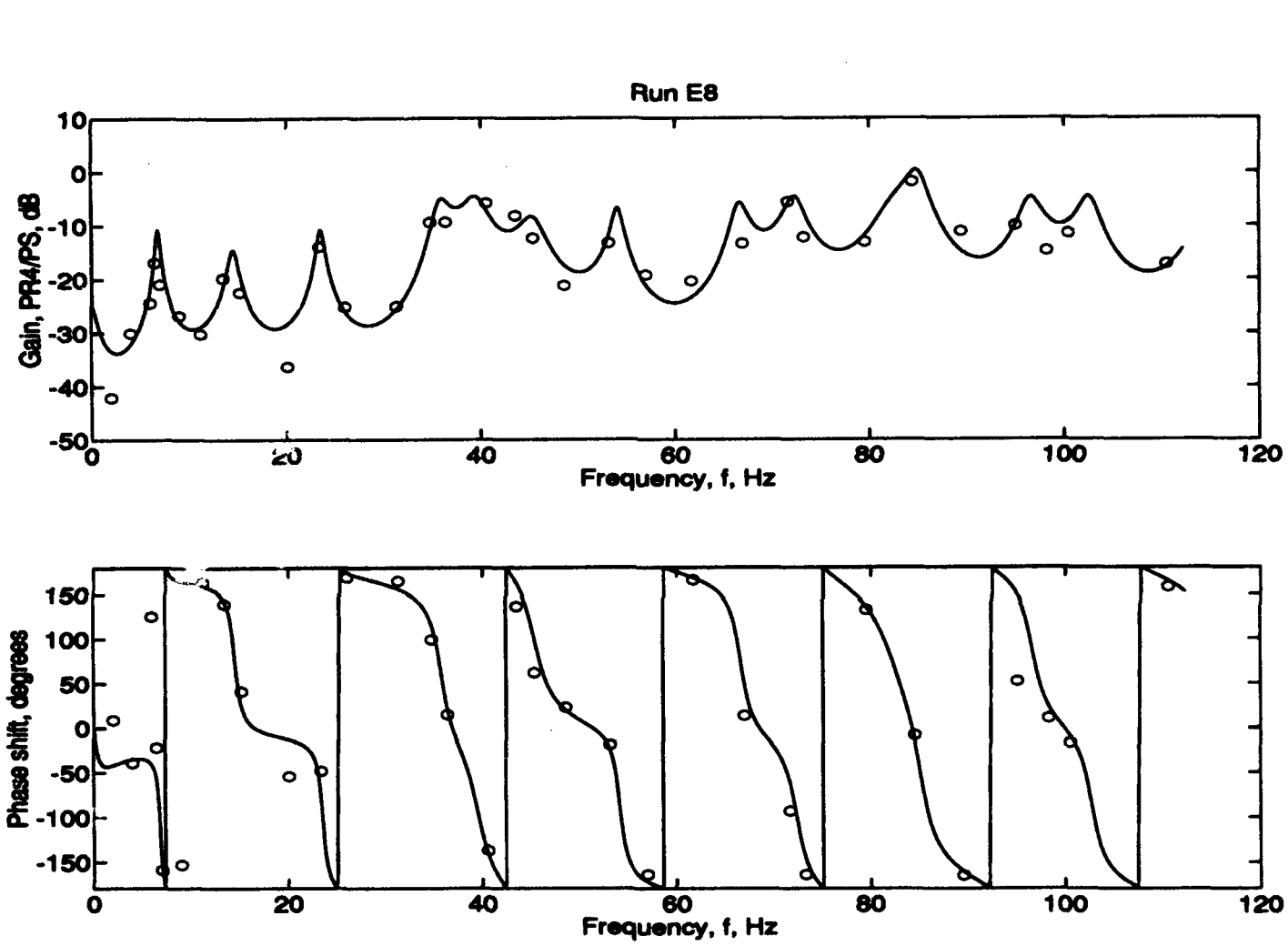

Figure 7.8. Model Frequency Response (PR4) with Washers for R_c = R3. Conditions: R_c = 3/16 in, $\dot{m}$ = 2.3 X 10^{-6} slug/s, basic length, washers.

conditioning elements. Data was taken with the screen only flow conditioning element section; however, the results differ little from the screen and honeycomb results. Therefore, the screen plots are not presented.

7.4 Model Response with Throughflow

In this section, model results are presented for the basic length configuration with screens and honeycomb installed for the flow conditioning elements and throughflow present in the system. Three experimental runs are presented, each for a different end radius. The experimental conditions are similar to the conditions for the results shown in section 7.2.2 - 7.2.4 except for the additional variable of throughflow. For the results presented in the following paragraphs, signal propagation is affected by the velocity of the throughflow. The velocity of the waves propagating in the direction of the throughflow are traveling at the speed of sound plus the throughflow velocity. Waves propagating against the direction of throughflow are traveling at a velocity of the speed of sound minus the throughflow velocity.

The results in Figures 7.9a through 7.9c are for an end radius of ¼R3 and a mass flow rate of 8.8×10^{-5} slug/s. This flow rate corresponds to a velocity of 31.7 ft/s in section 3 of the model. This velocity corresponds to a mass flow of 28

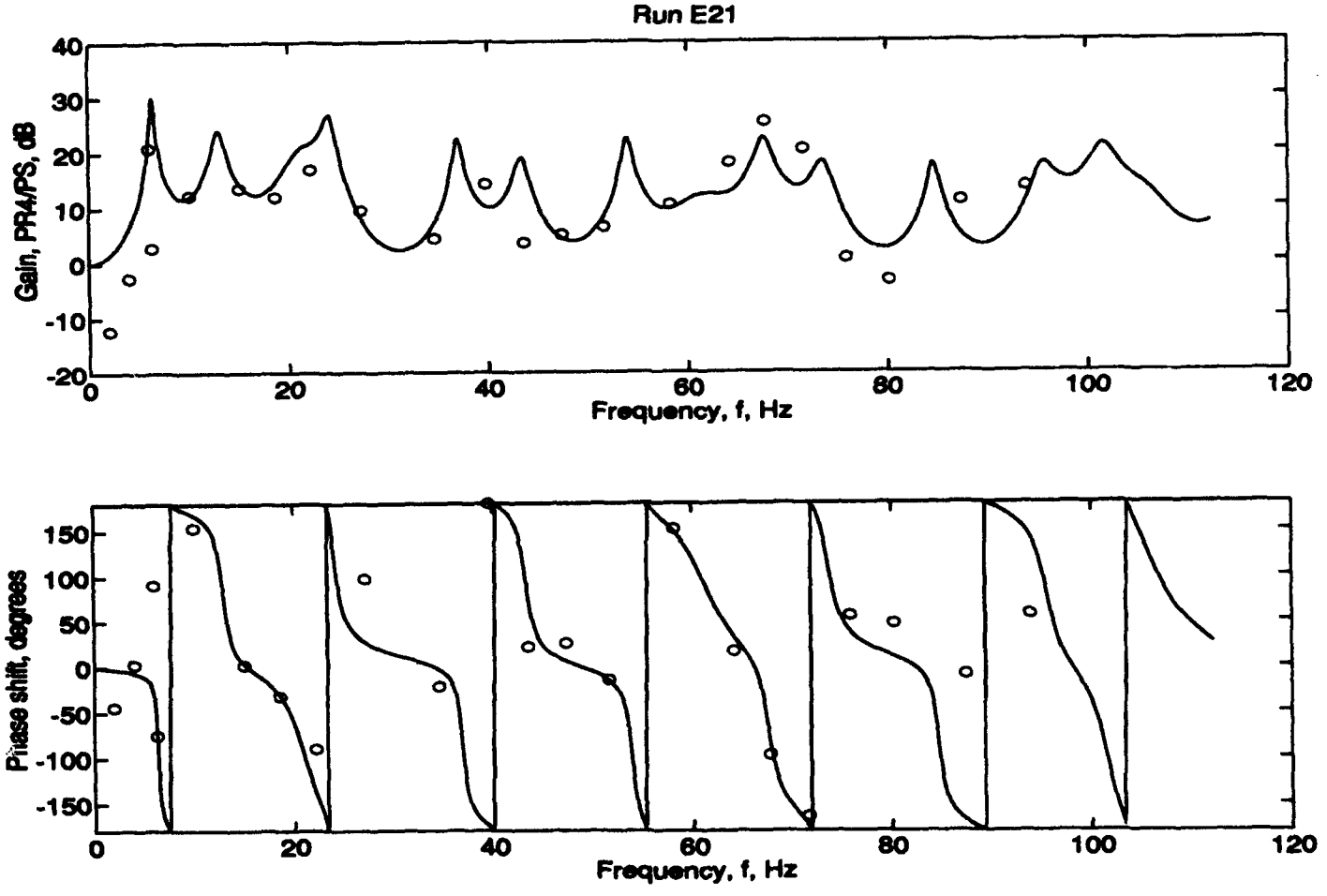

Figure 7.9a. Model Throughflow Frequency Response (PR4) for R_c = ½R3. Conditions: R_c = 3/64 in, $\dot{m}$ = 8.8 X 10^{-5} slug/s, basic length, screens and honeycomb.

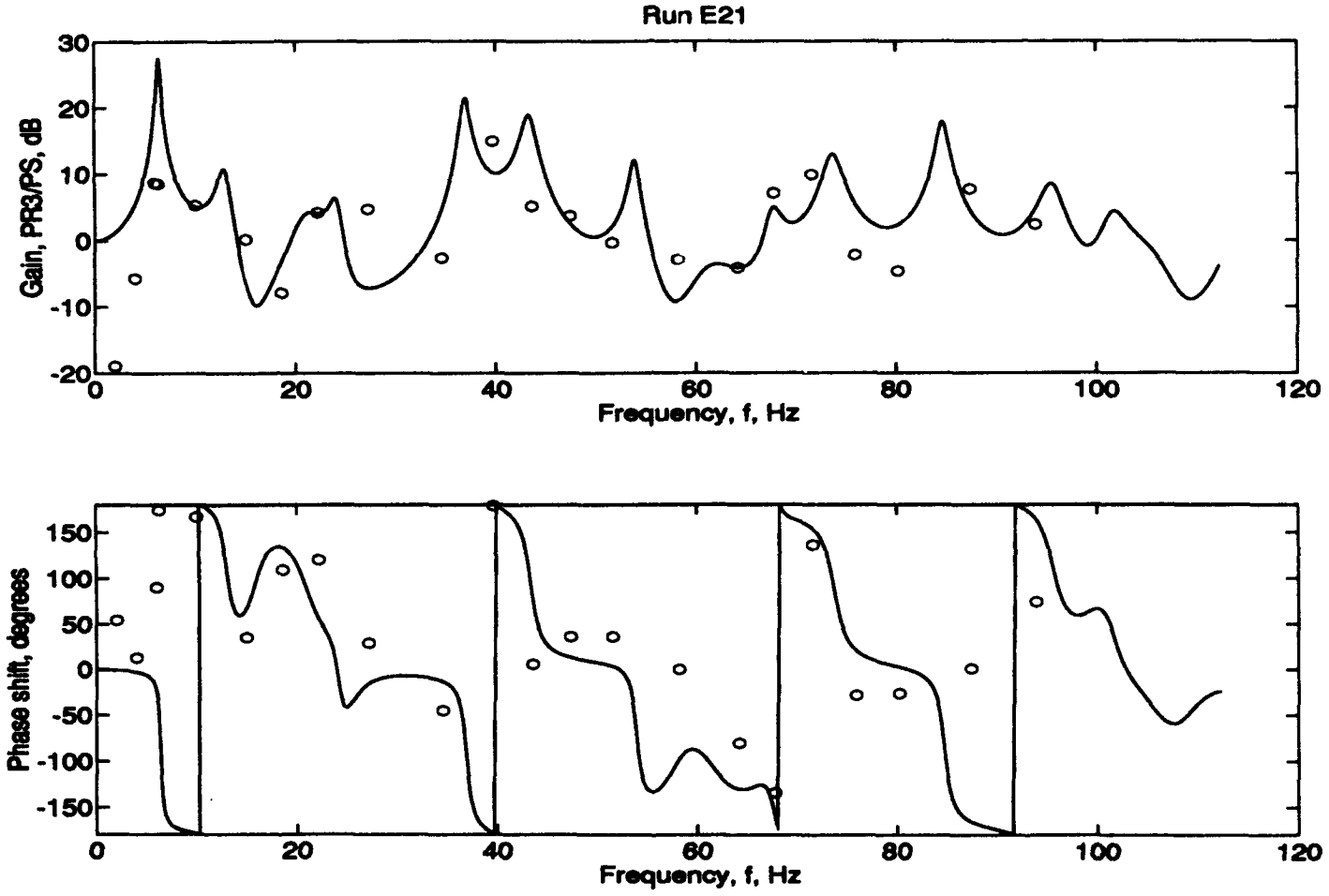

Figure 7.9b. Model Throughflow Frequency Response (PR3) for R_c = ¼R3. Conditions: R_c = 3/64 in, $\dot{m}$ = 8.8 X 10^{-5} slug/s, basic length, screens and honeycomb.

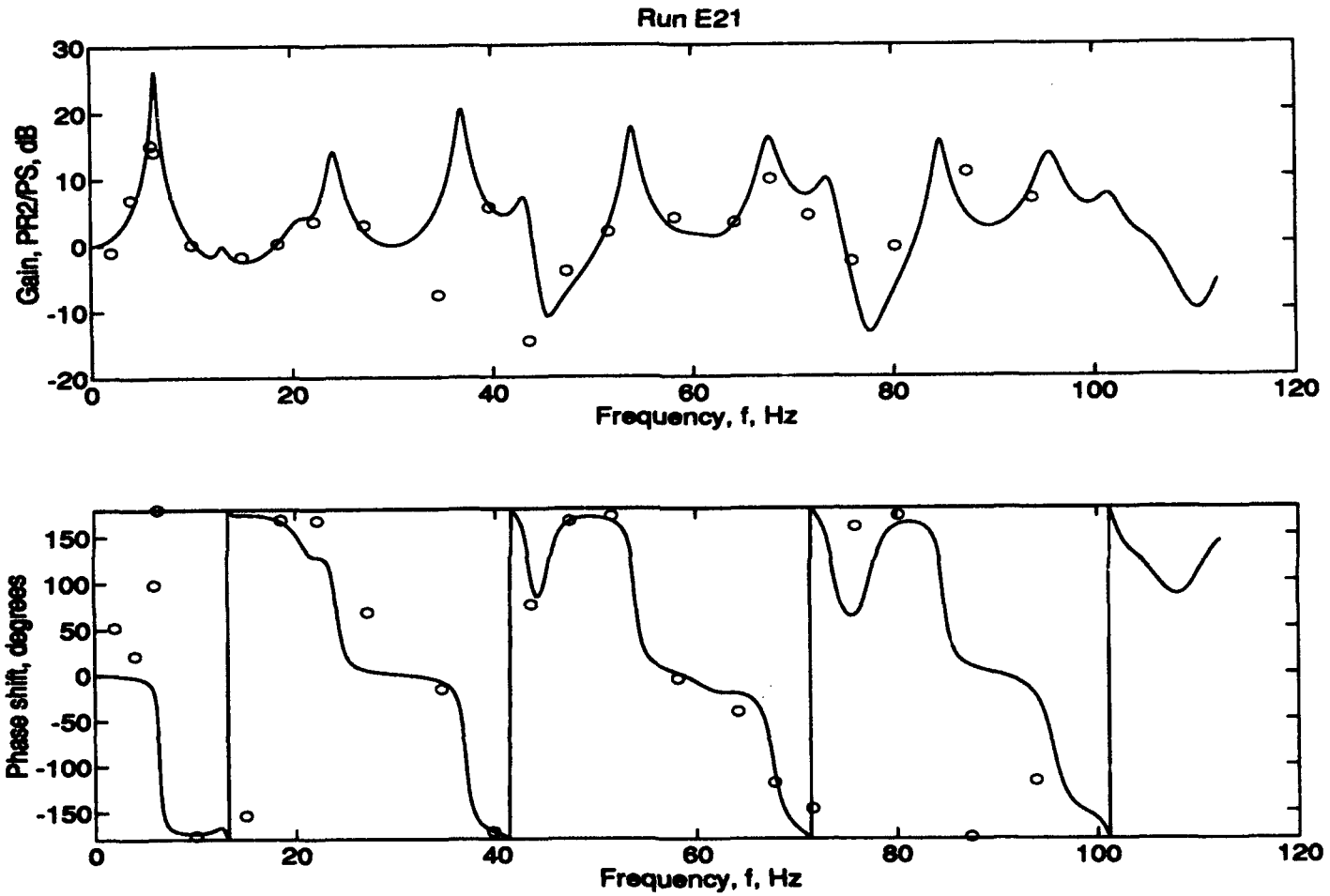

Figure 7.9c. Model Throughflow Frequency Response (PR2) for R_c = ½R3. Conditions: R_c = 3/64 in, $\dot{m}$ = 8.8 X 10^{-5} slug/s, basic length, screens and honeycomb.

lbm/s in the full-scale facility and is therefore similar to the 20 lbm/s analyses presented in Chapter VI.

Note the fairly good agreement of theory with the data for PR4 and PR2. PR3 data; however, does not agree with theory well at all. Recalling that PR3 is located just aft of the flow conditioning elements, it is probable that the flow is disturbed at this location and the data not very reliable. Since the transducers are configured to read any pressure changes in the line, any fluctuating pressure signal will be picked up by PR3. It is well known that screens cause a large pressure drop (Rae and Pope:74). It is likely that the pressure drop across the flow conditioning elements is unsteady and this fluctuation is picked up by the transducer. With fluctuations from the screen and throughflow interactions, the input signal is harder to distinguish when input into the spectral analysis program. This is primarily a local effect since PR2 data agrees well with theory and PR4 data is more dependent on end condition than flow quality.

Comparing Figure 7.9a with the results from the same configuration without throughflow, Figure 7.3a, it is noted that for PR4/PS, the data for throughflow agrees with theory about as well as the data for the case without throughflow. This is also true for PR2 as is clear when comparing Figures 7.8c and 7.3c. Also, the fundamental frequency is reduced from 6.6 Hz, for the no throughflow case, to 6.3 Hz for the

results with throughflow. Further, the peak levels are higher with throughflow than without. Both the lower frequency and the higher peaks are indicative of higher end impedance. This is indeed the case, as the end impedance for the throughflow case, computed from Equations (2-15) and (2-16), is 500 times higher than for the no throughflow case. The mass flow, then, does affect both the peaks and frequencies of the physical model.

Figures 7.10a through 7.10c show the data and analysis for the ½R3 case. Again the data shows good agreement with theory and when compared to the identical no throughflow cases in Figures 7.4a through 7.4c. The analysis for PR4/PS are slightly different for the no throughflow case in Figure 7.4a than for the throughflow case of 7.10a. Specifically, the throughflow PR4/PS curves illustrate higher gains. The fact that the data agrees with theory in both throughflow and no throughflow cases means that the model is sensitive to the changes in conditions of the flow. Note that in the throughflow case, PR4/PS data matches more closely with the analysis than in the case without throughflow. Also, PR3 and PR2 data more closely agree with theory than in the ¼R3 case, even though the theoretical curves from the two locations change very little from the no throughflow curves.

For this experiment, the mass flow is 1.73×10^{-4} slug/s and the velocities in sections 1, 2, and 3 are 2.4 ft/s, 9.7

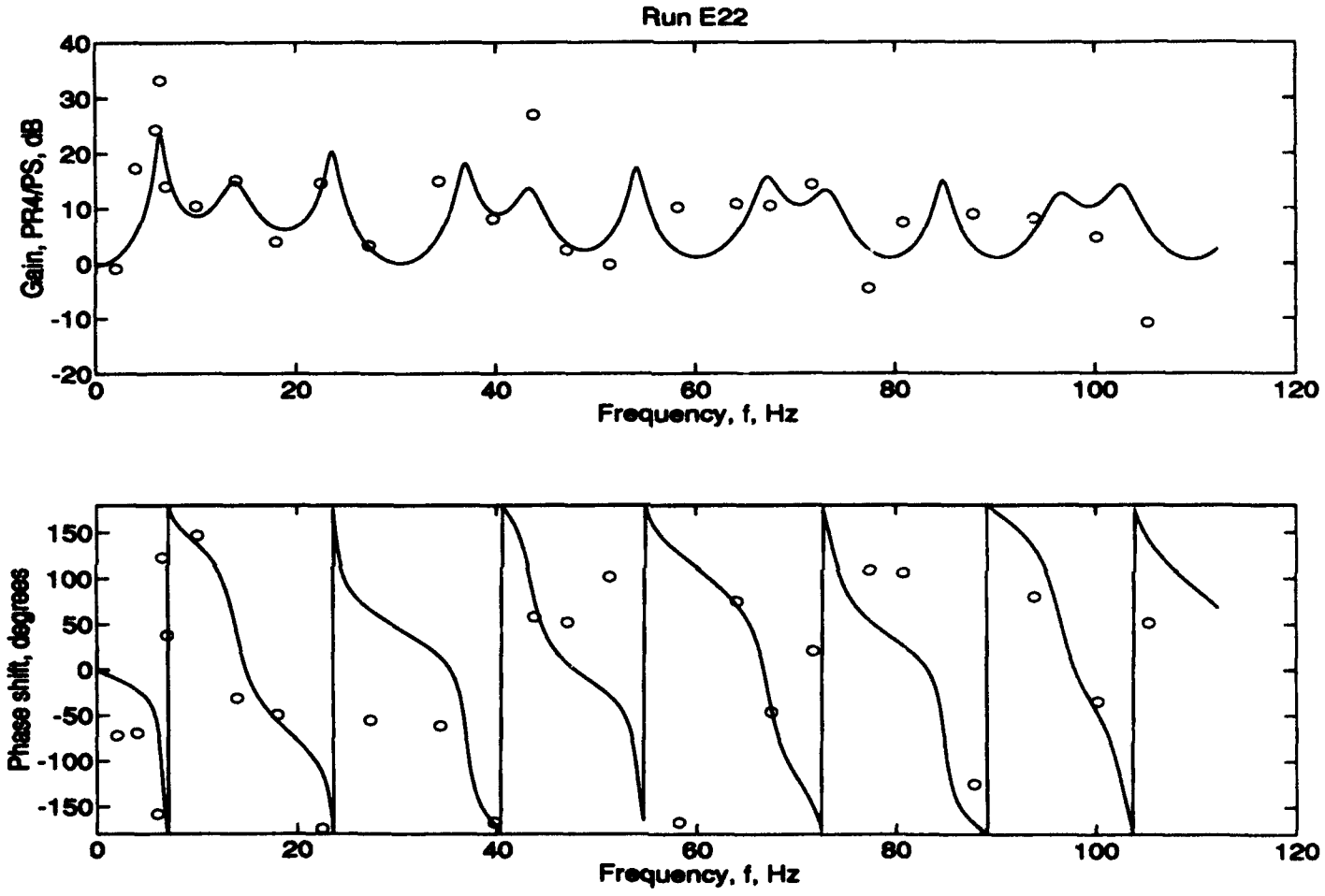

Figure 7.10a. Model Throughflow Frequency Response (PR4) for R_c = ½R3. Conditions: R_c = 3/32 in, $\dot{m}$ = 1.73 X 10^{-4} slug/s, basic length, screens and honeycomb.

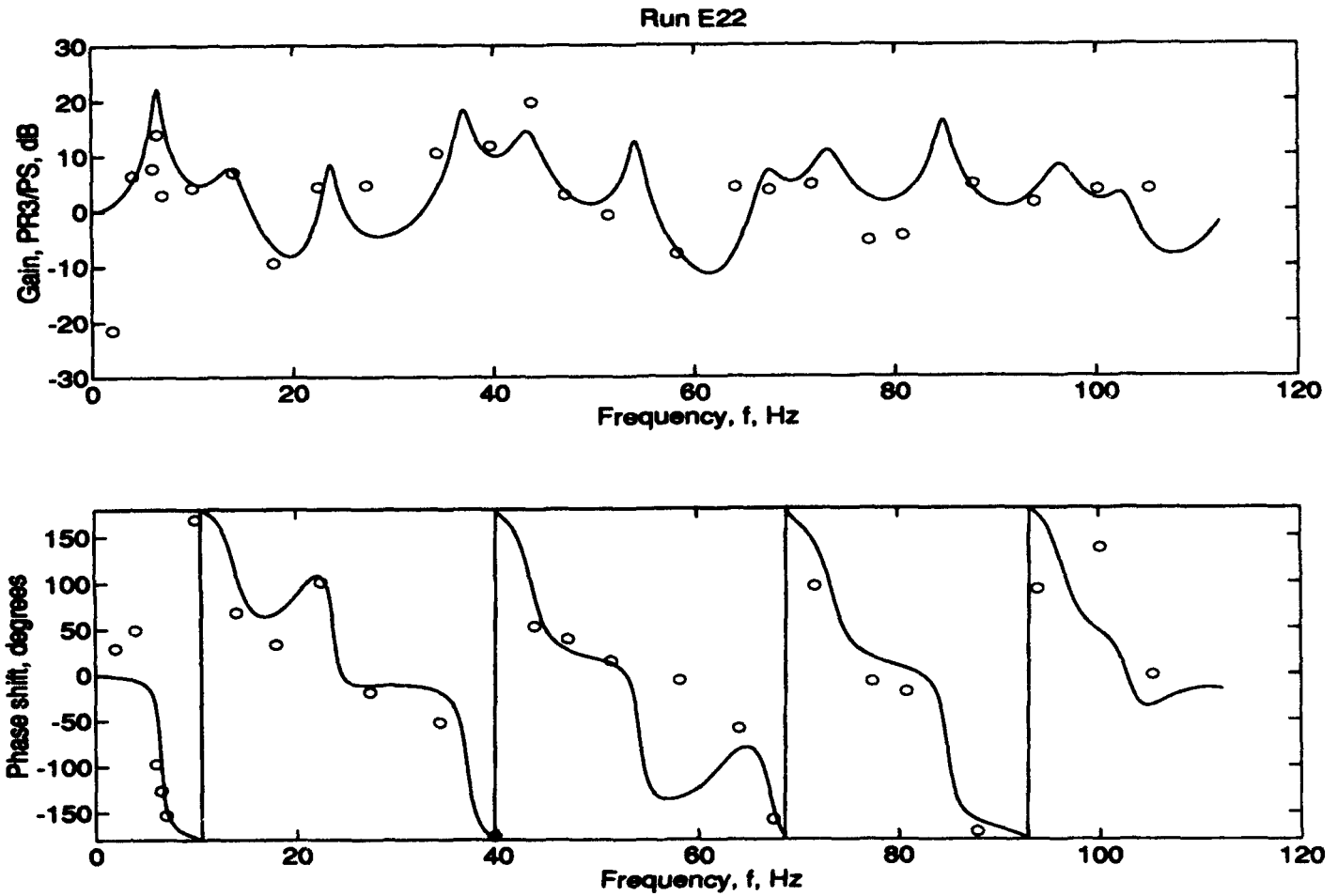

Figure 7.10b. Model Throughflow Frequency Response (PR3) for R_c = ½R3. Conditions: R_c = 3/32 in, $\dot{m}$ = 1.73 X 10^{-4} slug/s, basic length, screens and honeycomb.

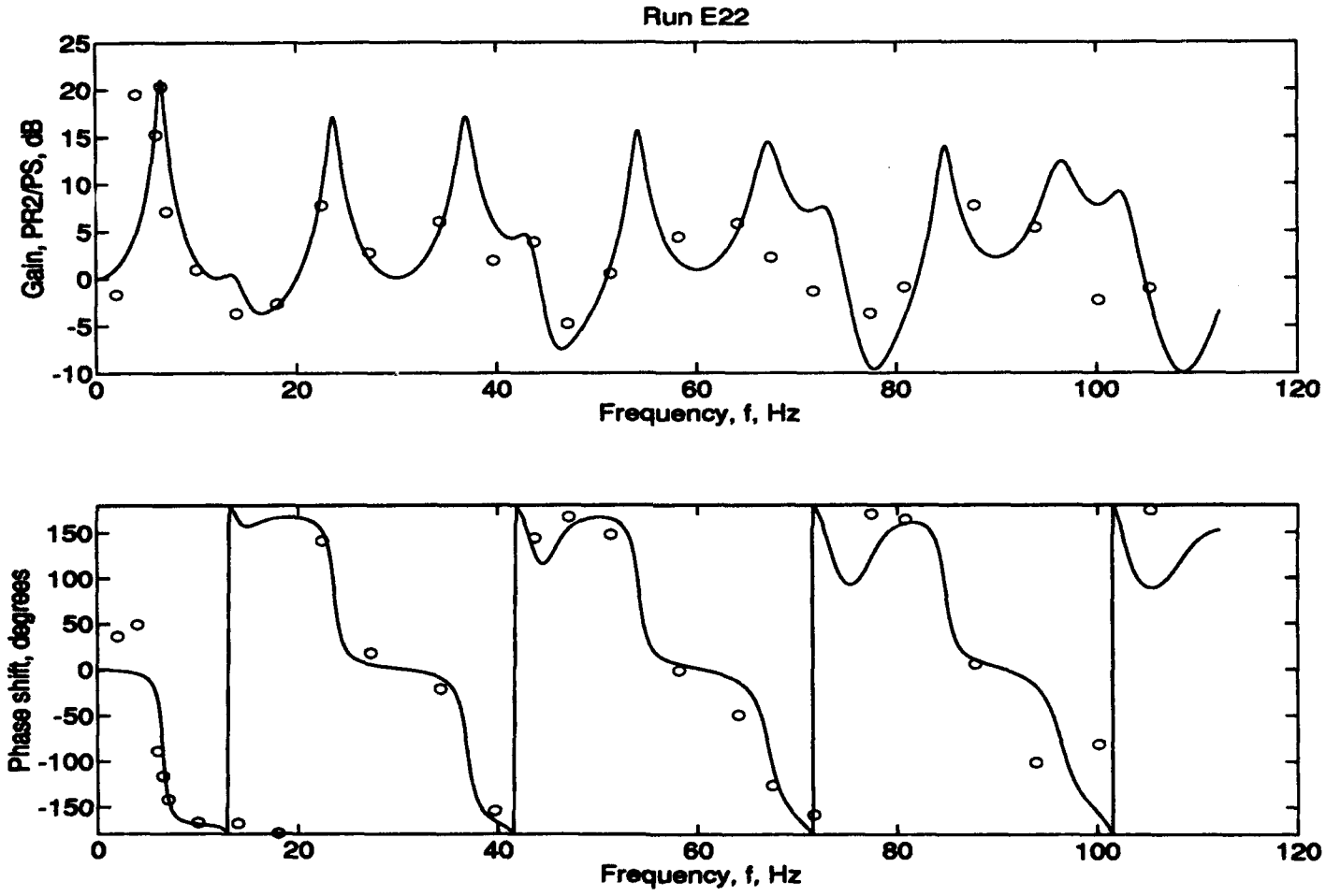

Figure 7.10c. Model Throughflow Frequency Response (PR2) for R_c = ½R3. Conditions: R_c = 3/32 in, $\dot{m}$ = 1.73 X 10^{-4} slug/s, basic length, screens and honeycomb.

ft/s, and 69.2 ft/s, respectively. The same section 3 velocity in the CRF corresponds to a mass flow of 60 lbm/s in the full-scale facility.

Compared with the conditions for the results in Figures 9a through 9c, the mass flow is increased and the end condition more open. This lowers the real part of the end impedance [Equation (2-15)]; however, it is still 680 times higher than the end impedance for the case without flow. As was the case with the ¼R3 end radius results, the fundamental frequency drops when flow is introduced. In this case, the fundamental frequency is 6.4 Hz for the results with flow and 6.7 Hz for the results without flow.

The last three Figures, 7.11a through 7.11c, are for an end radius of ¾R3. In this case, the mass flow is 2.2×10^{-4} slug/s and the velocity in section 3 is 90.5 ft/s. This velocity is most representative of flow conditions that would be seen in the full-scale facility. Specifically, this velocity in section 3 corresponds to a 80 lbm/s flow rate in the full-scale facility.

These results show that as the end orifice is increased from ½R3, the analytical and experimental gains decrease for PR4/PS. The fundamental frequency increases from 6.4 Hz, for the ½R3 case, to 6.7 Hz for the ¾R3 case.

In general, the fundamental frequency data in Figures 7.9 through 7.11 do not agree as well with theory as the no

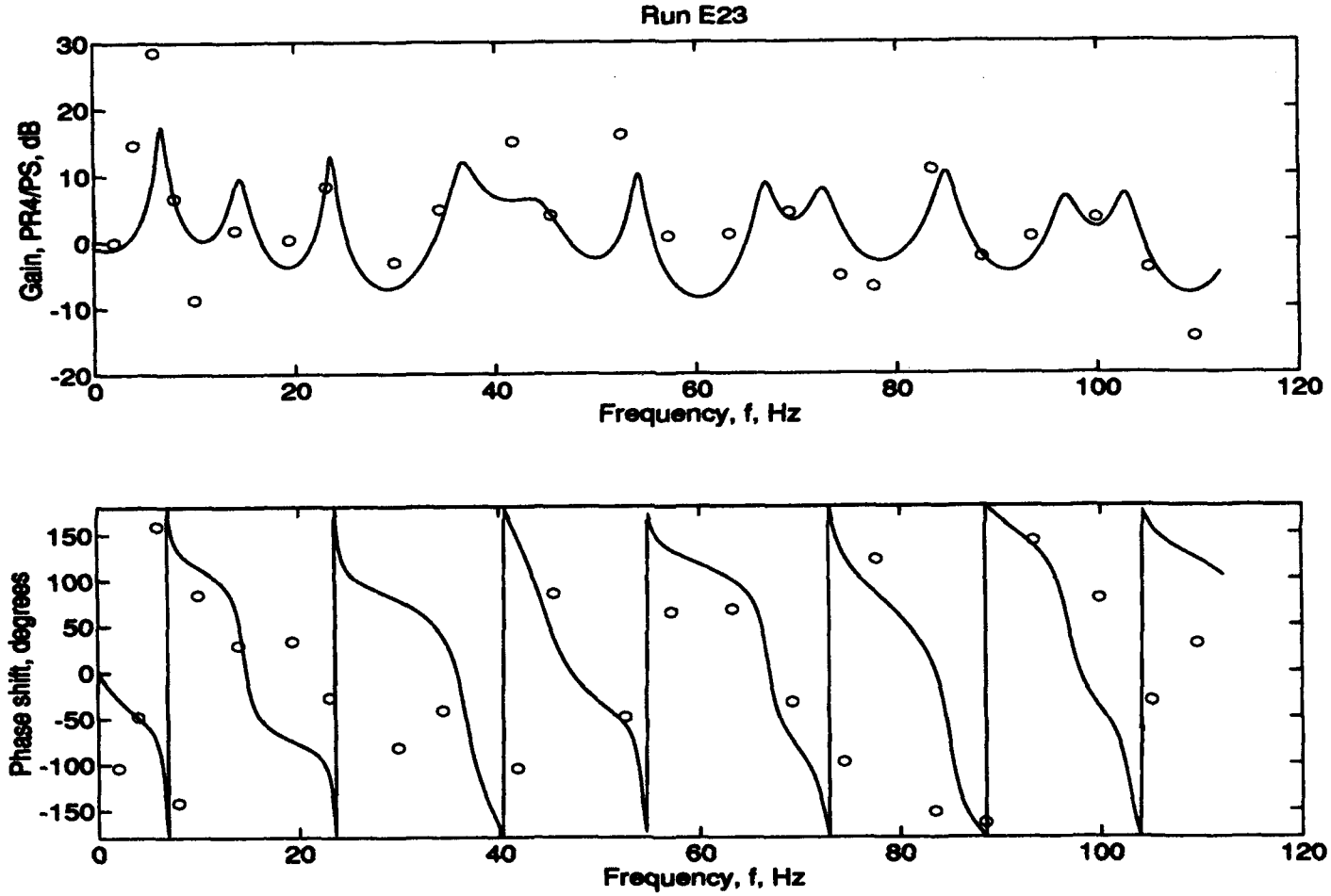

Figure 7.11a. Model Throughflow Frequency Response (PR4) for R_c = ¾R3. Conditions: R_c = 9/64 in, $\dot{m}$ = 2.2 X 10^{-4} slug/s, basic length, screens and honeycomb.

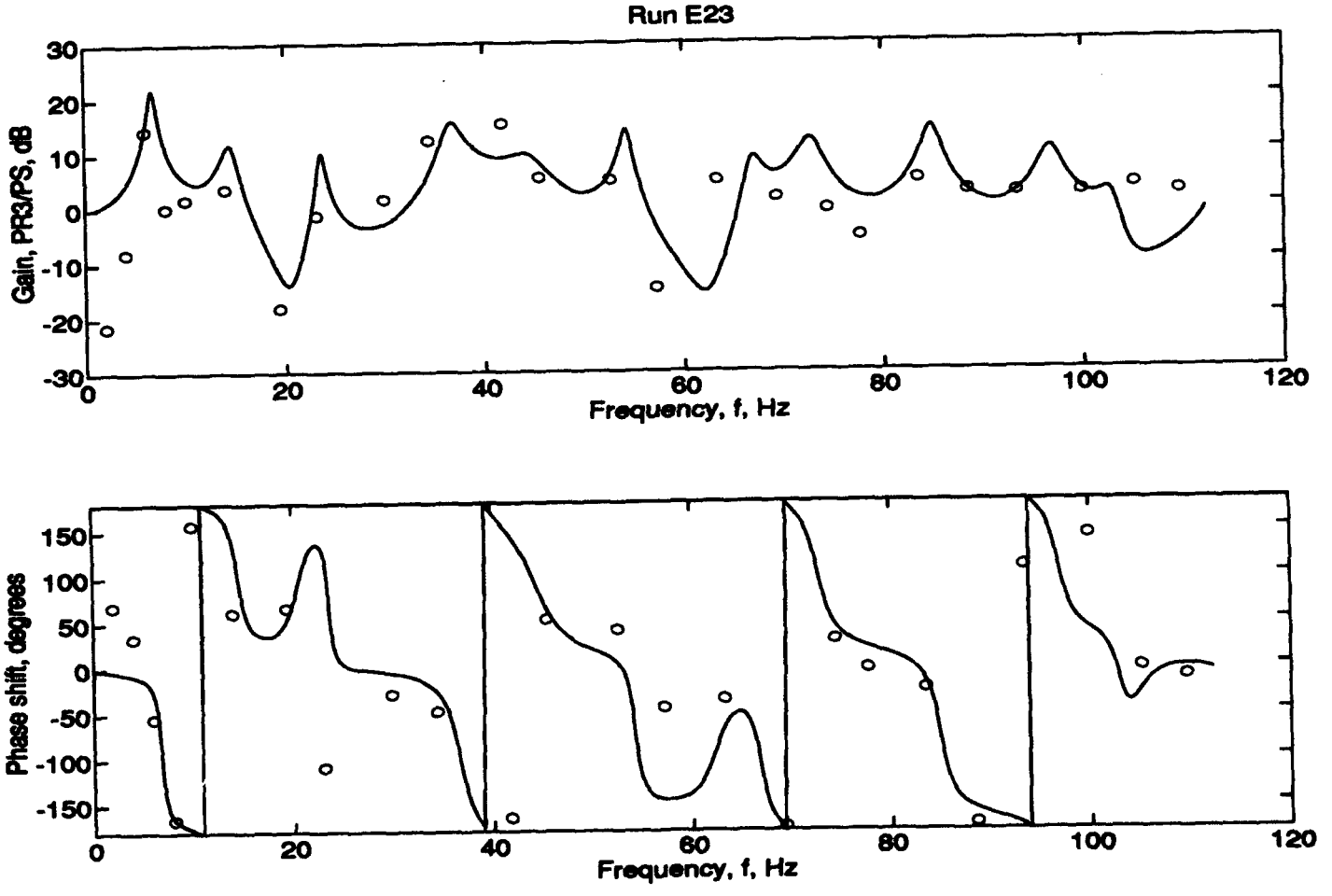

Figure 7.11b. Model Throughflow Frequency Response (PR3) for R_c = ¾R3. Conditions: R_c = 9/64 in, $\dot{m}$ = 2.2 X 10^{-4} slug/s, basic length, screens and honeycomb.

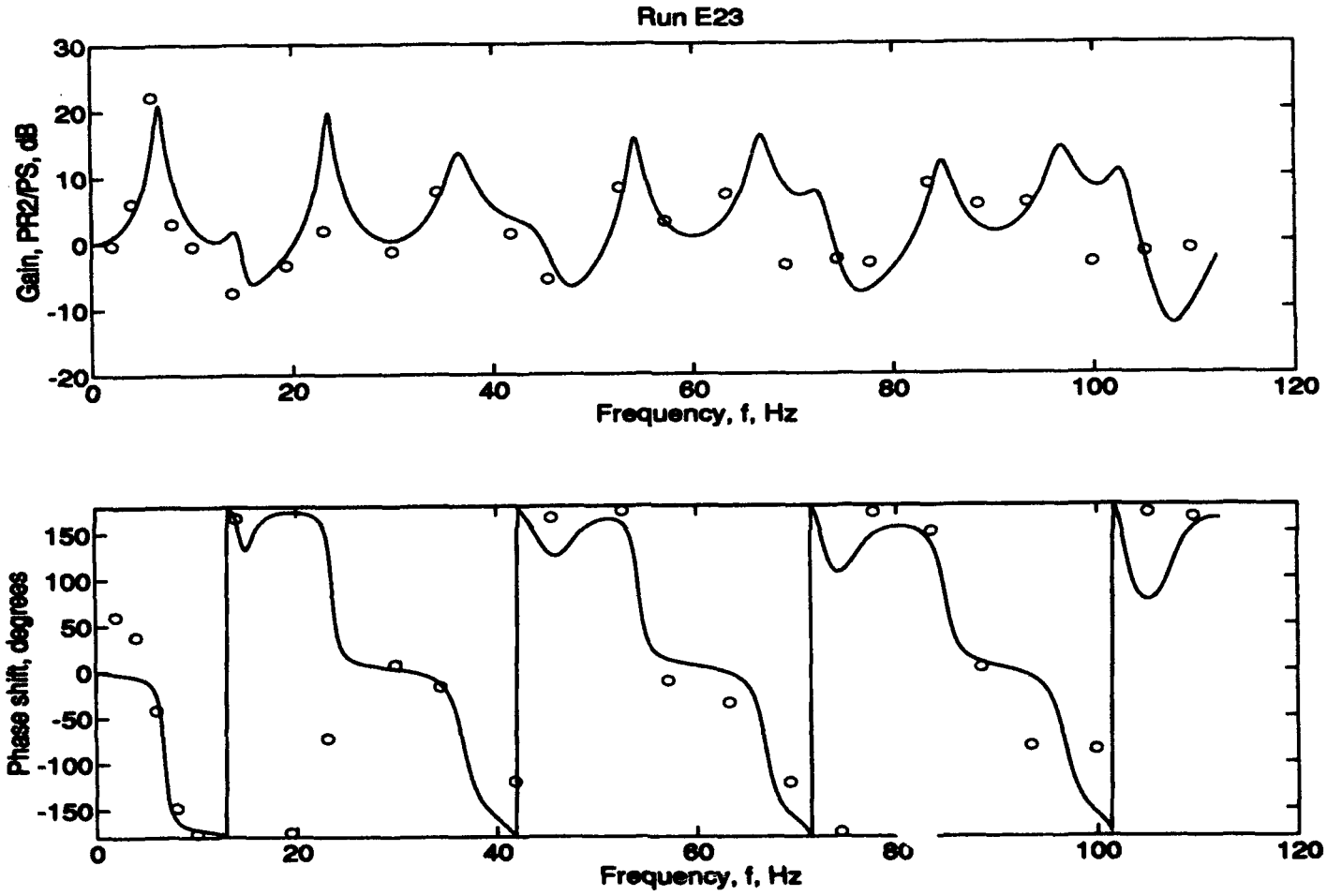

Figure 7.11c. Model Throughflow Frequency Response (PR2) for R_c = ¾R3. Conditions: R_c = 9/64 in, $\dot{m}$ = 2.2 X 10^{-4} slug/s, basic length, screens and honeycomb.

throughflow cases. Specifically, the end transducer data do not fall on the curve well at the fundamental frequencies. At low throughflow rates and high impedance (Figure 7.9), the theory overestimates the fundamental peak. At higher throughflow rates, the theory underestimates the fundamental peak. This is a result of the analysis not fully representing the physical system. Losses due to friction are computed but may not be exact, resulting in a mismatch between theory and the physical model data that is amplified when throughflow is introduced. Also, the end impedance model is only a best attempt at representing the line end and is most likely not the true representation of the end condition.

The frequency response results presented for the model support the analysis of the full-scale facility and illustrates some of the points made in Chapter VI concerning gain and frequency dependence on end impedance. Most importantly, the laboratory experiments verified that the fundamental frequency is near 6.5 Hz for the basic length case with a wide variety of flow conditions and end configurations.

Also, the model verified some trends in the analyses presented in Chapter VI. Specifically, under no throughflow conditions, opening up the end radius decreased the gains and increased the fundamental frequency for the model in the same manner as the full-scale facility. This was demonstrated both in the analysis and in the data. As with the full-scale

facility, the gains increased with increasing throughflow and the fundamental frequencies increased with increasing end radius.

7.5 Transient Response of the Model

The transient response tests were accomplished to determine the damping characteristics of the model. For the transient response tests, the model configuration includes screens and honeycomb, basic length, and an end radius of ¼R3. A solenoid valve was used to provide a positive pressure step.

The results are presented in four figures. Figure 7.12 illustrates the long time response for a 0.08 psig input step. For this pressure input and end condition, the model reaches a steady state condition in 4.5 seconds. For larger inputs, the model takes longer to reach a steady state pressure.

Figure 7.13 shows the unsteady response to the input signal at the end transducer, PR4. The valve opens at time t = - 0.06 seconds. At t = 0 seconds, the pressure is felt at the end transducer.

Initially, there is no flow in the model. At t = 0, the step function from the solenoid valve reaches the end of the line and PR4 senses the pressure rise. Immediately after the pressure front reaches the end of the line, the sudden flow constriction of the orifice causes a reflection of the front and the pressure immediately drops. The reflected wave

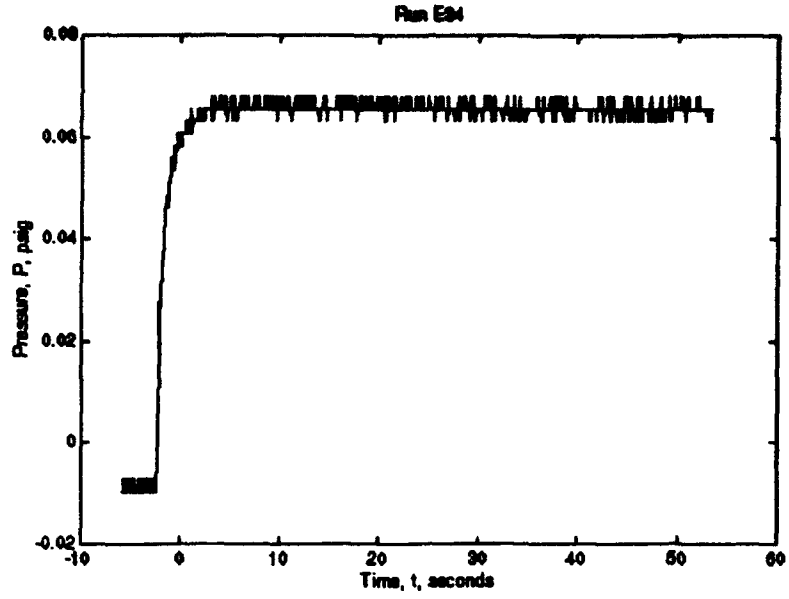

Figure 7.12: Long-Time Model Response (PR4) to a Positive Step Input. Conditions: R_c = ¼R3, basic length, screens and honeycomb.

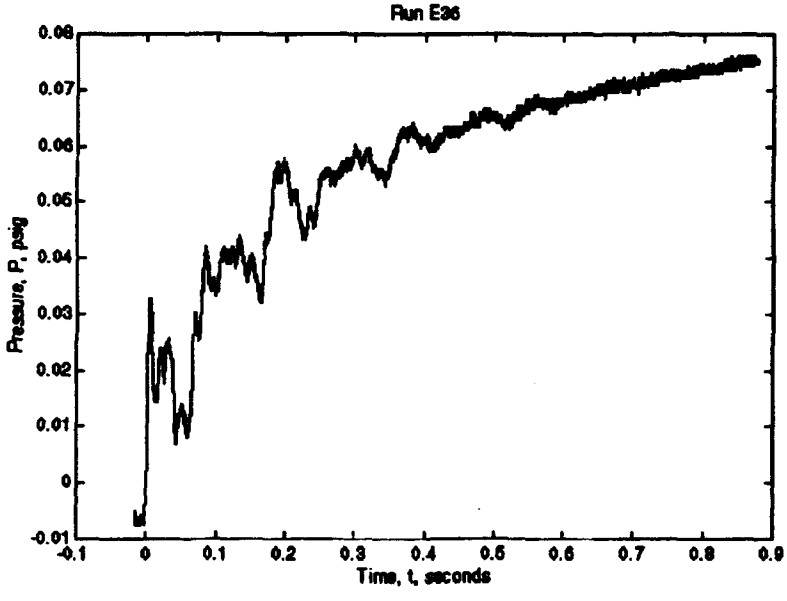

Figure 7.13: Model Transient Response (PR4) to a Small,Positive Step Input. Conditions: R_c = ¼R3, basic length, screens and honeycomb.

returns to the inlet, slightly damped from viscous interactions with the boundary layer, and reflects back to the end where PR4 again picks up its presence at time 0.12 seconds. These reflections continue until the wave is fully damped at t = 0.7 seconds. The pressure fluctuations from the wave reflecting back and forth between the inlet and exit are termed "ringing".

This pressure step, of 0.08 psig, is on the order of the pressure level of the signal introduced by the pneumatic signal generator for the frequency plots presented in the previous two sections. Figure 7.13 shows that for the small signal inputs in the frequency domain, the associated ringing is not very significant. In fact, the steady state pressure is not yet reached by the time the ringing is damped out. This means that, for the model, the transient response is controlled by the time required to reach steady state pressures and not by the ringing. This also means the model is well damped.

Figures 7.14 and 7.15 illustrate that the model also exhibits damped behavior for larger pressure steps. Figure 7.14 shows the ringing associated with a pressure step larger than 0.45 psig. Again, the ringing ceases in a short time; here, within 0.6 seconds. As with the small step, the ringing damps out before the steady state pressure is reached.

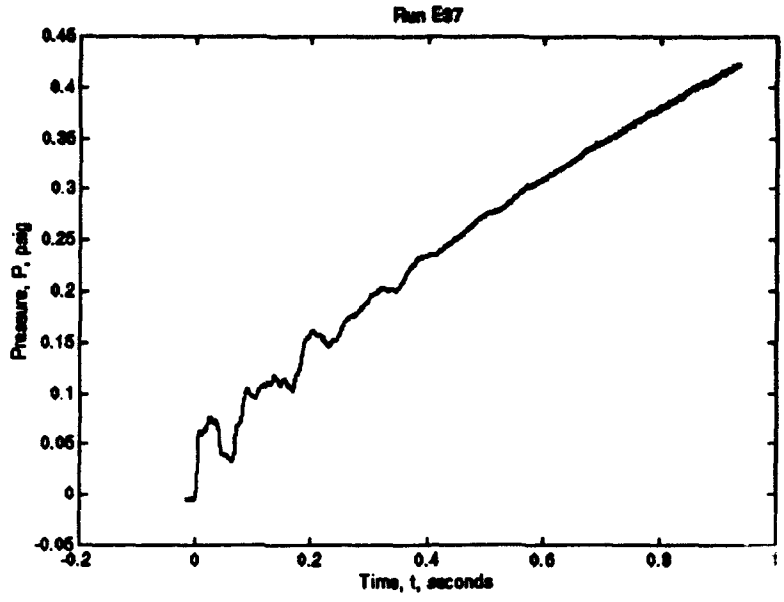

Figure 7.14: Model Transient Response (PR4) to a Large Positive Step Input. Conditions: R_c = ¼R3, basic length, screens and honeycomb, ΔP > .45 psig.

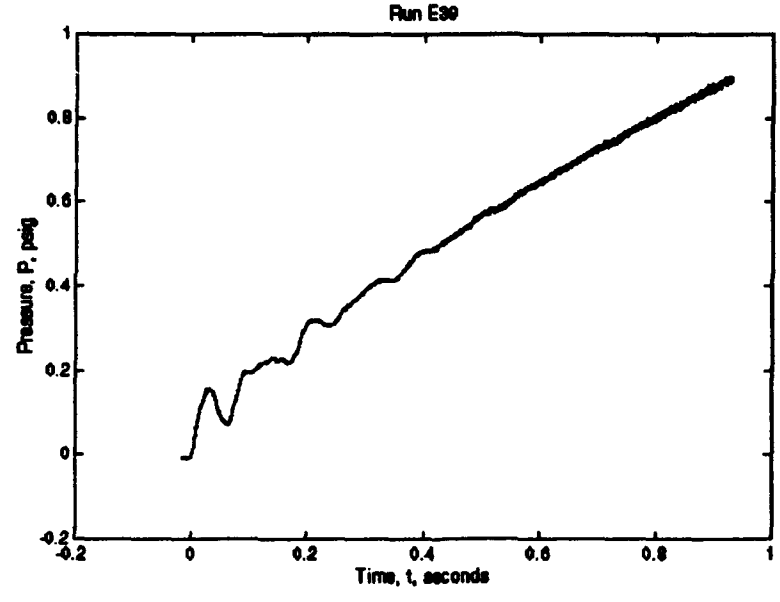

Figure 7.15: Model Transient Response (PR4) to a Very Large Positive Step Input. Conditions: R_c = ¼R3, basic length, screens and honeycomb, ΔP > 1 psig.

Figure 7.15 illustrates the ringing for an even larger pressure step, greater than 1 psig. Again the ringing ceases within 0.6 seconds and before the steady state pressure is achieved.

These results show that the model is well damped and the signal size may affect the ringing time. In Figure 7.13, with a small step, the ringing damps out in 0.7 seconds; whereas, with the larger pressure steps in Figures 7.14 and 7.15, the ringing damps out in 0.6 seconds. There is not enough evidence to make any broad statements about damping levels and signal sizes, but it is noted that the results tend to show the signal size is of some importance; particularity, the larger signals damp out more rapidly than the smaller ones.

Negative pressure step experiments were also run; however, the data is not presented here. Essentially, no ringing was observed for the negative step and therefore, the data provide no additional insight into the damping of signals in the model.

The transient analysis on the model can be loosely associated with the full-scale facility damping characteristics. In general, the model is well damped and, because of this, one might expect the full-scale facility also be well damped. Bear in mind; however, the radii of the model sections are 120 times smaller than the radii of the full-scale facility. Boundary layer interactions in the model will

be much more significant than in the full-scale facility, due to the smaller radius. As such, reflections will be damped out faster in the model than in the full-scale facility. In any case, it is not unreasonable to predict, on the basis of the model transient results, that the full-scale CRF damping is high. Further, it is reasonable to expect the input signal size is a factor in damping characteristics of the full-scale facility, just as it seems to be in the characteristics of the model damping.

As previously mentioned, the CRF damping is of significant importance to the control system design. At this time, the discussion postponed in Chapter VI is picked up again.

7.6 CRF Damping

Attempts were made by the controls designer to correlate the CRF frequency response curves presented in Chapter VI with the system damping (Hull:1993). Unfortunately, the attempt was unsuccessful. Hull's time response computations, based on the full-scale frequency response results, yielded a very lightly damped system. Several years of experience running the CRF has proven the system to be well damped (Hull:1993) and consequently, indicate error in the amplitude results of this analysis. Several sources of error are the end impedance model, the velocity adjustments to the propagation operator

and characteristic impedance, and the small pressure signal assumption. First, the errors associated with the end impedance model are discussed.

7.6.1 End Impedance Model Errors. Reviewing the results of the experimental runs, it is clear that the analysis and experimental data match up quite well for the low flow rate runs. However, it is also clear that the analysis does not correctly predict gains when the mass flow is increased. Since the experimental data yielded good agreement with theory at known end impedance conditions (blocked and fully open), this indicates that the analysis is lacking some element connected to the mass flow conditions.

The gains are dependent on mass flow in many ways; the most obvious of which is the end impedance. Recalling the results from this Chapter and Chapter VI, the end impedance has a significant effect on the amplitudes of the peaks. The overall gain of the CRF is highly dependent on the location of the end of the line as well as on the impedance model.

As was seen in section 7.2, the location of the end of the line can have a significant affect on the gains. In section 7.2, it was shown that under low flow conditions, PR4/PS gains are significantly different from PEND/PIN gains. PEN is located just 1 7/8 in downstream of PR4 and PIN is just 0.333 in upstream of PS. More study could be accomplished to

better define the end and inlet locations of the CRF, possibly resulting in different gain curves.

The end impedance model used for the full-scale analysis was determined from theory and is only a best attempt at a model. The solution was simplified by ignoring the compressor in all ways except size. Further study could be performed to more completely represent the compressor in the end impedance model and predict the peak amplitudes more accurately. If this study is performed, the velocity effects on the propagation operator and characteristic impedance should also be refined as discussed in the next section.

7.6.2 Errors with Velocity Effects. The equations used to include velocity effects [(2-17), (2-18), and (2-19)] are only an approximation. In this analysis, the approximation was used to simplify the calculations and consequently, may have contributed to the problem of high gains. Katz, Hausner, and Eisenberg (1974:282-285) present a more precise solution for including high velocities that requires simultaneous solution of the transmission line equations.

Including the velocity effects using the more precise solution may help reduce the gains. However, there is no way to estimate the extent to which the gains will decrease, if at all.

7.6.3 Validity of Governing Equation Assumptions. In order to truly present a transfer function useful to the controls designer, the governing equations must be refined to include large amplitude signals. The controls designer needs to input large pressure changes, of magnitude 2 - 5 psig. The analysis presented in this paper assumes small signals of order 2 or 3 lower than the required signal size.

The results of the transient tests with the model indicate that large pressure signals may damp out faster than small signals. Kantola (1971:279-281) has also shown this to be true. As such, an analysis for large input signals should result in lower gains than with this small signal analysis. In order to include this effect in the analysis; however, the Navier-Stokes equations cannot be linearized.

Another assumption that is most likely violated is the plane wave assumption. In lines with radii small compared to the length, such as in the model, this assumption is valid. However, in the large radii of the CRF, the signals traveling the 69.8 ft length of the line can develop disturbances in the radial direction, resulting in waves that are more spherically-shaped than plane-shaped.

VIII. Conclusion and Recommendations

8.1 Summary

The primary objective of this effort was to determine the fundamental frequency of the CRF and this was successfully accomplished. The resonant frequencies calculated for the full-scale facility were checked against basic pipe resonance equations and verified through experimental results.

8.2 Conclusion

All of the analyses place the fundamental frequency between 5.5 Hz and 6.9 Hz. The peak amplitudes for the full scale facility are questionable; however, the focus of this effort was to find the resonant frequencies and that has been accomplished.

As such, it is recommended the control system be designed, if practical, to operate at a frequency well below 5.5 Hz. This frequency occurs at the worst case conditions (Run 10.1, extended length, blocked line).

8.3 Recommendations

Future studies on the CRF, to determine the true gains, are possible if the effort is required for the control system design. Recommendations on improving the analysis for the CRF

were presented in Chapter VII and could be used to continue this study. At present; however, the control system design is proceeding without the correct gain information and, at this point, it appears that future studies on the CRF dynamic response are not required.

However, some basic studies could be accomplished to broaden the knowledge base of fluid transmission line theory. A simple fluid transmission line model could be constructed, from a single line of constant diameter, to study the effects of end impedance or the impedance presented by flow conditioning elements. In this manner, the geometry variables can be reduced, from those in the CRF model, so the research can concentrate on modeling one physical property of the fluid transmission line.

The simple model could be constructed from rigid tubing and have transducers located at the inlet and exit of the line. The frequency response of the simple model could be determined from a variety of input signals and flow conditions. From these tests, more baseline data would be gathered to use in future frequency response analyses of the type presented in this thesis.

Appendix A: Additional Data

The following pages contain additional data supporting Chapters VI and VII. Pages A-2 through A-10 contain data in support of Chapter VI. Pages A-11 through A-28 support Chapter VII.

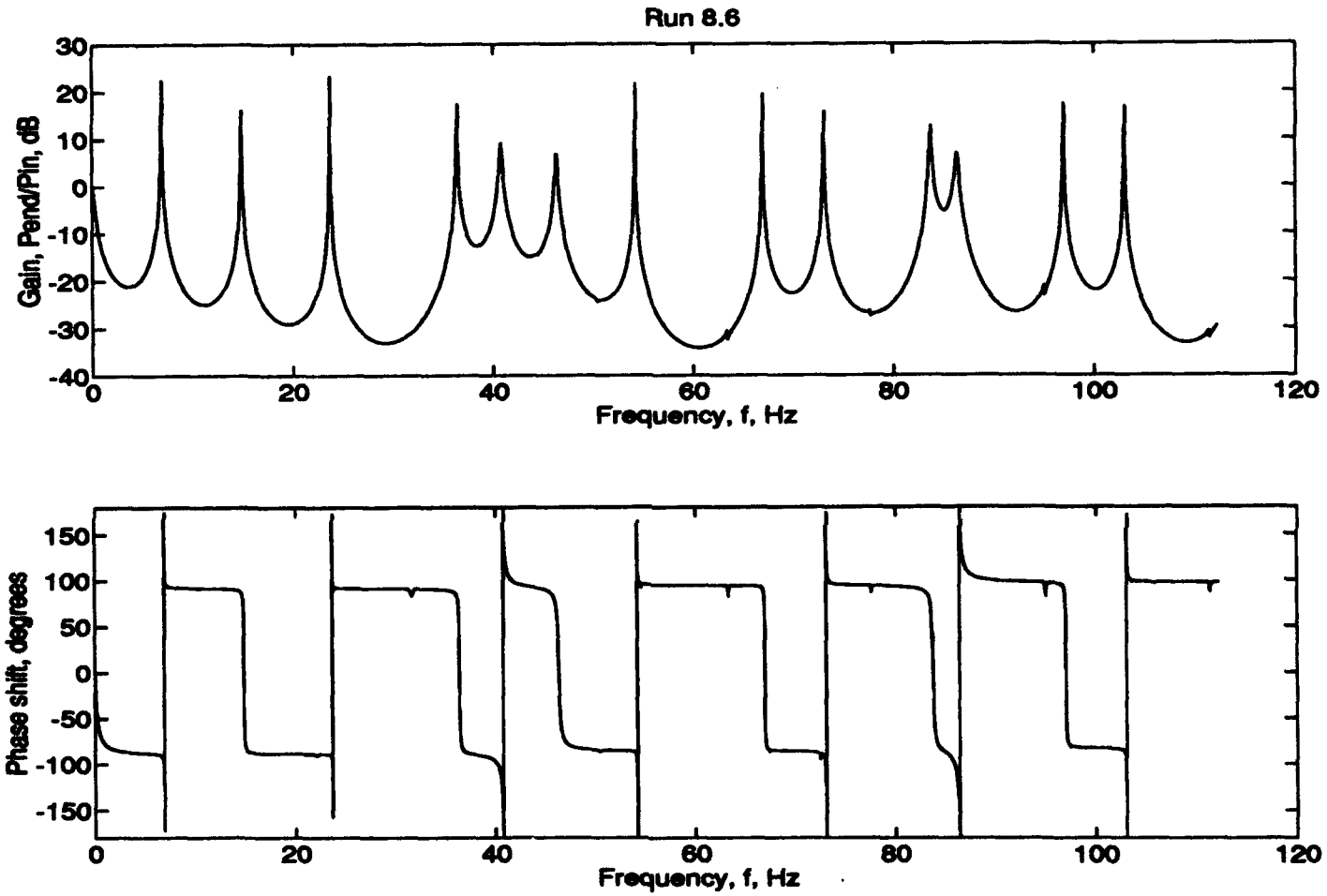

Figure A.1: CRF Response for Basic Length with 20 lbm/s Mass Flow Rate. Conditions: Run 8.6, R_c = 0.825 ft = ½R3. Fundamental Peak at 6.9 Hz.

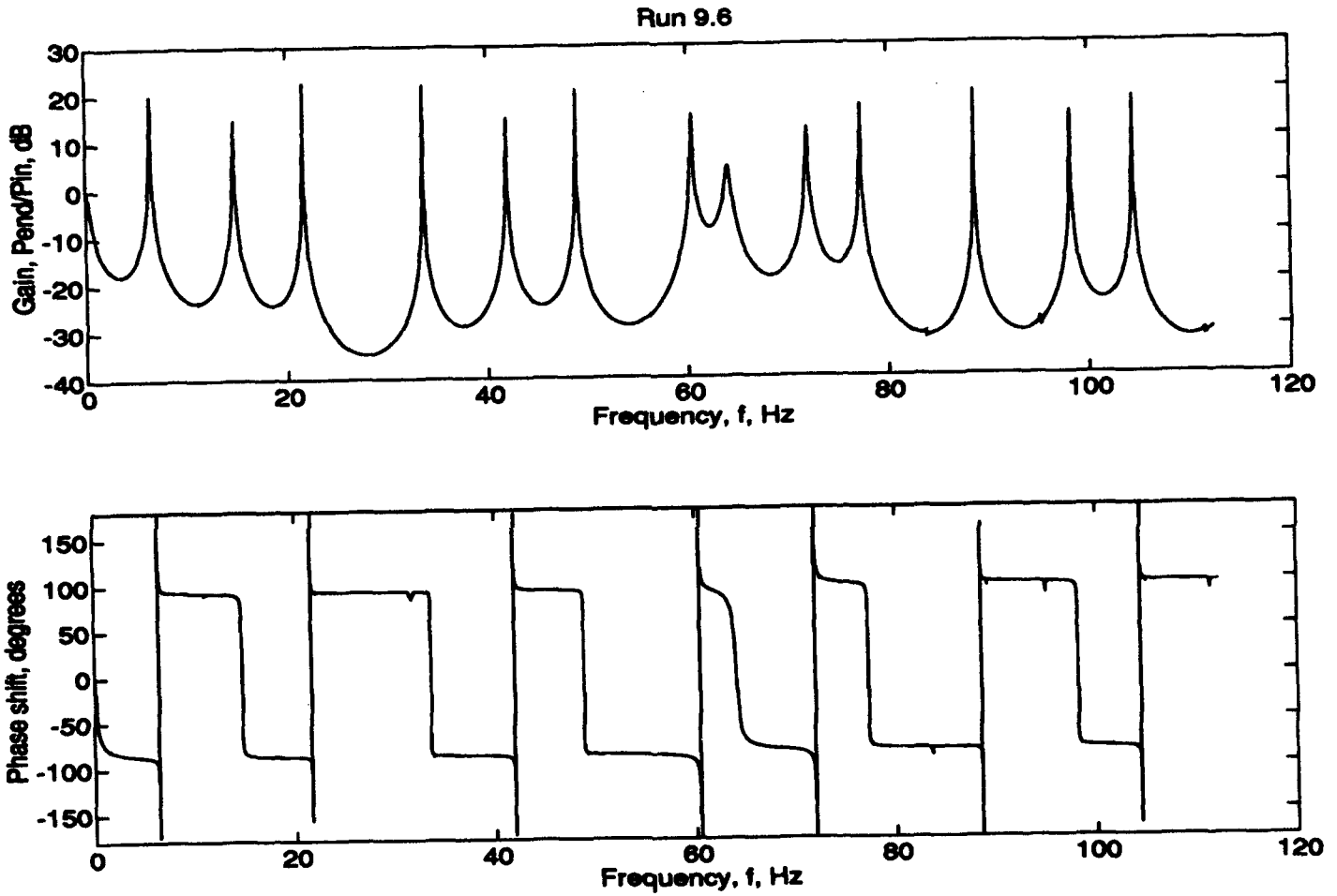

Figure A.2: CRF Response for Intermediate Length with 20 lbm/s Mass Flow Rate. Conditions: Run 9.6, R_c = 0.825 ft = ½R3. Fundamental Peak at 6.4 Hz.

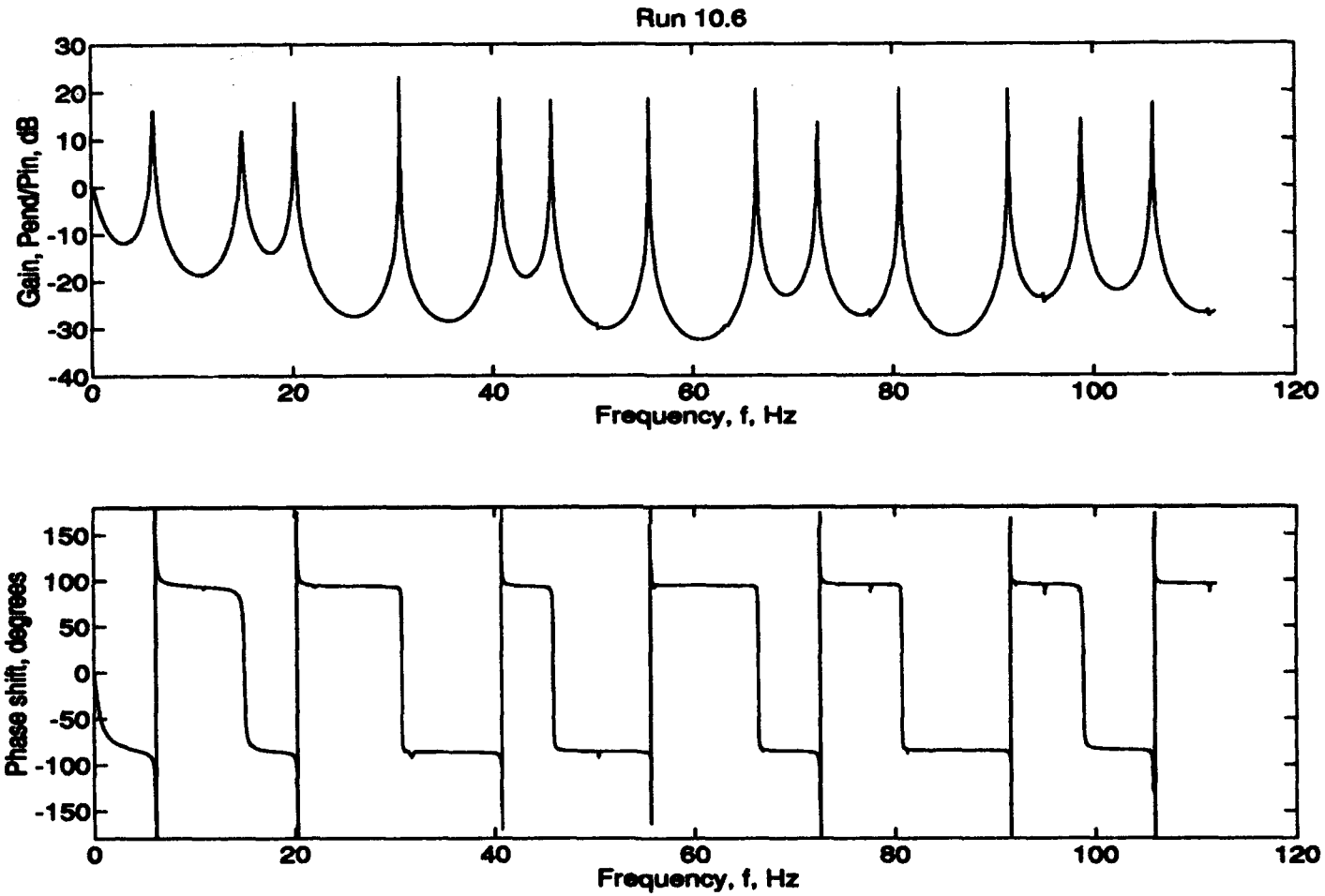

Figure A.3: CRF Response for Extended Length with 20 lbm/s Mass Flow Rate.
Conditions: Run 10.6, R_c = 0.825 ft = ½R3. Fundamental Peak at 6.1 Hz.

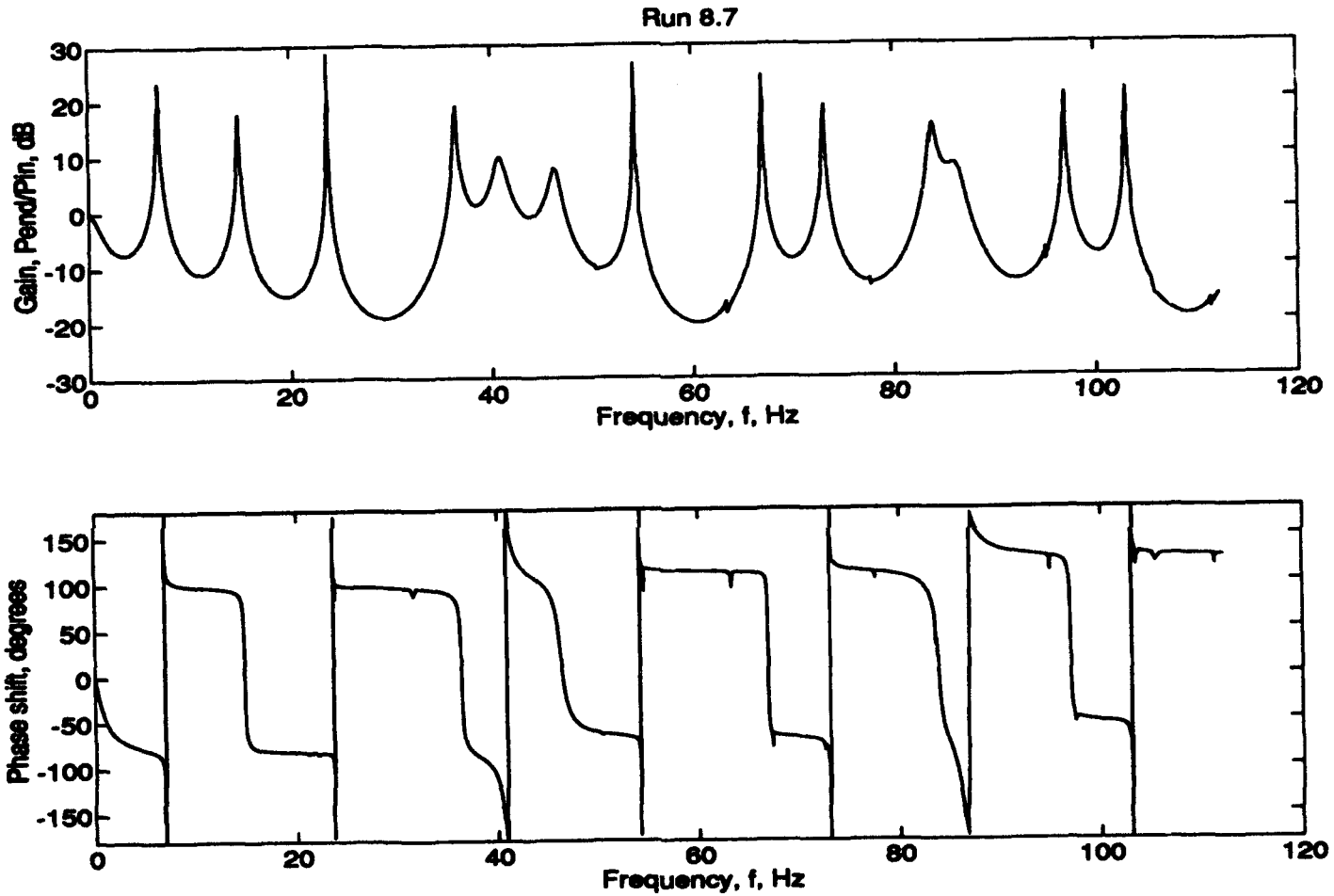

Figure A.4: CRF Response for Basic Length with 100 lbm/s Mass Flow Rate. Conditions: Run 8.7, R_c = 0.825 ft = ½R3. Fundamental Peak at 6.9 Hz.

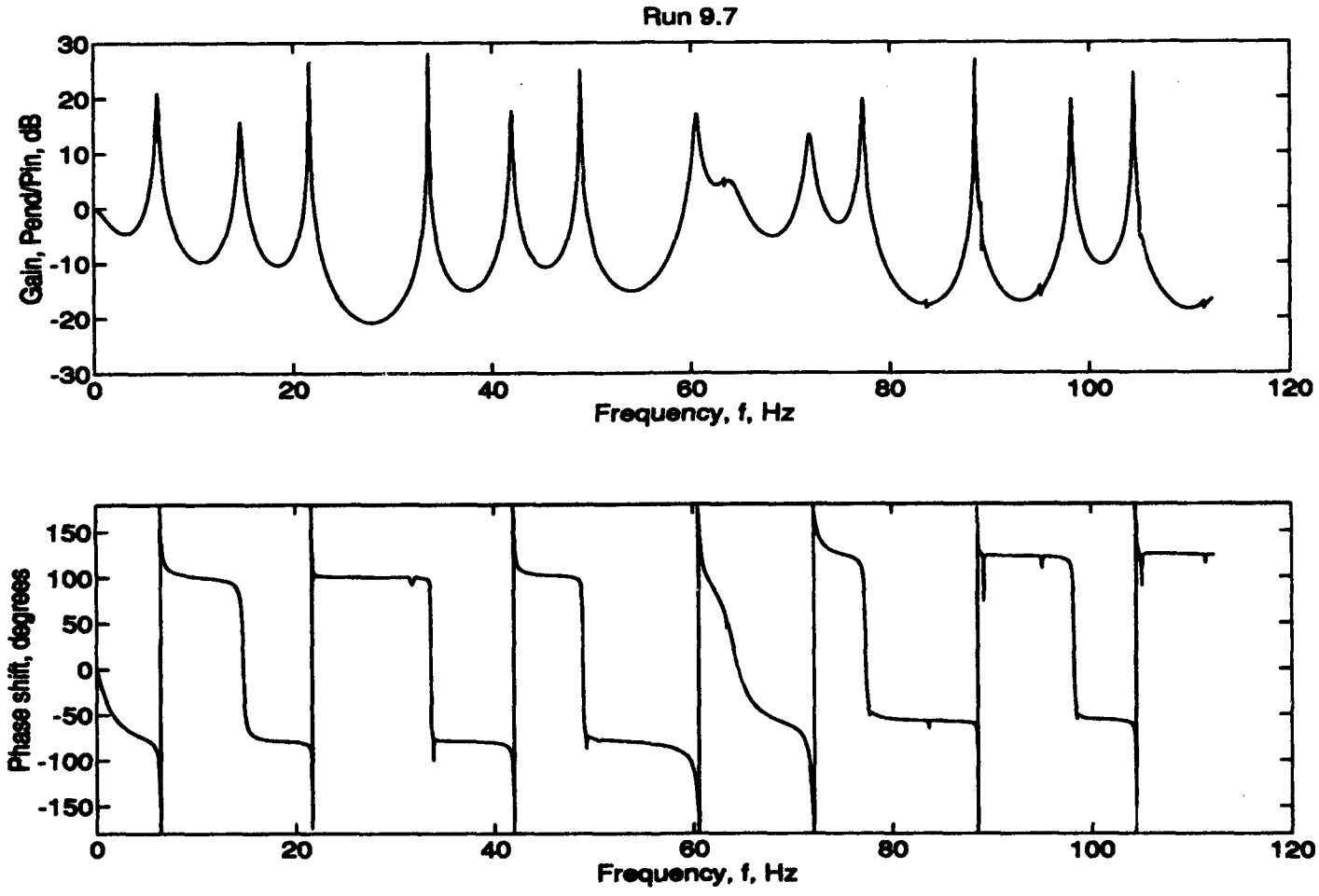

Figure A.5: CRF Response for Intermediate Length with 100 lbm/s Mass Flow Rate. Conditions: Run 9.7, R_c = 0.825 ft = ½R3. Fundamental Peak at 6.4 Hz.

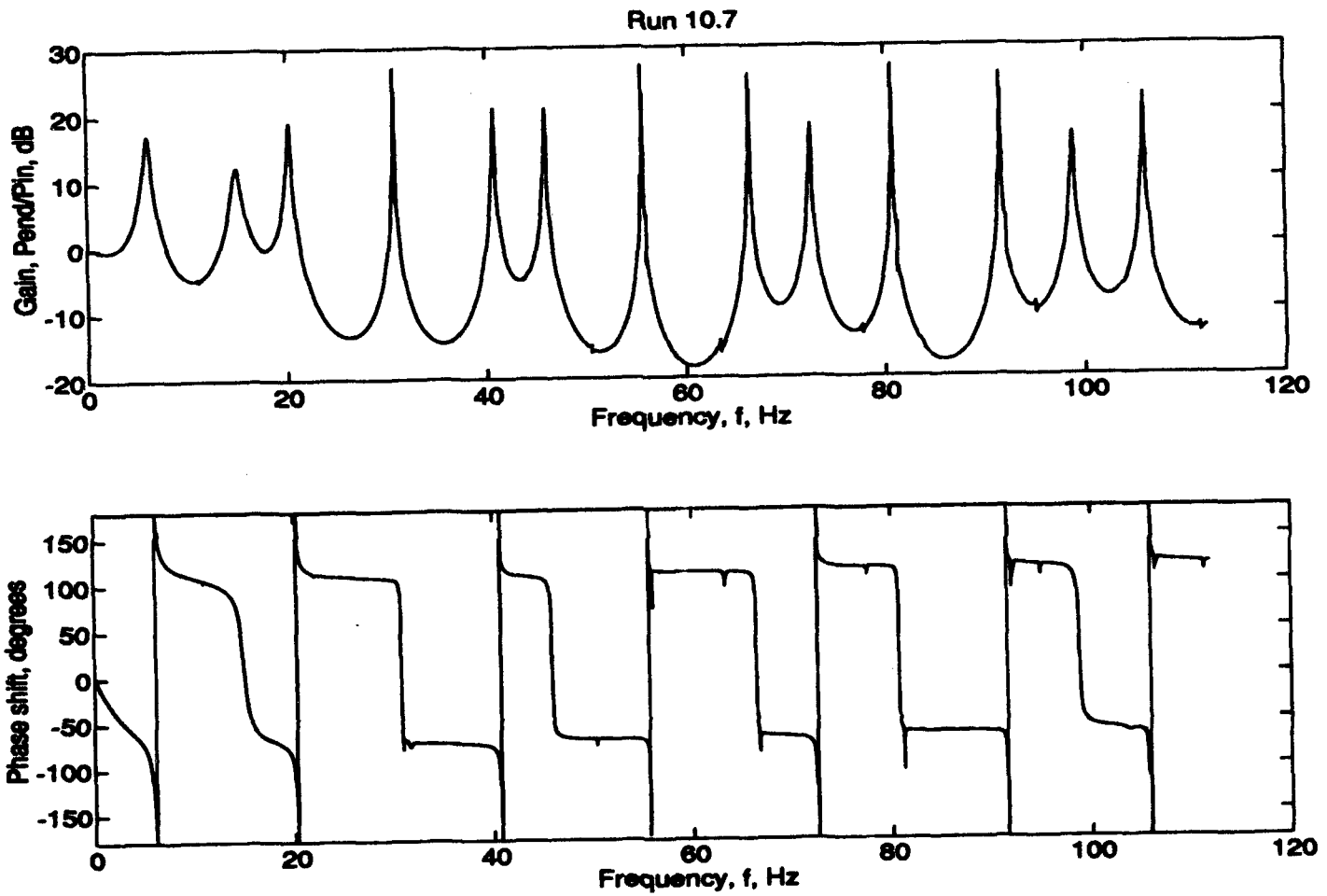

Figure A.6: CRF Response for Extended Length with 100 lbm/s Mass Flow Rate.
Conditions: Run 10.7, R_c = 0.825 ft = ½R3. Fundamental Peak at 6.0 Hz.

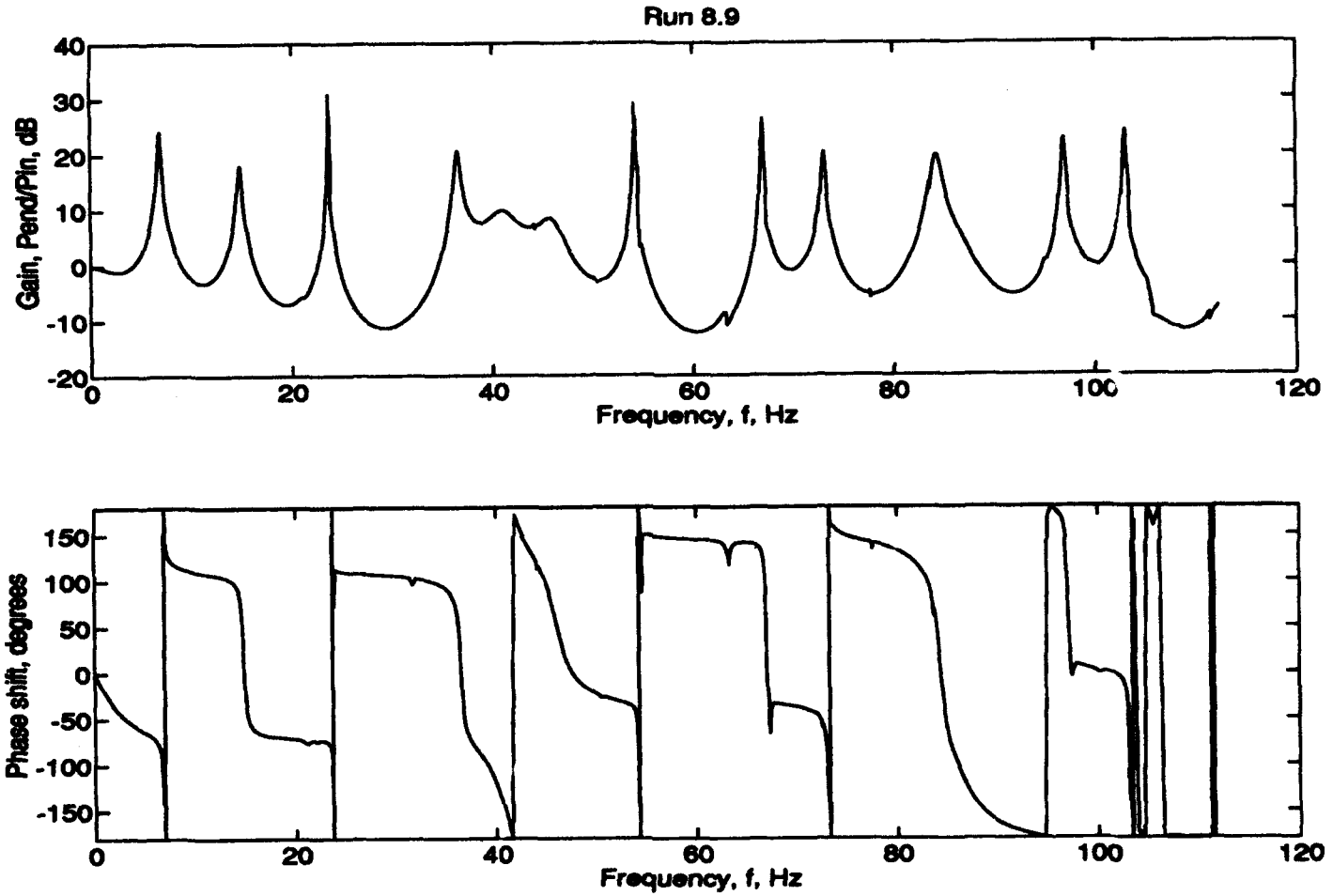

Figure A.7: CRF Response for Basic Length with 250 lbm/s Mass Flow Rate. Conditions: Run 8.9, R_c = 0.825 ft = ½R3. Fundamental Peak at 6.9 Hz.

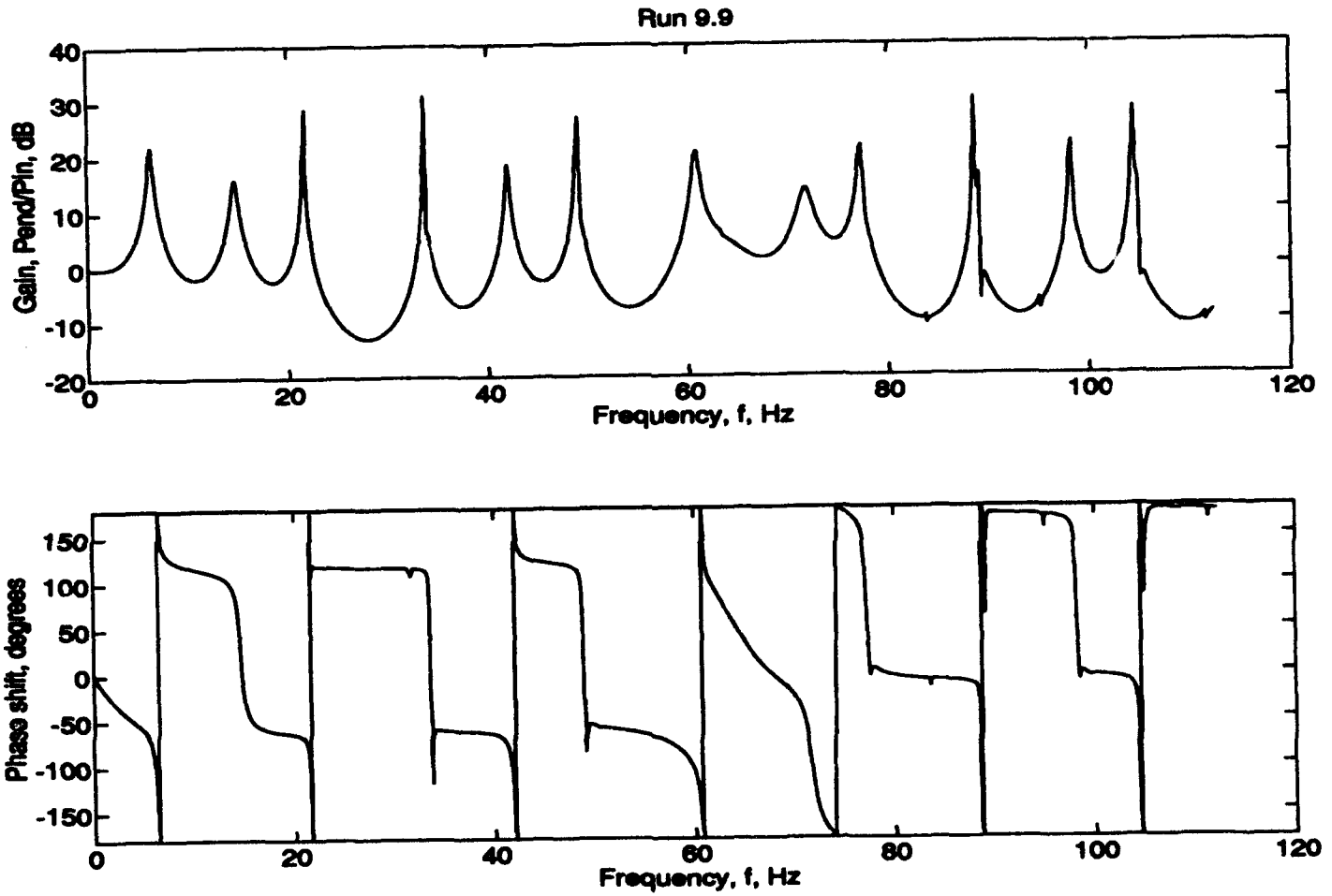

Figure A.8: CRF Response for Intermediate Length with 250 lbm/s Mass Flow Rate.
Conditions: Run 9.9, R_c = 0.825 ft = ½R3. Fundamental Peak at 6.3 Hz.

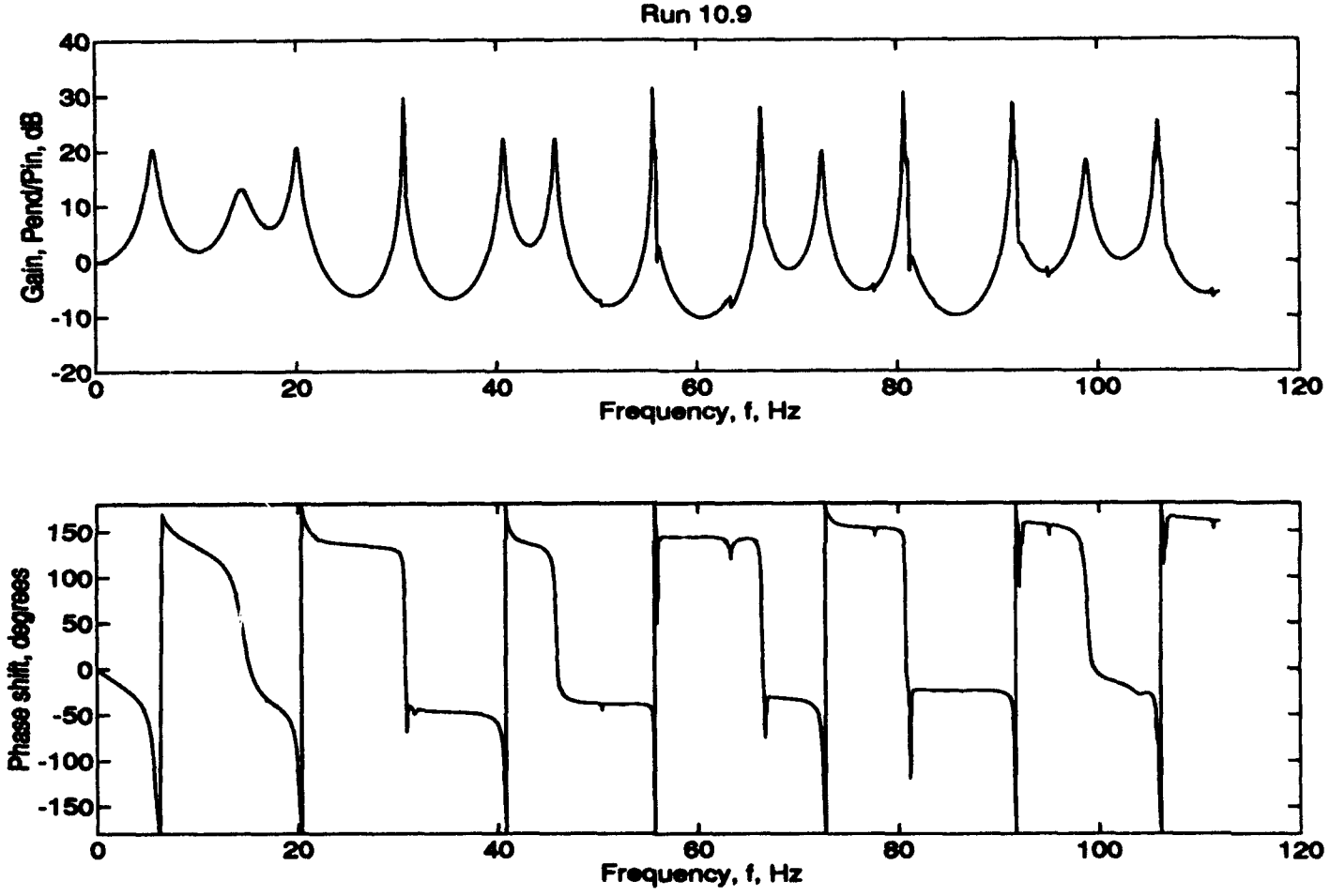

Figure A.9: CRF Response for Extended Length with 250 lbm/s Mass Flow Rate.
Conditions: Run 10.9, R_c = 0.825 ft = ½R3. Fundamental Peak at 5.7 Hz.

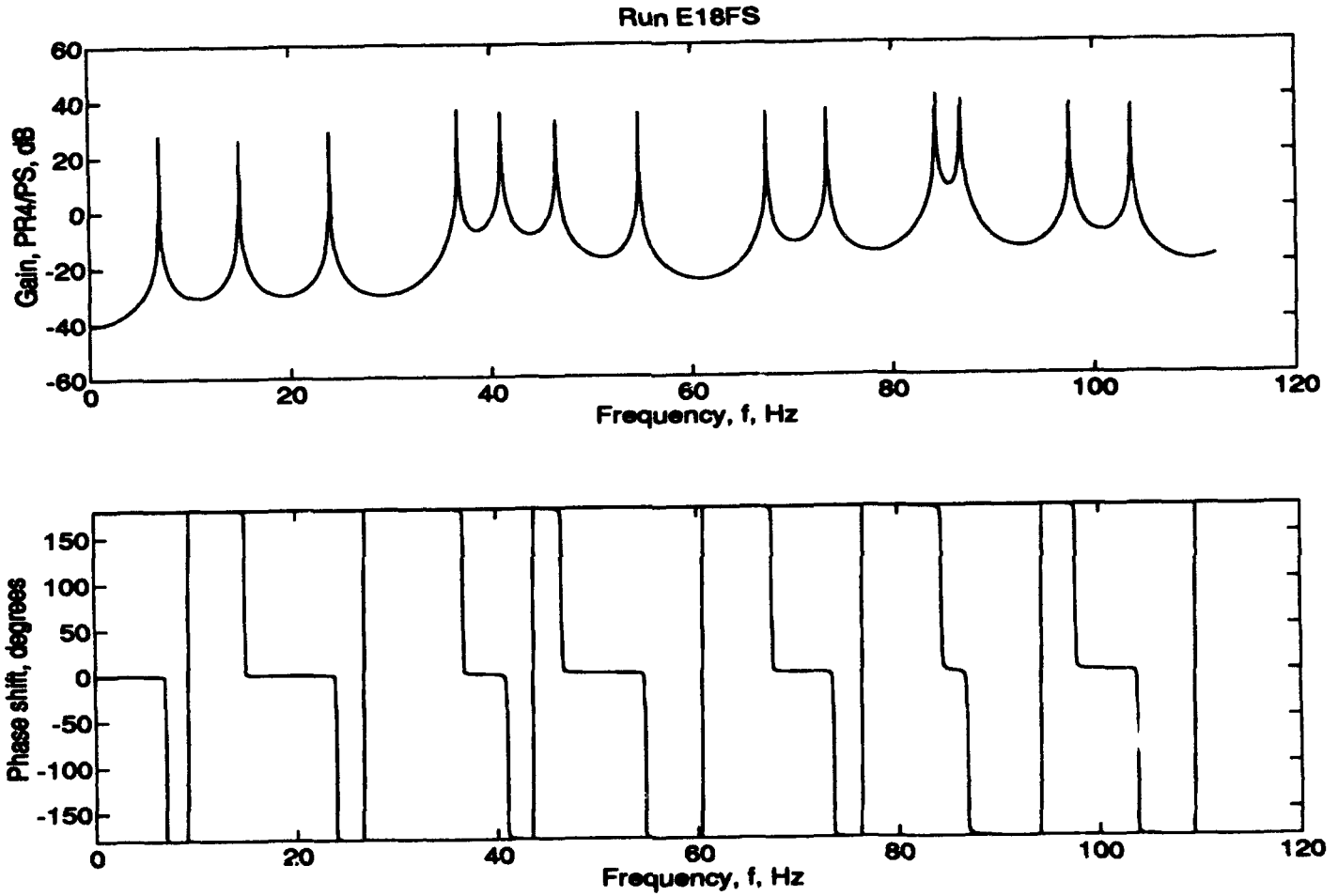

Figure A.10: CRF No Throughflow Response (PR4) for R_c = ½R3. Conditions: R_c = 0.4375 ft, $\dot{m}$ = 2.2 X 10^{-6} slug/s, basic length.

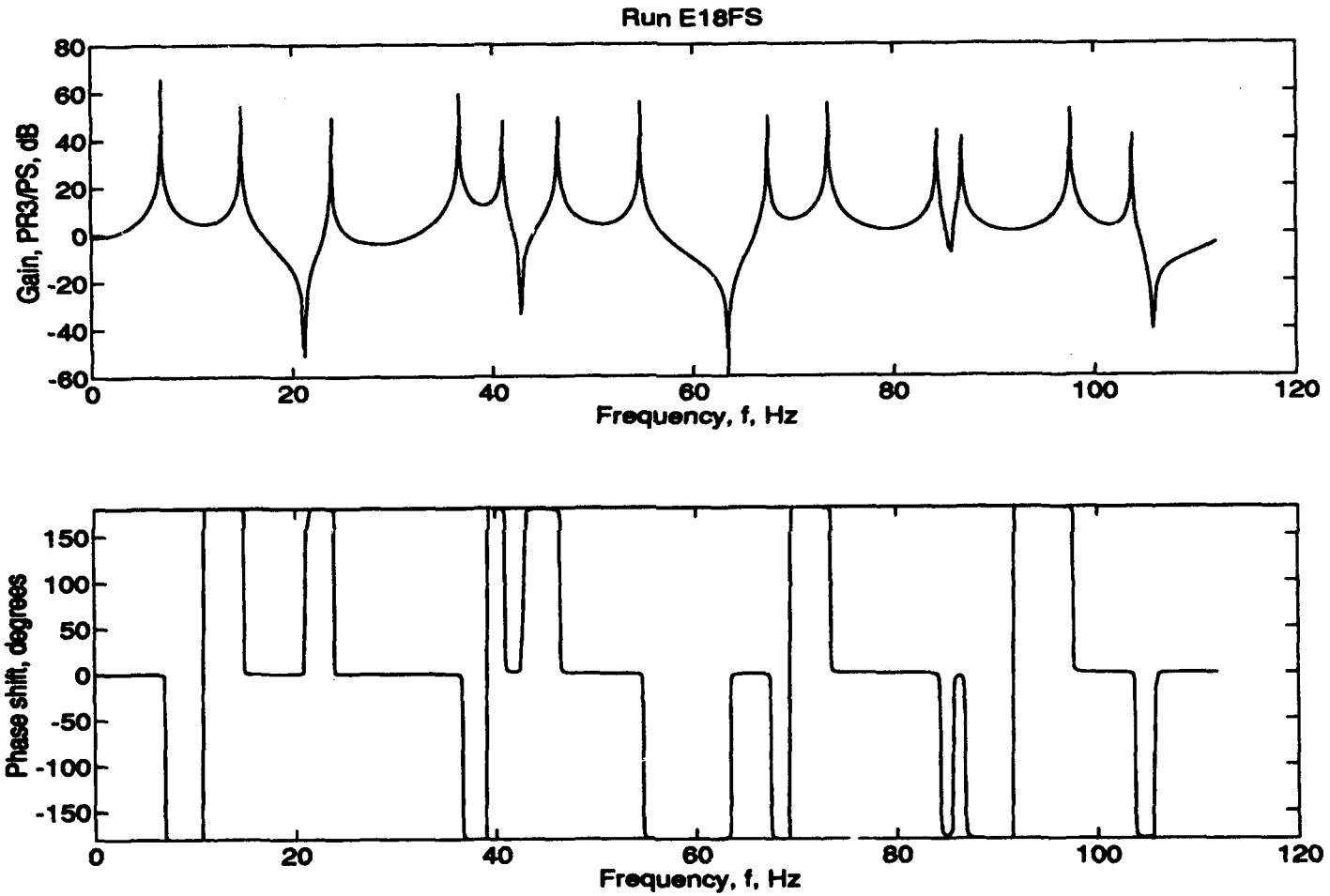

Figure A.11: CRF No Throughflow Response (PR3) for R_c = ½R3. Conditions: R_c = 0.4375 ft, $\dot{m}$ = 2.2 X 10^{-6} slug/s, basic length.

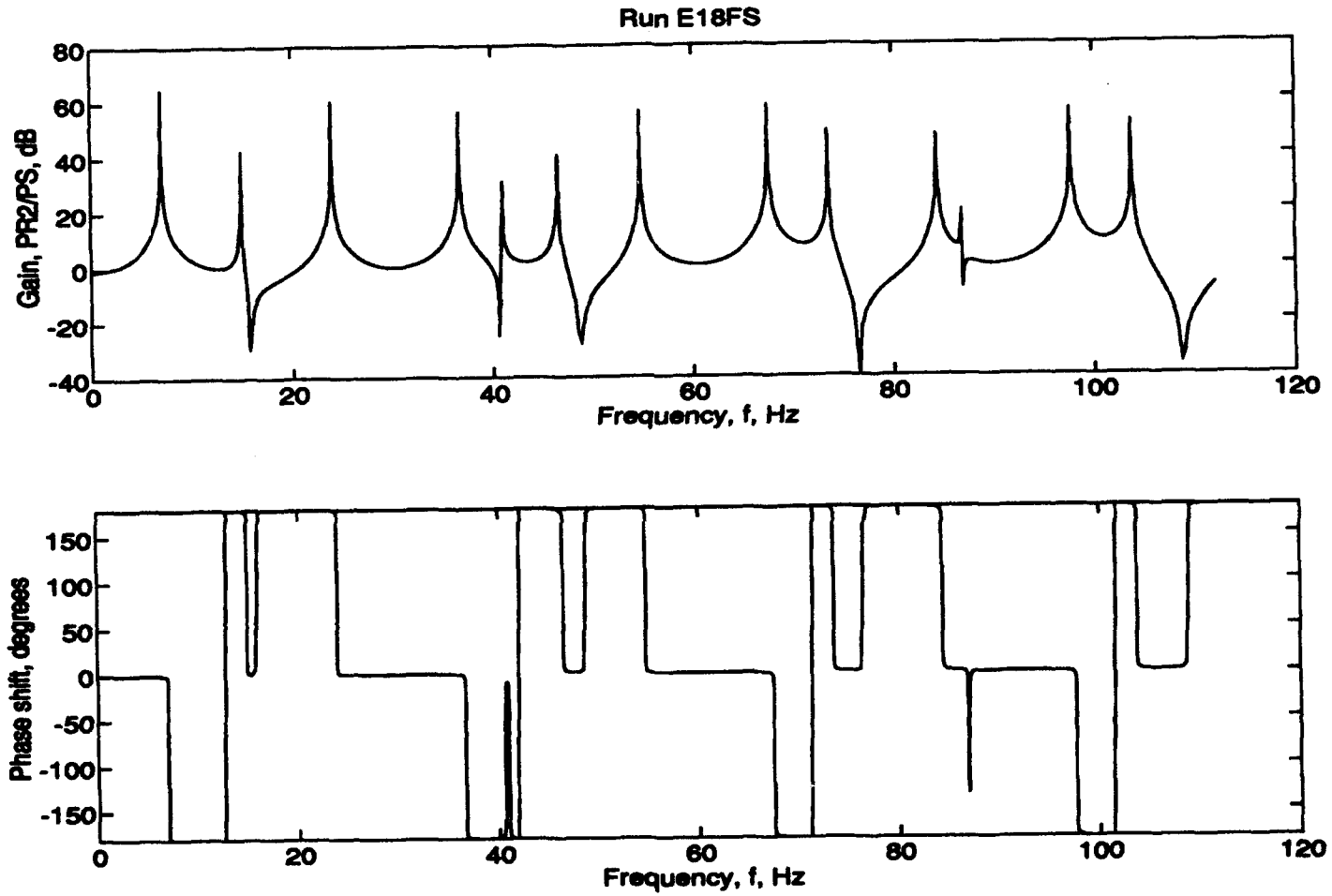

Figure A.12: CRF No Throughflow Response (PR2) for R_c = ¼R3. Conditions: R_c = 0.4375 ft, $\dot{m}$ = 2.2 X 10^{-6} slug/s, basic length.

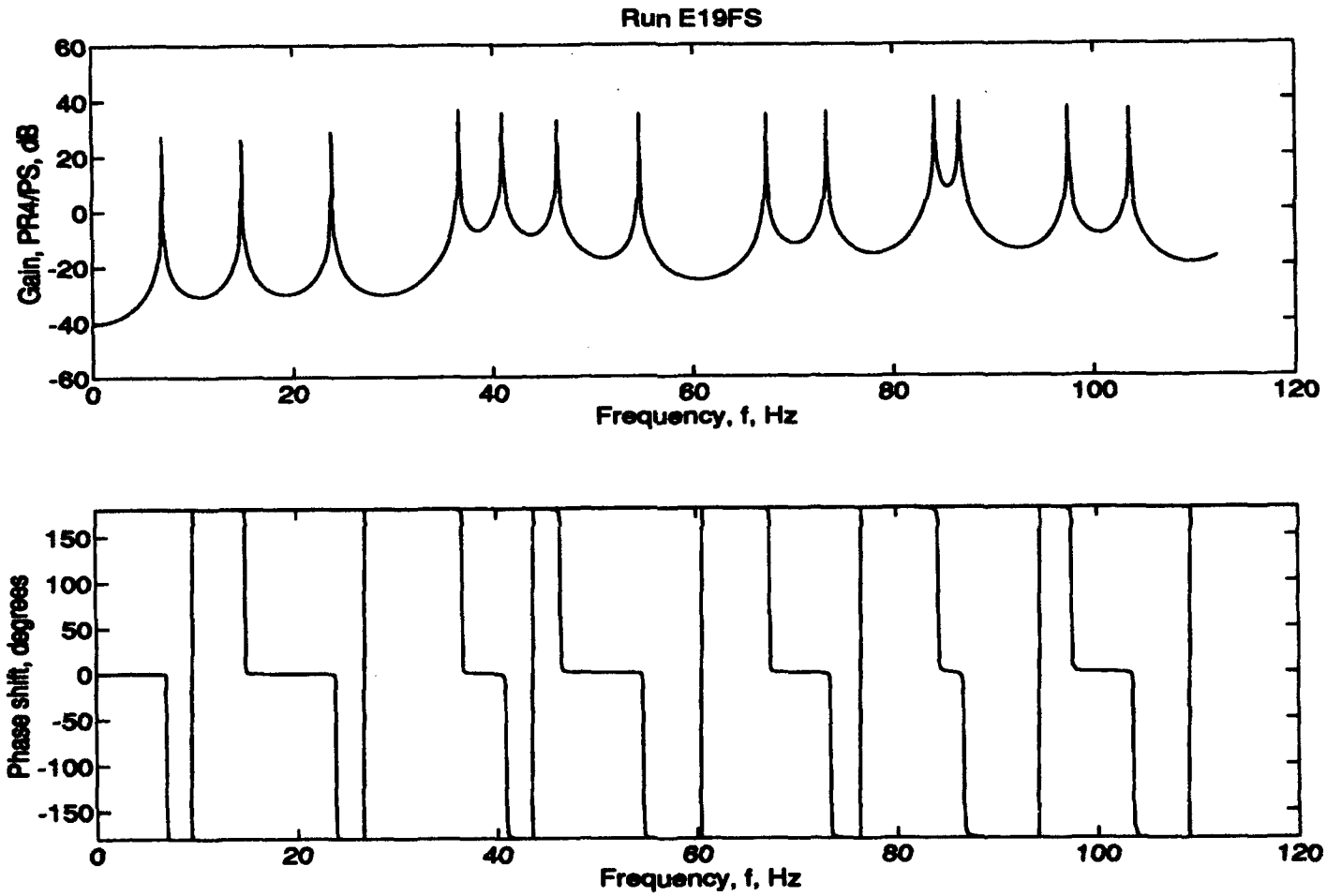

Figure A.13: CRF No Throughflow Frequency Response (PR4) for R_c = ½R3. Conditions: R_c = 0.825 ft, $\dot{m}$ = 2.3 X 10^{-6} slug/s, basic length.

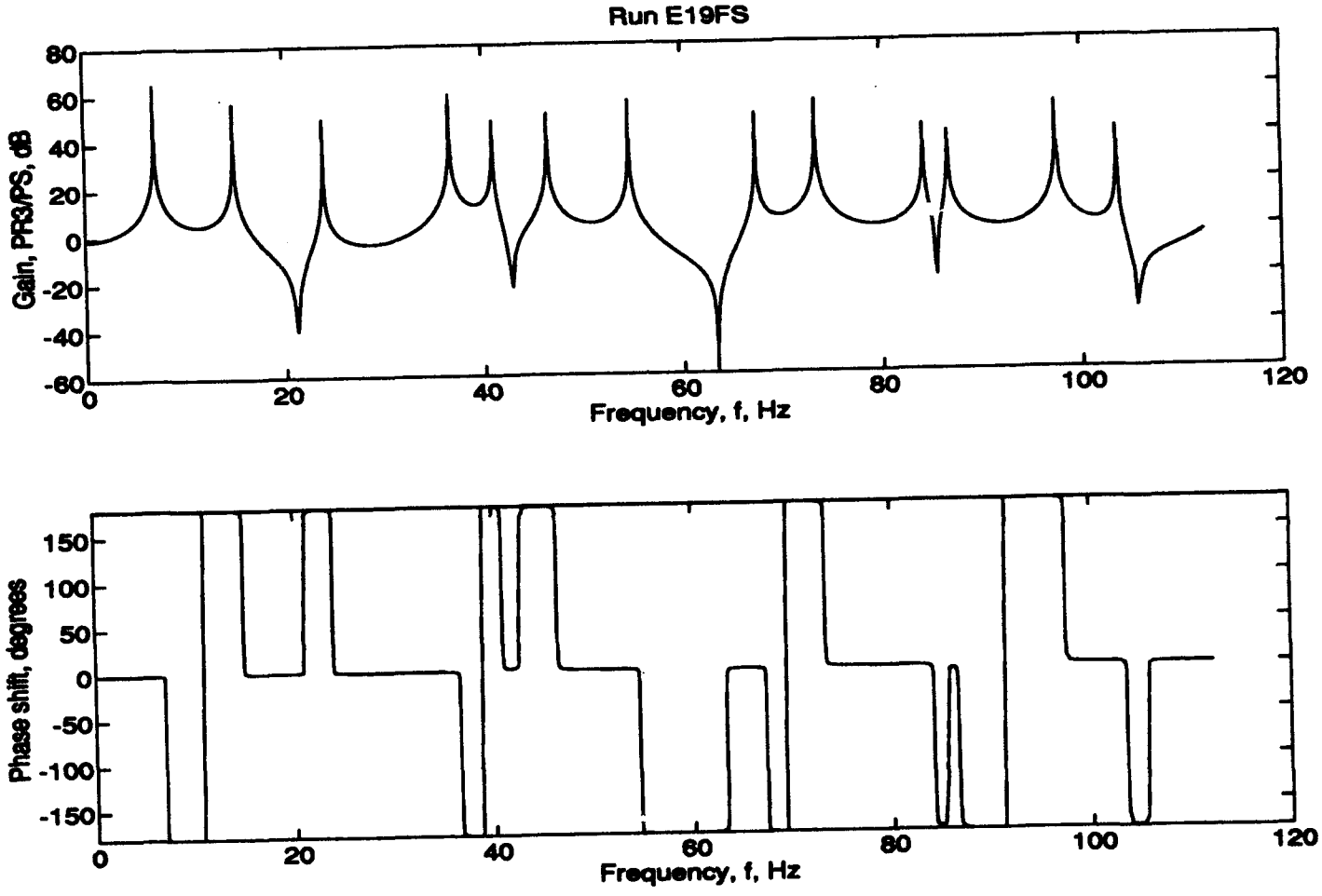

Figure A.14: CRF No Throughflow Frequency Response (PR3) for R_c = ½R3 . Conditions: R_c = 0.825 ft, $\dot{m}$ = 2.3 X 10^{-6} slug/s, basic leng[illegible].

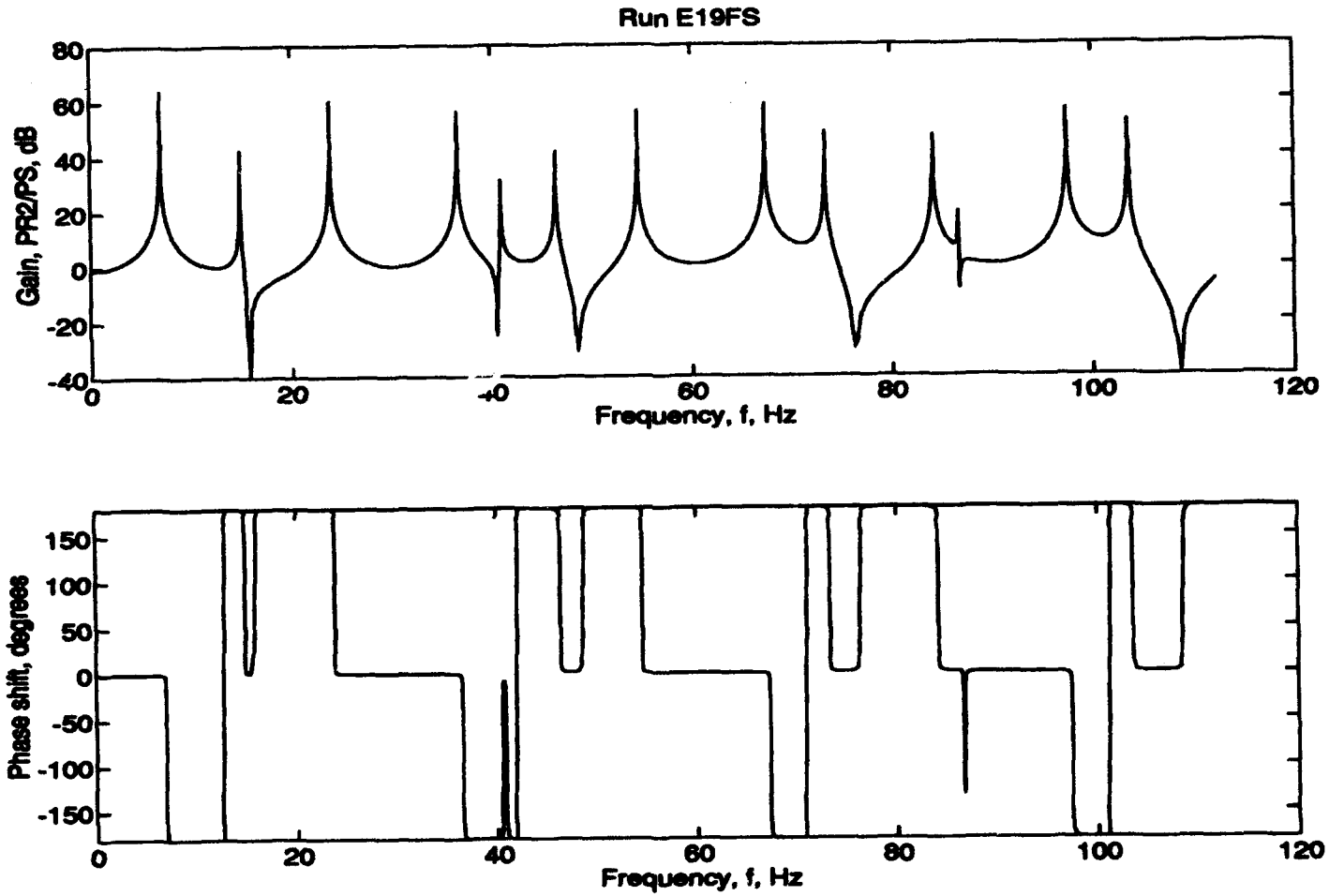

Figure A.15: CRF No Throughflow Frequency Response (PR2) for R_c = ½R3 . Conditions: R_c = 0.825 ft, $\dot{m}$ = 2.3 X 10^{-6} slug/s, basic length.

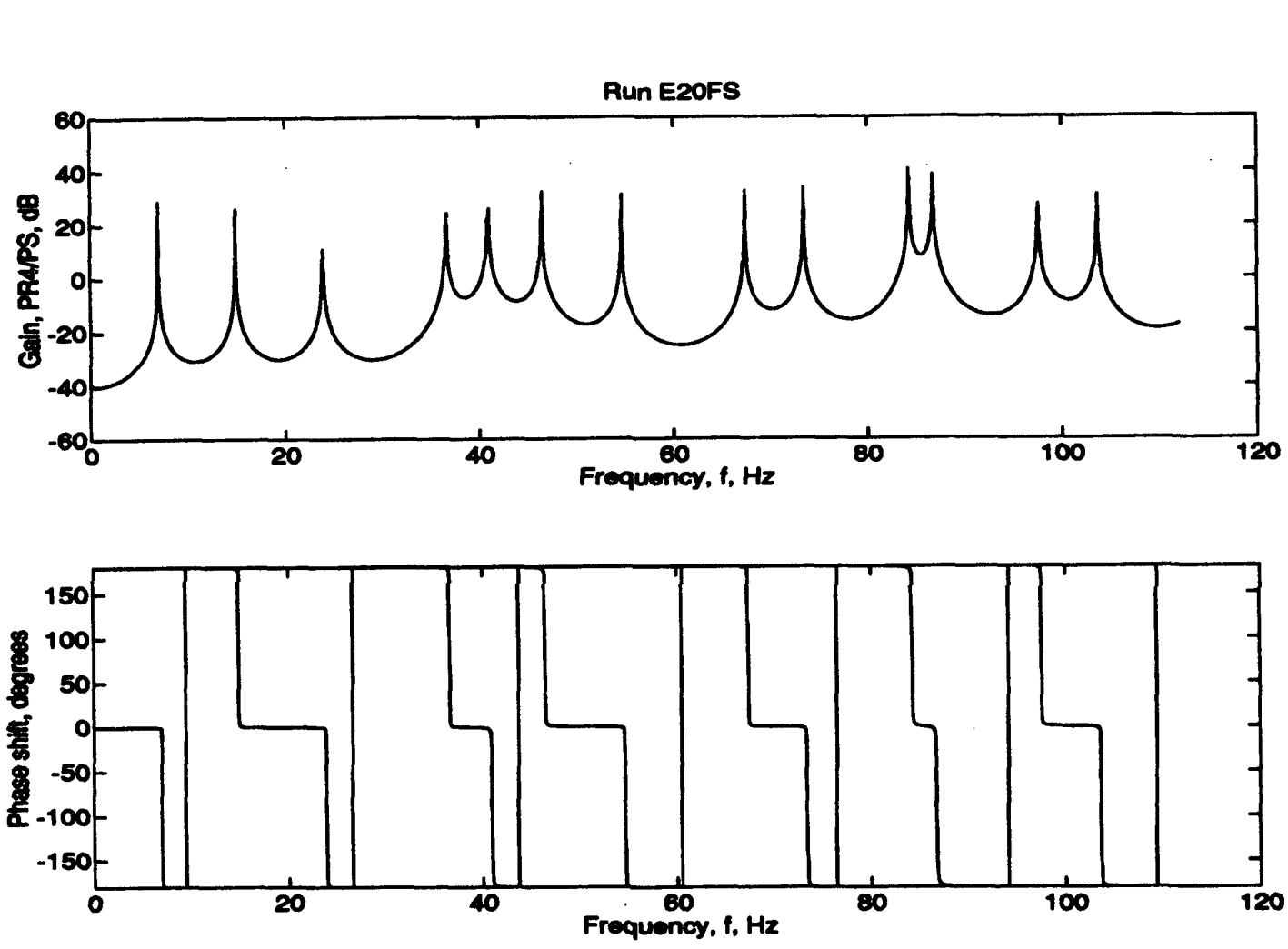

Figure A.16: CRF No Throughflow Frequency Response (PR4) for R_c = R3. Conditions: R_c = 1.65 ft, $\dot{m}$ = 2.1 X 10^{-6} slug/s, basic length.

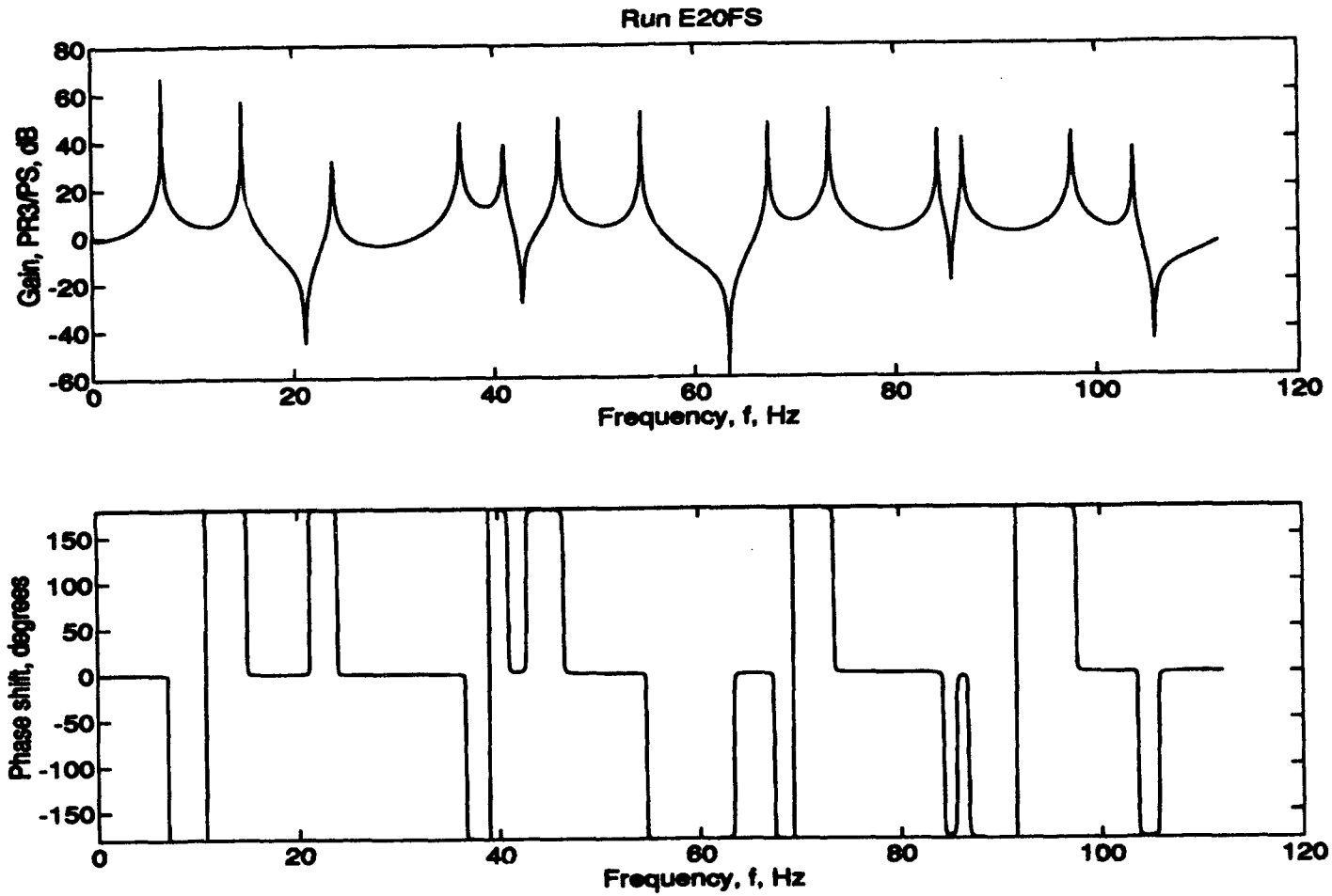

Figure A.17: CRF No Throughflow Frequency Response (PR3) for R_c = R3. Conditions: R_c = 1.65 ft, $\dot{m}$ = 2.1 X 10^{-6} slug/s, basic length.

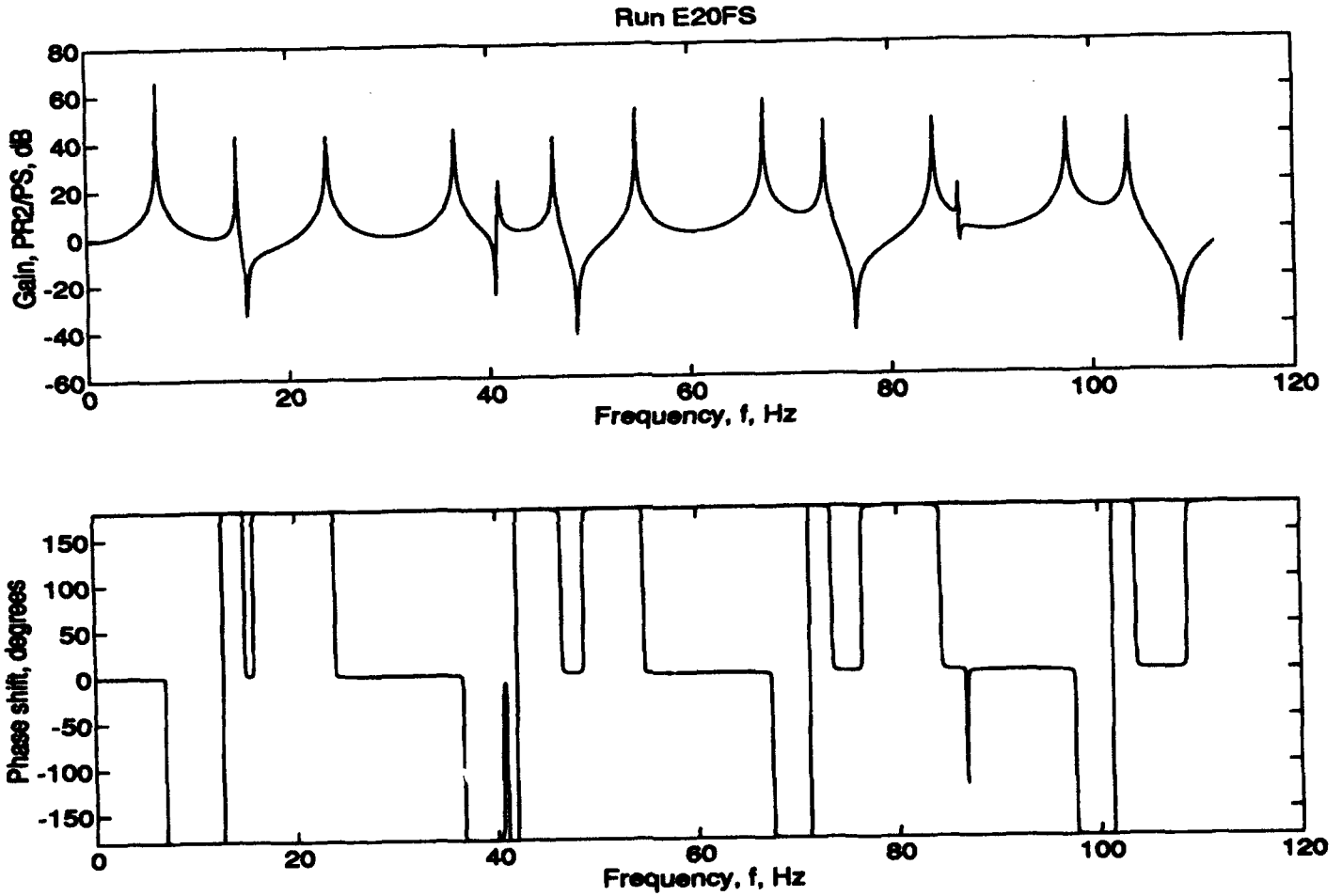

Figure A.18: CRF No Throughflow Frequency Response (PR2) for R_c = R3. Conditions: R_c = 1.65, $\dot{m}$ = 2.1 X 10^{-6} slug/s, basic length.

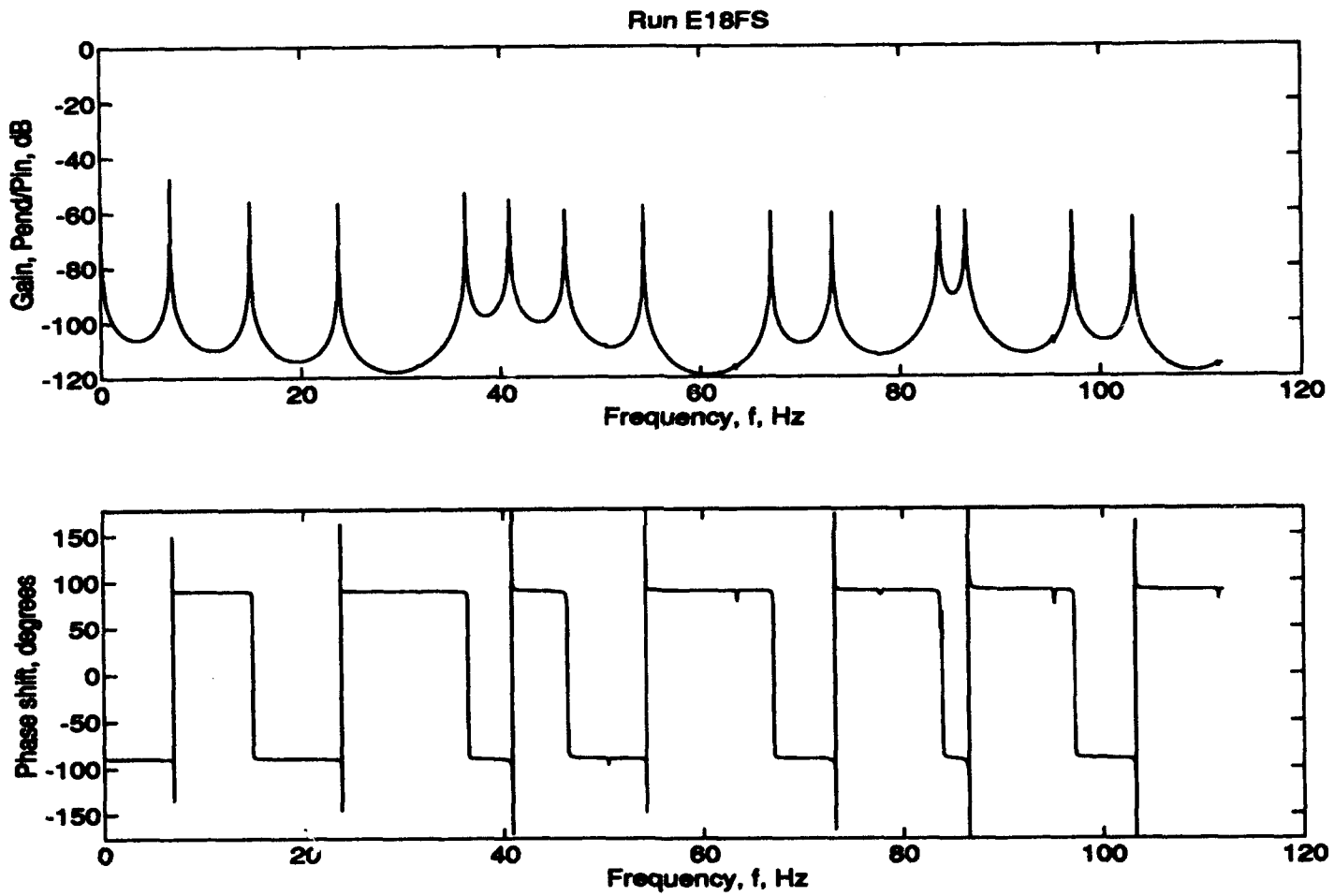

Figure A.19: CRF No Throughflow Response (PEND) for R_c = ½R3. Conditions: R_c = 0.4375 ft, $\dot{m}$ = 2.2 X 10^{-6} slug/s, basic length.

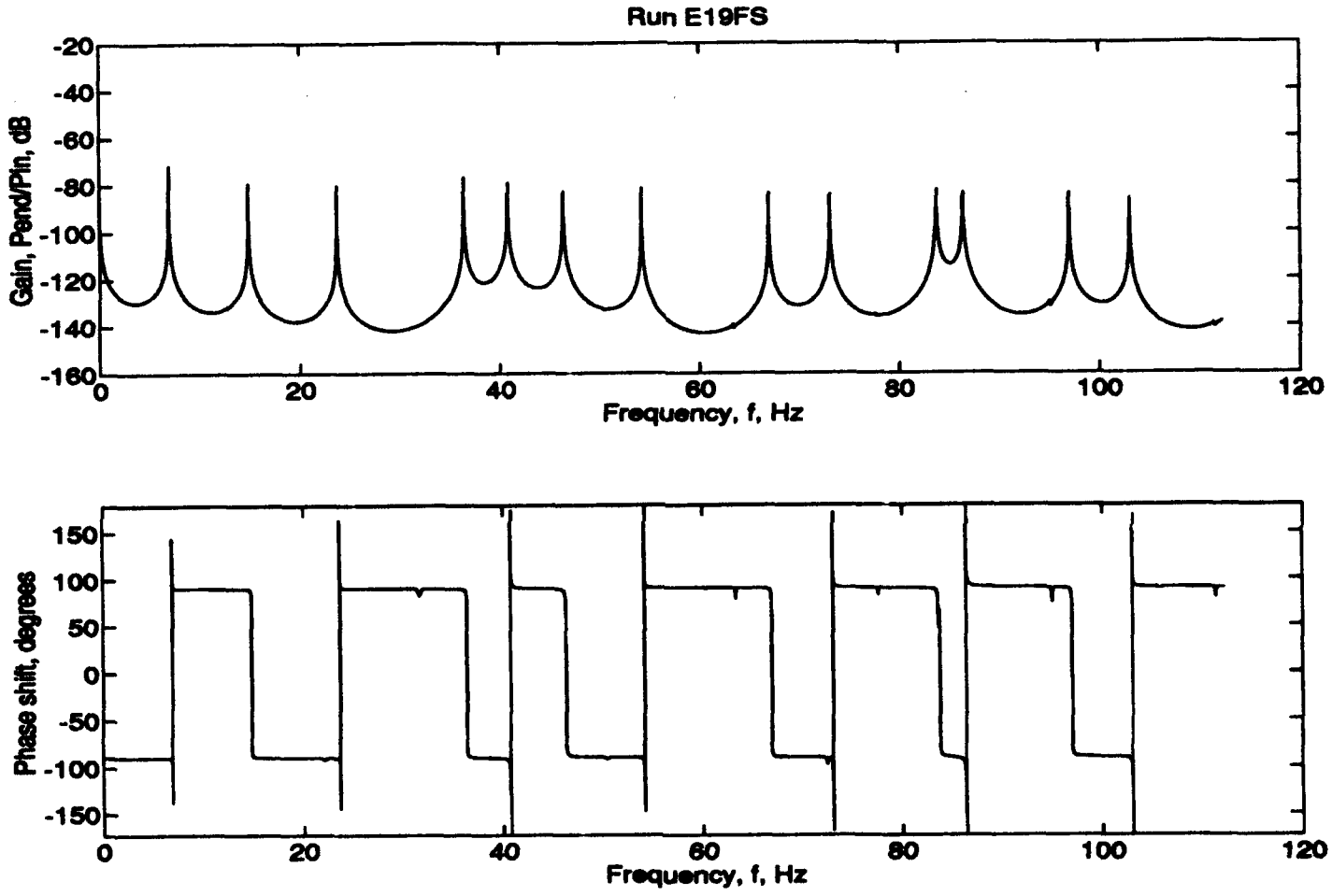

Figure A.20: CRF No Throughflow Response (PEND) for R_c = ½R3. Conditions: R_c = 0.825 ft, $\dot{m}$ = 2.3 X 10^{-6} slug/s, basic length.

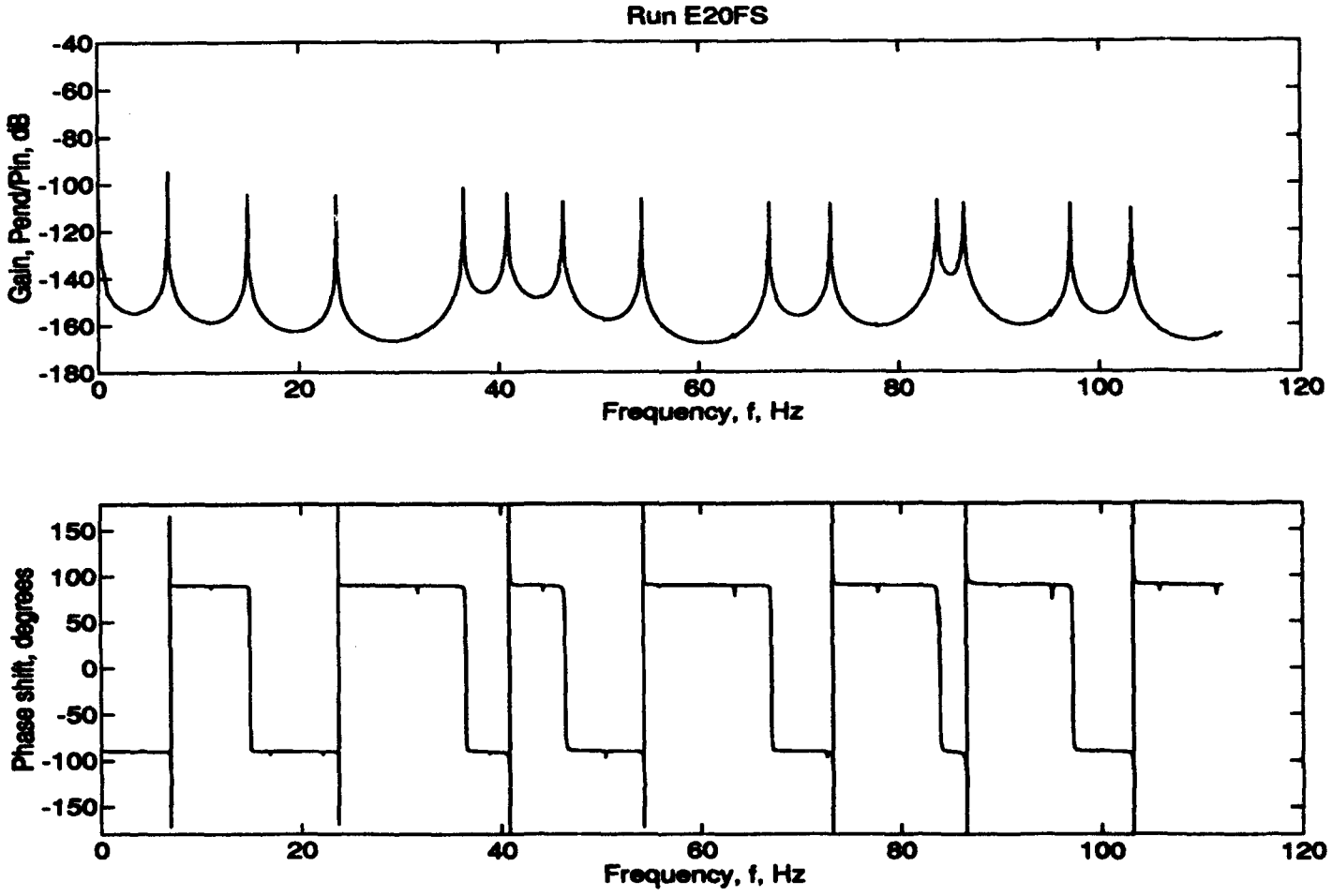

Figure A.21: CRF No Throughflow Frequency Response (PEND) for R_c = R3. Conditions: R_c = 1.65 ft, $\dot{m}$ = 2.1 X 10^{-6} slug/s, basic length.

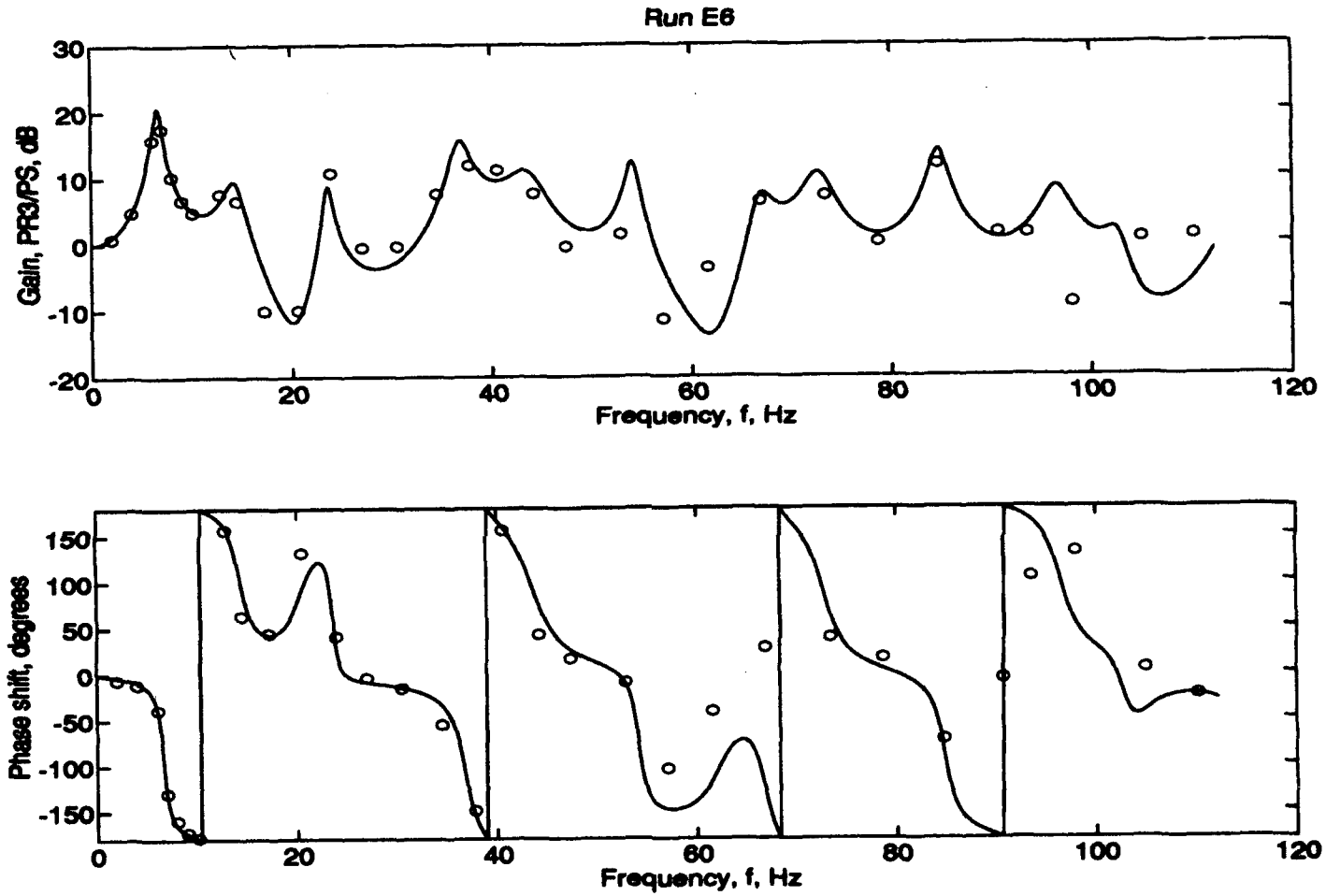

Figure A.22: Model Frequency Response (PR3) with Washers for R_c = ¼R3. Conditions: R_c = 3/64 in, $\dot{m}$ = 2.3 X 10^{-6} slug/s, basic length, washers.

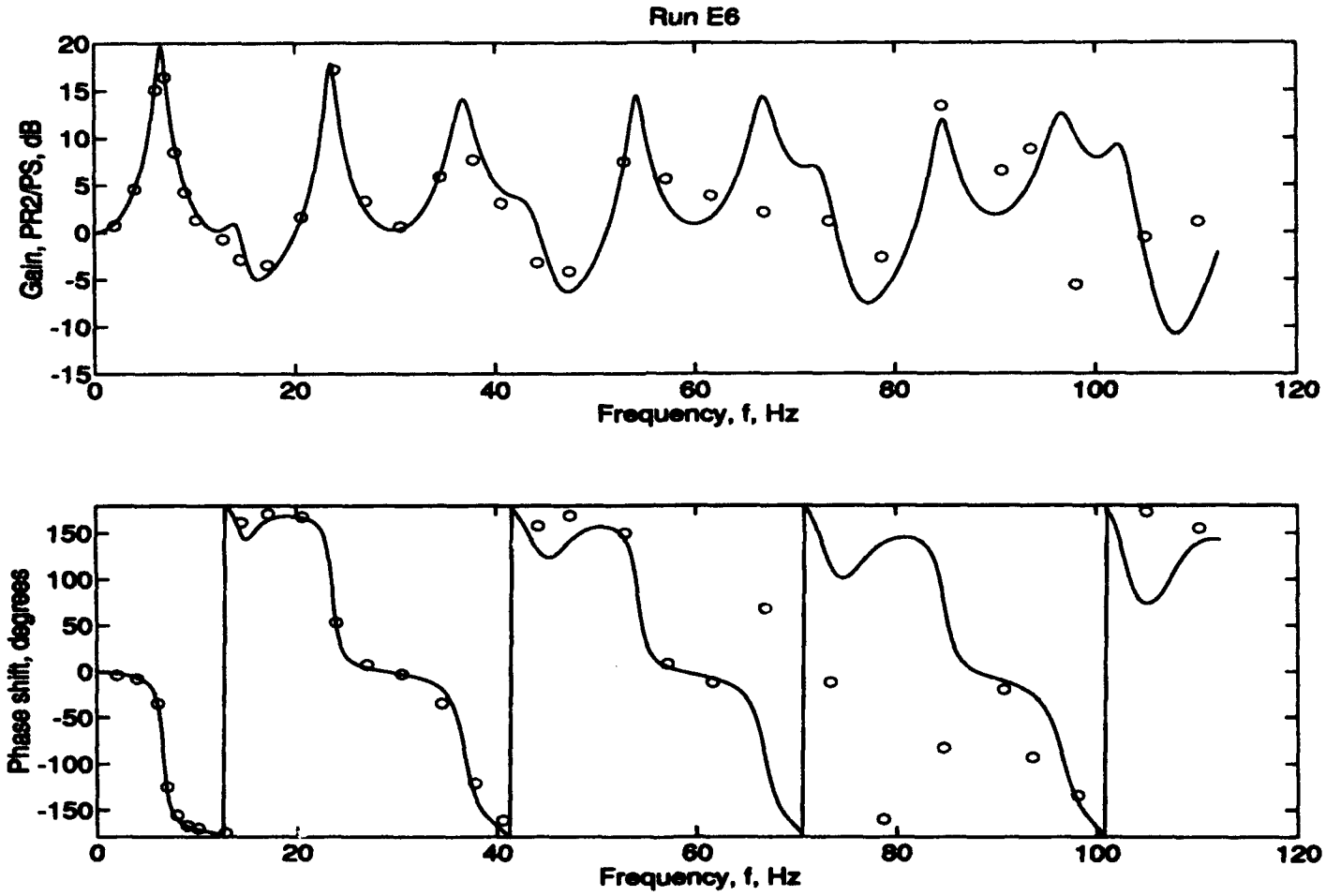

Figure A.23: Model Frequency Response (PR2) with Washers for R_c = ½R3. Conditions: R_c = 3/64 in, $\dot{m}$ = 2.3 X 10^{-6} slug/s, basic length, washers.

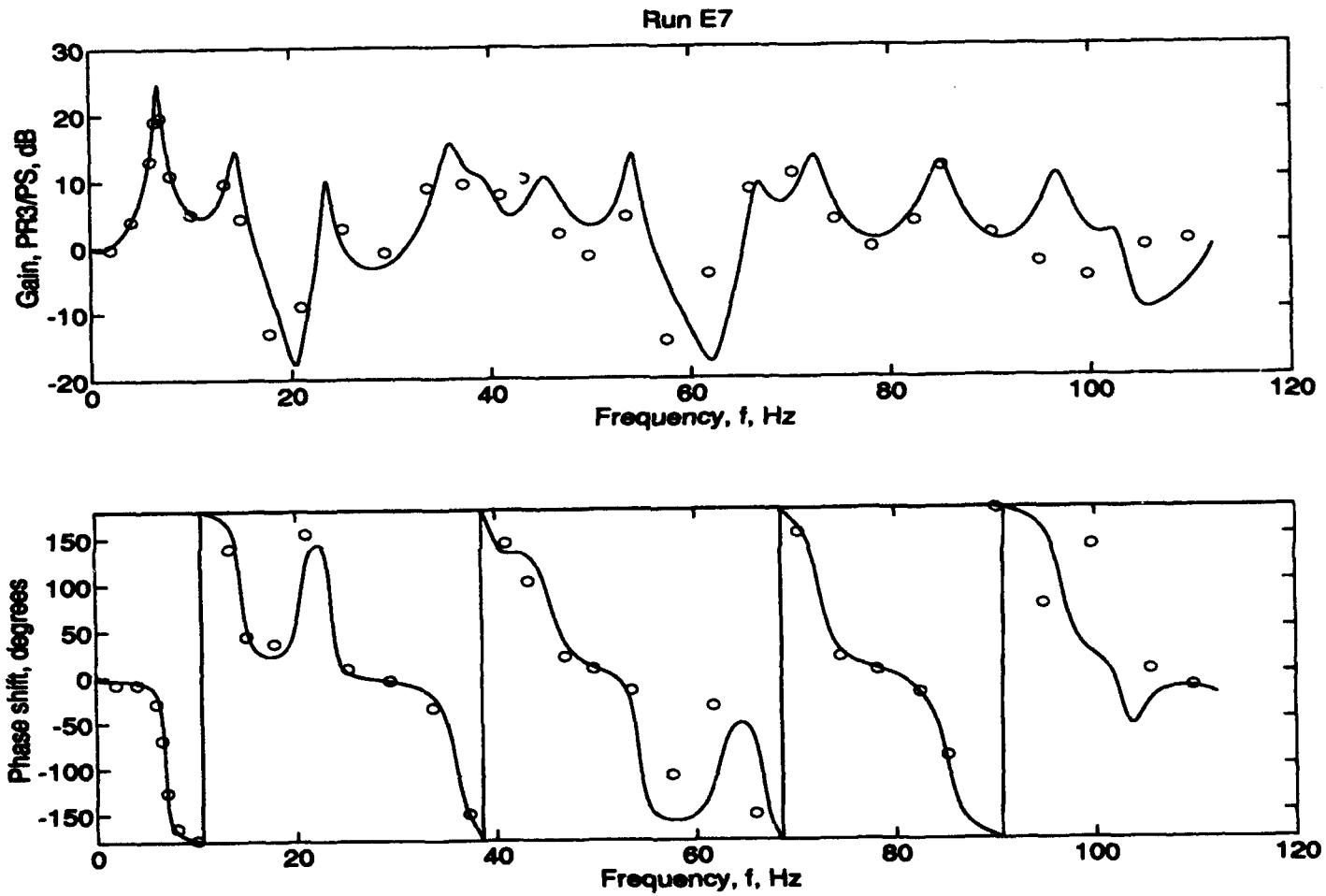

Figure A.24: Model Frequency Response (PR3) with Washers for R_c = ½R3. Conditions: R_c = 3/32 in, $\dot{m}$ = 2.3 X 10^{-6} slug/s, basic length, washers.

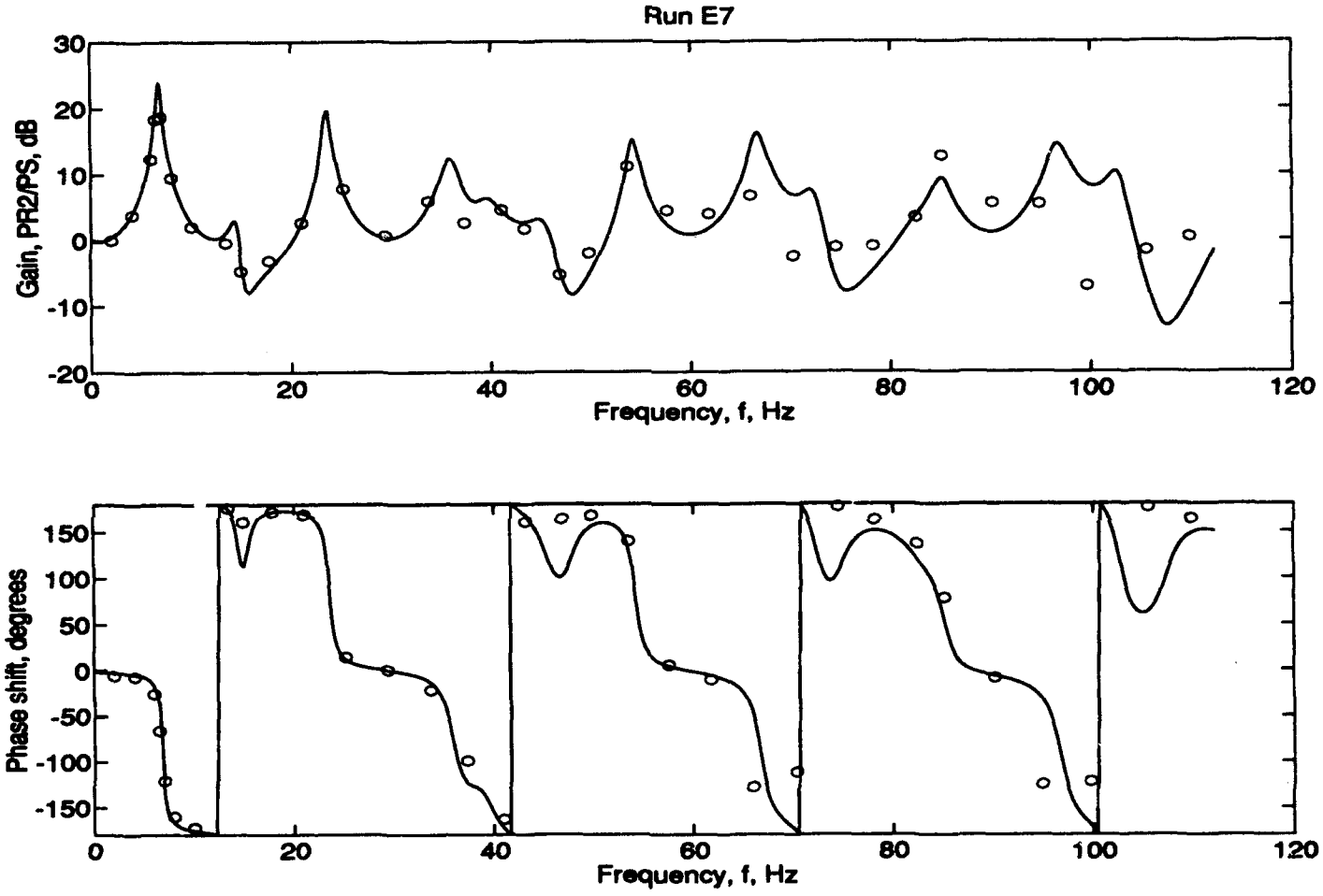

Figure A.25: Model Frequency Response (PR2) with Washers for R_c = ½R3. Conditions: R_c = 3/32 in, $\dot{m}$ = 2.3 X 10^{-6} slug/s, basic length, washers.

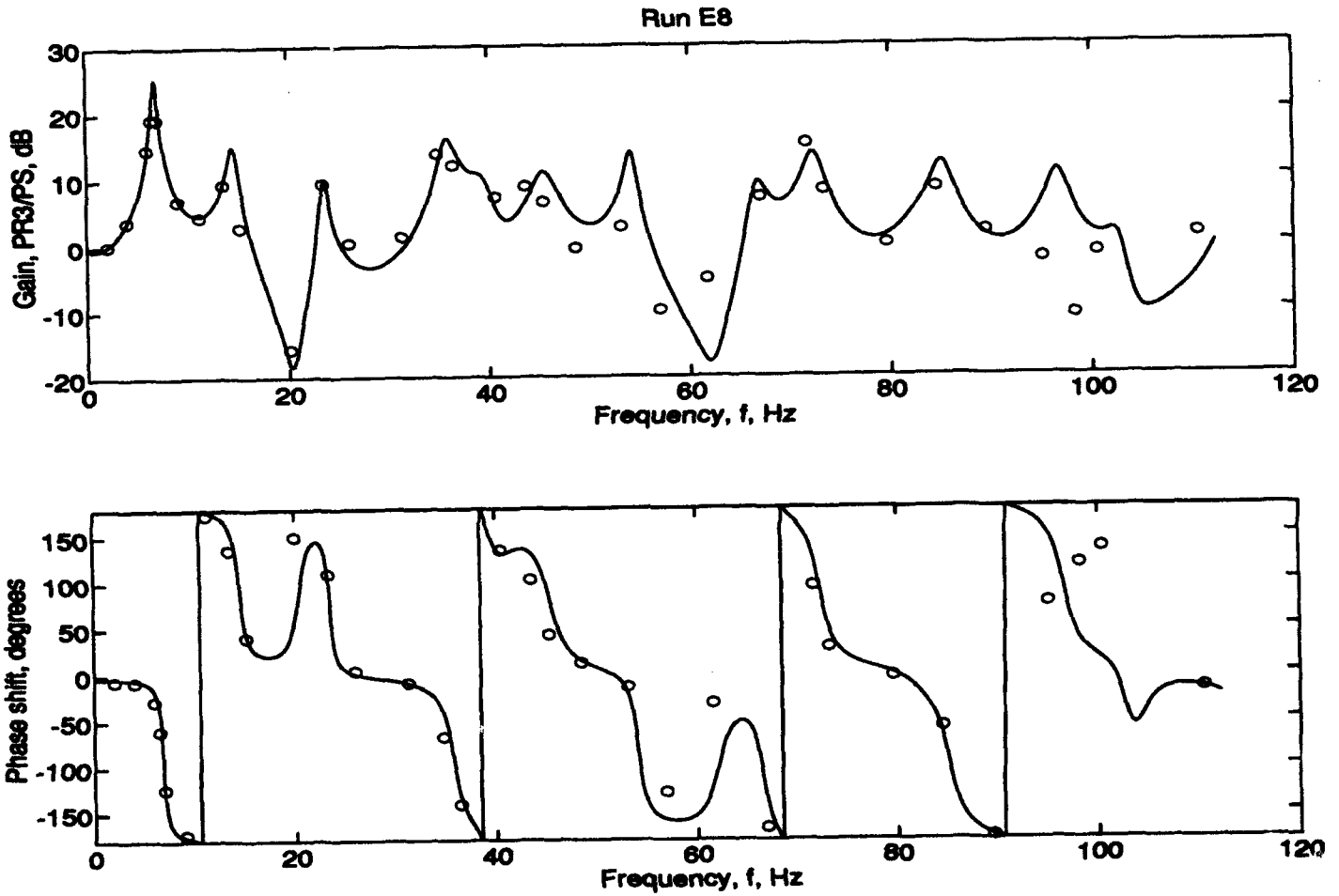

Figure A.26: Model Frequency Response (PR3) with Washers for R_c = R3. Conditions: R_c = 3/16 in, $\dot{m}$ = 2.3 X 10^{-6} slug/s, basic length, washers.

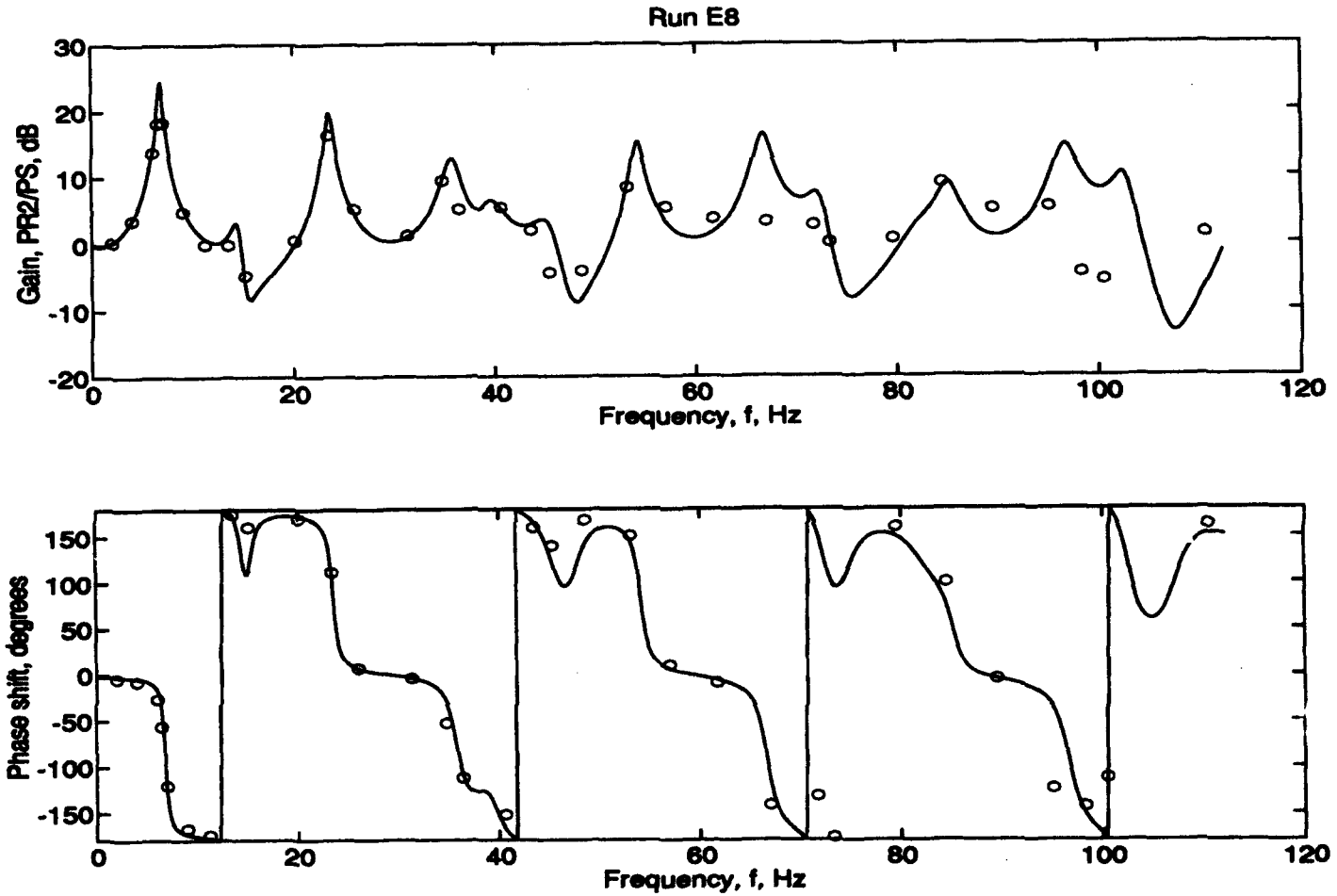

Figure A.27: Model Frequency Response (PR2) with Washers for R_c = R3. Conditions: R_c = 3/16 in, $\dot{m}$ = 2.3 X 10^{-6} slug/s, basic length, washers.

Appendix B. Geometry Effects on a Constant Diameter Line

This appendix presents a chronological overview of the development of the computer program used to solve the Nichols equations. The program was developed first for a constant diameter line with a blocked end. All of the geometry and flow effects were added in increments to determine how the solution is affected by each.

First, the Nichols solutions for a constant diameter blocked line were solved and verified. Next, a study on the effect of scaling the radius for the model dimensions was accomplished. The solution was then modified to account for cascaded lines of different diameter and orifice terminations. Finally, the flow conditioning elements, the pressure equalization pipe, and throughflow were added to the solution. Some of the above developments are discussed here. Others, such as the effect of end radius and throughflow, are covered in detail in Chapters VI and VII.

B.1 Constant Diameter, Blocked Line and Radius Scaling

The solution for a constant diameter line of 20 ft diameter and 69.8 ft in length is shown in Figure B.1. The gains smoothly attenuate through the frequency range; but, they are high (70 dB for the fundamental peak). In Figure B.2, a constant diameter line of 2 in and 69.8 ft in length

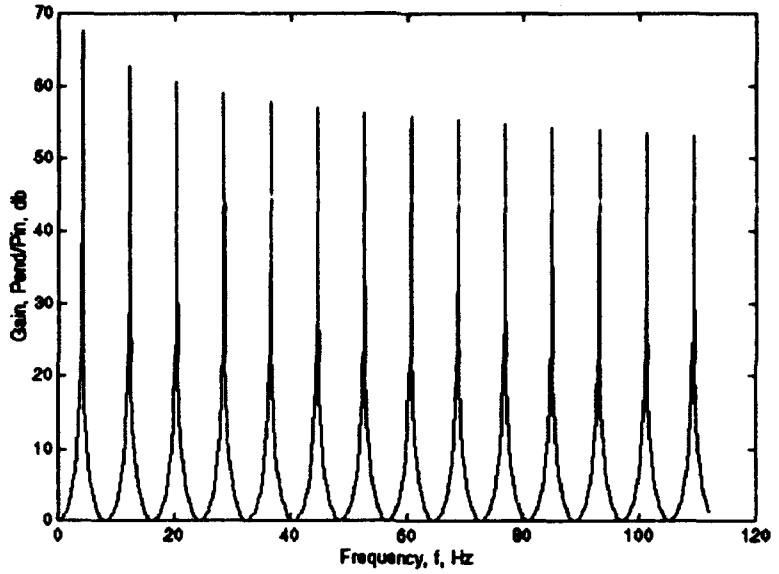

Figure B.1: Computer Output for a 20 ft Diameter Line.
Conditions: Constant Diameter, Blocked, 69.8 ft Long.

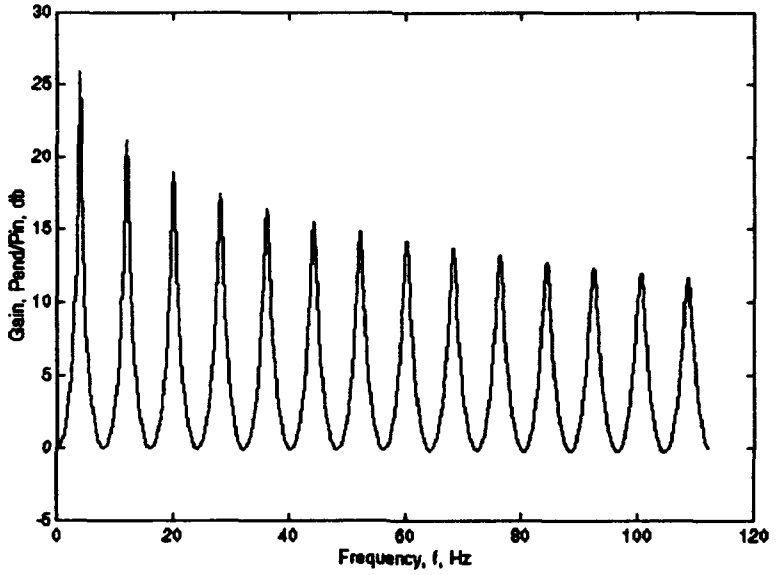

Figure B.2: Computer Output for a 2 in Diameter Line.
Conditions: Constant Diameter, Blocked, 69.8 ft Long.

is shown. Notice the gains are much lower but the shape of the curve is similar to Figure B.1. The diameter of the lines in Figures B.1 and B.2 represent section 1 of the CRF and model, respectively. The length, 69.8 ft, of both lines represents the overall length of the CRF and model.

Several other diameter lines were studied with the constant diameter solution. It was found that the gains are directly dependent on the radius of the line as:

$$Gain(D) = Gain(20\ ft\ dia)\ \frac{D}{20ft} \quad . \qquad \text{(B-1)}$$

For the 20 ft diameter line, the fundamental peak gain is 2400 (70 dB) and the 2 in line gain is 20 (26 dB). The gains are related by the above equations. The gains of other radius lines studied also follow equation B-1 as can be shown from the information in Table B.1.

The radius scaling also affects the fundamental frequency as is clear from Table B.1. The model scale is 1:120 for sections 1 and 2 and the pressure equalization pipe. According to the table, the model fundamental frequencies should be slightly lower than the full-scale CRF.

The fundamental frequency computed for the full-scale dimensions of 20 ft diameter, 4.08 Hz, is the equal to the fundamental frequency calculated from the basic pipe

resonance equation for a blocked line (2-1) of 69.8 ft in length. This indicates that the 20 ft diameter line is essentially lossless, since Equation (2-1) does not account for viscous effects. The smaller radius lines have lower fundamental frequencies than the 20 ft diameter line, indicating the viscous interactions present in the smaller lines have a greater affect the signal propagation than in the large diameter line.

B.2 Cascaded Lines of Different Diameter.

The addition of the 10 ft and 3.3 ft diameter sections to the 20 ft constant diameter, blocked line creates a cascade and alters the solution for the line. Figure B.3

Table B.1. Effects of Radius Scaling on a 69.8 ft Blocked Line. The speed of sound in all cases is 1130.5 ft/s.

Radius R (ft)	Scale	Fundamental Peak Amplitude (nondimensional)	Fundamental Frequency (Hz)
10	1:1	2400	4.08
0.5	1:20	120	4.03
0.25	1:40	60	4.01
0.125	1:80	30	3.97
0.10	1:100	24	3.94
0.083	1:120	20	3.92

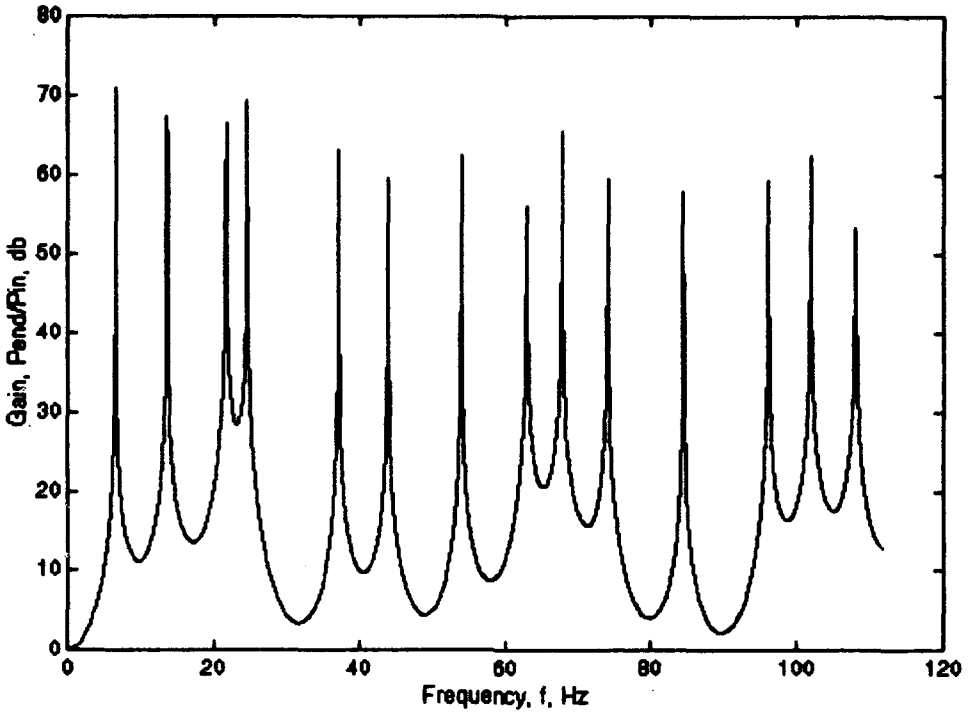

Figure B.3: CRF as a Three-Line Cascade. Conditions: Blocked, Basic Length.

shows the blocked line with a simple three-line cascade. This is the most fundamental solution for the CRF where section 1 is of 20 ft diameter, section 2 is of 10 ft diameter, and section 3 is of 3.3 ft diameter. Shown in Figure B.3 is the solution for the basic length line.

Introduction of the different diameter lines produces an impedance mismatch at the junctions of the individual lines. This causes the fundamental frequency to increase, in this case, to 6.5 Hz from 4.08.

Changing the length configuration from basic to intermediate decreases the fundamental frequency by 0.5 Hz. Another 0.5 Hz drop is evident by changing the length configuration from intermediate to extended.

Introduction of the cascaded lines does not change the peak amplitude of the fundamental frequency, but it does affect the harmonic peaks because the cascade causes signals to reflect at the junctions of the individual lines. These reflected signals interact with each other and the input signal, causing the attenuation to change from that of the constant diameter line (Figure B.1).

B.3 Flow Conditioning Elements

The addition of the flow conditioning elements is analytically modeled as area reductions in the locations where they are mounted. This increases the number of different diameter lines, changing the cascade from 3 to 13 lines of different diameter.

The solution; however, is unaffected by the addition of the flow conditioners. However, because the throughflow had not yet been modeled, the flow conditioning elements were left in the program for all subsequent runs.

B.4 Addition of the Pressure Equalization Pipe

The addition of the pressure equalization pipe to the solution for the cascaded lines changes the gain curve only slightly. Figures B.4 and B.5 illustrate the blocked cascaded line (with flow conditioning elements) for the CRF with and without the pressure equalization pipe.

The solution with the branch modeled shows small peaks at 30 and 111 Hz. These peaks are the only difference between the solution with and without the branch. Again, due to the fact that throughflow has not yet been accounted for, the pressure equalization pipe was left in the model for all subsequent runs.

B.5 Summary

The most significant effect on the solution for the CRF is the cascaded lines of different diameter created from sections 1, 2, and 3. The solution is highly dependent on the length configuration; however, it is not affected by the addition of flow straightening elements. The solution is slightly changed with the addition of the pressure equalization pipe; but this effect is at higher frequencies and does not change the fundamental frequency at all.

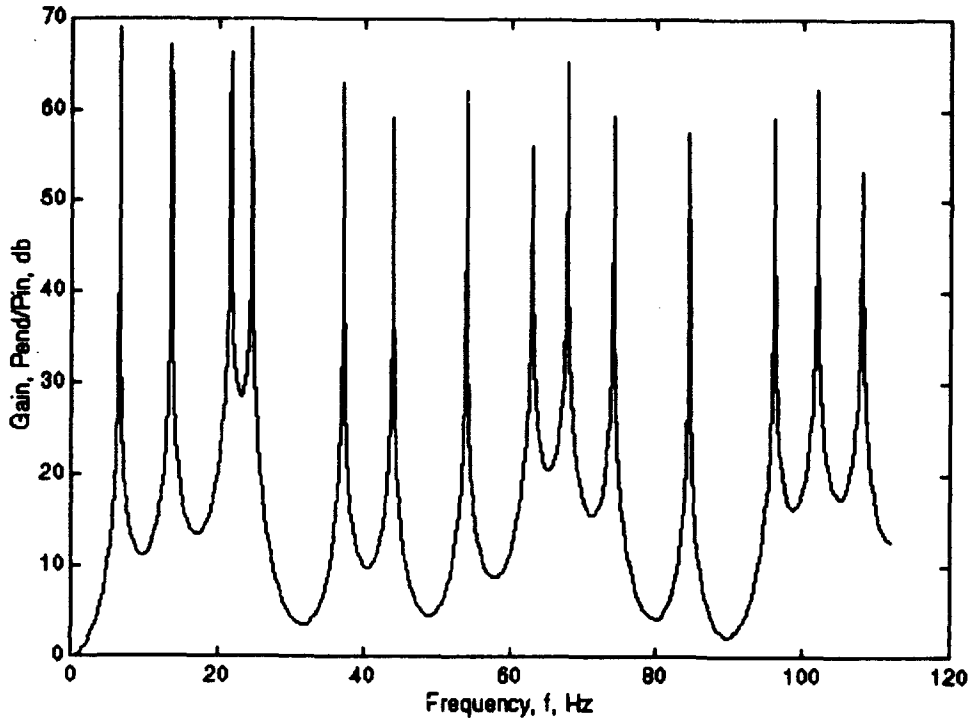

Figure B.4: CRF with Flow Conditioning Elements (no Pressure Equalization Pipe). Conditions: Blocked, Basic Length.

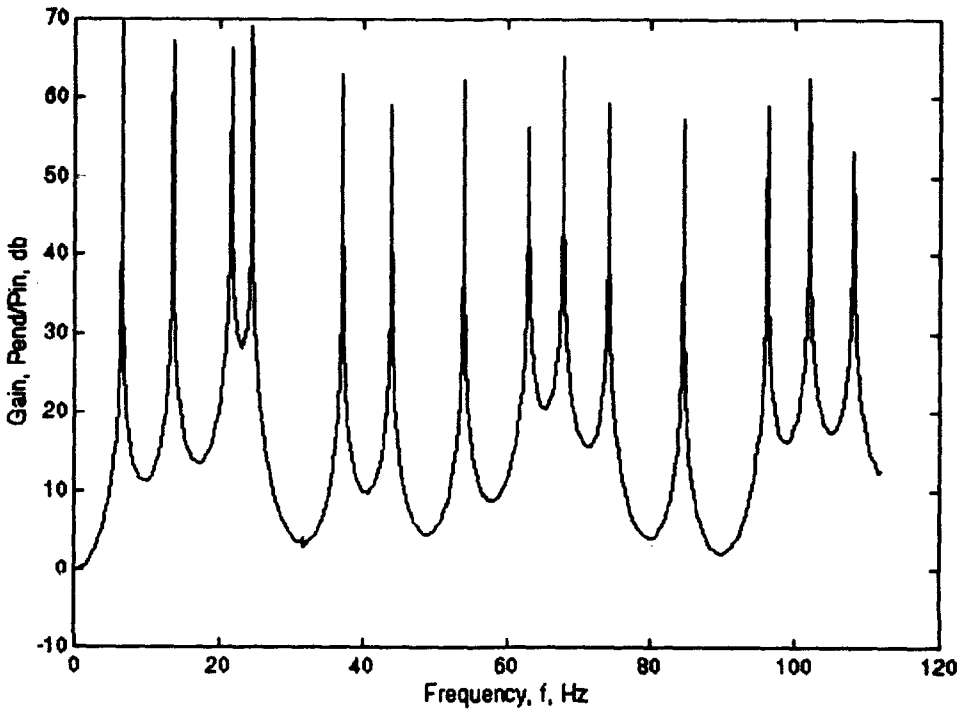

Figure B.5: CRF with Flow Conditioning Elements and Pressure Equalization Pipe. Conditions: Blocked, Basic Length.

Appendix C: Experimental Apparatus Specifications

Pneumatic Signal Generator: Manufacturer: Bendix. Includes

Pressure Regulator, S/N ENY-A296, 0 - 100 psig

Lambda Power Supplies, S/N ENY-A295/6, 0 - 600 V, 0 - 200 mA

Bendix Voltage Regulator, S/N ENY-A293

Hewlett-Packard Amplifier, Model 450A, S/N ENY-A297

Data Acquisition System:

Nicolet Multipro Pedestal, S/N IBK9300114. Includes four

Nicolet Multipro 120 digitizer cards, S/N IBM9300191/2/3/4

House Air Mean Pressure Transducer

Transducer: Endevco 8510-B100, S/N 20LG, 100 psig

Signal Conditioner: Endevco 4423, S/N BA88

Power Supply: Endevco 4425, S/N AF90

Orifice ΔP Transducer

Transducer: Statham 4347, S/N P6TC-2D-350, ± 2 psig

Signal Conditioner: Endevco 4423, S/N BA46

Power Supply: Endevco 4425, S/N AF68

Valve Transducer

Transducer: Endevco 8510-B5, S/N PP75, 5 psig

Signal Conditioner: Endevco 4423, S/N BA47

Power Supply: Endevco 4425, S/N AF68

Inlet (PS) Transducer

Transducer: Endevco 8510B-5, S/N 60HB, 5 psig

Signal Conditioner: Endevco 4423, S/N BA44

Power Supply: Endevco 4425, S/N AF70

Exit (PR4) Transducer

Transducer: Endevco 8510-B5, S/N B34Y, 5 psig

Signal Conditioner: Endevco 4423, S/N BA41

Power Supply: Endevco 4425, S/N AF70

Flow Conditioning Section Inlet (PR2) Transducer

Transducer: Endevco 8510-B5, S/N PP79, 5 psig

Signal Conditioner: Endevco 4423, S/N BA63

Power Supply: Endevco 442[illegible], S/N AF85

Flow Conditioning Section Exit (PR3) Transducer

Transducer: Endevco 8510-B5, S/N 90EK, 5 psig

Signal Conditioner: Endevco 4423, S/N BA63

Power Supply: Endevco 4425, S/N AF85

Section 1 Mean Pressure (Pmean) Transducer

Transducer: Endevco 8510-B100, S/N 80MB, 100 psig

Signal Conditioner: Endevco 4423, S/N BA44

Power Supply: Endevco 4425, S/N AF70

Function Generator: Wavetek 142-S-527, S/N 6700060

House Air Temperature: Thermocouple, OMEGA DP41-TC

Atmospheric Pressure: Transamerica Delaval Digital Barometer Type 2500-0103, S/N 258

Atmospheric Temperature: Bulb thermometer

Frequency Counter: Racal-Dana, Model 1992, S/N 990308

Valve Mass Flow Meter: Omega, FMA-408-V, S/N 7215

Solenoid Valve: Automatic Switch Company, Model 8320A15, S/N C78489S

Appendix D. Error Analysis

The errors associated with the dynamic pressure measurements are dependent on the accuracy of the transducer, amplifier (signal conditioner), and the digitizing card in the Nicolet MultiPro data acquisition system. These errors are tabulated below from information provided in the manufacturer's brochures.

Transducer (5 psig Endevco) Accuracy = ± .2%
Signal conditioner (Endevco) Accuracy = ± .5%
Nicolet MultiPro digitizer card Accuracy = ± 45 μV

For gain calculations, the peak voltage at the frequency of interest was determined from the spectral analysis program. A representative peak voltage from the gain data is 1.0 mV. For the 1.0 mV peak signal, the actual signal from the transducer is 50 μV since the signal conditioner amplifies the signal 20 times. Thus, assuming a transducer signal of 50 μV, subject to the accuracy of the transducer, the resulting transducer signal will be:

$$(50\ \mu V)\ X\ (\pm\ .2\%) = 50\ \mu V \pm 1\ \mu V.$$

When amplified by 20, the transducer signal and error become:

$$(50\ \mu V \pm 1\ \mu V)\ X\ (20) = 1000\ \mu V \pm 20\ \mu V.$$

This value is finally subject to the Nicolet accuracy of ± 45 μV, yielding a final range of actual voltages of:

$$1000\ \mu V \pm 65\ \mu V.$$

Thus, a 1 mV peak displayed in the spectral analysis program could actually be as small as 935 μV or as large as 1065 μV, yielding an overall error in the dynamic pressure measurement of ± 7%.

Appendix E: Computer Program

Several programs work off of a main program called maincrf.m. The main program and all of the subprograms are included in the following pages. A listing of the programs included is provided below.

```
% PROGRAM maincrf.m
%
% maincrf.malls all of the programs required to solve for the dynamic response
% of the CRF.  The variables are listed in the individual programs.
%
% PROGRAMS CALLED:
%
% crf.m          = Solves the Nichols equations
%
% out.m          = Prints output to the screen
%
% INPUT:
%
% RUNXXDATA.mat = Experimental run data, including mass flow, pressure, and
%                 temperature.
%
% inXX.mat       = Geometry data for the particular run
%
% OUTPUT
%
% CRFrunXX.mat   = Data file
%
% CRFrunXX.txt   = Text file
%
%%%%%%%%%%%%%%%%%%%%%%%%%%%%%%%%%%%%%%%%%%%%%%%%%%%%%%%%%%%%%%%%%%%%%%%%%%%%
clear variables
load RUN10DATA.mat
load inE10.mat
crf
save CRFrunE10.mat
diary CRFrunE10.txt
out
diary off
%
%
```

```
% This program is the analytical solution to the frequency response of the
% Compressor Research Facility (CRF) located at Wright-Patterson AFB, OH.
% This program is able to compute the fundamental frequencies of the full
% size facility as well as the fundamental frequencies for the laboratory model.
% There are two bessel function routines employed in this program.  For large
% scale input, algebraic approximations to the bessel functions are used.  When
% small scale input, i.e. scale model dimensions, are entered, the program uses
% the bessel functions intrinsic to matlab.  The approximations are required
% because Matlab intrinsic bessel functions will not compute the large
% argruments produced by the full scale geometry.
%
% This progam uses small signal assumptions.  For throughflow conditions, the
% facility is modeled in four sections.  The inlet section is section 1,
% the flow conditioning section is section 2, the inlet to the test article
% (end) is section 3, and the entrance to the compressor face (for full scale)
% or the exit from the model is section 4.  The program FSpipe.m solves for
% density, viscosity, velocities and the speed of sound for the full scale CRF.
% Program exppipe.m solves for the same variables for the scale model CRF.
% The unsteady solution divides the three sections into "J" + 2 sections to account
% for the individual flow straightening elements as well as the actual pressure
% transducer locations in the lab model.
%
% crf.m is started by a main program called maincrf.m.  All of the input
% variables are generated by maincrf.m.
%
% INPUT VARIABLES:
%
% Inputs from FSpipe.m or exppipe.m. Additional details about these variables
% are locacated in the comment sections of the program. All variables refer to
% the simplified geometry used in pipe.m.  For example, RADIUS(1) is the
% radius of the inlet section (36.8 + EXT feet long), RADIUS(2) is the
% radius of the flow conditioning section (19.8 feet long), RADIUS(3)
% is the radius of the end section (13.2 - EXT feet long), and RADIUS(4)
% is the exit radius or compressor radius.
```

```
%
% a(1,2,or 3)           = Speed of sound in air.  Units: ft/s.
% ENDIMP                = User specified end impedance.  Units: lb*s/ft^5.
% NU(1,2, or 3)         = Kinematic viscosity of air.  Units: ft^2/s.
% RHO(1,2, or 3)        = Density of air.  Units: lb*s^2/ft^4.
% RL3                   = End resistance.  Units: lb*s/ft^5.
% 'ELOCITY(1,2,3,or 4) = Velocity in each section.  Units: ft/s.
%
% Inputs from maincrf.m.  Additional details are given in the comments
% section of maincrf.m.
%
% B      = Number of sections in the branch.  Units: none.
% DATE   = Date of program run.
% EXT    = Extension of inlet section and subsequent contraction of exit
%          section.  Units: ft.
% J      = Number of sections in section 2. Units: none.
% L1     = Length of inlet section. Units: ft.
% L2(J)  = Length of a portion of the flow conditioning section. Units: ft.
% L3     = Length of inlet to test section. Units: ft.
% LB(B)  = Length of the branched line. Units: ft.
% MODEL  = Flags the program to use algebraic approximations for
%          full scale solutions (MODEL = 0) or intrinsic Bessel
%          functions for scale model solutions (MODEL = 1). Units: none.
% R1     = Radius of inlet section. Units: ft.
% R2(J)  = Radius of a portion of the flow conditioning section. Units: ft.
% R3     = Radius of inlet to test section. Units: ft.
% RB(B)  = Radius of the brached line. Units: ft.
% RO3    = Radius of orifice. Units: ft.
% RUN    = Tracking number to match input and output. Units: none.
% TAMB   = Ambient temperature. Units: degrees Rankine.
%
%
% OUTPUT VARIABLES:
%
% pltf(N)      = Discrete frequencies at which gain and phase angle are
```

```
%                 calculated. Units: hertz.
% pltG(N)       = Value of overall gain (Pend/Pin) at the "Nth" frequency. Units:
%                 decibels.
% pltP(N)       = Value of overall phase angle at the "Nth" frequency. Units:
%                 degrees.
% GAIN(N)       = Absolute value of the overall gain. Units: nondimensional.
% PR2PS(N)      = Value of the gain between the transducer located just ahead
%                 of the flow conditioning section (PR2) and the inlet transducer
%                 (PS). Units: nondimensional.
% pltG2(N)      = PR2PS in decibels.
% pltP2(N)      = Phase angle for PR2PS. Units: degrees.
% PR3PS(N)      = Value of the gain between the transducer located just behind
%                 of the flow conditioning section (PR3) and the inlet transducer
%                 (PS). Units: nondimensional.
% pltG3(N)      = PR3PS in decibels.
% pltP3(N)      = Phase angle for PR3PS. Units: degrees.
% PR4PS(N)      = Value of the gain between the transducer located at the end of
%                 the model (PR4) and the inlet transducer (PS). Units:
%                 nondimensional.
% pltG4(N)      = PR4PS in decibels.
% pltP4(N)      = Phase angle for PR4PS. Units: degrees.
% peak(x,y)     = Value of the "xth" peak gain at the "yth" frequency,
%                 based on overall gains. Units: decibels.
% valley(x,y)   = Value of the "xth" valley gain at the "yth" frequency, based on
%                 overall gains. Units: decibels.
%
% INTERMEDIATE VARIABLES:
%
% Ca1,Ca2(J),Ca3, CaB(B)    = Adiabatic capacitance per unit length.  Units:
%                             ft^4/lb.
% GAMMAL1, GAMMAL2(J), GAMMAL3, GAMMALB(B) = Propogation constant for line
%                             sections 1,2, 3, and branch, respectively.  Units:
%                             nondimensional.
% La1,La2(J),La3, LaB(B)    = Adiabatic inductance per unit length. Units:
%                             lb*(s^2)/ft^6.
```

```
% OMEGANU1, OMEGANU2(J), OMEGANU3, OMEGANUB(B) = Characteristic frequency.
%                                                nondimensional.
% PLPI2(J)                                     = Gain for "Jth" portion of line section 2. Units:
%                                                nondimensional.
% PLPIB(B)                                     = Gain for "Bth" portion of the branch. Units:
%                                                nondimensional.
% PL1PI1, PL2PI2, PL3PI3, PLBPIB = Gain for line sections 1, 2, 3, and branch,
%                                                respectively. Units: nondimensional.
% Y1, Y2(J), Y3, YB(B)                         = Shunt admittance for line sections 1, 2, 3, and
%                                                branch respectively; calculated through the use of
%                                                function adm.m. Units: ft^4/(lb*s).
% Z1, Z2(J), Z3, ZB(B)                         = Series Impedance for line sections 1, 2, 3, and
%                                                branch, repsectively; calculated through the use of
%                                                function imp.m. Units: lb*s/ft^6.
% ZC1, ZC2(J), ZC3, ZCB(B) = Characteristic Impedance for line sections 1, 2, 3,
%                                                and branch, respectively. Units lb*s/ft^5.
% ZI2(J), ZIB(B)                               = Impedance at the inlet to line section 2 and
%                                                branch, respectively. Units: lb*s/ft^5.
% ZL1, ZL2(J) ZLB(B)                           = Impedance at the end of sections 1, 2, and branch,
%                                                respectively. Units: lb*s/ft^5.
%
% OTHER VARIABLES:
%
% GAMAIR     = Ratio of specific heats for air. Units: nondimensional.
% I          = Loop counter. Units: none.
% INCREMENT = default value for stepomega.  Units: rad/s.
% N          = Counter for output arrays. Units: none.
% NP         = Prandtl number for air. Units: nondimensional.
% OMEGA      = Frequency of input signal, rad/s
% PLOTTER    = If PLOTTER = 1, signals the end of the program.  Data ready
%              to plot. Units: none.
% RANGE      = Maximum frequency for calculations. Units: hertz.
% repeat     = Flags the program to repeat calcultations, including refining
%              results around the peaks.  Units: none.
% stepomega = Determines the increment of advance through the frequency
```

```
%              range. Units: rad/s.
% v           = Counter for valley(x,y) array. Units: none.
% x           = Counter for peak(x,y) array. Units: none.
%
% FUNCTIONS:
%
%
% Four functions were written for the purpose of evaluating the propogation
% constants GAMMAL1, GAMMAL2, and GAMMAL3, as well as the characteristic
% impedance for each line section ZC1, ZC2, and ZC3.
%
% impa.m   = Accepts input variables OMEGARAT, La, and OMEGA and outputs
%            the impedance for the line section of interest. Approximates
%            the bessel function solution.
% imp.m    = Accepts input variables OMEGARAT, La, and OMEGA and outputs
%            the impedance for the line section of interest.  Uses internal
%            Bessel functions.
% adma.m   = Accepts input variables OMEGARAT, Ca, OMEGA, NP, GAMAIR and
%            outputs the admittance for the line section of interest.
%            Approximates the bessel function solution.
% adm.m    = Accepts input variables OMEGARAT, Ca, OMEGA, NP, GAMAIR and
%            outputs the admittance for the line section of interest.
%            Uses internal Bessel functions.
%
% Two functions were written for the purpose of evaluating the mach number
% effects due to mass flow.
%
% PENDPIN.m = Accepts input variables VELOCITY, La, Ca, ZC, GAMMAL, and ZL.
%           Outputs the gain for an individual line section based on
%           these inputs.
% ZC.m       = Accepts input variables La, Ca, VELOCITY, Z, and Y and outputs
%              the characteristic impedance for the individual line section
%              as adjusted for flow effects.
%
%
```

```
% Two programs were written to solve the dc conditions.
%
% exppipe.m = Solves for density, viscosity, velocity, speed of sound
%             and end resistance for the scale model CRF.
% FSpipe.m  = Solves for the density, viscosity, velocity, speed of sound,
%             and end resistance of the Full Scale CRF.
%
%
% Today's date: 1 October 1993
% Program Revision Number: 12
% Written for use on: Matlab Version 4.0a
% Programmer: Capt Janet Grondin
%
%%%%%%%%%%%%%%%%%%%%%%%%%%%%%%%%%%%%%%%%%%%%%%%%%%%%%%%%%%%%%%%%%%%%%%%%%%%%%%%
%
% Define conditions for air, range, and default step value
%
GAMAIR=1.4;
NP = .69;
if MODEL == 0
     FSpipe
else
     exppipe
end
%
% Set starting conditions
%
OMEGA = 0, N = 0, repeat = 0;
%
% Find characteristic values for section 3
%
La3 = RHO(3)/(pi*(R3^2));
Ca3 = (pi*(R3^2))/(RHO(3)*(a(3)^2));
OMEGANU3 = (8*NU(3))/(R3^2);
%
```

```
% Find characteristic values for the end if applicable
%
if mdot == 0 & RO3 >0
     LaEND = RHO(3)/(pi*(RO3^2));
     CaEND = (pi*(RO3^2))/(RHO(3)*(a(3)^2));
     OMEGANUEND = (8*NU(3))/(RO3^2);
end
%
% Find characteristic values for section 2
%
L = L1
%
% Because pipe.m only splits the CRF into 3 sections and crf.m splits
% the CRF into J+2 sections, determine the correlation between the
% data from pipe.m and the input required for each of the J+2 sections in
% crf.m
%
for I=1:J;
   L = L2(I) + L;
   if L >= 36.8+EXT
     HOLD1 = I-1;
   end
   if L >= 36.8+19.8+EXT
     HOLD2 = I-1;
   end
   I = I+1;
end
for I = 1:HOLD1
   OMEGANU2(I) = (8*NU(1))/(R2(I)^2);
   La2(I) = RHO(1)/(pi*(R2(I)^2));
   Ca2(I) = (pi*(R2(I)^2))/(RHO(1)*(a(1)^2));
end
for I = 1:HOLD1+1:HOLL2
   OMEGANU2(I) = (8*NU(2))/(R2(I)^2);
   La2(I) = RHO(2)/(pi*(R2(I)^2));
```

```
   Ca2(I) = (pi*(R2(I)^2))/(RHO(2)*(a(2)^2));
end
for I = HOLD2 + 1: J
   OMEGANU2(I) = (8*NU(3))/(R2(I)^2);
   La2(I) = RHO(3)/(pi*(R2(I)^2));
   Ca2(I) = (pi*(R2(I)^2))/(RHO(3)*(a(3)^2));
end
%
% Find characteristic values for section 1
%
La1 = RHO(1)/(pi*(R1^2));
Ca1 = (pi*(R1^2))/(RHO(1)*(a(3)^2));
OMEGANU1 = (8*NU(1))/(R1^2);
%
% Find characteristic values for branch
%
if B >0
   for I = 1:B
      OMEGANUB(I) = (8*NU(1))/(RB(I)^2);
      LaB(I) = RHO(1)/(pi*(RB(I)^2));
      CaB(I) = (pi*(RB(I)^2))/(RHO(1)*(a(1)^2));
   end
end
%
% Start a loop through the valid frequency range OMEGA < 702 (for CRF).  Allow
% for slightly higher frequencies than 702 so the calculations that
% depend on OMEGA being greater than or equal to 702 will not be missed.
%
while OMEGA < RANGE+10
if OMEGA < 1
        INCREMENT = .2;
else
     INCREMENT = 2;
end
    FLAG = 0;
```

```
    if repeat == 1
       for I=1:x
        if OMEGA >= ((peak(I,2)*2*pi) - 4) & OMEGA <= ((peak(I,2)*2*pi) + 4)
        if MODEL == 1
          stepomega = .2;
        else
                stepomega =.02;
        end
            FLAG = 1;
            I = x;
         else
         I = I+1;
         end
       end
%       for I=1:v
%     if OMEGA >= ((valley(I,2)*2*pi) - 4) & OMEGA <= ((valley(I,2)*2*pi) + 4)
%       if MODEL == 1
%         stepomega = .2;
%       else
%                 stepomega =.02;
%       end
%            FLAG = 1;
%            I = v;
%         else
%            I = I + 1;
%         end
%       end
       if FLAG == 1
         FLAG = 0;
       else
         stepomega = INCREMENT;
         end
    else
       stepomega = INCREMENT;
    end
```

```
OMEGA = OMEGA + stepomega;
freq = OMEGA/(2*pi)
N = N+1;
%
% Find the minimum OMEGA for calculations. (OMEGA/OMEGANU) > 1 is required for
% approximations to the Bessel functions to work.  Calculate the first 5
% points at the lowest allowable frequencies.
%
if N<5 & MODEL == 0
     minf = [OMEGANU1 min(OMEGANU2) OMEGANU3 min(OMEGANUB)]
     OMEGA = (N^2)*min(minf)
elseif N<5 & MODEL == 1
        OMEGA = (N^2)*1e-20
end
%
% Calculate the propogation constant GAMMAL3, characteristic impedance, ZC3, and
% gain for line section 3.
%
OMEGARAT3 = OMEGA/OMEGANU3;
%
% Use the approximations for bessel functions if MODEL = 0 or internal functions
% if MODEL = 1.
%
if MODEL==0
   Z3 = impa(OMEGARAT3, La3, OMEGA);
   Y3 = adma(OMEGARAT3, Ca3, OMEGA, NP, GAMAIR);
else
   Z3 = imp(OMEGARAT3, La3, OMEGA);
   Y3 = adm(OMEGARAT3, Ca3, OMEGA, NP, GAMAIR);
end
GAMMAL3 = (sqrt(Z3*Y3))*L3;
ZC3 = sqrt(Z3/Y3);
%
%  Determine end resistance
%
```

```
if RO3 >0 & mdot >0
     if MODEL == 1
          ZL3 = (RL3 + (j*OMEGA*RHO(3)/(12*AREA(4))));
     else
          ZL3 = RL3;
     end
     ZC3 = ZC(La3, Ca3, VELOCITY(3), Z3, Y3);
     ZI3 = ((ZL3*cosh(GAMMAL3)) + (ZC3*sinh(GAMMAL3)))/(cosh(GAMMAL3) +
((ZL3/ZC3)*sinh(GAMMAL3)));
     PL3PI3 = PENDPIN(VELOCITY(3), La3, Ca3, ZC3, GAMMAL3, ZL3);
elseif RO3 > 0 & mdot == 0
     OMEGARATEND = OMEGA/OMEGANUEND;
     if MODEL == 0
          LEND = 1
          ZEND = impa(OMEGARATEND, LaEND, OMEGA);
          YEND = adma(OMEGARATEND, CaEND, OMEGA, NP, GAMAIR);
     else
          LEND = 1/12
          ZEND = imp(OMEGARATEND, LaEND,OMEGA);
          YEND = adm(OMEGARATEND, CaEND, OMEGA, NP, GAMAIR);
     end
     GAMMALEND = (sqrt(ZEND*YEND))*LEND;
     ZCEND = (sqrt(ZEND/YEND))*LEND;
     ZL3 = ZCEND*tanh(GAMMALEND);
     ZI3 = ((ZL3*cosh(GAMMAL3)) + (ZC3*sinh(GAMMAL3)))/(cosh(GAMMAL3) +
((ZL3/ZC3)*sinh(GAMMAL3)));
     PL3PI3 = PENDPIN(VELOCITY(3), La3, Ca3, ZC3, GAMMAL3, ZL3);
elseif RO3 == 0
%
% For a blocked line:
%
     ZI3 = ZC3/tanh(GAMMAL3);
     PL3PI3 = 1/cosh(GAMMAL3);
end
%
```

```
% Calculate the propogation constant GAMMAL2 and characteristic impedance, ZC2 and
% gain for each portion of line section 2.  Use approximations if MODEL = 0 or
% internal bessel functions if MODEL = 1.
%
if MODEL==0;
   for I=1:J;
      OMEGARAT2(I) = OMEGA/OMEGANU2(I);
      Z2(I) = impa(OMEGARAT2(I), La2(I), OMEGA);
      Y2(I) = adma(OMEGARAT2(I), Ca2(I), OMEGA, NP, GAMAIR);
      GAMMAL2(I) = (sqrt(Z2(I)*Y2(I)))*L2(I);
   end
else
   for I=1:J;
      OMEGARAT2(I) = OMEGA/OMEGANU2(I);
      Z2(I) = imp(OMEGARAT2(I), La2(I), OMEGA);
      Y2(I) = adm(OMEGARAT2(I), Ca2(I), OMEGA, NP, GAMAIR);
      GAMMAL2(I) = sqrt(Z2(I)*Y2(I))*L2(I);
   end
end
%
% Calculate the properties at the end of line 2
%
ZC2(J) = ZC(La2(J), Ca2(J), VELOCITY(2), Z2(J), Y2(J));
ZL2(J) = ZI3;
ZI2(J) = ZC2(J)*((ZL2(J)*cosh(GAMMAL2(J)) +
ZC2(J)*sinh(GAMMAL2(J)))/(ZL2(J)*sinh(GAMMAL2(J)) + ZC2(J)*cosh(GAMMAL2(J))));
PLPI2(J) = PENDPIN(VELOCITY(2),La2(J),Ca2(J),ZC2(J),GAMMAL2(J),ZL2(J));
%
% Calculate the properties of the remaining portions of section 2
%
I=J-1;
while I>0
   ZC2(I) = ZC(La2(I), Ca2(I), VELOCITY(2), Z2(I), Y2(I));
   ZL2(I) = ZI2(I+1);
   ZI2(I) = ZC2(I)*((ZL2(I)*cosh(GAMMAL2(I)) +
```

```
ZC2(I)*sinh(GAMMAL2(I)))/(ZL2(I)*sinh(GAMMAL2(I)) +
ZC2(I)*cosh(GAMMAL2(I))));
   PLPI2(I) = PENDPIN(VELOCITY(2), La2(I),Ca2(I),ZC2(I),GAMMAL2(I),ZL2(I));
   I = I-1;
end
%
% Calculate the propagation constant GAMMALB, characteristic impedance ZCB, and
% gain for the branch.
%
if B >0
if MODEL == 0
   for I = 1:B
       OMEGARATB(I) = OMEGA/OMEGANUB(I);
       ZB(I) = impa(OMEGARATB(I), LaB(I), OMEGA);
       YB(I) = adma(OMEGARATB(I), CaB(I), OMEGA, NP, GAMAIR);
       GAMMALB(I) = (sqrt(ZB(I)*YB(I)))*LB(I);
       ZCB(I) = sqrt(ZB(I)/YB(I));
   end
else
   for I = 1:B
       OMEGARATB(I) = OMEGA/OMEGANUB(I);
       ZB(I) = imp(OMEGARATB(I), LaB(I), OMEGA);
       YB(I) = adm(OMEGARATB(I), CaB(I), OMEGA, NP, GAMAIR);
       GAMMALB(I) = (sqrt(ZB(I)*YB(I)))*LB(I);
       ZCB(I) = sqrt(ZB(I)/YB(I));
   end
end
%
% Line 2 of the branch is blocked.
%
ZIB(2) = ZCB(2)/tanh(GAMMALB(2));
%
% Line 3 of the branch is open.
%
ZIB(3) = ZCB(3)*tanh(GAMMALB(3));
```

```
ZLB(1) = (ZIB(2)*ZIB(3))/(ZIB(2) + ZIB(3));
ZIB(1) = ZCB(1)*((ZLB(1)*cosh(GAMMALB(1)) +
ZCB(1)*sinh(GAMMALB(1)))/(ZLB(1)*sinh(GAMMALB(1)) + ZCB(1)*cosh(GAMMALB(1 ))));
PLBPIB(N) = 1/(((ZCB(1)/ZLB(1))*sinh(GAMMALB(1))) + cosh(GAMMALB(1)));
end
%
% Calculate the propogation constant GAMMAL1, characteristic impedance, ZC1, and
% gain for line section 1.  Use approximations if MODEL = 0 or internal
% functions if model = 1.
%
if B >0
   ZL1 = (ZI2(1)*ZIB(1))/(ZI2(1) + ZIB(1));
else
   ZL1 = ZI2(1);
end
OMEGARAT1 = OMEGA/OMEGANU1;
if MODEL==0;
   Z1 = impa(OMEGARAT1, La1, OMEGA);
   Y1 = adma(OMEGARAT1, Ca1, OMEGA, NP, GAMAIR);
else
   Z1 = imp(OMEGARAT1, La1, OMEGA);
   Y1 = adm(OMEGARAT1, Ca1, OMEGA, NP, GAMAIR);
end
GAMMAL1 = L1 * (sqrt(Z1*Y1));
ZC1 = ZC(La1, Ca1, VELOCITY(1), Z1, Y1);
PL1PI1 = PENDPIN(VELOCITY(1), La1,Ca1,ZC1,GAMMAL1,ZL1);
%
% Calculate the total gain for line section 2
%
PL2PI2 = 1;
for I = 1:J;
   PL2PI2 = PL2PI2*PLPI2(I);
end
%
% Calculate the total gain for the CRF at the "Nth" frequency.  Also calculate
```

```
% the gains to be seen at the transducer locations in the model.
%
pltf(N) = OMEGA/(2*pi);
GAIN(N) = (PL1PI1*PL2PI2*PL3PI3);
pltP(N) = (atan2(imag(GAIN(N)),real(GAIN(N))))*(180/pi);
GAIN(N) = abs(GAIN(N));
pltG(N) = 20*log10(GAIN(N));
G = pltG(N)
PR2PS(N) = (PLPI2(2)*PLPI2(1));
pltP2(N) = (atan2(imag(PR2PS(N)),real(PR2PS(N))))*(180/pi);
PR2PS(N) = abs(PR2PS(N));
pltG2(N) = 20*log10(PR2PS(N));
PRPS3 = 1;
for I=1:J-2;
     PRPS3 = PRPS3*PLPI2(I);
end
pltP3(N) = (atan2(imag(PRPS3),real(PRPS3)))*(180/pi);
PR3PS(N) = abs(PRPS3);
pltG3(N) = 20*log10(PR3PS(N));
PR4PS(N) = (PL2PI2);
pltP4(N) = (atan2(imag(PR4PS(N)),real(PR4PS(N))))*(180/pi);
PR4PS(N) = abs(PL2PI2);
pltG4(N) = 20*log10(PR4PS(N));
save matlab2.m
%
% After the first "quick and dirty" cut, find the general locations of the peaks
% and valleys and refine stepomega around them to determine their actual value.
%
if OMEGA >= RANGE & repeat == 0
   x = 0
   v = 0
   repeat = 1
   FLAG = 0
   for I = 2: N-1
       if pltG(I) >= pltG(I+1) & FLAG == 0
```

```
            x = x + 1
            peak(x,1) = pltG(I)
            peak(x,2) = pltf(I)
            FLAG = 1
         elseif pltG(I-1) >= pltG(I) & pltG(I+1) >= pltG(I)
            v = v+1
            valley(v,1) = pltG(I)
            valley(v,2) = pltf(I)
            FLAG = 1
         end
         if pltG(I) <= pltG(I+1) & FLAG == 1
            FLAG = 0
         end
   end
   save matlab2.mat
   OMEGA = 7, N = 0
   clear GAIN PR1PS PR2PS PR3PS PR4PS pltf pltP pltG pltP2 pltG2 pltP3 pltG3
   clear pltG4 pltP4 PLBPIB
end
%
% If both iterations have been accomplished, find the values of the actual peaks and
% valleys.
%
if OMEGA >= RANGE & repeat == 1
   PLOTTER = 1;
   v = 1;
   x = 1;
   FLAG = 0;
   for I = 2:N-1
      if pltG(I) >= pltG(I+1) & FLAG == 0
         peak(x,1) = pltG(I);
         peak(x,2) = pltf(I);
         x = x + 1;
         FLAG = 1;
      elseif pltG(I-1) >=pltG(I) & pltG(I+1) >= pltG(I)
```

```
         valley(v,1) = pltG(I);
         valley(v,2) = pltf(I);
         v = v + 1
      end
      if pltG(I) <= pltG(I+1) & FLAG == 1
         FLAG = 0;
      end
   end
end
%
% Plot the results
%
if PLOTTER == 1
   OMEGA = RANGE + 20
end
end
```

```
%
%  Program exppipe.m solves for the dc flow conditions in the experimental
%  model of the CRF.  The program is written to solve for velocity,
%  density, viscosity, the speed of sound, and the end resistance for
%  the model only.  The equivalent program for the full scale CRF is called
%  FSpipe.m.  The two are different due to the different data available for
%  solution.  Also, the full scale CRF end impedance differers from the
%  model end impedance.  This program simplifies the geometry from that used to
%  solve for the transfer function of the CRF.  The CRF is broken into four
%  main sections in this program.  Section 1 is the inlet section of length
%  36.8 ft + EXT.  Section 2 is the constant length 19.8 ft flow conditioning
%  section.  Section 3 is the end section of length 13.2 ft - EXT. Section 4 is
%  the exit orifice, designated with length LO3 and radius RO3.
%
%  Program exppipe.m is called from program crf.m if the variable MODEL is
%  set to 1.
%
%  INPUT VARIABLES:
%
%  input from crf.m
%
%  GAMAIR = Ratio of specific heats for air.  Units: nondimensional
%  PAMB   = Ambient pressure.  Units: lb/ft^2 (absolute)
%  PMEAN1 = Mean pressure measured in the inlet section.  Units: lb/ft^2 (gage)
%  mdot   = Mass flow from RUNXXDATA.mat.  Units: slug/sec
%  TAMB   = Ambient temperature.  Units: degrees Rankine
%
%  input from inrunXX.m
%
%  MODEL  = If 0, program uses full scale radii.  If 1, program defaults
%           to scale model radii.%  R1 = Radius of inlet section.  Units: feet
%  R1     = Radius of inlet section.  Units: feet
%  RO3    = Radius of end orifice.  Units: feet
%
%  OUTPUT VARIABLES
```

```
%
%  a(I)    = Speed of sound in air.  Units: ft/s
%
%  ENDIMP = Specified end impedance.  This variable overrides the calculation
%           of end impedance (RL3) but does not change the flow conditions.
%           Units: lb*s/ft^5
%  NU(I)   = Kinematic viscosity in the inlet (NU(1)), flow conditioning section
%           (NU(2)), and end (NU(3)) sections based on the computed density
%           for that section.  Units: ft^2/s
%  PS(I)   = Static pressure in inlet(1), flow conditioning section (2), and
%           end (3).  MEANP(4) is the mean pressure at the exit of section
%           3 and is used to calculate the orifice resistance.  Units:
%           lb/ft^2 (gage)
%  RHO(I) =  Density of the inlet (RHO(1)), flow conditioning section (RHO(2)),
%            and end (RHO(3)) sections based on the mean pressure calculated in
%            each section and the input ambient pressure.  Units: slug/ft^3
%  RL3     = Computed end resistance.  Units: lb*s/ft^5
%  VELOCITY(I) = Velocities in inlet (1), flow conditioning section (2), and
%                end (3) sections.  Units: ft/s
%
%  INTERMEDIATE VARIABLES
%
%  AREA(I)      = Area of the inlet (1), flow conditioning section (2), and
%                 end (3).  Units: ft^2.
%  DELTAP       = Static pressure jump at exit of model, per unit length based
%                 on orifice length, lb/ft^3
%  friction(I) = Coefficient of friction for the 3 sections.  Based on
%                 smooth walls.  Units: nondimensional.
%  K            = Loss coefficient for individual elements such as area
%                 sections and screens and honeycomb.  Units: nondimensional
%  LENGTH(I)    = Length of the inlet (1), flow conditioning section (2), and
%                 end (3).  Units: feet.
%  LO3 = Orifice length, ft
%  RADIUS(I)    = Radius of the inlet (1), flow conditioning section (2), and
%                 end (3).  Units: feet.
```

```
%  ReD(I)       = Reynolds Number for the inlet (1), flow conditioning section
%                 (2), and end (3).  Units: nondimensional.
%
% Today's Date: 1 October 1993
% Program Revision Number: 4
% Written for use on: Matlab Version 4.0a
% Programmer: Capt Janet Grondin
%
%
%%%%%%%%%%%%%%%%%%%%%%%%%%%%%%%%%%%%%%%%%%%%%%%%%%%%%%%%%%%%%%%%%%%%%%%%%%%%%%%
%
% Density and Kinematic viscosity
%
for I = 1:9
     RHO(I) = (PAMB+PMEAN1)/(1716*TAMB);
     NU(I) = (1/RHO(I))*(3.584e-7)*(TAMB/491.4)*(691.2/(TAMB+199.8));
end
%
% If the end is orifice terminated, there will be flow through the crf.
%
if mdot == 0
     DENS = RHO(1);
     VISC = NU(1);
     clear RHO NU
    for I = 1:3
        RHO(I) = DENS;
     NU(I) = VISC;
        VELOCITY(I) = 0;
     a(I) = sqrt(GAMAIR*(PMEAN1+PAMB)/RHO(I));
    end
%
% Calculate pressure drops if mass flow is present
%
elseif mdot > 0
PS(1) = PMEAN1 + PAMB;
```

```
VELOCITY(1) = mdot/(RHO(1)*pi*(R1^2));
%
% Define dimensions and loss coefficients
%
RADIUS = [10/120 10/120 5/120 5/120 5/120 5/120 .375/24 .375/24 RO3];
LENGTH = [36.8+EXT 0 1.6 3 15.2 0 13.2-EXT 0 LO3];
K = [0 .2 0 2.365 0 .24 0  0  0];
%
% Calculate areas
%
for I = 1:9
     AREA(I) = (RADIUS(I)^2)*pi;
end
%
% Section velocities and Reynolds number
%
ReD(1) = 2*VELOCITY(1)*RADIUS(1)/NU(1);
for I = 2:9
     VELOCITY(I) = VELOCITY(I-1)*AREA(I-1)/AREA(I)
     ReD(I) = VELOCITY(I)*2*RADIUS(I)/NU(I);
end
%
% Friction coefficient for laminar flow
%
for I = 1:9
   if ReD(I) <2300
     friction(I) = 64/ReD(I);
%
% Friction coefficient for turbulent flow
%
   else
     friction(I) = .316/(ReD(I)^.25);
   end
end
%
```

```
% Static pressures in each section
%
for I = 1:8
     PS(I+1) = PS(I) + (RHO(I)/2)*((VELOCITY(I)^2) - (VELOCITY(I+1)^2) -
(K(I)*(VELOCITY(I+1)^2)) - (friction(I)*LENGTH(I)*(VELOCITY(I)^2)/(2*RADIUS(I))));
end
DENS = [RHO(1) RHO(3) RHO(7)];
VISC = [NU(1)  NU(3)  NU(7)];
vel = [VELOCITY(1) VELOCITY(3) VELOCITY(7)];
clear RHO NU VELOCITY
for I = 1:3
   VELOCITY(I) = vel(I);
   RHO(I) = DENS(I);
   NU(I) = VISC(I);
   a(I) = sqrt(GAMAIR*PS(I)/RHO(I));
end
  RL3 =  (mdot*(1.5 - .5*(RO3/R3)) + ((RO3/R3)^4)
+((LO3/(2*RO3))*friction(9))))/((pi^2)*(RO3^4))
getend = exist('ENDIMP')
%
% If end impedance has been specified, override RL3 calculation
%
if getend == 1
  RL3 = ENDIMP
end
end
end
```

```
% Program FSpipe.m solves for the end impedance, ZL3, and the velocities in
% each major section of the full scale CRF.  The flow is assumed to be
% incompressible and the end condition is a smooth contraction from R3 to RO3
% (Radius of the compressor).  The equivalent solution for the experimental
% model is exppipe.m.  Program crf.m calls FSpipe.m if the variable MODEL
% is equal to zero, indicating a full scale solution is desired.
%
% INPUT VARIABLES
%
%  GAMAIR = Ratio of specific heats for air.  Units: nondimensi nal
%  PAMB   = Ambient pressure.  Units: lb/ft^2 (absolute)
%  mdot   = Mass flow from RUNXXDATA.mat.  Units: slug/sec
%  MODEL  = If 0, program uses full scale radii.  If 1, program defaults
%           to scale model radii.%  R1 = Radius of inlet section.  Units: feet
%  RO3    = Radius of end orifice.  Units: feet
%  TAMB   = Ambient temperature.  Units: degrees Rankine
%
%  OUTPUT VARIABLES
%
%  a(I)   = Speed of sound in air.  Units: ft/s
%
%  ENDIMP = Specified end impedance.  This variable overrides the calculation
%           of end impedance (RL3) but does not change the flow conditions.
%           Units: lb*s/ft^5
%  NU(I)  = Kinematic viscosity in the inlet (NU(1)), flow conditioning section
%           (NU(2)), and end (NU(3)) sections based on the computed density
%           for that section.  Units: ft^2/s
%  RHO(I) =  Density of the inlet (RHO(1)), flow conditioning section (RHO(2)),
%            and end (RHO(3)) sections based on the mean pressure calculated in
%            each section and the input ambient pressure.  Units: slug/ft^3
%  RL3    = Computed end resistance.  Units: lb*s/ft^5
%  VELOCITY(I) = Velocities in inlet (1), flow conditioning section (2), and
%                end (3) sections.  Units: ft/s
%
%  INTERMEDIATE VARIABLE
```

```
%
%  AREA(I)      = Area of the inlet (1), flow conditioning section (2), and
%                 end (3).  Units: ft^2.
%
% Today's Date: 1 October 1993
% Program Revision Number: 4
% Written for use on: Matlab Version 4.0a
% Programmer: Capt Janet Grondin
%%%%%%%%%%%%%%%%%%%%%%%%%%%%%%%%%%%%%%%%%%%%%%%%%%%%%%%%%%%%%%%%%%%%%%%%%%%%%%%
%
% For full scale calculations, only mass flow is specified.  The flow conditions
% and end impedance are calculated.
%
if MODEL == 0
     for I = 1:3
          RHO(I) = PAMB/(1716*TAMB);
          NU(I) = (1/RHO(I))*(3.584e-7)*(TAMB/491.4)*(691.2/(TAMB+199.8));
          a(I) = sqrt(GAMAIR*1716*TAMB)
     end
     AREA = [pi*(100) pi*25 pi*(1.65^2) pi*(RO3^2)];
        if RO3 > 0
           for I = 1:3
          VELOCITY(I) = mdot/(RHO(I)*AREA(I));
        end
          RL3 = .04*mdot/((pi*(RO3^2))^2);

     else
          VELOCITY = [0 0 0];
     end
     getend = exist('ENDIMP')
        if getend == 1
           ZL3 = ENDIMP
        end
end
```

```
function Z = imp(OMEGARAT, La, OMEGA)
%
% This function calculates the series impedance for a line section and
% is to be used with program CRF.m
%
x = j*OMEGA*La;
y = sqrt( 8*OMEGARAT*(j^3));
CZRAT = 2/y;
JZRAT = bessela(1,y)/bessela(0,y);
Z = x/(1-(CZRAT*JZRAT));
end
```

```
function Z = impa(OMEGARAT, La, OMEGA)
%
%  This function is an algebraic approximation to the bessel functions
%  used in program CRFAPPRX.m
%
F = sqrt(OMEGARAT*8);
temp3 = 1/(sqrt(j) * F);
temp4 = (1 + (2*temp3) + (3*(temp3 ^ 2)) + ((15/64) *(temp3^3)));
Z = OMEGA*La*j*temp4;
end
```

```
function Y = adm(OMEGARAT, Ca, OMEGA, NP, GAMAIR)
%
% This program calculates the shunt admittance of a line and is to
% be used with program CRF.m
%
xy = j*OMEGA*Ca;
yy = sqrt(8*NP*OMEGARAT*j^3);
CYRAT = 2*(GAMAIR - 1)/yy;
JYRAT = bessela(1,yy)/bessela(0,yy);
Y = xy + (xy*CYRAT*JYRAT);
end
```

```
function Y = adma(OMEGARAT, Ca, OMEGA, NP, GAMAIR)
%
%  This function is an algebraic solution to the bessel functions required
%  to solve for shunt admittance in program CRFAPPRX.m
%
F = sqrt(8*OMEGARAT);
temp1 = 1/(F*sqrt(j*NP));
temp2 = ((2*temp1) - (temp1^2) - (.25*(temp1^3)));
Y = (OMEGA*Ca*j)*(1 + ((GAMAIR - 1)*temp2));
end
```

```
function thru = PENDPIN(VELOCITY, La, Ca, ZC, GAMMAL, ZL)
%
% PENDPIN.m is a function called from crf.m to evaluate the gain of
% a line.  This function accounts for velocity effects due to high
% mass flow.
%
% VARIABLE LIST
%
% Input Variables:
%
% Ca = Adiabatic capacitance per unit length.  Units: ft^4/lb.
% GAMMAL = Propagation operator.  Units: nondimensional.
% La = Adiabatic inductance per unit lenght.  Units: lb*(s^2)/ft^6.
% VELOCITY = Velocity in section of interest. Units: ft/s.
% ZC = Characteristic impedance in area of interest. Units: lb*s/ft^5.
% ZL = End impedance for section of interest.  Units: lb*s/ft^5.
%
% Intermediate Variables:
%
% GAMMATL = Propagation operator with throughflow. Units: nondimensional.
% NM = Mach number.  Units: nondimensional
% ZCA = Adiabatic characteristic impedance.  Units: lb*s/ft^5
%
% Output Variables:
%
% thru = Gain of the line of interest.  Units: nondimensional.
%
% Today's Date: 1 October 1993
% Program Revision Number: 1
% Written for use on: MATLAB Version 4.0a
% Programmer: Capt Janet Grondin
%%%%%%%%%%%%%%%%%%%%%%%%%%%%%%%%%%%%%%%%%%%%%%%%%%%%%%%%%%%%%%%%%%%%%%%%%%%%%%%
NM = sqrt(La*Ca*(VELOCITY^2));
ZCA = sqrt(La/Ca);
m = (NM/2)*((ZCA/ZC) - (ZC/ZCA));
```

```
bx = (.5*NM*GAMMAL*((ZCA/ZC)+(ZC/ZCA)))/(1-(NM^2));
GAMMATL = (GAMMAL*sqrt(1+(m^2)))/(1-(NM^2));
NUM = (exp(bx))*sqrt(1+(m^2));
DENOM = (sqrt(1+(m^2))*cosh(GAMMATL))+(((ZC/ZL) - m)*sinh(GAMMATL));
thru = NUM/DENOM;
end
```

```
% Function ZC.m calculates the characteristic impedance for a line with
% thrughflow.  This function is called by program crf.m.
%
% VARIABLE LIST
%
% Input Variables:
%
% Ca = Adiabatic capacitance per unit length. Units: ft^4/lb.
% La = Adiabatic inductance per unit lenght.  Units: lb*(s^2)/ft^6.
% VELOCITY = Velocity in section of interest. Units: ft/s.
% Z = Series impedance.  Units: lb*s/ft^6.
% Y = Shunt admittance.  Units: ft^4/(lb*s).
%
% Intermediate Variables:
%
% NM = Mach number.  Units: nondimensional
% ZC = Characteristic impedance without throughflow. Units: lb*s/ft^5.
% ZCA = Adiabatic characteristic impedance.  Units: lb*s/ft^5.
%
% Output Variables:
%
% thruzc = Characteristic impedance with throughflow.  Units: lb*s/ft^5.
%
% Today's Date: 1 October 1993
% Program Revision Number: 1
% Written for use on: MATLAB Version 4.0a
% Programmer: Capt Janet Grondin
%%%%%%%%%%%%%%%%%%%%%%%%%%%%%%%%%%%%%%%%%%%%%%%%%%%%%%%%%%%%%%%%%%%%%%%%%%%%%%%
function thruzc = ZC(La, Ca, VELOCITY, Z, Y)
ZC = sqrt(Z/Y);
NM = sqrt(La*Ca*(VELOCITY^2));
ZCA = sqrt(La/Ca);
m = (NM/2)*((ZCA/ZC) - (ZC/ZCA));
thruzc = sqrt(Z/Y)*((sqrt(1 + (m^2))) - m);
end
```

```
%
% Data set A.  Full scale CRF with flow straightening elements.
%
% Locations represent:
%
% L1      = Transducer 1 location, branch inlet (at the end of L1)
% L2(1)   = End of section 1
% L2(2)   = Location of Transducer 2 (at the end of L2(2))
% L2(3)   = Start of flow conditioning section
% L2(4)   = Grid
% L2(5)   = Screen
% L2(6)   = Honeycomb
% L2(7)   = Screen
% L2(8)   = Grid
% L2(9)   = 5 ft dia section, 1 ft long
% L2(10)  = Grid
% L2(11)  = Screen
% L2(12)  = Honeycomb
% L2(13)  = Screen
% L2(14)  = Grid
% L2(15)  = Location of Transducer 3 (at the end of L2(15))
% L2(16)  = End of section 2 (at the end of L2(16))
% L2(17)  = Location of Transducer 4 (at the end of L2)
% L3      = End of model
%
XT3 = 13.2-.15625-EXT
J = 17
R1 = 10
L1 = .33333333
R2 = [10 5 5 4.74 3.48 4.77 3.48 4.74 5 4.74 3.48 4.77 3.43 4.74 5 5 1.65]
L2 = [36.466667+EXT 1.58 1.02 .375 .017/12 .25 .017/12 .375 1 .375 .017/12 .25
.105/12 .375 .82 13.4 XT3]
R3 = 1.65
L3 = .15625
```

```
%
% Data set B.  Model scale CRF with flow straightening elements.
%
% Locations represent:
%
% L1      = Transducer 1 location, branch inlet (at the end of L1)
% L2(1)   = End of section 1
% L2(2)   = Location of Transducer 2 (at the end of L2(2))
% L2(3)   = Start of flow conditioning section
% L2(4)   = Grid
% L2(5)   = Screen
% L2(6)   = Honeycomb
% L2(7)   = Screen
% L2(8)   = Grid
% L2(9)   = 5 ft dia section, 1 ft long
% L2(10)  = Grid
% L2(11)  = Screen
% L2(12)  = Honeycomb
% L2(13)  = Screen
% L2(14)  = Grid
% L2(15)  = Location of Transducer 3 (at the end of L2(15))
% L2(16)  = End of section 2 (at the end of L2(16))
% L2(17)  = Location of Transducer 4 (at the end of L2)
% L3      = End of model
%
XT3 = 13.2 - .15625-EXT
J = 17
R1 = .083333
L1 = .33333333
R2 = [.0833333 .04166667 .0416667 .0395 .029 .03975 .029 .0395 .04166667 .0395 .029
.03975 .028583333 .0395 .04166667 .04166667 .015625]
L2 = [36.466667+EXT 1.58 1.02  .375 .017/12 .25 .017/12 .375 1 .375 .017/12 .25
.105/12 .375 .82 13.4 XT3]
R3 = .015625
L3 = .15625
```

```
%
% dataBF.m
% Data set for branch, full scale.
%
B =3
RB = [1.25 1.25 1.25]
LB = [35.7 48 17.8]
```

```
%
% dataBM.m
% Data set for branch, model scale.
%
B = 3
RB = [1.25 1.25 1.25]/12
LB = [35.7 48 17.8]
```

Bibliography

Bergh, H. and H. Tijdeman. "Theoretical and Experimental Results for the Dynamic Response of Pressure Measuring Systems," Report NLR-TR F.238, National Aero- and Astronautical Research Institute, Amsterdam, The Netherlands, 1965.

Brown, F. T., " The Transient Response of Fluid Lines," Journal of Basic Engineering, American Society of Mechanical Engineers, Vol. 4, 1962, 547-553.

Franke, M. E., R. W. Wilda, R. N. Miller, and C. V. Fada, "The Frequency Response of Volume-Terminated Pneumatic Lines with Circular and Rectangular Cross Sections," 1969 Joint Automatic Control Conference of the American Automatic Control Council, August 1969, pp 410-415.

-----, J.T. Karam and F.C. Lymburner, "Experimental Frequency Response of Fluid Transmission Lines," Proceedings of the Fourth Cranfield Conference, 1970, pp 1-12.

-----, A. J. Malanowski, and P. S. Martin, "Effects of Temperature, End-Conditions, Flow, and Branching on the Frequency Response of Pneumatic Lines," Journal of Dynamics, Systems, Measurement, and Control, Transactions of the American Society of Mechanical Engineers, March 1972, pp 15-20.

Gerhart, Philip M. and Richard J. Gross. Fundamentals of Fluid Mechanics. Reading, MA: Addison-Wesley, 1985.

Haliday, David and Robert Resnick. Fundamentals of Physics (Second Edition). New York: John Wiley & Sons, 1981.

Hull, Brian. " Automatic Pressure Control System for the Wright Laboratory Compressor Research Facility," M.S. Thesis, Air Force Institute of Technology, Wright-Patterson AFB OH, December 1993.

Iberall, A. S. "Attenuation of Oscillatory Pressures in Instrument Lines," Journal of Research, National Bureau of Standards, Vol. 45, 1950, pp 85-108.

Kantola, R. "Transient Response of Fluid Lines Including Frequency Modulated Inputs," Journal of Basic Engineering, Transactions of the American Society of Mechanical Engineers, June 1971, pp 274-281.

Karam, J. T. and M. E. Franke, "The Frequency Response of Pneumatic Lines," Journal of Basic Engineering, Transactions of the American Society of Mechanical Engineers, June 1967, pp 371-378.

Katz, Silas A., A. Hausner, and N. A. Eisenberg. "Effect of throughflow on signal propagation in fluid lines," Fluidic State-of-the-Art Symposium, Vol. IV, Harry Diamond Laboratories, Washington, D.C., 1974, pp 269-298.

Kirshner, Joseph M. and Silas Katz. Design Theory of Fluidic Components. New York: Academic Press, 1975.

Krishnayer, Ramesh and Thomas J. Lechner, Jr. "An Experimental Evaluation of Fluid Transmission Line Theory," Advances in Fluidics, ed: F.T. Brown et al., The American Society of Mechanical Engineers, New York, 1967, pp 367-389.

Luchuck, Wallace and John Pricket. "An Investigation of the Pressure Loss and Turbulence Attenuation Characteristics of Paired Screen Sets and Honeycomb Configurations," Arnold Engineering Development Center, Arnold Air Force Station, TN, May 1984, pp 1-29.

Nichols, N.B. "The Linear Properties of Pneumatic Transmission Lines," Transactions of the Instrument Society of America, Vol. 1, 1962, pp 5-14.

Nicolet Instrument Corporation. "Nicolet MultiPro Data Acquisition Systems Operation Manual," Madison, WI: Nicolet Instrument Corporation, 1991.

Rae, William H. and Alan Pope. Low-Speed Wind Tunnel Testing (Second Edition). New York: John Wiley & Sons, 1984.

Ross, Mark L. "Dynamic Characteristics of a Jet Engine Test Facility Air Supply," M.S. Thesis, Air Force Institute of Technology, Wright-Patterson AFB, OH, December 1983.

REPORT DOCUMENTATION PAGE

Form Approved
OMB No. 0704-0188

1. AGENCY USE ONLY (Leave blank)	2. REPORT DATE	3. REPORT TYPE AND DATES COVERED
	December 1993	Master's Thesis

4. TITLE AND SUBTITLE

DYNAMIC RESPONSE OF A COMPRESSOR RESEARCH FACILITY

5. FUNDING NUMBERS

6. AUTHOR(S)

Janet W. Grondin, Captain, USAF

7. PERFORMING ORGANIZATION NAME(S) AND ADDRESS(ES)

Air Force Institute of Technology
Wright-Patterson AFB, OH 45433-6583

8. PERFORMING ORGANIZATION REPORT NUMBER

AFIT/GAE/ENY/93D-16

9. SPONSORING/MONITORING AGENCY NAME(S) AND ADDRESS(ES)

Dr. Douglas Rabe
WL/POTX
Wright-Patterson AFB, OH 45433

10. SPONSORING/MONITORING AGENCY REPORT NUMBER

11. SUPPLEMENTARY NOTES

12a. DISTRIBUTION/AVAILABILITY STATEMENT

Approved for public release;
distribution unlimited

12b. DISTRIBUTION CODE

13. ABSTRACT *(Maximum 200 words)*

The response of the Wright Laboratory Compressor Research Facility to a small amplitude, acoustic, sinusoidal disturbance was investigated. The fluid transmission line equations for laminar, one-dimensional flow in a circular duct were solved and verified through a laboratory experiment using a scale model of the facility. The resonant frequencies of the facility were determined for a variety of flow conditions. Techniques for analytically modeling end impedance and flow straightening elements were also studied. The fundamental frequency of the facility was determined to be between 5.5 and 6.5 Hz depending on the flow conditions and geometry configurations specified.

14. SUBJECT TERMS

Fluid Transmission Line, Fluid Dynamics, Fluid Transients, Unsteady Pipe Flow

15. NUMBER OF PAGES

222

16. PRICE CODE

17. SECURITY CLASSIFICATION OF REPORT	18. SECURITY CLASSIFICATION OF THIS PAGE	19. SECURITY CLASSIFICATION OF ABSTRACT	20. LIMITATION OF ABSTRACT
Unclassified	Unclassified	Unclassified	UL